

Mustafa Ashry¹ 



*PHENOMENOLOGICAL IMPLICATIONS OF
NON-MINIMAL SUPERSYMMETRIC MODELS*

By
Mustafa Ashry Ibrahim Seif

SUBMITTED IN PARTIAL FULFILLMENT OF THE
REQUIREMENTS FOR THE DEGREE OF
DOCTOR OF PHILOSOPHY
AT
CAIRO UNIVERSITY
CAIRO, EGYPT
OCTOBER 2024

© Copyright by Mustafa Ashry Ibrahim Seif, 2024

¹mustafa@sci.cu.edu.eg, mustafa@cu.edu.eg,

CAIRO UNIVERSITY

DEPARTMENT OF MATHEMATICS

The undersigned hereby certify that they have read and recommend to the Faculty of Graduate Studies for acceptance a thesis entitled "***Phenomenological Implications of Non-Minimal Supersymmetric Models***" by **Mustafa Ashry Ibrahim Seif** in partial fulfillment of the requirements for the degree of **Doctor of Philosophy**.

Dated: October 2024

External Referees:

Prof. Qaisar Shafi
Department of Physics and Astronomy,
Delaware University, USA

Prof. Alakabha Datta
Department of Physics and Astronomy,
University of Mississippi, USA

Research Supervisors:

Prof. Ahmad A. Amer
and
Prof. Adel A. Mosharafa
Department of Mathematics,
Faculty of Science, Cairo University, Egypt

Prof. Shaaban S. Khalil
Center for Fundamental Physics (CFP),
Zewail City of Science and Technology, Egypt

CAIRO UNIVERSITY

Date: **October 2024**

Author: **Mustafa Ashry Ibrahim Seif**

Title: ***Phenomenological Implications of Non-Minimal
Supersymmetric Models***

Department: **Mathematics**

Degree: **Ph.D.** Convocation: **October** Year: **2024**

Permission is herewith granted to cairo university to circulate and to have copied for non-commercial purposes, at its discretion, the above title upon the request of individuals or institutions.

Signature of Author

THE AUTHOR RESERVES OTHER PUBLICATION RIGHTS, AND NEITHER THE THESIS NOR EXTENSIVE EXTRACTS FROM IT MAY BE PRINTED OR OTHERWISE REPRODUCED WITHOUT THE AUTHOR'S WRITTEN PERMISSION.

THE AUTHOR ATTESTS THAT PERMISSION HAS BEEN OBTAINED FOR THE USE OF ANY COPYRIGHTED MATERIAL APPEARING IN THIS THESIS (OTHER THAN BRIEF EXCERPTS REQUIRING ONLY PROPER ACKNOWLEDGEMENT IN SCHOLARLY WRITING) AND THAT ALL SUCH USE IS CLEARLY ACKNOWLEDGED.

To

my wife, Samira

&

my little angel, Aisha

&

my beloved parents . . .

Table of Contents

Table of Contents	v
List of Tables	ix
List of Figures	x
Abstract	xii
Acknowledgements	xiv
Introduction	1
1 SUPERSYMMETRY AND THE MINIMAL SUPERSYMMETRIC STANDARD MODEL	12
1.1 SUPERSYMMETRY	12
1.1.1 Introduction and Motivations	12
1.1.2 Spinors	20
1.1.3 Algebra and Supermultiplets	23
1.1.4 Superfields and Superpotential	26
1.2 The Minimal Supersymmetric Standard Model	34
1.2.1 MSSM Lagrangian	34
1.2.2 MSSM Spectrum	40
1.2.3 Radiative Electroweak Symmetry Breaking	45
2 SUPERSYMMETRIC $B - L$ EXTENSION OF THE STANDARD MODEL	49
2.1 Neutrino Masses in MSSM	49
2.1.1 Dirac Mass Term	50
2.1.2 Seesaw Mechanisms	53
2.2 BLSSM Model	58
2.2.1 BLSSM Structure	58
2.2.2 Gauge Kinetic Mixing in BLSSM	61

2.2.3	$B - L$ symmetry breaking	65
2.2.4	BLSSM Spectrum	68
2.2.5	BLSSM Higgs Sector	70
2.2.6	BLSSM Gauge Sector	74
3	PHENOMENOLOGY OF BLSSM	76
3.1	Introduction	76
3.2	The BLSSM BPs and Spectrum	79
3.3	Search for a heavy neutral CP-even Higgs boson at the LHC	85
3.3.1	$h' \rightarrow W^+W^- \rightarrow 2\ell + \cancel{E}_T$ Channel	88
3.3.2	$h' \rightarrow ZZ \rightarrow 4\ell$ Channel	91
3.3.3	$h' \rightarrow hh \rightarrow b\bar{b}\gamma\gamma$ Channel	93
3.3.4	Historical Significance	95
3.3.5	ML Analysis	96
3.4	Conclusion	98
4	LEFT RIGHT INVERSE SEESEW	100
4.1	Introduction	100
4.2	Supersymmetric Left-Right Model	102
4.3	Inverse Seesaw Mechanism	105
4.4	Left Right Model with Inverse Seesaw	106
4.5	Spontaneous Symmetry Breaking in LRIS	113
4.5.1	Gauge Boson Masses	115
4.5.2	Fermion Masses	118
4.6	Higgs Sector in LRIS	120
4.6.1	Singly Charged Scalars	120
4.6.2	Neutral Pseudoscalars	121
4.6.3	Neutral Scalars	123
5	PHENOMENOLOGY OF LRIS	127
5.1	Search for a heavy neutral Higgs boson in LRIS at the LHC	127
5.1.1	Heavy Neutral CP-Even Higgs Boson in LRIS	128
5.1.2	Search for Heavy Higgs Bosons at the LHC	134
5.1.3	Conclusion	146
5.2	Muon $g - 2$ anomaly in LRIS	146
5.2.1	LRIS Couplings for a_μ	147
5.2.2	LRIS Contributions to a_μ	154
5.2.3	LFV Constraints on a_μ	162
5.2.4	Conclusion	165

6 SEMI-VISIBLE DARK PHOTON IN A MODEL WITH VECTOR-LIKE LEPTONS FOR THE $(g-2)_{e,\mu}$ AND W-BOSON MASS ANOMALIES	166
6.1 The VLSM model	166
6.1.1 Gauge boson sector	166
6.1.2 Fermion sector	168
6.1.3 Fermion interactions	170
6.2 Anomalous magnetic moments and W -boson mass	172
6.2.1 Anomalous magnetic moments	172
6.2.2 W -boson mass	175
6.3 Signals of light particles	179
6.3.1 Semi-visible dark photon	179
6.3.2 The light vector-like neutrino and $U(1)'$ scalar	181
6.3.3 Vector-like lepton search at the LHC	182
6.4 Conclusions	183
7 Conclusion	185
A LRIS Appendix	189
A.0.1 Tadpole Equations and Potential Minimization	189
A.0.2 Copositivity Conditions of the Higgs Potential	190
A.0.3 Neutral CP -even Higgs Rotations and Determinant	191
B The muon anomalous magnetic moment a_μ in QED and the EW Theory	193
B.1 Algebra and Useful Relations	195
B.2 Theory of Magnetic Moment	198
B.3 a_μ in QED	201
B.4 a_μ in EW Theory	207
B.4.1 $W - \nu$ -loop	208
B.4.2 Z -loop	215
B.4.3 Higgs loop	220
C VLSM Appendix	224
C.1 Details of the model	224
C.1.1 Diagonalization of vector boson mass matrix	224
C.1.2 Diagonalization of the fermion mass matrices	226
C.1.3 Lepton couplings	229
C.2 Loop functions	230

Bibliography **232**

List of Tables

1.1	Particle content of the MSSM	35
2.1	BLSSM field and superfield content	60
3.1	Chiral superfields and their quantum numbers in the BLSSM.	79
3.2	BP and relevant outputs.	84
3.3	Heavy Higgs production and decays values	88
3.4	Heavy Higgs Signal and Back ground rates in BLSSM	89
3.5	Used HEP Tools	96
4.1	The LRIS particle Content	107
5.1	LRIS parameters h' searches BPs	133
5.2	h' production cross section and its $h' \rightarrow hh$ decay branching ratio . .	137
5.3	Cut flow for the h' signal and background	139
5.4	h' production cross section and its $h' \rightarrow ZZ$ decay branching ratio . .	144
5.5	BP of $g - 2$ in LRIS	160
5.6	Yukawa BP of $g - 2$ in LRIS	161
5.7	Results of muon and electron $g - 2$ and LFV in LRIS	162
6.1	Quantum numbers of the scalars and leptons in VLSM	167
6.2	BPs inputs and outputs in VLSM	178

List of Figures

1.1	One-loop self-energy graph in ϕ^4 theory [31, 147, 255]	16
1.2	Fermionic loop contribution to the scalar two point function [31, 147, 255]	17
1.3	Sfermion loop contributions to Higgs self energy [31, 147, 255]	19
1.4	Different supermultiplets of massless particles [147]	25
1.5	Running of the soft MSSM masses from GUT to EW scale	46
1.6	SM failure and MSSM success of gauge coupling unification	48
2.1	Type I seesaw neutrino masses process	54
2.2	The evolution of the $B - L$ scalar masses from GUT to TeV scale . .	67
3.1	Heavy Higgs mixing versus \tilde{g} in BLSSM	82
3.2	Feynman diagrams for h' production and decays	85
3.3	Heavy Higgs mass, production and decays versus \tilde{g}	86
3.4	Signal and background without and with cuts in WW channel	91
3.5	Signal and background without and with cuts in ZZ channel	92
3.6	Signal and background without and with cuts in hh channel	94
3.7	Significance versus integrated luminosity	95
3.8	BDT response in WW and hh channels	97
3.9	Correlation matrix and the ROC curves	98
4.1	Gauge coupling unification [57, 88]	105
4.2	The Charged Higgs boson mass M_H vs parameter α_{32}	122
4.3	The CP-odd Higgs boson mass M_A vs parameter α_{32} and λ_{23}	123
5.1	The next lightest Higgs boson mass and its mixing	132
5.2	The next lightest Higgs boson production and its decay branching ratios	134
5.3	Number of Sg and Bkg h' production and decay events in LRIS . . .	137
5.4	Feynman diagram for the h' ggF production and decay	138

5.5	Number of signal and background events of $h' \rightarrow b\bar{b}\gamma\gamma$ events	140
5.6	Significances of h' channels in LRIS	142
5.7	Number of signal events for $h' \rightarrow b\bar{b}\gamma\gamma$ in LRIS	142
5.8	Feynman diagram for $gg \rightarrow h' \rightarrow ZZ \rightarrow 4\ell$ in LRIS	143
5.9	Number of signal events for $pp \rightarrow h' \rightarrow ZZ \rightarrow 4\ell$ in LRIS	145
5.10	Significance of the $pp \rightarrow h' \rightarrow ZZ \rightarrow 4\ell$ signal in LRIS	145
5.11	LRIS one-loop Feynman diagrams contributions to lepton $g_\ell - 2$	155
5.12	The muon and electron magnetic moment anomalies in LRIS	157
5.13	The branching ratio $\text{BR}(\mu \rightarrow e\gamma)$ in LRIS	162
6.1	The Feynman diagrams dominantly contribute to the $\Delta a_{e,\mu}$	172
6.2	Leptonic magnetic anomalies $\Delta a_{e,\mu}$ in VLSM	173
6.3	CDF II m_W in VLSM	177
6.4	Dominant dark photon semi-visible decay.	179
B.1	spin precession about a magnetic field.	194
B.2	One-loop QED contributions to a_μ	202
B.3	One-loop EW W, Z, H contributions to a_μ	207
B.4	The Goldston ϕ_W contributions to a_μ	212
B.5	EW Z and ϕ_Z loops contributions to a_μ	215
B.6	One-loop Goldston boson ϕ_Z -loops contribution to a_μ	217
B.7	One-loop EW Higgs-loop contribution to a_μ	220

Abstract

The detection of a heavy neutral CP-even Higgs boson of the $B - L$ Supersymmetric Standard Model (BLSSM), h' , with $m_{h'} \simeq 400$ GeV, at the Large Hadron Collider (LHC) for a center-of-mass energy of $\sqrt{s} = 14$ TeV, is investigated. The following production and decay channels are considered: $gg \rightarrow h' \rightarrow ZZ \rightarrow 4\ell$ and $gg \rightarrow h' \rightarrow W^+W^- \rightarrow 2\ell + \cancel{E}_T$ (with \cancel{E}_T being the Missing Transverse Energy (MET)), where $\ell = e, \mu$, with integrated luminosity $L_{\text{int}} = 300 \text{ fb}^{-1}$ (Run 3). Furthermore, we also look into the di-Higgs channel $gg \rightarrow h' \rightarrow hh \rightarrow b\bar{b}\gamma\gamma$ at the High-Luminosity LHC (HL-LHC) with an integrated luminosity of $L_{\text{int}} = 3000 \text{ fb}^{-1}$. We demonstrate that promising signals with high statistical significance can be obtained through the three aforementioned channels.

We develop a low scale left-right symmetric model based on $SU(3)_C \times SU(2)_L \times SU(2)_R \times U(1)_{B-L} \times Z_2$ with a simplified Higgs sector consisting of only one bidoublet and one $SU(2)_R$ doublet. In this model, the tiny values of light neutrino masses are generated through an inverse-seesaw mechanism. We emphasize that in this setup, the tree-level flavor changing neutral current can be strongly suppressed, consistent with the current experimental constraints. We show that the lightest CP -even Higgs boson, which is like the standard model Higgs boson, and the next lightest Higgs boson, h' , are generated from the neutral components of the bidoublet. We show that the mass of the next lightest Higgs boson can be of an order a few hundred GeVs. We analyze the detection of h' at the LHC for a center-of-mass energy $\sqrt{s} = 14$ TeV and integrated luminosity $L_{\text{int}} = 300 \text{ fb}^{-1}$ via di-Higgs channel: $h' \rightarrow hh \rightarrow b\bar{b}\gamma\gamma$ and also in the ZZ channel: $h' \rightarrow ZZ \rightarrow 4\ell$ ($\ell = e, \mu$) at an integrated luminosity $L_{\text{int}} = 3000 \text{ fb}^{-1}$. We consider three benchmark points for this analysis with $m_{h'} = 250$ GeV, 400 GeV, and 600 GeV. We show that promising signals with good statistical significances can be obtained in di-Higgs channel, with $2\gamma + 2b$ -jets final states.

We investigate the possibility of explanation for the muon anomalous magnetic moment $g_\mu - 2$ in a left-right model with an inverse seesaw mechanism. We emphasize that the observed deviation from the Standard Model predictions can be accommodated in a large part of the parameter space of this class of models, where loops with

massive neutrinos and charged Higgs boson as well as the weak W boson contribute significantly to $g_\mu - 2$. Stringent constraints due to lepton flavor violation $\mu \rightarrow e\gamma$, μ - e conversion and the electron anomalous magnetic moment $g_e - 2$ are considered, and the results are compatible.

We propose a model realizes that a semi-visible dark photon which can contribute to the anomalous magnetic moment ($g - 2$) of both electron and muon. In this model, the electron $g - 2$ is deviated from the Standard Model (SM) prediction by the 1-loop diagrams involving the vector-like leptons, while that of muon is deviated due to a non-vanishing gauge kinetic mixing with photons. We also argue that the W -boson mass can be deviated from the SM prediction due to the vector-like lepton loops, so that the value obtained by the CDF II experiment can be explained. Thus, this model simultaneously explains the recent three anomalies in $g - 2$ of electron and muon as well as the W -boson mass. The constraints on the $\mathcal{O}(1)$ GeV dark photon can be avoided because of the semi-visible decay of the dark photon, $A' \rightarrow 2N \rightarrow 2\nu 2\chi \rightarrow 2\nu 4e$, where N is a SM singlet vector-like neutrino and χ is a CP-even Higgs boson of the $U(1)'$ gauge symmetry.

Acknowledgements

I would like to start by expressing my sincere gratitude and appreciation to my advisors Prof. *Ahmad Amer* and Prof. *Adel Mosharafa* for their support, and encouragement.

It is with gratitude that I acknowledge my advisor Prof. *Shaaban Khalil* for his support for my Ph.D. study and research. His guidance helped me in research and in writing this thesis.

I hope that my Prof. *Ahmed Khalil* is resting in peace. My sincere gratefulness to him for motivating me towards modern fields of science. I am indebted to Prof. *Hamdy Abdalgawad* and Prof. *Nabil Youssef* for helping me in the first steps of research. Also thanking both Prof. *Adel awad* and Prof. *Elsayed Lashin* is necessary for their deep and fundamental discussions.

My deep thanks to my colleagues *Ahmad Moursy*, *Waleed Abdallah*, and *Ahmed Hammad*, for their fruitful discussions. My deep thanks to Dr. *Nefertity Megahed* for her kind support. Also, I am grateful to my junior collaborators *Merna Ibrahim*, and *Kareem Ezzat* for their practical discussions and hard work.

I wish to express deep gratitude to the Mathematics Department, Faculty of Science, Cairo University. I had the honor of being an undergraduate student and MSc student in such a department. Luckily, I became a senior member of staff there. Also I would like to thank the Center for Fundamental Physics (CFP) at Zewail City for Science and Technology for providing everything I need to complete my work.

Last but not least, I would like to thank my family: my wife, *Samira*, and my little angel *Aisha* for their graceful accompany, my parents for their endless love and care, and for supporting me spiritually throughout my life, and my sisters and brothers for their unstoppable support and belief in me. All love to my nephew *Youssef M. Ashry*, being always proud of me!

Cairo, Egypt.
October 7, 2024

Mustafa Ashry

Introduction

The search for a heavy neutral CP-even Higgs boson at the current Run 3 of the LHC and a future HL-LHC is an active area of research [5,6,23,64,67,107,176,188,302]. This is so because virtually any extension of the Higgs sector beyond the single doublet structure of the Standard Model (SM), in which the only neutral CP-even state of it is identified with the particle that was discovered in 2012 at the LHC by the ATLAS and CMS experiments [3, 103], contains it. As a result, probing such a heavy Higgs boson is one of the main goals of the LHC experiments, as it could well provide the first hint for physics Beyond the SM (BSM). Both ATLAS and CMS have searched for a heavy Higgs boson and the corresponding analyses typically involve looking for events in which the heavy Higgs boson is produced and then decays into SM particles, such as W^\pm or Z bosons, in turn decaying into leptons or jets [5], or into the SM Higgs boson itself [109], which then decays into b quarks or τ leptons.

Supersymmetric extensions of the SM are one of the BSM frameworks that consistently predict the existence of several Higgs bosons, including a heavy neutral CP-even one. Such a Higgs boson mass can be significantly larger than the one of the SM Higgs state, potentially reaching several hundred GeV. For example, the Minimal Supersymmetric Standard Model (MSSM) contains five Higgs bosons: two CP-even (h and H , with $m_h < m_H$), one CP-odd (A) and two charged states (H^+ and H^-): for reviews, see, e.g., [145]. This is the simplest construct implementing supersymmetry, where the lightest CP-even Higgs boson, h , is designated as the SM Higgs boson, with a mass of 125 GeV, which, however, imposes a strenuous configuration

on the MSSM parameter space, forcing the other CP-even Higgs boson, H , to be rather heavy and significantly decoupled. Some other models have similar situations too [221]. However, if supersymmetry is non-minimal, in either its gauge or Higgs sector or both, then the mass of additional CP-even Higgs states can become rather less constrained [254]. An example of this is the so-called BLSSM, which indeed offers the possibility of LHC signals for a CP-even Higgs state not only above the SM Higgs mass, e.g., in the range up to 500 GeV [188], but also afford one with a lighter mass spectrum, in turn able to explain past [15, 187] and present data anomalies [16].

The BLSSM is a theoretical extension of the MSSM that includes an additional $U(1)$ gauge symmetry known as $B - L$ (baryon number minus lepton number) [69, 70, 214, 259] as well as an extended Higgs sector. The $B - L$ symmetry is motivated by the observation that the difference between baryon and lepton number is conserved in many particle physics processes. In the BLSSM, the $B - L$ symmetry may be broken at the few TeV scale, giving rise to new particles such as two new extra neutral CP-even Higgs bosons. One of them, labeled h' , can have energies in the hundreds of GeV range. It is indeed the presence of such a h' state that causes the aforementioned new phenomenology to emerge in collider experiments, which can then be used to test the BLSSM hypothesis.

We emphasize that the SM-like Higgs state, henceforth labeled h throughout, is derived from the real parts of the neutral components of the Electro-Weak (EW) scalar doublets H_u and H_d whereas the (typically) next-to-lightest Higgs boson, h' , stems from the real parts of the neutral components of the $B - L$ scalar singlets χ_1 and χ_2 . Despite the fact that the mass mixing between these two types of Higgs bosons is negligible, a non-vanishing kinetic mixing allows for relevant couplings between h' and the SM particles, resulting in a total cross section of h' production and decay into W^+W^- , ZZ or hh of $\mathcal{O}(1)$ fb. These signals are typically smaller than the associated backgrounds but, by using appropriate selection strategies, they can be probed with

a reasonably high sensitivity. However, given that current experimental limits have significantly constrained also the BLSSM parameter space above and beyond what allowed for in Ref. [188], which targeted Run 2 sensitivities, we revisit here the scope of Run 3 and the HL-LHC in accessing the heavy neutral CP-even Higgs boson of the BLSSM, h' , in the mass region of 400 GeV or so.

The SM of particle physics is in an excellent agreement with most of the confirmed experimental results. However, there exist several compelling arguments that indicate that the SM is only an effective low energy limit of a more fundamental underlying theory. Indeed, there are a number of theoretical and phenomenological outstanding issues in particle physics that can not be explained and the SM fails to address them adequately. Here, we may just mention the puzzles of dark matter and tiny neutrino masses [26, 29, 40, 151, 166], which can not be explained within the SM. One of the most popular extensions of the SM is the grand unified theory (GUT), where the SM gauge symmetry $SU(3)_C \times SU(2)_L \times U(1)_Y$ is extended to a bigger (simple or semisimple) group. Nonvanishing neutrino masses motivate the existence of right-handed neutrinos, and hence, all known fermions would have both left and right chirality. In this respect, the SM gauge group would be extended to the left-right (LR) symmetric gauge group, which is based on $SU(3)_C \times SU(2)_L \times SU(2)_R \times U(1)_{B-L}$, where left and right chirality are treated equally at high energy scales. In this class of models, the Majorana right-handed neutrinos are naturally heavy, and hence small left-handed neutrino masses are generated through seesaw mechanisms.

In the conventional LR model proposed by Mohapatra *et al.* [249, 250, 279], the SM fermions (including the right-handed neutrino) are assigned in left- or right-handed doublets, and the following Higgs sector has been assumed: one bidoublet to construct the Yukawa couplings of quarks and leptons, in addition to a left- and right-handed scalar triplets for seesaw neutrino masses. The $SU(2)_R \times U(1)_{B-L}$ symmetry is broken down to $U(1)_Y$, at a high energy scale, by the vacuum expectation value (VEV) of the

neutral component of the right-handed triplet, while the VEVs of neutral components of the bidoublet and the left-handed triplet contribute in breaking the electroweak symmetry, $SU(2)_L \times U(1)_Y$, down to $U(1)_{\text{em}}$. It was clear that the Higgs sector of this model is not minimal, with several neutral and singly and doubly charged components. Also, the left-handed triplet was introduced only to preserve LR symmetry, although its VEV must be fine-tuned to a very small value to avoid stringent constraints from the observed neutrino masses. Moreover, the Higgs triplets may induce tree level flavor violating processes that contradict the current experimental limits. Therefore, different variants of the conventional LR model have been considered [55, 58, 87, 141, 236, 256].

Here, we consider an example of a LR model, with a Higgs sector consisting of one scalar bidoublet and a scalar right-handed doublet. In this case and in order to generate light neutrino masses, we adopt the inverse-seesaw (IS) mechanism [93, 173, 247, 248, 306]. As known, this mechanism requires introducing other singlet fermions that couple with right-handed neutrinos and have a small mass [$\sim \mathcal{O}(1)$ KeV], which may be generated radiatively. The IS mechanism is quite motivated by having the TeV scale LR model that can be probed in current and future colliders, while in the conventional LR model, the GUT scale is the typical scale of breaking LR symmetry, where right-handed neutrino masses are generated. Moreover, in the limit of vanishing the above mentioned tiny mass, we will have massless left-handed neutrinos and the lepton number symmetry is restored. Thus, such a small scale can be considered, according to 't Hooft naturalness criteria [293], as a natural scale of a global symmetry (lepton number) breaking. We also argue that in this class of models the tree-level flavor changing neutral current (FCNC) is under control. It turns out that the right-handed doublet is essentially decoupled from the two Higgs doublets, generated from the bidoublet; hence the Higgs sector of this model mimics the scenario of two the Higgs doublet model [128, 183, 184]. We

show that the lightest CP -even Higgs boson, the SM-like Higgs boson, and the next lightest are generated from the neutral components of the bidoublet. For a wide range of the parameter space, one can show that the mass of the next lightest Higgs boson is of the order a few hundred GeVs.

In this paper we analyze the discovery prospects of the next lightest CP -even neutral Higgs boson, h' , at the Large Hadron Collider (LHC). Our searches are performed by looking for resonant peaks in two processes, namely $h' \rightarrow hh \rightarrow b\bar{b}\gamma\gamma$ and $h' \rightarrow ZZ \rightarrow 4\ell$ ($\ell = e, \mu$). The analysis is pivoted on three benchmark points, with $m_{h'} = 250$ GeV, 400 GeV, and 600 GeV, for a center-of-mass energy $\sqrt{s} = 14$ TeV and $L_{\text{int}} = 300 \text{ fb}^{-1}$, and 3000 fb^{-1} , respectively. After imposing various sets of cuts to reduce backgrounds (B) and improve the statistical significance (S/\sqrt{B}), where S refers to the signal, we find that the SM-like Higgs boson pair production, with $b\bar{b}\gamma\gamma$ final states, is the most promising channel for probing our heavy Higgs boson at the LHC. The channel of the Z -pair production, decay to 4ℓ is less significant as its cross section is very small for $m_{h'} \gtrsim 300$ GeV, and the associated background is quite large for $m_{h'} \simeq 200$ GeV. We show that to probe h' through this channel, L_{int} must be increased up to $L_{\text{int}} = 3000 \text{ fb}^{-1}$.

Non-vanishing neutrino masses inferred from neutrino oscillation experiments [26, 29, 40, 151, 166], provided strong evidence for new BSM physics. The extensions of the SM to account for neutrino masses and mixing imply new sources of lepton flavor violation (LFV), which could explain the long-standing discrepancy between the SM prediction for the muon anomalous magnetic moment $a_\mu = (g_\mu - 2)/2$ and its experimental measurement.

Recent experimental results indicate a possible 4.2σ difference between the measured value of the anomalous magnetic moments of muons a_μ and the SM expectations [19, 162, 209, 215], namely

$$\delta a_\mu = a_\mu^{\text{exp}} - a_\mu^{\text{SM}} = (2.51 \pm 0.59) \times 10^{-9}. \quad (0.0.1)$$

We consider the explanation of the a_μ anomaly in the left-right (LR) model with inverse seesaw mechanism (LRIS) to generate light neutrino masses and mixing at low energy scale. The salient feature of this class of models is the large neutrino Yukawa couplings, which allow for significant nonuniversal leptonic contributions to the a_μ anomaly via diagrams mediated by charged Higgs bosons and right-handed neutrinos (RHNs). As constraints, we impose the experimental limits of the LFV $\mu \rightarrow e\gamma$, $\mu\text{-}e$ conversion, and the electron anomalous magnetic moment [22, 36, 99, 129].

The LR model is among the most natural extensions of the SM, which is motivated by grand unified theories (GUTs) and accounts for measured neutrino masses as well as providing an elegant explanation for the origin of parity violation in low-energy weak interactions. The LRIS has been analyzed in detail in Ref. [160]. We recall that it has a Higgs sector that consists of one scalar bidoublet and a scalar right-handed (RH) doublet only. In addition, the LRIS contains singlet fermions S_1, S_2 for adopting the IS mechanism of neutrino masses. Such a TeV scale LR model can be probed in current and future experiments as emphasized in Ref. [160]. Also, it was argued in Ref. [161] that the tension between the SM prediction and the experimental results of the R_D and R_{D^*} ratios, defined by $R(\{D^*, D\}) = \frac{\text{BR}(B \rightarrow \{D^*, D\}\tau\nu)}{\text{BR}(B \rightarrow \{D^*, D\}\ell\nu)}$, where $\ell = e, \mu$, can be resolved in this class of LRIS models. In fact there are several new physics scenarios that have been proposed to accommodate δa_μ and δa_e results. See Refs. [61, 75, 80, 90, 106, 122, 123, 137, 138, 157, 180, 189, 201, 229, 230].

There is the long-standing discrepancy in the anomalous magnetic moment ($g-2$) of muon between the Standard Model (SM) prediction [45–47, 81, 84, 112–114, 125, 130, 131, 169, 172, 197, 198, 210, 211, 222, 241, 244] and the experimental measurement [20, 78]. The latest world average of Δa_μ reports the 5.1σ discrepancy [25],

$$\Delta a_\mu := a_\mu^{\text{exp}} - a_\mu^{\text{SM}} = 2.49(48) \times 10^{-9}. \quad (0.0.2)$$

Whereas the recent lattice calculation [89] and the experiment determination [200]

of the hadron vacuum polarization contribution to the muon $g-2$ point the value closer to the SM prediction, and hence the tension relaxes to a few sigma level. Nonetheless, we shall assume that the discrepancy is given by Eq. (0.0.2), since the current situation is not conclusive. The electron $g-2$ may also deviate from the SM prediction according to the recent precise measurement of the fine structure constant using Cs atoms [262], and the discrepancy is given by [133]

$$\Delta a_e := a_e^{\text{exp}} - a_e^{\text{SM}} = -8.7 \text{ (3.6)} \times 10^{-13}, \quad (0.0.3)$$

and hence there is a 2.4σ discrepancy from the experimental value [190, 191]. Similarly to the muon $g-2$, however, the situation is not conclusive because the fine structure constant determined by Rb atoms shows the value consistent with the SM [253]. Nonetheless, we also assume that there is the discrepancy in Eq. (0.0.3), especially the negative sign of its discrepancy. Simultaneous explanations for both anomalies have been studied in Refs. [12, 33, 54, 61, 75, 94, 95, 118, 123, 133, 150, 157, 170, 189, 233, 262].

The model with a $U(1)'$ gauge symmetry and the vector-like fourth family of SM (VLSM) is studied in Refs. [207, 208]², to explain the muon $g-2$ and another anomaly in the $b \rightarrow s\ell\ell$ process [24, 32, 35, 49, 111, 127, 136, 195, 217, 220]³. In these works, the $U(1)'$ gauge boson is assumed to be heavier than 100 GeV, so the gauge boson is called a Z' -boson. The muon $g-2$ is explained by the 1-loop diagrams involving the vector-like leptons via mixing with muons. In this case, however, the electron $g-2$ can not be explained simultaneously because it causes the lepton flavor violations if the mixing with electrons is introduced. In Ref. [206], it has been shown that the W -boson mass measured by the CDF II [9],

$$m_W^{\text{CDF}} = 80.4335 \text{ (94) GeV}, \quad (0.0.4)$$

²Other types of models with vector-like fermions and a $U(1)'$ are studied in Refs. [34, 37, 86, 126, 134, 144, 219, 224, 225, 243, 273, 313].

³The recent measurement of $R_{K^{(*)}}$ shows the consistent value with the SM prediction [8].

which is larger than the previous measurements $m_W^{\text{PDG}} = 80.379$ (12) GeV and the SM prediction $m_W^{\text{SM}} = 80.361$ (6) GeV [314], can be explained by the 1-loop diagrams involving the vector-like leptons lighter than about 200 GeV.

In this work, we study a new parameter space of the model proposed in Ref. [207, 208], where the $U(1)'$ gauge boson is much lighter than the Z -boson mass and therefore we call it a dark photon A' throughout this work. In such a scenario, the dark photon can explain Δa_μ if it is lighter than $\mathcal{O}(1)$ GeV and its gauge kinetic mixing with the photon is $\mathcal{O}(10^{-5} - 10^{-2})$ depending on the dark photon mass [272]. Note that the dark photon contribution from the gauge kinetic mixing can not explain the negative shift of the electron $g - 2$ in Eq. (0.0.3), since it is predicted to be positive. In this model, we can explain Δa_e by the 1-loop diagrams involving the vector-like leptons as for Δa_μ in the heavy Z' scenario [207, 208], without lepton flavor violations. We also point out that the W -boson mass measured by the CDF II can be explained in the same manner as in Ref. [206]. Altogether, we study the light dark photon region of the model in Ref. [207, 208] in order to explain both electron and muon $g-2$, as well as m_W measured by the CDF II experiment without extending the model.

The dark photon explaining Δa_μ is excluded by the experiments if it decays dominantly to e^+e^- [7, 74, 226] or invisible particles [42, 227]. This limit will be relaxed and the dark photon explanation is still viable if the dark photon decays to both visible and invisible particles [17, 100, 148, 149, 252], namely if the dark photon is semi-visible. Interestingly, in this model, the SM singlet vector-like neutrino N can be lighter than the dark photon, and then N can decay to the $U(1)'$ breaking Higgs boson χ whose dominant decay mode is e^+e^- . Thus, the decay of the dark photon A' proceeds as $A' \rightarrow 2N \rightarrow 2\nu 2\chi \rightarrow 2\nu 4e$ which is a semi-visible decay.

The thesis has the following structure:

-
- 0.0.1. In chapter 1, we review the SUSY structure, and the MSSM model.
- 0.0.2. In chapter 2, we review BLSSM model.
- 0.0.3. In chapter 3 we discuss BLSSM Phenomenology. In Sec. 3.1, we discuss at some length the Higgs sector. Studies of h' signals at the LHC are then carried out too, wherein a detailed Monte Carlo (MC) analysis for h' production via (mostly) gluon-gluon fusion (ggF) and decay via $W^+W^- \rightarrow 2\ell + \cancel{E}_T$, $ZZ \rightarrow 4\ell$ and $hh \rightarrow b\bar{b}\gamma\gamma$ is performed.
- 0.0.4. In chapter 4, we introduce the LR model with IS mechanism. The gauge, fermion, and Higgs sectors of the model are discussed. The SSB is introduced and different spectra were worked out.
- 0.0.5. In chapter 5 is devoted for the LRIS phenomenology. In Sec. 5.1, we show that the SM-like Higgs, h , and the next lightest h' are stemmed from the real part of neutral components of the bidoublet. Searches for h' at the LHC are comprehensively studied. A detailed analysis for the SM Higgs pair production from h' , followed by the decays into $b\bar{b}\gamma\gamma$, is provided. We show that the total cross section of this process is of order $\mathcal{O}(1)$ fb. In general the signal of this channel is much smaller than the background, however by selecting an appropriate set of cuts we can probe the signal with a reasonable significance. We also analyze a possible signature through the Z -gauge boson pair production from h' followed by the decays to 4ℓ .

In Sec. 5.2, we highlight relevant interactions in the LRIS, as the details of the model are given in previous papers [160, 161]. Then we analyze new LRIS contributions to a_μ , specifically those due to the light and heavy Z, W, Z', W' gauge bosons and neutral and charged Higgs bosons with heavy neutrinos. Finally, we is devoted a part for for the LFV constraints in LRIS.

0.0.6. In chapter 6, we study the VLSM model and its phenomenology. In Sec. 6.1, we briefly review the model with particular interests in the gauge kinetic mixing. We study the observables, including Δa_e , Δa_μ and m_W in Sec. 6.2, and then discuss signals from the dark photon in Sec. 6.3. Finally, we draw our conclusions in Sec. 6.4. The details of the model and the loop functions for the oblique parameters are respectively in Appendices C.1 and C.2.

PUBLICATIONS

The main work of the thesis is based on these papers [10, 53, 54, 56, 160]:

- 0.0.1. M. Ashry, S. Khalil and S. Moretti, *Searching for a Heavy Neutral CP-Even Higgs Boson in the BLSSM at the LHC Run 3 and HL-LHC*, Eur. Phys. J. C 84 (2024), 433. ([arXiv: 2305.11712](#))
- 0.0.2. M. Ashry, K. Ezzat and S. Khalil, *Muon $g-2$ anomaly in a left-right model with an inverse seesaw mechanism*, Physical Review D 107, 055044, (2023) ([arXiv: 2207.05828](#))
- 0.0.3. M. Ashry, K. Ezzat and S. Khalil, *Search for a heavy neutral Higgs boson in a left-right model with an inverse seesaw mechanism at the LHC*, Physical Review D 104, 015016 (2021) ([arXiv: 2101.08255](#))
- 0.0.4. M. Ashry, K. Ezzat and S. Khalil, *Search for heavy neutral Higgs bosons at the LHC*, The International Conference on Beyond Standard Model: From Theory To Experiment (BSM-2021), Andromeda Proceedings (2021) ([DOI: 10.31526/ACP.BSM-2021.21](#))
- 0.0.5. Waleed Abdallah, Mustafa Ashry, Junichiro Kawamura, and Ahmad Moursy, *Semi-visible dark photon in a model with vector-like leptons for the $(g-2)_{e,\mu}$ and W -mass anomalies*, Physical Review D 109, 015031 (2024) ([arXiv: 2308.05691](#))

1

SUPERSYMMETRY AND THE MINIMAL SUPERSYMMETRIC STANDARD MODEL

1.1 SUPERSYMMETRY

Symmetries are very important in modern physics. They give the most consistent way to construct Lagrangians. Well known examples of symmetries are Lorentz transformations, translations in space-time, and symmetry under isospin transformations. Supersymmetry is different from all those symmetries; it's action transforms bosons into fermions and vice versa, that is, it does not conserve statistics.

1.1.1 Introduction and Motivations

Supersymmetry is the most elegant and promising theory beyond the standard model. In this section we will give, in points, why do physicists interest in supersymmetry, and then we give, in brief, what is the supersymmetry and its foundations. For supersymmetry References, we suggest [31, 65, 255, 309].

1.1 SUPERSYMMETRY

In fact, there are many theoretical arguments can be given in favor of supersymmetry. Some of them are:

- It seems appealing in its own right to have a theory which unifies the two different classes of particles, bosons and fermions, into a common representation, called the superfield.
- It is necessary to superstring theory, which is believed by many physicists to be the best candidate of a “Theory Of Everything”(TOE). In particular, local SUSY gives rise to supergravity, which could possibly be the answer to the attempts to unify general relativity (GR) with quantum field theory(QFT).
- It solves the problem with quadratic divergences “The Hierarchy Problem” in a very elegant natural way.
- The minimal supersymmetric extension of the Standard Model (MSSM) leads to the gauge coupling unification, which can't be satisfied in the SM.
- While the quadratic and quartic terms of the Higgs potential, which are necessary in order to break the electroweak symmetry have to be postulated ‘adhoc’ in the case of the SM, they appear in a natural way in the context of MSSM.

“The price one pays for such a beautiful theory is the abundance of many new particles that must be included into the theory”¹, since, in order to satisfy the requirements of supersymmetry, each particle must have a superpartner (a boson for a fermion and vice versa). In fact, supersymmetry ensures that the particle and its superpartner must have the same masses. So, for example, there would be a superpartner for the electron (selectron) with the electron mass (0.5 MeV). However, a particle with this mass must be founded by an experiment, which does not occur. Therefor, if

¹said by prof. S. Khalil about the supersymmetry in his book “Supersymmetry Phenomenology”

supersymmetry will go farther being a mathematical theory by describing physics, it must be broken at a scale of energy which is far from our present experimental data. It is worth noting that, there are many models which inform us that the superpartners masses should be in the range of 100 GeV to 1 TeV. This is such an interesting mass range, since it is just what the LHC is going to explore. “*If the LHC discovered SUSY, this will certainly be one of the greatest achievements in the history of theoretical physics*”¹.

At present, Quantum Field Theory (QFT) is the theoretical framework of the particle physics. The Special Relativity (SR) is one of the QFT assumptions. The symmetries of the spacetime in QFT are included by the Poincaré group. Under this group, coordinates transform as

$$x_\mu \rightarrow x'_\mu = \Lambda_\mu^\nu x_\nu + a_\mu, \quad (1.1.1)$$

where Λ_μ^ν is the Lorentz transformation, and a_μ is a spacetime translation. The generators of these transformations are the angular momentum 4-tensor $M^{\mu\nu}$, which represents the Lorentz transformations, and the four-momentum P^μ , which represents the spacetime translations. They follow the algebra

$$[P^\mu, P^\nu] = 0, \quad (1.1.2)$$

$$[M^{\mu\nu}, P^\lambda] = i(P^\mu \eta^{\nu\lambda} - P^\nu \eta^{\mu\lambda}), \quad (1.1.3)$$

$$[M^{\mu\nu}, M^{\lambda\sigma}] = i(M^{\mu\sigma} \eta^{\nu\lambda} + M^{\nu\lambda} \eta^{\mu\sigma} - M^{\mu\lambda} \eta^{\nu\sigma} - M^{\nu\sigma} \eta^{\mu\lambda}), \quad (1.1.4)$$

where $\eta^{\mu\nu} = \text{diag}(1, -1, -1, -1)$ is the Minkowski metric tensor.

Of a great importance to any theory are the so called Casimir operators. Casimir operators are, by definition, the operators that commute with all the generators of the algebra. The Casimir operators of the Poincaré algebra are P^2 and W^2 , where

$$W_\mu := -\frac{i}{2} \epsilon_{\mu\nu\lambda\sigma} M^{\nu\lambda} P^\sigma, \quad (1.1.5)$$

which is called the Pauli-Lubanski operator. The eigenvalues of the P^2 operator are the masses of the particles, whereas the eigenvalues of the W^2 operator are related to the spin of the particle. Therefore, an irreducible representation of the Poincaré group will be characterized by the mass and spin².

“Is it possible to extend the Poincaré group in order to combine it with internal symmetries of the particles in a non-trivial way?” was a very important question in the sixties. By internal symmetries we mean symmetry groups that affect the fields of the particles and not the spacetime. Well known examples of such symmetries are the $SU(2)$ isospin symmetry, and the $U(1)$ electromagnetism symmetry. The answer of that question was given by the famous no-go theorem by Coleman and Mandula [115], and was that the most general symmetry of the S matrix is the direct product of the Poincaré group times an internal symmetry group. That is, the combination of these two groups of symmetries are trivial. However, the proof contained a loophole [179]; it was based on the fact that apart from the vector momentum operator P^μ , and the antisymmetric tensor angular momentum operator $M^{\mu\nu}$, any other conserved operator must be Lorenz scalar. Supersymmetry is considered as the possible loophole of this theorem, since it contains additional generators that are not Lorenz scalars, but spinors. The possibility of unifying the Poincaré group with the internal symmetries arose when we allowed for such anticommuting operators. Now, we go directly, and briefly, into the construction of the supersymmetry.

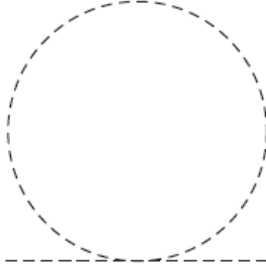
SM Fine-Tuning and Hierarchy Problems

(a) Tree-Level Fine-Tuning

The adhoc wrong -ve sign in the mass term $-\mu^2$ of the Higgs potential $V(\phi)$ is essential

²Note that, particles are represented by the irreducible representations.

Figure 1.1: One-loop self-energy graph in ϕ^4 theory [31, 147, 255]



for spontaneous symmetry breaking (SSB), where

$$V(\phi) = -\mu^2 \phi^\dagger \phi + \frac{\lambda}{4} (\phi^\dagger \phi)^2, \quad \phi = \begin{pmatrix} \phi^+ \\ \phi^0 \end{pmatrix}, \quad (\mu^2, \lambda > 0). \quad (1.1.6)$$

Moreover, μ^2 is not protected by any symmetry, $\mu^2 \rightarrow 0$ doesn't increase the symmetry of the SM, and it can be set to have any value. We have only one parameter v , the vev of the Higgs field, which defines the scale of the theory, where

$$\Re \phi^0 = \frac{h + v}{\sqrt{2}}, \quad |\langle \phi^0 \rangle_0| = \frac{v}{\sqrt{2}}, \quad v = \frac{2\mu}{\sqrt{\lambda}} \approx 246 \text{ GeV}. \quad (1.1.7)$$

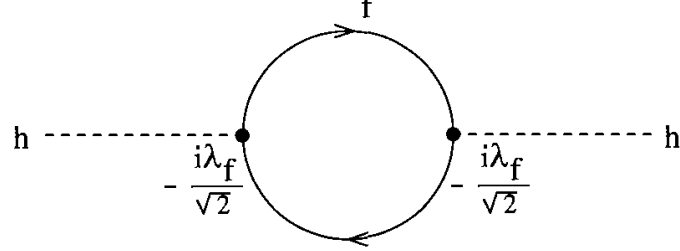
v sets the masses of all particles in the SM, however, it is adjustable.

(b) Loop-Level Fine-Tuning and Hierarchy Problem

The SM is renormalizable but regarded as an effective theory which is valid up to a finite, however high, cut-off scale $\Lambda \sim M_P \approx 10^{19}$ GeV. The 4-boson self-interaction $\frac{\lambda}{4} (\phi^\dagger \phi)^2$ in (1.1.6) generates, at one-loop order, a contribution to the Higgs mass term $-\mu^2 \phi^\dagger \phi$ in (1.1.6). The corresponding self-energy diagram is illustrated in Fig. 1.1. It produces the following positive correction to the Higgs mass term

$$(\lambda \int^\Lambda \frac{d^4 k}{(2\pi)^4} \frac{1}{k^2 - m_h^2} \sim \lambda \Lambda^2) \phi^\dagger \phi. \quad (1.1.8)$$

Figure 1.2: Fermionic loop contribution to the scalar two point function [31, 147, 255]



A Yukawa coupling of a generic matter fermion field f to the Higgs filed is

$$\mathcal{L}_{\bar{f}f\phi} = -\lambda_f \bar{f}_L \phi f_R + h.c. = -\frac{\lambda_f}{\sqrt{2}} h \bar{f} f - \frac{\lambda_f v}{\sqrt{2}} \bar{f} f. \quad (1.1.9)$$

The self-energy fermion loop generated by (1.1.9) is illustrated in Fig. 1.2 and generates a negative contribution to the Higgs mass term in (1.1.6)

$$(-2\lambda_f^2) \int^\Lambda \frac{d^4 k}{(2\pi)^4} \frac{k^2 + m_f^2}{(k^2 - m_f^2)^2} \sim -2\lambda_f^2 \Lambda^2 + \mathcal{O}(\lambda_f^2 m_f^2 / 8\pi) \phi^\dagger \phi. \quad (1.1.10)$$

The two quadratically divergent contributions in (1.1.8) and (1.1.10) together have the form

$$(\lambda - 2\lambda_f^2) \Lambda^2 \phi^\dagger \phi. \quad (1.1.11)$$

Relevant one-loop radiative corrections to the Higgs mass, from gauge bosons, Higgs self-coupling and fermions, give (Veltman [305])

$$\delta m_h^2 = \frac{3\Lambda^2}{16\pi^2 v^2} (m_h^2 + 2m_W^2 + m_Z^2 - 4m_t^2) + \mathcal{O}\left(\frac{\lambda_f^2 m_f^2}{8\pi}\right). \quad (1.1.12)$$

Despite one could renormalize such quadratic divergences away, the legacy of their severity would still remain. In the SM, residual finite correction $\mathcal{O}(\lambda_f^2 m_f^2 / 8\pi)$ in (1.1.10) would be managably small for t-quark. In Grand Unification Theoreies (GUTs), such a leading fermion contribution, with m_f expected to be $\mathcal{O}(M_{\text{GUT}})$, causes the loop correction to the scalar mass squared to be $\mathcal{O}(M_{\text{GUT}}^2)$.

SUSY motivations

SM Problems [31, 147, 255]: The bare coefficient μ^2 of $\phi^\dagger\phi$ in (1.1.6) is then replaced by the one-loop corrected physical value such that the scalar mass at the one-loop is

$$m_h^2 = 2\mu^2 - \delta m_h^2. \quad (1.1.13)$$

One would have to do an unnatural amount of fine tuning between the bare scalar mass squared μ^2 and the renormalization δm_h^2 in order to keep the renormalized mass squared (1.1.13) to be $\mathcal{O}(\text{GeV})$. For this possible solutions arise with composite Higgs models [292], supersymmetry [179, 305, 310], and models with extra dimensions [274, 280].

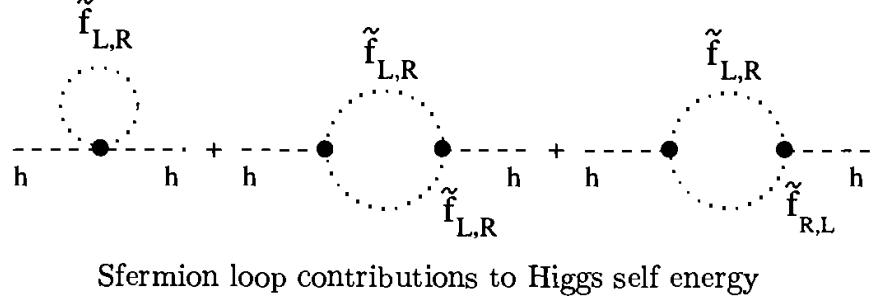
SUSY Naturalness and Nonrenormalization

In QED, both gauge and chiral symmetries guarantees both masslessness of the photon and smallness of the electron mass, respectively ('t Hooft [294]). SUSY is a spacetime symmetry which groups scalar particles with either massless fermions or massless vector bosons. Then the scalars would enjoy the same protection from divergences as their symmetry partners. In SUSY, the existence of sparticle superpartners with masses near the weak scale, cures the problem of quadratic divergences through cancellations between fermionic and bosonic loops. Loops induced by other scalar fields, contributing to the Higgs two point function, can also be considered. SUSY introduces two additional complex scalar (“sfermion”) fields \tilde{f}_L , \tilde{f}_R with the following coupling to the Higgs field:

$$\begin{aligned} \mathcal{L}_{\tilde{f}\tilde{f}\phi} &= \tilde{\lambda}_f |\phi|^2 (|\tilde{f}_L|^2 + |\tilde{f}_R|^2) + (\lambda_f A_f \phi \tilde{f}_L \tilde{f}_R^* + h.c.) \\ &\supset \tilde{\lambda}_f \left(\frac{1}{2} h^2 + v h \right) (|\tilde{f}_L|^2 + |\tilde{f}_R|^2) + \frac{h}{\sqrt{2}} (\lambda_f A_f \tilde{f}_L \tilde{f}_R^* + h.c.). \end{aligned} \quad (1.1.14)$$

(1.1.14) makes the following additional contribution to the Higgs two point function

Figure 1.3: Sfermion loop contributions to Higgs self energy [31, 147, 255]



via the loops of Fig. 1.3

$$\begin{aligned}
 & -\tilde{\lambda}_f \int \frac{d^4 k}{(2\pi)^4} \left(\frac{1}{k^2 - m_{\tilde{f}_L}^2} + \frac{1}{k^2 - m_{\tilde{f}_R}^2} \right) \\
 & + (\tilde{\lambda}_f v)^2 \int \frac{d^4 k}{(2\pi)^4} \left(\frac{1}{(k^2 - m_{\tilde{f}_L}^2)^2} + \frac{1}{(k^2 - m_{\tilde{f}_R}^2)^2} \right) \\
 & + |\lambda_f A_f|^2 \int \frac{d^4 k}{(2\pi)^4} \frac{1}{k^2 - m_{\tilde{f}_L}^2} \frac{1}{k^2 - m_{\tilde{f}_R}^2}. \tag{1.1.15}
 \end{aligned}$$

SUSY cancels the quadratic divergence in the first term in (1.1.15) with that in the fermionic contribution (1.1.10) by enforcing the following coupling constant equality:

$$\tilde{\lambda}_f = -\lambda_f^2. \tag{1.1.16}$$

Moreover, we have the choice $m_{\tilde{f}_L} = m_{\tilde{f}_R} = m_{\tilde{f}}$. The sum of the scalar and fermionic contributions to the Higgs two point function with the choices (1.1.16) and the one after is

$$\begin{aligned}
 & i \frac{\lambda_f^2}{16\pi^2} \left[-2m_f^2 \left(1 - \ln \frac{m_f^2}{\mu^2} \right) + 4m_f^2 \ln \frac{m_f^2}{\mu^2} \right. \\
 & \left. + 2m_{\tilde{f}}^2 \left(1 - \ln \frac{m_{\tilde{f}}^2}{\mu^2} \right) - 4m_{\tilde{f}}^2 \ln \frac{m_{\tilde{f}}^2}{\mu^2} - |A_f|^2 \ln \frac{m_{\tilde{f}}^2}{\mu^2} \right]. \tag{1.1.17}
 \end{aligned}$$

For exact SUSY, $m_f = m_{\tilde{f}}$ and $A_f = 0$ and (1.1.17) vanishes identically. The above results holds in all perturbation orders as a consequence of the **nonrenormalization**

theorem valid in supersymmetric theories. The **naturalness** aspect is also made clear by the introduction of a certain kind of small supersymmetry breaking

$$\delta_f^2 = m_{\tilde{f}}^2 - m_f^2; \quad \delta_f, A_f \ll m_f, \quad \forall f. \quad (1.1.18)$$

Approximately, the one loop renormalization of the Higgs self energy is linearly proportional to the small SUSY breaking parameters δ_f^2 and $|A_f|^2$, restricting the correction to one of modest magnitude, though m_f may be quite large:

$$-i \frac{\lambda_f^2}{16\pi^2} \left[4\delta_f^2 + (2\delta_f^2 + |A_f|^2) \ln \frac{m_f^2}{\mu^2} \right] + \mathcal{O}(\delta_f^4, \delta^2 |A_f|^2). \quad (1.1.19)$$

Conclusion: The introduction of the superpartners \tilde{f}_L, \tilde{f}_R with the interactions of (1.1.14) has served two purposes:

- 1.1.1. the quadratic divergence in the scalar self energy is cancelled;
- 1.1.2. the scalar mass is shielded from large loop corrections involving heavy particles so long as the mass splitting between the heavy fermion and boson superpartners is itself of the order of the scalar mass.

The same conclusions follow if loop contributions from gauge bosons and their superpartners are combined or Higgs bosons and their superpartners are added together.

1.1.2 Spinors

The first step to study SUSY is to become a professional in spinors (specially, Weyl spinors) terminology. In this subsection, we work out some identities which are useful to work in supersymmetric theories.

Weyl Spinors

A Weyl spinor is, by definition, a two complex component spinor

$$\psi = \begin{pmatrix} \psi_1 \\ \psi_2 \end{pmatrix}, \quad (1.1.20)$$

that transforms under any element $M \in SL(2, C)$, (*i.e.*, M is a 2×2 complex matrix such that $\det M = 1$) as follows:

$$\psi_\alpha \rightarrow \psi'_\alpha = M_\alpha^\beta \psi_\beta, \quad (1.1.21)$$

where $\alpha, \beta \in \{1, 2\}$. Also we can define another type of Weyl spinors to be a two complex component spinor

$$\bar{\psi} = \begin{pmatrix} \psi^1 \\ \psi^2 \end{pmatrix}, \quad (1.1.22)$$

that transforms under M^* as

$$\bar{\psi}^{\dot{\alpha}} \rightarrow \bar{\psi}'^{\dot{\alpha}} = (M^*)^{\dot{\alpha}}_{\dot{\beta}} \bar{\psi}^{\dot{\beta}}. \quad (1.1.23)$$

where $\dot{\alpha}, \dot{\beta} \in \{1, 2\}$. Sometimes we call the undotted spinors ψ_α *left-handed Weyl spinors*, whereas, the dotted spinors $\bar{\psi}_{\dot{\alpha}}$ are called *right-handed Weyl spinors*.

Now define the antisymmetric two index symbols,

$$\varepsilon^{\alpha\beta} := \varepsilon^{\dot{\alpha}\dot{\beta}} := \begin{pmatrix} 0 & 1 \\ -1 & 0 \end{pmatrix}, \quad \varepsilon_{\alpha\beta} := \varepsilon_{\dot{\alpha}\dot{\beta}} := \begin{pmatrix} 0 & -1 \\ 1 & 0 \end{pmatrix}. \quad (1.1.24)$$

These objects usage is to raise or lower the Weyl spinors indices as follows

$$\psi^\alpha = \varepsilon^{\alpha\beta} \psi_\beta, \quad \psi_\alpha = \varepsilon_{\alpha\beta} \psi^\beta, \quad (1.1.25)$$

$$\bar{\psi}^{\dot{\alpha}} = \varepsilon^{\dot{\alpha}\dot{\beta}} \bar{\psi}_{\dot{\beta}}, \quad \bar{\psi}_{\dot{\alpha}} = \varepsilon_{\dot{\alpha}\dot{\beta}} \bar{\psi}^{\dot{\beta}}. \quad (1.1.26)$$

It is worth noting that

$$\varepsilon_{\alpha\beta} \varepsilon^{\beta\gamma} = \delta_\alpha^\gamma \quad \text{and} \quad \varepsilon_{\dot{\alpha}\dot{\beta}} \varepsilon^{\dot{\beta}\dot{\gamma}} = \delta_{\dot{\alpha}}^{\dot{\gamma}}.$$

Since these spinors anticommute, $\psi_1 \chi_2 = -\chi_2 \psi_1$ and $\psi_1 \bar{\chi}_2 = -\bar{\chi}_2 \psi_1$, the scalar products $\psi\chi$ and $\bar{\psi}\bar{\chi}$ must be carefully defined as

$$\psi\chi = \psi^\alpha \chi_\alpha = \varepsilon^{\alpha\beta} \psi_\beta \chi_\alpha = -\varepsilon^{\alpha\beta} \chi_\alpha \psi_\beta = \varepsilon^{\beta\alpha} \chi_\alpha \psi_\beta = \chi^\beta \psi_\beta = \chi\psi, \quad (1.1.27)$$

$$\bar{\psi}\bar{\chi} = \bar{\psi}_{\dot{\alpha}}\bar{\chi}^{\dot{\alpha}} = \varepsilon_{\dot{\alpha}\dot{\beta}}\bar{\psi}^{\dot{\beta}}\bar{\chi}^{\dot{\alpha}} = -\varepsilon_{\dot{\alpha}\dot{\beta}}\bar{\chi}^{\dot{\alpha}}\bar{\psi}^{\dot{\beta}} = \varepsilon_{\dot{\beta}\dot{\alpha}}\bar{\chi}^{\dot{\alpha}}\bar{\psi}^{\dot{\beta}} = \bar{\chi}_{\dot{\beta}}\bar{\psi}^{\dot{\beta}} = \bar{\chi}\bar{\psi}, \quad (1.1.28)$$

$$(\chi\psi)^\dagger = (\chi^\alpha\psi_\alpha)^\dagger = \bar{\psi}_{\dot{\alpha}}\bar{\chi}^{\dot{\alpha}} = \bar{\psi}\bar{\chi} = \bar{\chi}\bar{\psi}. \quad (1.1.29)$$

The σ_μ matrices are defined to have a dotted index as well as an undotted index

$$(\sigma^\mu)_{\alpha\dot{\alpha}} := (1, \sigma_i)_{\alpha\dot{\alpha}}. \quad (1.1.30)$$

The raised indices σ -matrices are defined by using the ε -symbols

$$(\bar{\sigma}^\mu)^{\dot{\alpha}\alpha} = \varepsilon^{\dot{\alpha}\dot{\beta}}\varepsilon^{\alpha\beta}(\sigma^\mu)_{\beta\dot{\beta}} = (1, -\sigma_i)^{\dot{\alpha}\alpha}. \quad (1.1.31)$$

The hermiticity of σ^μ matrices implies that

$$(\sigma_{\alpha\dot{\alpha}}^\mu)^* = (\sigma^{\mu*})_{\dot{\alpha}\alpha} = (\sigma^{\mu\dagger})_{\alpha\dot{\alpha}} = (\sigma^\mu)_{\alpha\dot{\alpha}}. \quad (1.1.32)$$

Therefore, the vector representation under Lorentz group can be written in terms of Weyl spinors as $V^\mu = \psi^\alpha\sigma_{\alpha\dot{\alpha}}^\mu\bar{\psi}^{\dot{\alpha}}$.

Dirac Spinors

A Dirac spinor is a four-component spinor constructed by using the two types of the Weyl spinors

$$\Psi = \begin{pmatrix} \psi_\alpha \\ \bar{\chi}^{\dot{\alpha}} \end{pmatrix}. \quad (1.1.33)$$

Also, to work with the Dirac spinor notations, one should introduce the Dirac matrices instead of the Pauli matrices. Dirac matrices can be formulated in terms of Pauli matrices as follows

$$\gamma^\mu = \begin{pmatrix} 0 & \sigma^\mu \\ \bar{\sigma}^\mu & 0 \end{pmatrix}, \quad \gamma_5 = i\gamma^0\gamma^1\gamma^2\gamma^3 = \begin{pmatrix} -1 & 0 \\ 0 & 1 \end{pmatrix} \quad (1.1.34)$$

Both chiralities are contained in one Dirac spinor. The chirality eigenstates are

$$\Psi_L = \frac{1 - \gamma_5}{2}\Psi = \begin{pmatrix} \psi_\alpha \\ 0 \end{pmatrix}, \quad \Psi_R = \frac{1 + \gamma_5}{2}\Psi = \begin{pmatrix} 0 \\ \bar{\chi}^{\dot{\alpha}} \end{pmatrix} \quad (1.1.35)$$

Majorana Spinors

The charge conjugation matrix C is defined to be

$$C := i\gamma^0\gamma^2, \quad (1.1.36)$$

and the charge conjugated spinor definition is

$$\Psi^c = C\bar{\Psi}^T. \quad (1.1.37)$$

If the Dirac spinor Ψ describes a particle, then Ψ^c describes its antiparticle. In two components formulation,

$$\Psi = \begin{pmatrix} \psi_\alpha \\ \bar{\chi}^\dot{\alpha} \end{pmatrix} \quad \longrightarrow \quad \Psi^c = \begin{pmatrix} \chi_\alpha \\ \bar{\psi}^\dot{\alpha} \end{pmatrix}. \quad (1.1.38)$$

A Dirac spinor $\Psi = \begin{pmatrix} \psi_\alpha \\ \bar{\chi}^\dot{\alpha} \end{pmatrix}$ is said to be a Majorana spinor iff $\psi \equiv \chi$, *i.e.*, it is of the form

$$\Psi_M = \begin{pmatrix} \psi_\alpha \\ \bar{\psi}^\dot{\alpha} \end{pmatrix}. \quad (1.1.39)$$

Therefore, a Majorana spinor can be define as the two degrees of freedom, four component spinor that is equal to its charge conjugated spinor

$$\Psi_M^c = \Psi_M. \quad (1.1.40)$$

1.1.3 Algebra and Supermultiplets

For a spinor quantity SUSY generator Q , the SUSY Algebra is given by [31, 147, 255]

$$\{Q_a, Q_b^\dagger\} = (\sigma^\mu)_{ab} P_\mu, \quad (1.1.41)$$

$$\{Q_a, Q_b\} = \{Q_a^\dagger, Q_b^\dagger\} = 0, \quad (1.1.42)$$

$$[Q_a, P_\mu] = [Q_a^\dagger, P_\mu] = 0. \quad (1.1.43)$$

A supermultiplet contains states which are connected to each other by the action of the SUSY generators. From (1.1.43), the Casimir operator P^2 commutes with all the generators Q_a, Q_a^\dagger

$$[Q_a, P^2] = [Q_a^\dagger, P^2] = 0. \quad (1.1.44)$$

This means physically that states in a supermultiplet must be degenerate in mass (and, more generally, have the same 4-momentum). The same holds for internal symmetry generators and therefore all internal quantum numbers are also invariant within a supermultiplet. Both Q_1, Q_2^\dagger are lowering operators and Q_1^\dagger, Q_2 are raising operators by $\frac{1}{2}$ in the spectrum of the third angular momentum component J_3

$$[J_3, Q_1] = -\frac{1}{2}Q_1, \quad [J_3, Q_1^\dagger] = \frac{1}{2}Q_1^\dagger, \quad (1.1.45)$$

$$[J_3, Q_2] = \frac{1}{2}Q_2, \quad [J_3, Q_2^\dagger] = -\frac{1}{2}Q_2^\dagger. \quad (1.1.46)$$

There are two states in a supermultiplet of massless particles, one with helicity $\pm|j|$ and the other with helicity $\pm|j - \frac{1}{2}|$. A left chiral supermultiplet ($j = \frac{1}{2}$) consisting of the two states containing a massless LH spin- $\frac{1}{2}$ state and a massless scalar state. A right chiral supermultiplet ($j = \frac{1}{2}$) consisting of the two states containing a massless RH spin- $\frac{1}{2}$ state and a massless scalar state. A vector, or gauge supermultiplet ($j = 1$), consists of a massless spin-1 state with a massless LH spin- $\frac{1}{2}$ state. Formally, we enlarge the space of coordinates x^μ to include also fermionic (spinor) degrees of freedom (DoF) θ and θ^* in the ‘superspace’. Accordingly, ‘superfields’ defined on superspace depend on spinorial DoF θ and θ^* as well as on x , and the extended space of x^μ, θ and θ^* is called superspace. The most general form of superfield is expanded in terms of the superspace variables as follows

$$\begin{aligned} \mathcal{F}(x, \theta, \bar{\theta}) &= f(x) + \sqrt{2}\theta\xi(x) + \sqrt{2}\bar{\theta}\bar{\chi}(x) + \theta^2M(x) + \bar{\theta}^2N(x) \\ &\quad + \theta\sigma^\mu\bar{\theta}A_\mu + \theta^2\bar{\theta}\bar{\lambda} + \theta\bar{\theta}^2\zeta(x) + \frac{1}{2}\theta^2\bar{\theta}^2D(x). \end{aligned} \quad (1.1.47)$$

1.1 SUPERSYMMETRY

Figure 1.4: Different supermultiplets of massless particles [147].

j_0	Name	Helicities	States	Particles	Degrees of freedom
$\frac{1}{2}$	Chiral supermultiplet(s)	$-\frac{1}{2}$ or $\frac{1}{2}$	$1+1$	1 spin 1/2 complex chiral fermion + 1 complex scalar	2
		0	$1+1$		2
1	Gauge supermultiplet	-1	1	1 spin one gauge boson +	2
		1	1	1 spin 1/2 Majorana gaugino	
		$-\frac{1}{2}$	1		
		$\frac{1}{2}$	1		2
2	$N = 1$ supergravity multiplet	-2	1	1 spin two graviton	2
		2	1	+ 1 spin 3/2 Majorana gravitino	
		$-\frac{3}{2}$	1		
		$\frac{3}{2}$	1		2

Different supermultiplets of massless particles.

The fields $f(x), M(x), N(x), D(x)$ are scalars. The field A_μ is a vector. The fields $\xi(x), \zeta(x)$ are left handed spinor fields and the fields $\bar{\chi}, \bar{\lambda}$ are right handed spinor fields. A general superfield constitute a reducible SUSY representation. SUSY transforms the **D -term** of Φ into itself plus a spacetime derivative. Hence, such a term in the Lagrangian density leads to a supersymmetry invariant action when surface terms can be discarded. A SUSY transformation element can be written in the form

$$U(x, \theta, \bar{\theta}) = e^{ix \cdot P} e^{i\theta \cdot Q} e^{i\bar{\theta} \cdot \bar{Q}}. \quad (1.1.48)$$

The product $U(a, \xi, \bar{\xi})U(x, \theta, \bar{\theta})$ induces the transformations

$$\theta' = \theta + \xi, \quad \bar{\theta}' = \bar{\theta} + \bar{\xi}, \quad x'^\mu = x^\mu + a^\mu - i\theta\sigma^\mu\bar{\xi}. \quad (1.1.49)$$

Thus the chiral covariant derivatives

$$\mathcal{D}_a = \partial_a - i\sigma_{ab}^\mu \bar{\theta}^b \partial_\mu, \quad \bar{\mathcal{D}}^a = \bar{\partial}^a - i\bar{\sigma}^{\mu ab} \theta_b \partial_\mu \quad (1.1.50)$$

have covariant supersymmetric transformations.

1.1.4 Superfields and Superpotential

Chiral and Antichiral Superfields

Chiral and antichiral superfields are irreducible susy representations which contains propagating complex scalar and two-component spinor. Chiral and antichiral superfields Φ and its conjugate Φ^\dagger are defined to satisfy the constraints

$$\bar{\mathcal{D}}^a \Phi = 0, \quad \mathcal{D}^a \Phi^\dagger = 0. \quad (1.1.51)$$

They have component expansions

$$\begin{aligned} \Phi(x, \theta, \bar{\theta}) &= \phi(x) + \sqrt{2}\theta\psi(x) + \theta^2 F(x) - i\theta\sigma^\mu\bar{\theta}\partial_\mu\phi(x) \\ &\quad - \frac{1}{4}\theta^2\bar{\theta}^2\partial^\mu\partial_\mu\phi(x) + \frac{i}{\sqrt{2}}\theta^2\partial_\mu\psi(x)\sigma^\mu\bar{\theta}, \end{aligned} \quad (1.1.52)$$

$$\begin{aligned} \Phi^\dagger(x, \theta, \bar{\theta}) &= \phi^\dagger(x) + \sqrt{2}\bar{\theta}\bar{\psi}(x) + \bar{\theta}^2 F^\dagger(x) + i\theta\sigma^\mu\bar{\theta}\partial_\mu\phi^\dagger(x) \\ &\quad - \frac{1}{4}\theta^2\bar{\theta}^2\partial^\mu\partial_\mu\phi^\dagger(x) - \frac{i}{\sqrt{2}}\bar{\theta}^2\theta\sigma^\mu\partial_\mu\bar{\psi}(x). \end{aligned} \quad (1.1.53)$$

Products of any number of chiral (antichiral) superfields is again a chiral (antichiral) superfield. SUSY transforms the ***F-term*** of Φ into itself plus a spacetime derivative. Hence, such a term in the Lagrangian density leads to a supersymmetry invariant action when surface terms can be discarded.

$$\Phi_i \Phi_j|_{\theta^2} = \phi_i F_j + \phi_j F_i - \psi_i \psi_j, \quad (1.1.54)$$

$$\begin{aligned} \Phi_i \Phi_j \Phi_k|_{\theta^2} &= F_i \phi_j \phi_k + F_j \phi_k \phi_i + F_k \phi_i \phi_j \\ &\quad - \psi_i \psi_j \phi_k - \psi_j \psi_k \phi_i - \psi_k \psi_i \phi_j. \end{aligned} \quad (1.1.55)$$

Superpotential

In SUSY, superpotential describe the nongauge interactions, and is defined by

$$W(\Phi) = h_i \Phi_i + \frac{1}{2} m_{ij} \Phi_i \Phi_j + \frac{1}{6} y_{ijk} \Phi_i \Phi_j \Phi_k. \quad (1.1.56)$$

This gives the F -term part of the Lagrangian

$$\mathcal{L}_{F,\text{chiral}} = W(\Phi)|_{\theta^2} + \bar{W}(\bar{\Phi})|_{\bar{\theta}^2} \quad (1.1.57)$$

$$= (h_k + m_{ik}\phi_i + \frac{1}{2}y_{ijk}\phi_i\phi_j)F_k - \frac{1}{2}\psi_i\psi_j(m_{ij} + y_{ijk}\phi_k) + h.c. \quad (1.1.58)$$

Products of a chiral superfield with antichiral superfield is neither. But

$$\Phi_i^\dagger\Phi_j|_{\theta^2\bar{\theta}^2} = F_i^\dagger F_j + \frac{1}{2}\partial_\mu\phi_i^\dagger\overleftrightarrow{\partial^\mu}\phi_j - \frac{1}{2}\phi_i^\dagger\overleftrightarrow{\partial_\mu}\partial^\mu\phi_j + i\psi_j\sigma^\mu\overleftrightarrow{\partial_\mu}\bar{\psi}_i. \quad (1.1.59)$$

Kähler potential

On the other hand, Kähler potential contains kinetic terms of scalar fields and their fermioninc superpartners. For chiral sufeields

$$K_{\text{chiral}}(\Phi_i^\dagger, \Phi_j) = \Phi_i^\dagger\Phi_j. \quad (1.1.60)$$

This gives the D -term of the chiral superfields

$$\mathcal{L}_{D,\text{chiral}} = K_{\text{chiral}}(\Phi_i^\dagger, \Phi_j)|_{\theta^2\bar{\theta}^2}. = i\psi_i\sigma^\mu\overleftrightarrow{\partial_\mu}\bar{\psi}_i + \partial_\mu\phi_i^\dagger\partial^\mu\phi_i + F_i^\dagger F_i. \quad (1.1.61)$$

The most general supersymmetric two-derivative Lagrangian involving only chiral supermultiplets Φ_i can then be written as

$$\mathcal{L}_{\text{chiral}} = \mathcal{L}_{D,\text{chiral}} + \mathcal{L}_{F,\text{chiral}} = K_{\text{chiral}}(\Phi_i^\dagger, \Phi_j)|_{\theta^2\bar{\theta}^2} + W(\Phi)|_{\theta^2} + \bar{W}(\bar{\Phi})|_{\bar{\theta}^2}. \quad (1.1.62)$$

The Kähler potential K is a real function of the chiral superfields and their conjugates. The superpotential W is a holomorphic function of the chiral superfields only. The Lagrangian \mathcal{L} describes a renormalizable field theory if and only if K is quadratic and W is at most cubic. The auxiliary F field can be fixed by the EoM as follows [31, 147, 255]:

$$\frac{\partial\mathcal{L}_{\text{chiral}}}{\partial F_i} = 0, \quad (1.1.63)$$

which gives

$$F_i^\dagger = -W_i(\phi) = -\frac{\partial W}{\partial\Phi_i}|_{\theta=0=\bar{\theta}} = -h_i - m_{ij}\phi_j - \frac{1}{2}y_{ijk}\phi_j\phi_k. \quad (1.1.64)$$

Substituting in (1.1.58), (1.1.61) and (1.1.62), we get

$$\mathcal{L}_{\text{chiral}} = i\psi_i \sigma^\mu \overleftrightarrow{\partial}_\mu \bar{\psi}_i + \partial_\mu \phi_i^\dagger \partial^\mu \phi_i - \left(\frac{1}{2} \psi_i \psi_j W_{ij} + h.c. \right) - V(\phi^\dagger, \phi). \quad (1.1.65)$$

The scalar potential is

$$V(\phi^\dagger, \phi) = |W_i(\phi)|^2 = F_i^\dagger F_i = |h_k + m_{ik}\phi_i + \frac{1}{2}y_{ijk}\phi_i\phi_j|^2. \quad (1.1.66)$$

The double superfield derivative $W_{ij}(\phi)$ of the superpotential evaluated with nonzero scalar fields only, contains both the fermion mass terms and the Yukawa interaction terms

$$W_{ij}(\phi) = \frac{\partial W}{\partial \Phi_i \partial \Phi_j}|_{\theta=0=\bar{\theta}} = m_{ij} + y_{ijk}\phi_k. \quad (1.1.67)$$

The Yukawa potential is

$$\mathcal{L}_{\text{Yukawa}} = -\frac{1}{2}(\psi_i \psi_j W_{ij} + h.c.) = -\frac{1}{2}\psi_i \psi_j (m_{ij} + y_{ijk}\phi_k) + h.c. \quad (1.1.68)$$

Real Superfields

Real Superfields satisfy the constraint $V^\dagger = V$. They contain the DoF for a gauge field and its gaugino superpartner. Super-gauge transformations (Wess-Zumino gauge) can be used to bring its component expansion into the form [147, 281]

$$V(x, \theta, \bar{\theta}) = \theta \sigma^\mu \bar{\theta} A_\mu + i\theta^2 \bar{\theta} \lambda^\dagger - i\bar{\theta}^2 \theta \lambda + \frac{1}{2}\theta^2 \bar{\theta}^2 D(x). \quad (1.1.69)$$

We define the chiral superfields [147]

$$W_A = -\frac{1}{4}\bar{\mathcal{D}}^2 \mathcal{D}_A V, \quad W_{\dot{A}} = -\frac{1}{4}\mathcal{D}^2 \bar{\mathcal{D}}_{\dot{A}} V. \quad (1.1.70)$$

Expanding the superfield W^a in terms of its components

$$W_A = \lambda_A + \theta_A D - (\sigma^{\mu\nu}\theta)_A F_{\mu\nu} + i\theta^2 \sigma_{A\dot{B}}^\mu \partial_\mu \bar{\lambda}^{\dot{B}}. \quad (1.1.71)$$

Again, from the products of chiral superfields, we extract the F -terms to obtain the free gauge and gaugino part of the Lagrangian

$$\mathcal{L}_{F,\text{gauge}} = \frac{1}{4}\{W^A W_A|_{\theta^2} + h.c.\} = \frac{1}{2}D^2 - \frac{1}{4}F^{\mu\nu}F_{\mu\nu} + i\lambda\sigma^\mu \overleftrightarrow{\partial}_\mu \lambda. \quad (1.1.72)$$

The F -term of the Lagrangian containing gauge and chiral superfields

$$\mathcal{L}_F = \mathcal{L}_{F,\text{chiral}} + \mathcal{L}_{F,\text{gauge}}. \quad (1.1.73)$$

Abelian Gauge Interactions

The Kähler potential (1.1.60) is not invariant under the supergauge transformations

$$\Phi'_i = e^{-2igt_i\Lambda} \Phi_i, \quad \Phi'^{\dagger}_i = \Phi^{\dagger}_i e^{2igt_i\Lambda^{\dagger}}; \quad (\mathcal{D}_A \Lambda^{\dagger} = 0, \bar{\mathcal{D}}^{\dot{A}} \Lambda = 0). \quad (1.1.74)$$

Since $\Lambda^{\dagger} \neq \Lambda$, the kinetic energy D -term in (1.1.60) is not gauge invariant by itself. This is rectified by introducing a gauge vector superfield V with the gauge transformation

$$V' = V + i(\Lambda - \Lambda^{\dagger}), \quad (1.1.75)$$

and by generalizing the kinetic energy term to $\Phi_i^{\dagger} e^{2gq_i V} \Phi_i$. The vector superfield in (1.1.69) satisfies [147, 281]

$$V^2 = \frac{1}{2}\theta^2\bar{\theta}^2 A^{\mu}A_{\mu}, \quad V^n = 0, \quad \forall n \geq 3. \quad (1.1.76)$$

Therefore its exponential is given by [147, 281]

$$e^V - 1 = V + \frac{1}{2}V^2 = \theta\sigma^{\mu}\bar{\theta}A_{\mu} + i\theta^2\bar{\theta}\lambda^{\dagger} - i\bar{\theta}^2\theta\lambda + \frac{1}{2}\theta^2\bar{\theta}^2(D(x) + \frac{1}{2}A^{\mu}A_{\mu}). \quad (1.1.77)$$

Moreover, with chiral superfields [147, 281]

$$\begin{aligned} \Phi_i^{\dagger} V \Phi_j|_{\theta^2\bar{\theta}^2} &= \frac{1}{2}(D\phi_i^{\dagger}\phi_j - 2iA^{\mu}\phi_i^{\dagger}\overleftrightarrow{\partial}_{\mu}\phi_j - \bar{\psi}_i\bar{\sigma}^{\mu}\psi_j A_{\mu} \\ &\quad - \sqrt{2}\phi_j\bar{\lambda}\bar{\psi}_i - \sqrt{2}\phi_i^{\dagger}\lambda\psi_j), \end{aligned} \quad (1.1.78)$$

$$\Phi_i^{\dagger} V V' \Phi_j|_{\theta^2\bar{\theta}^2} = \frac{1}{2}A^{\mu}A'_{\mu}\phi_i^{\dagger}\phi_j. \quad (1.1.79)$$

We promote the Kähler potential (1.1.60) to

$$K(\Phi_i^{\dagger}, e^{2gq_j V} \Phi_j) = \Phi_i^{\dagger} e^{2gq_i V} \Phi_i = \Phi_i^{\dagger}(1 + 2gq_i V + 2(gq_i V)^2)\Phi_i. \quad (1.1.80)$$

The D -term of the Lagrangian containing gauge and chiral superfields

$$\mathcal{L}_{D,\text{gauge}} = K(\Phi_i^\dagger, (e^{gq_i V} - 1)\Phi_i)|_{\theta^2 \bar{\theta}^2} + \eta V|_{\theta^2 \bar{\theta}^2} \quad (1.1.81)$$

$$\begin{aligned} &= \eta D(x) + g^2 q_i^2 A^\mu A_\mu \phi_i^\dagger \phi_i + g q_i (D \phi_i^\dagger \phi_i - 2i A^\mu \phi_i^\dagger \overleftrightarrow{\partial}_\mu \phi_i \\ &\quad - \bar{\psi}_i \bar{\sigma}^\mu \psi_i A_\mu - \sqrt{2} \phi_i \bar{\lambda} \bar{\psi}_i - \sqrt{2} \phi_i^\dagger \lambda \psi_i). \end{aligned} \quad (1.1.82)$$

The D -term of the Lagrangian containing gauge and chiral superfields

$$\mathcal{L}_D = \mathcal{L}_{D,\text{chiral}} + \mathcal{L}_{D,\text{gauge}} = K(\Phi_i^\dagger, e^{gq_i V} \Phi_i)|_{\theta^2 \bar{\theta}^2} + \eta V|_{\theta^2 \bar{\theta}^2}. \quad (1.1.83)$$

The most general supersymmetric two-derivative Lagrangian involving gauge and chiral supermultiplets can then be written as

$$\mathcal{L}_{\text{gauge}} = \mathcal{L}_{D,\text{gauge}} + \mathcal{L}_{F,\text{gauge}}. \quad (1.1.84)$$

The auxiliary D field can be fixed by the EoM as follows [31, 147, 255]:

$$\frac{\partial \mathcal{L}_{\text{gauge}}}{\partial D} = 0 \quad \rightarrow \quad D = -g q_i \phi_i^\dagger \phi_i - \eta. \quad (1.1.85)$$

Substituting in (1.1.84), we obtain

$$\begin{aligned} \mathcal{L}_{\text{gauge}} &= -\frac{1}{2} D^2 - \frac{1}{4} F^{\mu\nu} F_{\mu\nu} + i \lambda \sigma^\mu \overleftrightarrow{\partial}_\mu \lambda + g^2 q_i^2 A^\mu A_\mu \phi_i^\dagger \phi_i \\ &\quad + g q_i (-2i A^\mu \phi_i^\dagger \overleftrightarrow{\partial}_\mu \phi_i - \bar{\psi}_i \bar{\sigma}^\mu \psi_i A_\mu - \sqrt{2} \phi_i \bar{\lambda} \bar{\psi}_i - \sqrt{2} \phi_i^\dagger \lambda \psi_i). \end{aligned} \quad (1.1.86)$$

The total Lagrangian for a supersymmetric abelian gauge theory coupled to chiral superfields can be written as the sum of both (1.1.65) and (1.1.86)

$$\begin{aligned} \mathcal{L} &= \mathcal{L}_{\text{chiral}} + \mathcal{L}_{\text{gauge}} \\ &= i \psi_i \sigma^\mu D_\mu \bar{\psi}_i + |D_\mu \phi_i|^2 - \frac{1}{4} F^{\mu\nu} F_{\mu\nu} + i \lambda \sigma^\mu \overleftrightarrow{\partial}_\mu \lambda \\ &\quad - \sqrt{2} g q_i (\phi_i \bar{\lambda} \bar{\psi}_i + h.c.) + \mathcal{L}_{\text{Yukawa}} - V(\phi^\dagger, \phi), \end{aligned} \quad (1.1.87)$$

where the covariant derivative is $D_\mu = \partial_\mu + ig q_i A_\mu$ and the Yukawa potential as (1.1.68). The scalar potential (1.1.66) was generalized in (1.1.87) to

$$V(\phi^\dagger, \phi) = F_i^\dagger F_i + \frac{1}{2} D^2 = |h_k + m_{ik} \phi_i + \frac{1}{2} y_{ijk} \phi_i \phi_j|^2 + (g q_i \phi_i^\dagger \phi_i + \eta)^2. \quad (1.1.88)$$

The supersymmetric gaugino-scalar-chiral fermion (g-s-cf) interaction respectively is

$$\mathcal{L}_{g-s-cf} = -\sqrt{2}gq_i(\phi_i\bar{\lambda}\bar{\psi}_i + h.c.). \quad (1.1.89)$$

Non-Abelian Gauge Interactions

The Kähler potential (1.1.60) is not invariant under the supergauge transformations

$$\Phi'_i = e^{-2ig\Lambda^a T^a} \Phi_i, \quad \Phi'^\dagger_i = \Phi^\dagger_i e^{2ig\Lambda^{a\dagger} T^a}; \quad (\mathcal{D}_\Lambda^\dagger = 0, \bar{\mathcal{D}}^{\dot{a}} \Lambda = 0). \quad (1.1.90)$$

where $\Lambda^a \equiv \Lambda^a(x^\mu, \theta, \bar{\theta})$ are the gauge complex chiral superfunctions. Also, T^a 's are the hermitian generators of the nonabelian gauge group G . Thus

$$[T^a, T^b] = iq^{abc}T^c. \quad (1.1.91)$$

To maintain gauge invariance one introduces a gauge vector superfield V with the gauge transformation

$$e^{V'} = e^{-i\Lambda^\dagger} e^V e^{i\Lambda}, \quad e^{-V'} = e^{-i\Lambda} e^{-V} e^{i\Lambda^\dagger}, \quad (1.1.92)$$

where Λ and V are promoted to take their values in the Lie algebra

$$\Lambda = 2g\Lambda^a T^a, \quad V = 2gV^a T^a. \quad (1.1.93)$$

The transformation (1.1.92) ensures the gauge invariance of $\text{Tr}(\Phi^\dagger e^V \Phi)$. The field-strength superfields in (1.1.70) are extended to

$$W_A = -\frac{1}{4}\bar{\mathcal{D}}^2 e^{-V} \mathcal{D}_A e^V, \quad W_{\dot{A}} = -\frac{1}{4}\mathcal{D}^2 \bar{\mathcal{D}}_{\dot{A}} V. \quad (1.1.94)$$

Expanding in powers of V , one has

$$W_A = -\frac{1}{4}\bar{\mathcal{D}}^2 \mathcal{D}_A V - \frac{1}{8}\bar{\mathcal{D}}^2 [\mathcal{D}_A V, V]. \quad (1.1.95)$$

We define W_A^a , in analogy with V , by $W_A = 2gW_A^a T^a$ and thus

$$W_A^a = -\frac{1}{4}\bar{\mathcal{D}}^2 \{\mathcal{D}_A V^a + iq^{abc}(\mathcal{D}_A V^b)V^c\} \quad (1.1.96)$$

$$= \lambda_A^a + \theta_A D^a - (\sigma^{\mu\nu} \theta)_A F_{\mu\nu}^a + i\theta^2 \sigma_{A\dot{B}}^\mu D_\mu \bar{\lambda}^{a\dot{B}}, \quad (1.1.97)$$

where

$$F_{\mu\nu}^a = \partial_\mu A_\nu^a - \partial_\nu A_\mu^a - g q^{abc} A_\mu^b A_\nu^c, \quad D_\mu \bar{\lambda}^{a\dot{B}} = \partial_\mu \bar{\lambda}^{a\dot{B}} - g q^{abc} \bar{\lambda}^{c\dot{B}}. \quad (1.1.98)$$

The total Lagrangian for a supersymmetric non-abelian gauge theory coupled to chiral superfields can be written as the sum of both (1.1.65) and (1.1.86)

$$\begin{aligned} \mathcal{L} = & i\psi_i \sigma_\mu D_{ij}^\mu \bar{\psi}_j + |D_{ij}^\mu \phi_i|^2 - \frac{1}{4} F^{a\mu\nu} F_{\mu\nu}^a + i\lambda^a \sigma^\mu D_\mu \lambda^a \\ & - \sqrt{2}g(\bar{\lambda}^a \bar{\psi}_i T_{ij}^a \phi_j + h.c.) + \mathcal{L}_{\text{Yukawa}} - V(\phi^\dagger, \phi), \end{aligned} \quad (1.1.99)$$

where the covariant derivative is $D_{ij}^\mu = \delta_{ij} \partial^\mu + ig A^{a\mu} T_{ij}^a$ and the Yukawa potential as (1.1.68). The scalar potential and the auxiliary field in (1.1.99) are

$$V(\phi^\dagger, \phi) = F_i^\dagger F_i + \frac{1}{2} D^a D^a, \quad D^a = -g \phi_i^\dagger T_{ij}^a \phi_j. \quad (1.1.100)$$

In compact form, the exact supersymmetric Lagrangian is

$$\begin{aligned} \mathcal{L}_{\text{susy}} = & \frac{1}{4} (W^{aA} W_A^a + \bar{W}_{\dot{A}}^a \bar{W}^{a\dot{A}})_F + [\Phi_i^\dagger (e^{2gV^a T^a})_{ij} \Phi_j]_D \\ & + [h_i \Phi_i + \frac{1}{2} m_{ij} \Phi_i \Phi_j + \frac{1}{6} y_{ijk} \Phi_i \Phi_j \Phi_k + h.c.]_F. \end{aligned} \quad (1.1.101)$$

Soft SUSY Breaking Terms

In an exactly supersymmetric world, sparticles would be degenerate in mass with particles and they would have the same abundance. In reality, such is not the case as no sparticle has yet been observed. Thus SUSY must be broken severely. The most general soft SUSY breaking gauge invariant terms are [31, 147, 255]

$$\begin{aligned} \mathcal{L}_{\text{soft}} = & -\phi_i^\dagger M_{ij}^2 \phi_j + \left(\frac{1}{6} A_{ijk} \phi_i \phi_j \phi_k - \frac{1}{2} B_{ij} \phi_i \phi_j + C_i \phi_i + h.c. \right) \\ & - \frac{1}{2} (M \lambda^a \lambda^a + h.c.). \end{aligned} \quad (1.1.102)$$

1.1 SUPERSYMMETRY

The explicit SUSY breaking terms (1.1.102) can be rewritten in a form analogous to that of (1.1.101) as

$$\begin{aligned} -\mathcal{L}_{\text{soft}} = & \left[\theta^2 \left(-\frac{1}{6} A_{ijk} \Phi_i \Phi_j \Phi_k + \frac{1}{2} B_{ij} \Phi_i \Phi_j - C_i \Phi_i + h.c. \right. \right. \\ & \left. \left. + \frac{1}{2} (MW^{aA} W_A^a + h.c.) \right) \right]_F + \left[\theta^2 \bar{\theta}^2 \eta \Phi_i^\dagger M_{ij}^2 (e^V)_{jk} \Phi_k \right]_D. \end{aligned} \quad (1.1.103)$$

SUSY Transformations

The SUSY Action is invariant under the SUSY transformations of a chiral superfield

$$\delta_\xi \phi_i = \xi \cdot \chi_i, \quad \delta_\xi \phi_i^\dagger = \bar{\xi} \cdot \bar{\chi}_i, \quad (1.1.104)$$

$$\delta_\xi \chi_i = -i\sigma^\mu \bar{\xi} \partial_\mu \phi_i + \xi F_i, \quad \delta_\xi \chi_i^\dagger = -i\partial_\mu \phi_i^\dagger \bar{\sigma}^\mu \xi + F_i^\dagger \bar{\xi}, \quad (1.1.105)$$

$$\delta_\xi F_i = -i\xi^\dagger \bar{\sigma}^\mu \partial_\mu \chi_i, \quad \delta_\xi F_i^\dagger = i\partial_\mu \chi_i^\dagger \bar{\sigma}^\mu \xi. \quad (1.1.106)$$

The SUSY transformation $\delta_\xi F$ of the F -term is a total derivative. The SUSY Action is also invariant under the SUSY transformations of a vector superfield of some abelian gauge group

$$\delta_\xi A^\mu = -\frac{1}{\sqrt{2}} (\xi^\dagger \bar{\sigma}^\mu \lambda + \lambda^\dagger \bar{\sigma}^\mu \xi), \quad (1.1.107)$$

$$\delta_\xi D = \left(-\frac{1}{\sqrt{2}} \right) - i(\xi^\dagger \bar{\sigma}^\mu \partial_\mu \lambda - (\partial_\mu \lambda)^\dagger \bar{\sigma}^\mu \xi), \quad (1.1.108)$$

$$\delta_\xi \lambda = -\frac{1}{\sqrt{2}} \left(\frac{1}{2} i\sigma^\mu \bar{\sigma}^\nu \xi F_{\mu\nu} + \xi D \right), \quad (1.1.109)$$

$$\delta_\xi \lambda^\dagger = -\frac{1}{\sqrt{2}} \left(-\frac{1}{2} i\xi^\dagger \bar{\sigma}^\nu \sigma^\mu F_{\mu\nu} + \xi^\dagger D \right), \quad (1.1.110)$$

$$\delta_\xi F_i \rightarrow -\sqrt{2}q \lambda^\dagger \cdot \xi^\dagger \phi_i - i\xi^\dagger \bar{\sigma}^\mu \partial_\mu \chi_i, \quad (1.1.111)$$

$$\delta_\xi F_i^\dagger \rightarrow -\sqrt{2}q \xi \cdot \lambda \phi_i^\dagger + i\partial_\mu \chi_i^\dagger \bar{\sigma}^\mu \xi. \quad (1.1.112)$$

The SUSY transformation $\delta_\xi D$ of the D -term is a total derivative. The SUSY Action is also invariant under the SUSY transformations of a vector superfield of some non-abelian gauge group

$$\delta_\xi W^{a\mu} = -\frac{1}{\sqrt{2}} (\xi^\dagger \bar{\sigma}^\mu \lambda^a + \lambda^{a\dagger} \bar{\sigma}^\mu \xi), \quad (1.1.113)$$

$$\delta_\xi D^a = \left(-\frac{1}{\sqrt{2}}\right) - i(\xi^\dagger \bar{\sigma}^\mu (D_\mu \lambda)^a - (D_\mu \lambda)^{a\dagger} \bar{\sigma}^\mu \xi), \quad (1.1.114)$$

$$\delta_\xi \lambda^a = -\frac{1}{\sqrt{2}} \left(\frac{1}{2} i \sigma^\mu \bar{\sigma}^\nu \xi F_{\mu\nu}^a + \xi D^a \right), \quad (1.1.115)$$

$$\delta_\xi \lambda^{a\dagger} = -\frac{1}{\sqrt{2}} \left(-\frac{1}{2} i \xi^\dagger \bar{\sigma}^\nu \sigma^\mu F_{\mu\nu}^a + \xi^\dagger D^a \right), \quad (1.1.116)$$

$$\delta_\xi F_i \rightarrow -\sqrt{2} g \lambda^{a\dagger} \cdot \xi^\dagger T^a \phi_i - i \xi^\dagger \bar{\sigma}^\mu \partial_\mu \chi_i, \quad (1.1.117)$$

$$\delta_\xi F_i^\dagger \rightarrow -\sqrt{2} g \phi_i^\dagger T^a \xi \cdot \lambda^a + i \partial_\mu \chi_i^\dagger \bar{\sigma}^\mu \xi. \quad (1.1.118)$$

The SUSY transformation $\delta_\xi D^a$ of the D -term is a total derivative.

1.2 The Minimal Supersymmetric Standard Model

The so called MSSM is nothing but a straightforward supersymmetrization of the SM with a minimal number of parameters. This section is devoted to construct, briefly, the MSSM. Detailed reviews of the MSSM can be found in Refs. [30, 31, 62, 240, 254].

1.2.1 MSSM Lagrangian

The gauge group of the MSSM is the same as of the SM, $SU(3)_C \times SU(2)_L \times U(1)_Y$.

The particle content of the MSSM model is summarized in the following table

The Lagrangian of the MSSM is given by

$$\mathcal{L}_{\text{MSSM}} = \mathcal{L}_{\text{gauge}} + \mathcal{L}_{\text{matter}} + W + \mathcal{L}_{\text{soft}}, \quad (1.2.1)$$

where $\mathcal{L}_{\text{gauge}}$ is given by

$$\mathcal{L}_{\text{gauge}} = -\frac{1}{4} F_G^{a\mu\nu} F_G^a{}_{\mu\nu} + i \bar{\lambda}_G^a \bar{\sigma}^\mu D_\mu \lambda_G^a + \frac{1}{2} D^a D_a, \quad (1.2.2)$$

where the index G runs over the color, weak isospin and hypercharge of gauge group, and the index a refers to the adjoint representations of the non-abelian subgroups.

SM Particles		SUSY partners	
Particles	States	Particles	States
quarks(q) (spin - $\frac{1}{2}$)	$(\begin{smallmatrix} u \\ d \end{smallmatrix})_L, u_R, d_R$ $(\begin{smallmatrix} c \\ s \end{smallmatrix})_L, c_R, s_R$ $(\begin{smallmatrix} t \\ b \end{smallmatrix})_L, t_R, b_R$	squarks(\tilde{q}) (spin - 0)	$(\begin{smallmatrix} \tilde{u} \\ \tilde{d} \end{smallmatrix})_L, \tilde{u}_R, \tilde{d}_R$ $(\begin{smallmatrix} \tilde{c} \\ \tilde{s} \end{smallmatrix})_L, \tilde{c}_R, \tilde{s}_R$ $(\begin{smallmatrix} \tilde{t} \\ \tilde{b} \end{smallmatrix})_L, \tilde{t}_R, \tilde{b}_R$
leptons(ℓ) (spin - $\frac{1}{2}$)	$(\begin{smallmatrix} \nu_e \\ e \end{smallmatrix})_L, e_R$ $(\begin{smallmatrix} \nu_\mu \\ \mu \end{smallmatrix})_L, \mu_R$ $(\begin{smallmatrix} \nu_\tau \\ \tau \end{smallmatrix})_L, \tau_R$	sleptons($\tilde{\ell}$) (spin - 0)	$(\begin{smallmatrix} \tilde{\nu}_e \\ \tilde{e} \end{smallmatrix})_L, \tilde{\nu}_{eR}, \tilde{e}_R$ $(\begin{smallmatrix} \tilde{\nu}_\mu \\ \tilde{\mu} \end{smallmatrix})_L, \tilde{\mu}_R$ $(\begin{smallmatrix} \tilde{\nu}_\tau \\ \tilde{\tau} \end{smallmatrix})_L, \tilde{\tau}_R$
gauge/Higgs bosons (spin-1, spin-0)	g, Z, γ, h, H, A W^\pm, H^\pm	gauginos/Higgsinos (spin - $\frac{1}{2}$)	$\tilde{g}, \tilde{Z}, \tilde{\gamma}, \tilde{H}_1^0$ $\tilde{W}^\pm, \tilde{H}^\pm$

Table 1.1: Particle content of the MSSM

λ_G is the associated gaugino fields. The field strength tensors $F_G^{a\mu\nu}$ are given by

$$F_G^{a\mu\nu} = \partial_\mu W_\nu^a - \partial_\nu W_\mu^a - g_G f^{abc} W_\mu^b W_\nu^c, \quad (1.2.3)$$

while the covariant derivative D_μ is defined as

$$D_\mu = \partial_\mu + ig_G W_\mu^a T^a, \quad (1.2.4)$$

where T^a are the gauge group generators.

Also, $\mathcal{L}_{\text{matter}}$ is given by

$$\begin{aligned} \mathcal{L}_{\text{matter}} = & (D^\mu \phi_i)^\dagger (D_\mu \phi_i) + i \bar{\psi}_i \gamma^\mu D_\mu \psi_i + F_i^* F_i \\ & + ig_a \sqrt{2} (\phi^* T^a \lambda^a \psi + \text{h.c.}) - \frac{1}{2} g_a^2 (\phi_i^* T^a \phi_i)^2, \end{aligned} \quad (1.2.5)$$

where ϕ and ψ run over the MSSM scalars and fermions respectively.

The Yukawa interactions are included, as usual, in the superpotential, W . This superpotential is given by

$$W = Y_u \hat{Q}_L \hat{U}_L^c \hat{H}_u + Y_d \hat{Q}_L \hat{D}_L^c \hat{H}_d + Y_e \hat{L}_L \hat{E}_L^c \hat{H}_d - \mu \hat{H}_d \hat{H}_u. \quad (1.2.6)$$

Here the summation over generational indices is implicit. Furthermore, due to the fact that the $SU(3) \times SU(2)_L \times U(1)_Y$ quantum numbers of the Higgs and lepton

doublet superfields are the same, we have the additional undesired terms

$$W' = \lambda_{ijk} \hat{L}_i \hat{L}_j \hat{E}_k^c + \lambda'_{ijk} \hat{L}_i \hat{Q}_j \hat{D}_k^c + \lambda''_{ijk} \hat{D}_i^c \hat{D}_j^c \hat{U}_k^c + \mu'_i \hat{L}_i \hat{H}_u. \quad (1.2.7)$$

These terms violate baryon and lepton number explicitly and lead to proton decay at unacceptable rates³. To avoid this problem of too rapid proton decay, imposing a smaller symmetry like the R -parity, $R_P = (-1)^{3B+L+2S}$, where B and L are baryon and lepton number and S is the spin, would be sufficient.

The soft SUSY breaking Lagrangian, $\mathcal{L}_{\text{soft}}$, is given by

$$\begin{aligned} \mathcal{L}_{\text{soft}} = & -\frac{1}{2} M_a \lambda^a \lambda^a - m_{\tilde{q}_{ij}}^2 \tilde{q}_i^* \tilde{q}_j - m_{\tilde{u}_{ij}}^2 \tilde{u}_i^* \tilde{u}_j - m_{\tilde{d}_{ij}}^2 \tilde{d}_i^* \tilde{d}_j - m_{\tilde{l}_{ij}}^2 \tilde{l}_i^* \tilde{l}_j \\ & - m_{\tilde{e}_{ij}}^2 \tilde{e}_i^* \tilde{e}_j - m_{H_u}^2 |H_u|^2 - m_{H_d}^2 |H_d|^2 - [A_u^{ij} Y_u^{ij} \tilde{q}_i \tilde{u}_j H_u \\ & + A_d^{ij} Y_d^{ij} \tilde{q}_i \tilde{d}_j H_d + A_e^{ij} Y_e^{ij} \tilde{\ell}_i \tilde{e}_j H_d - B \mu H_u H_d + h.c.]. \end{aligned} \quad (1.2.8)$$

This means that about 100 free parameters have been added into the model, which reduce the predictiveness of the MSSM. To reduce this large number of parameter, a kind of universality among the soft SUSY breaking terms at grand unification scale, $M_X = 3 \times 10^{16}$ GeV, is assumed. That is, we assume

$$m_{\tilde{q}_{ij}}^2 = m_{\tilde{u}_{ij}}^2 = m_{\tilde{d}_{ij}}^2 = m_{\tilde{l}_{ij}}^2 = m_{\tilde{e}_{ij}}^2 = m_0^2 \delta_{ij}, \quad (1.2.9)$$

$$m_{H_u}^2 = m_{H_d}^2 =: m_0^2, \quad (1.2.10)$$

$$A_u^{ij} = A_d^{ij} = A_e^{ij} =: A_0, \quad (1.2.11)$$

$$M_1 = M_2 = M_3 =: M_{1/2}. \quad (1.2.12)$$

The parameters m_0 , A_0 , and $M_{1/2}$ are, respectively, called “universal scalar mass”, “universal trilinear coupling”, and “universal gaugino mass”.

³This can be seen from the fact that the term $\lambda''_{211} D_2^c D_1^c U_1^c$ and $\lambda'_{112} L_1 Q_1 D_2^c$ form, through the exchange of \tilde{s} , the four fermion operator $\frac{\lambda''_{211} \lambda'_{112}}{m_s^2} (u_R d_R) (u_L e_L)$. This operator would contribute to the proton decay process, $p \rightarrow e^+ \pi^0$, making the lifetime of the proton is of order $\mathcal{O}(10^{-13})$ sec, which is far from the experimental limit on the proton lifetime, $\tau_p > 1.6 \times 10^{33}$ year.

The complete scalar potential of the MSSM is given by

$$V = V_F + V_D + V_{soft}, \quad (1.2.13)$$

where V_F is derived from the F-term ($\sum_i |\frac{\partial W}{\partial \phi_i}|^2$), that is,

$$\begin{aligned} V_F = & |Y_u \tilde{u}^c \tilde{q} + \mu H_d|^2 + |Y_d \tilde{d}^c \tilde{q} + Y_e \tilde{e}^c \tilde{\ell} + \mu H_u|^2 + |Y_u \tilde{q} H_u|^2 \\ & + |Y_d \tilde{q} H_d + Y_e \tilde{\ell} H_d|^2 + |Y_u \tilde{u}^c H_u + Y_d \tilde{d}^c H_d|^2 + |Y_e \tilde{e}^c H_d|^2. \end{aligned} \quad (1.2.14)$$

Also, V_D is derived from the D-term ($D^a = g^a \sum_i \phi_i^* T^a \phi_i$), that is,

$$\begin{aligned} V_D = & \frac{g_1^2}{2} \left[\frac{1}{6} |\tilde{q}|^2 - \frac{2}{3} |\tilde{u}^c|^2 + \frac{1}{3} |\tilde{d}^c|^2 - \frac{1}{2} |\tilde{\ell}|^2 + |\tilde{e}^c|^2 + \frac{1}{2} |H_u|^2 \right. \\ & - \frac{1}{2} |H_d|^2 \Big]^2 + \frac{g_3^2}{8} \left(\tilde{q}^\dagger \lambda^A \tilde{q} - \tilde{d}^{c\dagger} \lambda^A \tilde{d}^c - \tilde{u}^{c\dagger} \lambda^A \tilde{u}^c \right)^2 \\ & + \frac{g_2^2}{8} \left(\tilde{q}^\dagger \tau^i \tilde{q} + \tilde{\ell}^\dagger \tau^i \tilde{\ell} + H_u^\dagger \tau^i H_u + H_d^\dagger \tau^i H_d \right)^2, \end{aligned} \quad (1.2.15)$$

where g_3 , g_2 and g_1 are the $SU(2)_L$ and $U(1)_Y$ gauge coupling constants respectively. Finally V_{soft} is given as the scalar part of \mathcal{L}_{soft} , shown in eq. (1.2.8). Now we can, easily, extract the Higgs potential from the complete scalar potential. It is given by

$$\begin{aligned} V(H_u, H_d) = & (|\mu|^2 + m_{H_u}^2) (|H_u^+|^2 + |H_u^0|^2) + (|\mu|^2 + m_{H_d}^2) (|H_d^-|^2 + |H_d^0|^2) \\ & + [B\mu (H_u^+ H_d^- - H_u^0 H_d^0) + h.c.] + \frac{g_2^2 + g_1^2}{8} [|H_u^+|^2 + |H_u^0|^2 \\ & - |H_d^0|^2 - |H_d^-|^2]^2 + \frac{g_2^2}{2} |H_u^+ H_d^{0+} + H_u^0 H_d^{-+}|^2. \end{aligned} \quad (1.2.16)$$

The only parameter, in the above equation, which can be complex is $B\mu$. However, the phase of it can be absorbed by a redefinition of the phases of H_u^0 and H_d^0 . Therefore, all obtained VEVs are assumed to be real. The vacuum expectation values of the Higgs fields are given by

$$\langle \text{Re}H_{u,d}^0 \rangle = \frac{v_{u,d}}{\sqrt{2}}, \quad \langle \text{Im}H_{u,d}^0 \rangle = 0 = \langle H_{u,d}^{+-} \rangle \quad (1.2.17)$$

The potential of neutral Higgs fields can be written as

$$V(v_u, v_d) = m_2^2 v_u^2 + m_1^2 v_d^2 + 2m_3^2 v_u v_d + \frac{g_2^2 + g_1^2}{8} (v_u^2 - v_d^2)^2 \quad (1.2.18)$$

where

$$m_1^2 = m_{H_d}^2 + |\mu|^2, \quad m_2^2 = m_{H_u}^2 + |\mu|^2, \quad m_3^2 = B\mu. \quad (1.2.19)$$

In order to avoid the unboundedness from below for this potential, we must impose the condition (sometimes called the stability condition)

$$m_1^2 + m_2^2 > 2m_3^2. \quad (1.2.20)$$

Now we go directly to explore the condition of the symmetry breaking. This happens when the origin, $v_u = v_d = 0$, is not a local minimum of the potential (1.2.18). Thus, define $T(v_u, v_d) := \left(\frac{\partial^2 V(v_u, v_d)}{\partial v_u^2} \right) \left(\frac{\partial^2 V(v_u, v_d)}{\partial v_d^2} \right) - \left(\frac{\partial^2 V(v_u, v_d)}{\partial v_u \partial v_d} \right)^2$. Now, In order for the point $(0, 0)$ to be a local minimum of $V(v_u, v_d)$, it must be satisfied that $T(0, 0) > 0$ and $\frac{\partial V(0,0)}{\partial^2 v_u^2} > 0$. Recall that $\frac{\partial V(0,0)}{\partial^2 v_u^2} = 2m_1^2$ is always positive. Therefore, we must impose the condition $T(0, 0) < 0$, in order to break the electroweak symmetry, that is, we must have

$$m_1^2 m_2^2 < m_3^4. \quad (1.2.21)$$

It is remarkable that the two conditions (1.2.20), and (1.2.21) are not consistent with each other. This paradox is solved by recalling that the boundary conditions, eq. (1.2.19), are valid only at GUT scale, while the running from GUT scale down to the electroweak scale shows that m_1 and m_2 get renormalized differently - since H_d and H_u couple with different strengths to fermions - so that m_2^2 become negative at the symmetry breaking scale, at which the condition (1.2.21) is satisfied. This will be discussed in the following section.

R-Parity

Other gauge invariant and renormalizable terms which could also be included in the superpotential of the MSSM violate lepton and baryon numbers conservations by one unit of L and B , respectively

$$W_{\Delta L=1} = \lambda_e^{ijk} L_i L_j \bar{e}_k + \lambda_L^{ijk} L_i Q_j \bar{d}_k + \mu_L^i L_i H_u, \quad (1.2.22)$$

$$W_{\Delta B=1} = \lambda_B^{ijk} \bar{u}_i \bar{L}_j \bar{d}_k. \quad (1.2.23)$$

B - and L -violating processes have never been seen experimentally. If both the couplings λ_L and λ_B were present, the proton could decay via channels such as $e^+ \pi^0$, $\mu^+ \pi^0$, ..., etc. The R -parity discrete symmetry forbids (1.2.22) and (1.2.23), while allowing all the interactions of the MSSM. The R -parity is multiplicatively conserved, and is defined by

$$R = (-1)^{3B+L+2S}. \quad (1.2.24)$$

SM particles has $R = 1$ and their sparticles has $R = -1$.

Every interaction vertex in the MSSM superpotential contains an even number of $R = -1$ sparticles. The lightest sparticle ('LSP') is absolutely stable, and if electrically uncharged it could be an attractive candidate for non-baryonic dark matter. The decay products of all other sparticles must contain an odd number of LSP's. In accelerator experiments, sparticles can only be produced in pairs. In the context of the MSSM, the LSP must lack electromagnetic and strong interactions. An important implication is that in collider experiments LSP's will carry away energy and momentum while escaping detection.

Since all sparticles will decay into at least one LSP (plus SM particles), and since in the MSSM sparticles are pair produced, it follows that at least $2m_{\tilde{\chi}_1^0}$ missing energy will be associated with each SUSY event, where $m_{\tilde{\chi}_1^0}$ is the mass of the LSP (often taken to be a neutralino). In $e^- e^+$ machines, the total visible energy and momentum

can be well measured, and the beams have very small spread, so that the missing energy and momentum can be well correlated with the energy and momentum of the LSP's. In hadron colliders, the distribution of energy and longitudinal momentum of the partons (i.e. quarks and gluons) is very broad, so in practice only the missing transverse momentum (or missing transverse energy \cancel{E}_T) is useful.

1.2.2 MSSM Spectrum

Now we will briefly review the important spectrum of the MSSM.

The masses of the gauge bosons, W and Z , are generated, as usual, after the electroweak symmetry breaking from the kinetic terms of H_u and H_d by inserting the VEVs. That is we get

$$M_Z^2 = \frac{1}{4}(g_2^2 + g_1^2)v^2, \quad (1.2.25)$$

$$M_W^2 = \frac{1}{4}g_2^2v^2, \quad (1.2.26)$$

where $v = \sqrt{v_u^2 + v_d^2} \simeq 246$ GeV.

Higgs Sector

To obtain the masses of the physical Higgs fields, we make the usual redefinition of the Higgs fields:

$$H_u = \begin{pmatrix} H_u^+ \\ \frac{v_u + \text{Re}H_u^0}{\sqrt{2}} + i \text{Im}H_u^0 \end{pmatrix}, \quad H_d = \begin{pmatrix} \frac{v_d + \text{Re}H_d^0}{\sqrt{2}} + i \text{Im}H_d^0 \\ H_d^- \end{pmatrix}. \quad (1.2.27)$$

The real parts correspond to the CP-even Higgs bosons and the imaginary parts correspond to the CP-odd Higgs bosons. The squared-mass matrix of the neutral Higgs fields is given by

$$\mathcal{M}_{ij}^2 = \frac{1}{2} \left. \frac{\partial^2 V_H}{\partial H_i \partial H_j} \right|_{\langle H_1^0 \rangle = v_1/\sqrt{2}, \langle H_2^0 \rangle = v_2/\sqrt{2}, \langle H_{1,2}^\pm \rangle = 0}, \quad (1.2.28)$$

where $H_i = \text{Re}H_u^0, \text{Im}H_u^0, \text{Re}H_d^0, \text{Im}H_d^0$. Thus the neutral Higgs bosons squared-mass matrix, in the basis $(\text{Re}H_d^0, \text{Re}H_u^0, \text{Im}H_d^0, \text{Im}H_u^0)$, is given by⁴

$$\mathcal{M}_0^2 = \begin{pmatrix} -\bar{m}_3^2 \tan \beta + M_Z^2 \cos^2 \beta & \bar{m}_3^2 - M_Z^2 \sin \beta \cos \beta & 0 & 0 \\ \bar{m}_3^2 - M_Z^2 \sin \beta \cos \beta & -\bar{m}_3^2 \cot \beta + M_Z^2 \sin^2 \beta & 0 & 0 \\ 0 & 0 & -\bar{m}_3^2 \tan \beta & \bar{m}_3^2 \\ 0 & 0 & \bar{m}_3^2 & -\bar{m}_3^2 \cot \beta \end{pmatrix}, \quad (1.2.31)$$

where $\tan \beta = v_u/v_d$. It is clear that no CP-violation occurs in the neutral Higgs sector. Indeed, the block-diagonal form of the above matrix proves that there is no mixing between the CP-even (real) Higgs fields and the CP-odd (imaginary) ones. Another straightforward observation from the matrix in eq. (1.2.31) is that the determinant of the second (down-right) 2×2 matrix is zero which corresponds to the Goldstone boson mass. Therefore, the other pseudoscalar Higgs mass is given by

$$M_A^2 = -\bar{m}_3^2(\tan \beta + \cot \beta) = -\frac{2\bar{m}_3^2}{\sin 2\beta} \quad (1.2.32)$$

The mixing angle of the pseudo physical fields is simply the angle β , i.e.

$$\begin{pmatrix} G^0 \\ A \end{pmatrix} = \begin{pmatrix} \cos \beta & \sin \beta \\ -\sin \beta & \cos \beta \end{pmatrix} \begin{pmatrix} \text{Im}(H_d)^0 \\ \text{Im}(H_u)^0 \end{pmatrix}. \quad (1.2.33)$$

Exactly the same procedure of the pseudoscalar A boson can be done as for obtaining the charged Higgs fields. That is, the squared-mass matrix of the charged Higgs fields is a 2×2 matrix with a zero determinant. This corresponds to the charged goldstone boson which will be eaten to give the W^\pm its mass. Also, the mixing angle of the charged Higgs fields is simply the same angle β , i.e.

$$\begin{pmatrix} G^\pm \\ H^\pm \end{pmatrix} = \begin{pmatrix} \cos \beta & \sin \beta \\ -\sin \beta & \cos \beta \end{pmatrix} \begin{pmatrix} H_d^\pm \\ H_u^\pm \end{pmatrix}. \quad (1.2.34)$$

⁴To obtain the eigenvalues (masses) and the eigenvectors (mixings) of any 2×2 matrix, there are some useful relations, which are

$$\text{Tr}(A) = \lambda_1 + \lambda_2, \quad \text{Det}(A) = \lambda_1 \lambda_2 \quad (1.2.29)$$

$$\sin 2\theta = \frac{2A_{12}}{\sqrt{(A_{11} - A_{22})^2 + 4A_{12}^2}}, \quad \cos 2\theta = \frac{A_{11} - A_{22}}{\sqrt{(A_{11} - A_{22})^2 + 4A_{12}^2}} \quad (1.2.30)$$

where λ_1 and λ_2 are the eigenvalues (masses) and θ is the mixing angle.

The mass of the massive charged Higgs boson is given by

$$M_{H^\pm}^2 = M_A^2 + M_W^2 \quad (1.2.35)$$

Nothing remaining except the CP-even Higgs fields mass matrix, which is the first (up-left) block in the matrix in eq. (1.2.31). The eigenvalues (masses) of the 2×2 matrix is given by

$$M_{h,H}^2 = \frac{1}{2} \left[M_A^2 + M_Z^2 \mp \sqrt{(M_A^2 + M_Z^2)^2 - 4M_A^2 M_Z^2 \cos^2 2\beta} \right] \quad (1.2.36)$$

The mixing angle of the physical CP-even Higgs bosons is given by

$$\cos 2\alpha = -\frac{M_A^2 - M_Z^2}{M_H^2 - M_h^2} \cos 2\beta, \quad \sin 2\alpha = -\frac{M_H^2 + M_h^2}{M_H^2 - M_h^2} \sin 2\beta \quad (1.2.37)$$

or equivalently

$$\alpha = \frac{1}{2} \arctan \left(\frac{M_A^2 + M_Z^2}{M_A^2 - M_Z^2} \tan 2\beta \right), \quad -\frac{\pi}{2} \leq \alpha \leq 0 \quad (1.2.38)$$

It is worth mentioning that from eq. (1.2.35) and eq. (1.2.36) one can easily extract the relations:

$$M_{H^\pm} > \max(M_A, M_W), \quad (1.2.39)$$

$$M_H > \max(M_A, M_Z). \quad (1.2.40)$$

It is important to note that for the lightest Higgs mass, M_h , we can get an upper bound from observing that M_h is an increasing function of $\cos^2 2\beta$, and reaches its maximum when $\cos^2 2\beta = 1$. This gives the very important relation

$$M_h \leq M_z. \quad (1.2.41)$$

It is clear that such a relation could be a reason to rule out the nice mathematical theory of MSSM. This is due to the upper bound $M_h \lesssim 90$ GeV derived from eq. (1.2.41) which contradicts the recent experimental data $M_h > 114.5$ GeV. The loop radiative corrections solved this problem. It was found [154, 155, 181, 258] that the lightest Higgs mass receives non-trivial corrections at the 1-loop level.

Chargino/Neutralino Sector

“Charginos” are linear combinations of the superpartners of the W^\pm and H^\pm , and the “neutralinos” are linear combinations of the superpartners of the Z and γ (B and W_3) and the neutral Higgses.

The general chargino mass matrix is given by [178, 182]

$$\mathcal{M}_C = \begin{bmatrix} M_2 & \sqrt{2}M_W s_\beta \\ \sqrt{2}M_W c_\beta & \mu \end{bmatrix} \quad (1.2.42)$$

where $s_\beta \equiv \sin \beta$, $c_\beta \equiv \cos \beta$. Like any non-symmetric square matrix, chargino mass matrix requires two real matrices U and V , in order to diagonalize it :

$$\mathcal{M}_C^{\text{diag}} = U \mathcal{M}_C V^{-1}, \quad (1.2.43)$$

where

$$U = \mathcal{O}_-, \quad (1.2.44)$$

$$V = \begin{cases} \mathcal{O}_+ & \text{if } \det \mathcal{M}_C > 0 \\ \sigma_3 \mathcal{O}_+ & \text{if } \det \mathcal{M}_C < 0 \end{cases}, \quad (1.2.45)$$

where σ_3 is the diagonal Pauli matrix introduced to make the chargino masses positive and \mathcal{O}_\pm are rotation matrices with angles θ_\pm defined by

$$\tan 2\theta_- = \frac{2\sqrt{2}M_W(M_2 c_\beta + \mu s_\beta)}{M_2^2 - \mu^2 - 2M_W^2 c_\beta}, \quad (1.2.46)$$

$$\tan 2\theta_+ = \frac{2\sqrt{2}M_W(M_2 s_\beta + \mu c_\beta)}{M_2^2 - \mu^2 + 2M_W^2 c_\beta}. \quad (1.2.47)$$

This diagonalization leads to the two chargino masses

$$m_{\chi_{1,2}^\pm}^2 = \frac{1}{2} \left\{ M_2^2 + \mu^2 + 2M_W^2 \mp \left[(M_2^2 - \mu^2)^2 + 4M_W^2(M_W^2 c_{2\beta}^2 + M_2^2 + \mu^2 + 2M_2 \mu s_{2\beta}) \right]^{\frac{1}{2}} \right\}. \quad (1.2.48)$$

The mass matrix of the neutralinos is a four-dimensional symmetric mass matrix. It is given, in the basis $(-i\tilde{B}, -i\tilde{W}_3, \tilde{H}_1^0, \tilde{H}_2^0)$, by [178, 182]

$$\mathcal{M}_N = \begin{bmatrix} M_1 & 0 & -M_Z s_W c_\beta & M_Z s_W s_\beta \\ 0 & M_2 & M_Z c_W c_\beta & -M_Z c_W s_\beta \\ -M_Z s_W c_\beta & M_Z c_W c_\beta & 0 & -\mu \\ M_Z s_W s_\beta & -M_Z c_W s_\beta & -\mu & 0 \end{bmatrix} \quad (1.2.49)$$

Since it is symmetric real square matrix, it can be diagonalized analytically [152, 177] by a single real matrix Z . The expressions of the matrix elements Z_{ij} with $i, j = 1, \dots, 4$ as well as the resulting masses $m_{\chi_i^0}$ have too complicated expressions. Nevertheless, the limit of large $|\mu|$ values, i.e. $|\mu| \gg M_{1,2} \gg M_Z$, is quite useful to simplify the mass expressions of the physical neutralino states. In this limit we get [146]

$$\begin{aligned} m_{\chi_1^0} &\simeq M_1 - \frac{M_Z^2}{\mu^2} (M_1 + \mu s_{2\beta}) s_W^2 \\ m_{\chi_2^0} &\simeq M_2 - \frac{M_Z^2}{\mu^2} (M_2 + \mu s_{2\beta}) c_W^2 \\ m_{\chi_{3/4}^0} &\simeq |\mu| + \frac{1}{2} \text{sign}(\mu) \frac{M_Z^2}{\mu^2} (1 \mp s_{2\beta}) (\mu \pm M_2 s_W^2 \mp M_1 c_W^2). \end{aligned} \quad (1.2.50)$$

Sfermions Sector

The squared-mass matrix of an sfermion \tilde{f} is generally given by

$$\mathcal{M}_{\tilde{f}}^2 = \begin{pmatrix} m_f^2 + m_{LL}^2 & m_f X_f \\ m_f X_f & m_f^2 + m_{RR}^2 \end{pmatrix}, \quad (1.2.51)$$

where

$$\begin{aligned} m_{LL}^2 &= m_{\tilde{f}_L}^2 + (I_f^{3L} - Q_f s_W^2) M_Z^2 c_{2\beta} \\ m_{RR}^2 &= m_{\tilde{f}_R}^2 + Q_f s_W^2 M_Z^2 c_{2\beta} \\ X_f &= A_f - \mu (\tan \beta)^{-2I_f^{3L}}. \end{aligned} \quad (1.2.52)$$

The mixing matrix which diagonalize the sfermion squared-mass matrix is given by

$$R^{\tilde{f}} = \begin{pmatrix} c_{\theta_f} & s_{\theta_f} \\ -s_{\theta_f} & c_{\theta_f} \end{pmatrix}, \quad (1.2.53)$$

where,

$$s_{2\theta_f} = \frac{2m_f X_f}{m_{\tilde{f}_1}^2 - m_{\tilde{f}_2}^2}, \quad (1.2.54)$$

$$c_{2\theta_f} = \frac{m_{LL}^2 - m_{RR}^2}{m_{\tilde{f}_1}^2 - m_{\tilde{f}_2}^2}. \quad (1.2.55)$$

The masses of the sfermions are given by

$$m_{\tilde{f}_{1,2}}^2 = m_f^2 + \frac{1}{2} \left[m_{LL}^2 + m_{RR}^2 \mp \sqrt{(m_{LL}^2 - m_{RR}^2)^2 + 4m_f^2 X_f^2} \right] \quad (1.2.56)$$

1.2.3 Radiative Electroweak Symmetry Breaking

In this subsection, we will turn our attention to explore how the electroweak symmetry may be broken in the context of the MSSM. To do so, we will concentrate our attention on the Renormalization Group Equations (RGE) of the Higgs potential parameters. In what follows, we use the third family approximation. Also we consider the limit $Y_\tau, Y_b \ll Y_t$, which simplifies the RGEs significantly. That is we neglect all the Yukawa couplings compared to Y_t of the top quark:

$$Y_u \simeq \begin{pmatrix} 0 & 0 & 0 \\ 0 & 0 & 0 \\ 0 & 0 & Y_t \end{pmatrix}, \quad Y_i \simeq \begin{pmatrix} 0 & 0 & 0 \\ 0 & 0 & 0 \\ 0 & 0 & 0 \end{pmatrix}, \quad i = d, e \quad (1.2.57)$$

$$(1.2.58)$$

$$A_u \simeq \begin{pmatrix} 0 & 0 & 0 \\ 0 & 0 & 0 \\ 0 & 0 & A_t Y_t \end{pmatrix}, \quad A_i \simeq \begin{pmatrix} 0 & 0 & 0 \\ 0 & 0 & 0 \\ 0 & 0 & 0 \end{pmatrix}, \quad i = d, e \quad (1.2.59)$$

In this respect, the RGEs of the relevant parameters are given by

$$16\pi^2 \frac{dm_{H_d}^2}{dt} = \frac{1}{4\pi} \left(-\frac{6}{5}\alpha_1 M_1^2 - 6\alpha_2 M_2^2 \right) \quad (1.2.60)$$

$$16\pi^2 \frac{dm_{H_u}^2}{dt} = \frac{1}{4\pi} \left(3\frac{m_4^2}{4\pi} - \frac{6}{5}\alpha_1 M_1^2 - 6\alpha_2 M_2^2 \right), \quad (1.2.61)$$

where $t = \ln Q$ is the logarithm of the energy scale Q , $\alpha_i = \frac{g_i^2}{4\pi}$, and

$$m_4^2 = 2Y_t^2 \left(m_{H_u}^2 + m_{\tilde{Q}_3}^2 + m_{\tilde{u}_3}^2 + A_t^2 \right). \quad (1.2.62)$$

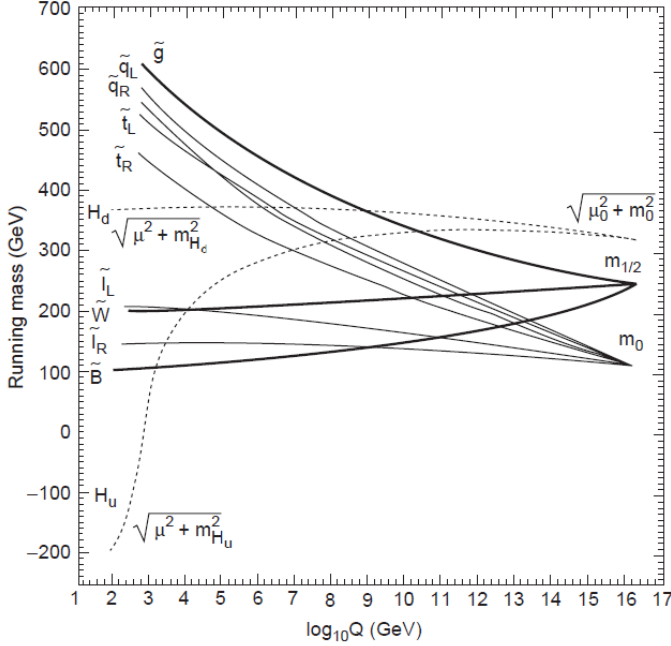
Now, in order to solve these equations, we should take into account the following RGEs

$$16\pi^2 \frac{d\alpha_i}{dt} = -\frac{b_i}{2\pi} \alpha_i^2, \quad (1.2.63)$$

$$16\pi^2 \frac{dM_i}{dt} = -\frac{b_i}{2\pi} \alpha_i M_i, \quad (1.2.64)$$

$$16\pi^2 \frac{dY_t}{dt} = \frac{Y_t}{4\pi} \left(6\frac{Y_t^2}{4\pi} - \frac{13}{15}\alpha_1 - 3\alpha_2 - \frac{16}{3}\alpha_3 \right) \quad (1.2.65)$$

Figure 1.5: The running of the soft MSSM masses from the GUT scale to the electroweak scale [31, 203]



$$16\pi^2 \frac{dm_{\tilde{Q}_3}^2}{dt} = \frac{1}{4\pi} \left(\frac{m_4^2}{4\pi} - \frac{2}{15}\alpha_1 M_1^2 - 6\alpha_2 M_2^2 - \frac{32}{3}\alpha_3 M_3^2 \right), \quad (1.2.66)$$

$$16\pi^2 \frac{dm_{\tilde{u}_3}^2}{dt} = \frac{1}{4\pi} \left(2\frac{m_4^2}{4\pi} - \frac{32}{15}\alpha_1 M_1^2 - \frac{32}{3}\alpha_3 M_3^2 \right), \quad (1.2.67)$$

$$16\pi^2 \frac{dA_t}{dt} = \frac{1}{4\pi} \left(12\frac{Y_t^2}{4\pi} A_t + \frac{26}{15}\alpha_1 M_1 + 6\alpha_2 M_2 + \frac{32}{3}\alpha_3 M_3^2 \right), \quad (1.2.68)$$

where $b_i = -\frac{33}{5}, -1, 3$ respectively. From these equations, it is remarkable that H_u couples to the top (s)quark with the large Yukawa coupling Y_t , while H_d don't. Therefore, the running from GUT scale down to the electroweak scale, as shown in Fig. 1.5, decreases $m_2^2 = m_{H_u}^2 + \mu^2$ as the energy scale decrease. Around the right electroweak scale, m_2 reaches a negative value. On the contrary, $m_1^2 = m_{H_d}^2 + \mu^2$ increases slightly as the energy scale decrease. This means that the running of the RGEs of $m_{1,2}^2$ proves that at the electroweak scale, the condition eq. (1.2.21) is satisfied and the gauge symmetry is broken. “In fact, this is an appealing feature in SUSY models

that explains the mechanism of the electroweak symmetry breaking. In the SM with a single Higgs doublet, the assumption that its mass squared is negative is an ad hoc assumption. From the previous discussion we have shown that the Higgs boson mass becomes negative around the electroweak scale due to the effect of the large top Yukawa coupling⁵.

Higgs Mass Limit

The precision fits to electroweak data show that the Higgs mass $M_H = 125$ GeV, at the 99% confidence level [4, 104]. In the SM, we have no constraint on M_H . The MSSM predicts that the lightest Higgs particle should be no heavier than about 140 GeV

$$m_h^2 \leq m_Z^2 + \frac{3m_t^4}{2\pi^2 v^2} \ln\left(\frac{m_S}{m_t}\right) \sim 140 \text{ GeV}, \quad (1.2.69)$$

where m_S is the average of the stop particles $m_S = \frac{1}{2}(m_{\tilde{t}_1}^2 + m_{\tilde{t}_2}^2)$.

Gauge Coupling Unification

In terms of the gauge couplings $g_i = \sqrt{\frac{5}{3}}g', g, g_s$ of the $U(1)_Y$, $SU(2)_L$, $SU(3)_C$ groups of the hypercharge, the weak and the strong interactions, the couplings α_i 's are defined such that $\alpha_i = g_i^2/4\pi$. Their running with the energy scale Q , to one loop order, is governed by the renormalization group equations (RGEs) [31, 312]

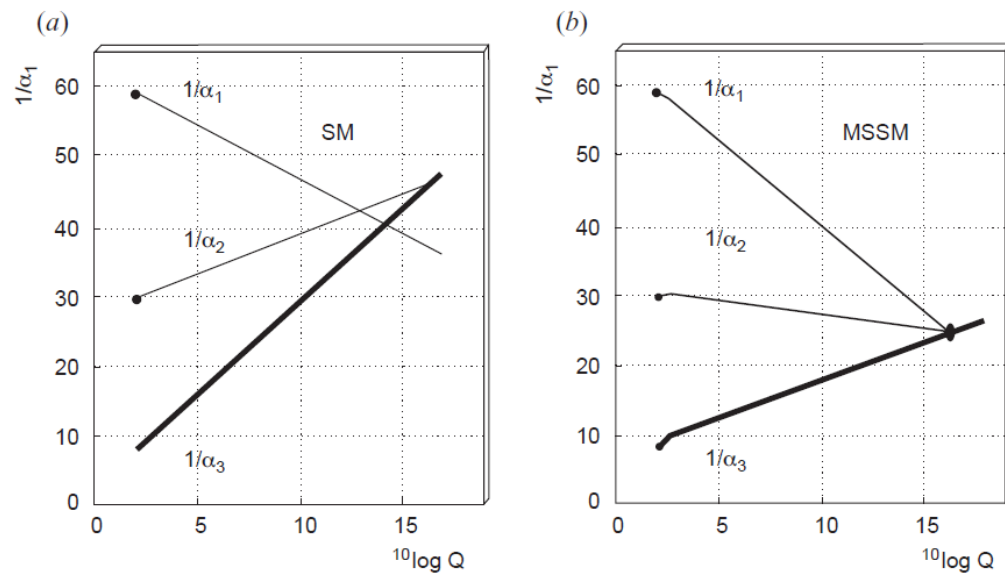
$$\frac{d}{d \ln Q} (\alpha_i^{-1}) = \frac{b_i}{2\pi}, \quad (1.2.70)$$

where b_i 's are functions which depend on the particle content of the model and the corresponding charges. In the MSSM, at the GUT scale $Q_U = m_U \simeq 2.2 \times 10^{16}$ GeV, the gauge couplings are equal and the three fundamental forces are unified (see Fig. 1.6)

$$\alpha_1(m_U) = \alpha_2(m_U) = \alpha_3(m_U) = \alpha_U. \quad (1.2.71)$$

⁵said by professor Shaaban Khalil in his book “Supersymmetry Phenomenology”

Figure 1.6: (Left) Failure of the SM couplings to unify. (Right) Gauge coupling unification in the MSSM [31, 312]



2

SUPERSYMMETRIC $B - L$ EXTENSION OF THE STANDARD MODEL

2.1 Neutrino Masses in MSSM

Neutrinos are massless, by construction, in MSSM. In this section we review several possible modifications of the MSSM in order to overcome this problem.

An important phenomenological motivation to extend the SM and MSSM is neutrinos masses. many experiments were performed that neutrinos are massive particles, through the discovery of neutrino oscillations. In the SM, neutrinos are massless particles. Explicit Majorana mass terms for the LH neutrinos are forbidden by gauge invariance. Inclusion of any type of neutrino mass terms implies extending either of the fermion or scalar sectors or both with extra degrees of freedom nonexisting in the SM. Therefore, BSM is required for, at least, neutrino masses. In the literature, seesaw mechanisms are famous ways to generate neutrino masses.

2.1.1 Dirac Mass Term

The most straightforward way to generate the neutrino masses is to introduce a new MSSM singlet superfield \hat{N} , whose fermionic member accounts for a right handed neutrino ν_R . This allows the formulation of the Yukawa term $Y_\nu \hat{L} \hat{H}_u \hat{N}^c$ in the superpotential. After EWSB, a Dirac mass term

$$m_D \bar{\nu}_L \nu_R \quad (2.1.1)$$

is formed, where $m_D = Y_\nu v_u$. Now it is worth to mention that, in order to get the tiny neutrino masses given by the experimental results, $m_\nu \sim \mathcal{O}(10^{-13})$, we should impose the condition that the neutrino Yukawa coupling must be so small, $Y_\nu \sim \mathcal{O}(10^{-11})$, which is far from the smallest known Yukawa coupling $Y_e \sim \mathcal{O}(10^{-6})$. This is the reason for which the physicist does not favor this scenario.

For massive Dirac neutrinos, in addition to the ν_L , one must introduce a chirally RH neutrino field, ν_R , to the SM. These RH neutrinos are weak isospin singlets and can therefore couple to the ν_L and ϕ , the SM Higgs doublet, to form the Yukawa term:

$$y_\nu \overline{\ell}_L \phi \nu_R + \text{h.c.}, \quad (2.1.2)$$

which induces a Dirac mass term for the neutrino, when the neutral component of the Higgs field ϕ acquires a VEV, normally just like all other fermions get their masses. However, in order to explain tiny neutrino masses, one has to impose a hierarchy in the Yukawas: $y_\nu \ll y_e$, making it seem rather ad-hoc. We shall discuss some possible resolutions to this later.

In principle, for massive Majorana neutrinos, only one type of Weyl field is required. Hence, given ν_L , one can already construct a Majorana mass term for the neutrino. But since $\overline{\ell}_L \ell_L^c$ is a weak isospin triplet, within the framework of the SM, the

2.1 Neutrino Masses in MSSM

simplest possibility is therefore the dimension-5 mass term of the form [307,308,311]:

$$-\frac{y}{\Lambda} \overline{\ell}_L \phi \phi^T \ell_L^c + \text{h.c.}, \quad (2.1.3)$$

where y denotes some dimensionless coupling constant and Λ is the high-energy cutoff scale above which this renormalisability scale. After SSB, the term in (2.1.3) induces an effective Majorana mass for the LH neutrino:

$$m_\nu = \frac{y v^2}{2 \Lambda}. \quad (2.1.4)$$

In general, with 3 families, m_ν is not diagonal, so if we want to read the neutrino masses we must diagonalize it. We can do it performing a unitary transformation

$$\nu_L \rightarrow U_\nu \nu_L, \quad (2.1.5)$$

in such a way that:

$$m_\nu \rightarrow m_{\nu_i}^{diag} \equiv U_\nu^\dagger m_\nu U_\nu. \quad (2.1.6)$$

Now we can read the neutrino masses, which are:

$$m_{\nu_i}^{diag} = \frac{y_i^{diag} v^2}{2 \Lambda}. \quad (2.1.7)$$

When we perform (2.1.5) in the whole SM Lagrangian, together the charged lepton rotations with V_e , the leptonic sector of the weak charged current becomes

$$J_\mu^- = \cdots + \overline{\nu}_L \gamma_\mu \underbrace{U_\nu^\dagger V_e}_{U_{\text{PMNS}}} e_L. \quad (2.1.8)$$

As for quarks, a flavor mixing in the leptonic charge current arises, but this time controlled by the neutrino Pontecorvo-Maki-Nakagawa-Sakata (PMNS) unitary mixing matrix [231, 237, 268, 269], U_{PMNS}^\dagger , analogous to V_{CKM} for quarks mixing, and it is often parametrized as

$$U_{\text{PMNS}} = \begin{pmatrix} c_{12}c_{13} & s_{12}c_{13} & s_{13}e^{-i\delta} \\ -s_{12}c_{23} - c_{12}s_{23}s_{13}e^{i\delta} & c_{12}c_{23} - s_{12}s_{23}s_{13}e^{i\delta} & s_{23}c_{13} \\ -s_{12}s_{23} + c_{12}c_{23}s_{13}e^{i\delta} & c_{12}s_{23} + s_{12}c_{23}s_{13}e^{i\delta} & -c_{23}c_{13} \end{pmatrix}, \quad (2.1.9)$$

When we compare the neutrino masses of (2.1.6) to other fermion masses, we see that the former are suppressed by the factor v/Λ with respect to the latter. Experimental bounds indicate that approximately [245]

$$m_\nu < 1 \text{ eV}.$$

Since $v \sim \mathcal{O}(100)$ GeV , if we take $\lambda \sim \mathcal{O}(1)$ we can get a lower bound for the scale Λ :

$$m_\nu \sim v^2 \Lambda < 1 \text{ eV} \Rightarrow \Lambda > 10^{13} \text{ GeV}. \quad (2.1.10)$$

However, smaller values of the effective coupling λ allow for smaller value of the cut-off scale Λ . It is interesting to note here that if $\Lambda \gg v$, then expression (2.1.4) suggests that neutrinos can naturally have a much smaller mass than other fermions without the need to fine-tune y with the corresponding Yukawa coupling of the charged leptons. Given this potential benefit in models with Majorana neutrino masses, and the fact that no SM symmetry forbids their inclusion, it seems natural that neutrinos ought to be Majorana particles. Consequently, we shall assume throughout this work that neutrinos are Majorana unless otherwise indicated.

To summarize, introducing an effective dimension-5 mass term we can give neutrinos a mass, and we can explain why it is so small with respect to the other fermion masses. This term spoils the renormalizability of the SM, but it is so suppressed at ordinary energies that we cannot notice it, except for the small effect that makes neutrinos massive. The above construction leads to Majorana neutrino masses instead of a Dirac masses, at variance with the charged SM fermions: giving LH neutrinos a mass without introducing RH neutrinos forces the former to be Majorana particles.

Returning to the initial problem of how to modify the SM to incorporate neutrino masses, we see that both the Dirac mass term of (2.1.2) and the non-renormalisable

term of (2.1.3) imply that some new physics must be introduced. While (2.1.2) demands the addition of RH singlet neutrinos, (2.1.3) can lead to many possibilities. So, it is the subject of the next few subsections to explore several possible scenarios which can achieve this within framework of renormalisable interactions.

2.1.2 Seesaw Mechanisms

In this subsection, we provide the most elegant mechanisms to generate the neutrino masses. These mechanisms are called “Seesaw Mechanisms”. The idea behind the seesaw mechanisms is to explain the smallness of the neutrino masses by using the largeness of some other mass scale or so. There are several types of seesaw mechanisms:

- Seesaw Type I,
- Seesaw Type II,
- Seesaw Type III,
- Linear Seesaw,
- Inverse Seesaw.

The formalization of each mechanism is different from the others. Therefore, since reviewing the several types of seesaw mechanisms is not our goal, we will review briefly the only two types that are needed in this thesis. These are the seesaw type I as well as the Inverse seesaw mechanisms.

Type I Seesaw

Within the class of renormalisable models that can give neutrinos a mass in the same way as for all the other SM fermions, through a Dirac mass term, the type I seesaw

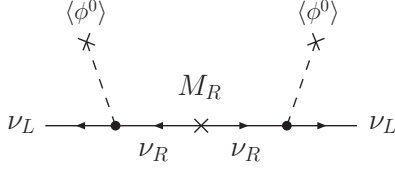


Figure 2.1: The type I seesaw realisation of the small Majorana mass for the LH neutrino with $m_\nu \simeq vev\phi^{02} y_\nu M_R^{-1} y_\nu^T$.

mechanism [68, 168, 228, 246, 251] is perhaps the most elegant solution of all. It provides a way to generate tiny but nonzero neutrino masses.

The idea of the type I seesaw model is quite simple. We must add to the fermion sector of the SM a heavy neutral singlet fermions, RH neutrino ν_R , for each family. These *sterile* neutrinos participate in some Yukawa interactions, but have no SM gauge interactions.

We can then extend the SM Lagrangian with the following terms

$$\mathcal{L}^\nu = i\bar{\nu}_R \partial_\mu \gamma^\mu \nu_R - (y_\nu \bar{\ell}_L \tilde{\phi} \nu_R + y_\nu^T \bar{(\nu_R)^c} \tilde{\phi} \ell_L^c + \frac{1}{2} M_R \bar{(\nu_R)^c} \nu_R + h.c.), \quad (2.1.11)$$

where y_ν is 3×3 complex matrix and M_R denotes the bare mass for the RH neutrino. It is useful to notice, for future use, that it is not restrictive to work in a field basis where the RH Majorana mass matrix M_R is diagonal, with real and positive eigenvalues, since we can always go to such a basis by a suitable redefinition of the RH neutrino fields.

Since the SM does not predict or restrict the size of M_R , we may assume that it is arbitrarily large. So, by integrating out the heavy RH neutrino field, one gets an effective Lagrangian that is of the same form as (2.1.3):

$$\mathcal{L}_{\text{eff}}^\nu = \frac{y_\nu^2}{2M_R} \bar{\ell}_L \phi \phi^T \ell_L^c, \quad (2.1.12)$$

if we identify y and Λ of Eq. (2.1.3) with y_ν and M_R respectively. The interaction of (2.1.12) will naturally give rise to a very small Majorana neutrino mass: $m_\nu \simeq vev\phi^0 y_\nu M_R^{-1} y_\nu^T$ if one assumes that $M_R \gg vev\phi^0$. This situation is illustrated in Fig. 2.1.

After the spontaneous breaking of the gauge symmetry, we have the neutrino mass terms

$$\mathcal{L}_m^\nu = -m_D \bar{\nu}_L \nu_R - m_D^T \overline{(\nu_R)^c} (\nu_L)^c - \frac{1}{2} M_R \overline{(\nu_R)^c} \nu_R + h.c., \quad (2.1.13)$$

where $m_D = y_\nu v / \sqrt{2}$ is the Dirac neutrino mass matrix and we have used the fact: $\bar{\nu}_L \nu_R \equiv \overline{(\nu_R)^c} (\nu_L)^c$. Then, (2.1.13) can be re-packaged into:

$$-\mathcal{L}_m^\nu = \begin{pmatrix} \bar{\nu}_L & \overline{(\nu_R)^c} \end{pmatrix} \underbrace{\begin{pmatrix} 0 & m_D \\ m_D^T & M_R \end{pmatrix}}_{M_\nu} \begin{pmatrix} (\nu_L)^c \\ \nu_R \end{pmatrix} + h.c., \quad (2.1.14)$$

Using the assumption that all eigenvalues of m_D are much less than those of M_R , the neutrino mass matrix in (2.1.14) may be block-diagonalised (to first order in $m_D M_R^{-1}$) by:

$$M_\nu^{diag} = V M_\nu V^T \simeq \begin{pmatrix} -m_D M_R^{-1} m_D^T & 0 \\ 0 & -M_R \end{pmatrix}, \quad (2.1.15)$$

where

$$V = \begin{pmatrix} -1 & m_D M_R^{-1} \\ m_D^T M_R^{-1} & 1 \end{pmatrix} \begin{pmatrix} i & 0 \\ 0 & -i \end{pmatrix}. \quad (2.1.16)$$

The second matrix in the definition of (2.1.16) is included to ensure all mass eigenvalues are positive. Let

$$\begin{pmatrix} \nu' \\ N' \end{pmatrix} = V \begin{pmatrix} \nu_L \\ (\nu_R)^c \end{pmatrix}, \quad \begin{pmatrix} \nu'^c \\ N'^c \end{pmatrix} = V \begin{pmatrix} (\nu_L)^c \\ \nu_R \end{pmatrix},$$

and define a set of Majorana fields:

$$\begin{pmatrix} \nu \\ N \end{pmatrix} \equiv \begin{pmatrix} \nu' + \nu'^c \\ N' + N'^c \end{pmatrix}. \quad (2.1.17)$$

That is,

$$\begin{pmatrix} \nu \\ N \end{pmatrix} = V \begin{pmatrix} \nu_L + (\nu_L)^c \\ \nu_R + (\nu_R)^c \end{pmatrix}.$$

Therefore, the Lagrangian (2.1.14) becomes

$$\begin{aligned} \mathcal{L}_m^\nu &= (m_D M_R^{-1} m_D^T) \bar{\nu} \nu + M_R \bar{N} N + h.c. \\ &= m_\nu \bar{\nu} \nu + M_N \bar{N} N + h.c. . \end{aligned} \quad (2.1.18)$$

So from this, it is easy to see that this model gives rise to two sets of Majorana neutrinos: the light ones (ν) with mass matrix $m_\nu \simeq m_D M_R^{-1} m_D^T$, and the heavy ones (N) with $M_N \simeq M_R$.

Besides type I seesaw, there exist other extensions to the SM which can lead to the effective Majorana mass term in (2.1.3). These seesaw-like models provide alternative ways to understand the smallness of neutrino mass [235], and hence are of great interest to many model builders¹. So, we will briefly review some of them here.

In MSSM, and being MSSM singlets, the three, one per generation, added right handed neutrinos can have what is known by a “Majorana” mass term:

$$M \hat{N}^c \hat{N}^c. \quad (2.1.19)$$

Whenever there is no symmetry to prevent such a term to be allowed, it should be added into the superpotential, i.e. the relevant neutrino terms in the superpotential should be modified to be

$$\hat{W}^\nu = Y_\nu \hat{L}_L \hat{H}_u \hat{N}^c + M \hat{N}^c \hat{N}^c. \quad (2.1.20)$$

¹Small neutrino masses can also be generated without seesaw in models with extra dimensions [50, 175].

Inverse Seesaw

In the type I seesaw mechanism, we assume that the M_R is a very large scale. From another point view, M_R represents the strength of breaking the lepton number in the Lagrangian. That is, in the seesaw type I we assume that the lepton number is strongly violated, which is a non widely acceptable assumption in the physicists community. As a result, another types of seesaw mechanisms that ‘respects’² the lepton number arose. One of these mechanisms is the so called ”Inverse Seesaw” mechanism. The construction of this mechanism requires the existence of another SM singlet fermions S other than the RH neutrino ν_R . Explicitly, we have to add a fermion S whose lepton number is opposite to that of ν_R . In this case, the most general neutrino part of the Lagrangian is given by

$$\mathcal{L}_{\text{ISS}}^\nu = y_\nu \overline{\ell_L} \tilde{\phi} \nu_R + M_R \overline{(\nu_R)^c} S + y_S \overline{\ell_L} \tilde{\phi} S + \mu_R \overline{(\nu_R)^c} \nu_R + \mu_S \overline{(S)^c} S + h.c. , \quad (2.1.21)$$

where y_S , μ_R and μ_S are naturally small because of the so called ’t Hooft criteria. Indeed, in the limit y_S , μ_R , $\mu_S \rightarrow 0$, the lepton number is restored as a conserved symmetry.

After the electroweak symmetry breaking, the mass matrix of the neutrinos are given, for one generation, by

$$\begin{pmatrix} 0 & m_D & M_S \\ m_D^T & \mu_R & M_R \\ M_S^T & M_R^T & \mu_S \end{pmatrix}, \quad (2.1.22)$$

where $m_D = y_\nu v$ and $M_S = y_S v$. As mentioned before, $M_S, \mu_R, \mu_S \ll m_D, M_R$, thus the neutrino masses can be given, with a very good approximation, by

$$m_{\nu_\ell} = \frac{m_D(m_D \mu_S - 2M_R M_S)}{M_R^2 + m_D^2}, \quad (2.1.23)$$

$$m_{\nu_{H,H'}} = \frac{M_R(M_R \mu_S + 2m_D M_S)}{2(M_R^2 + m_D^2)} + \frac{\mu_R}{2} \mp \sqrt{M_R^2 + m_D^2}. \quad (2.1.24)$$

²‘respects’ here in the sense that the violation of the lepton number must be weak.

It is worth mentioning that in the ISS scenario, the neutrino Yukawa coupling can be of order $\mathcal{O}(1)$ and the large scale M_R can be brought to be the TeV scale. This is because the suppression factor needed to account for light neutrino masses are played by the naturally small parameters M_S, μ_S instead of the Yukawa coupling y_ν . Indeed, If $y_\nu \sim \mathcal{O}(1)$, $M_R \sim 1$ TeV and $\mu_S \sim 10 M_S \sim \mathcal{O}(10^{-7})$ GeV, then a 1 eV neutrino mass can be obtained.

In type I seesaw mechanism, we assume that the M is a very large scale. From another point view, M represents the strength of breaking the lepton number in the superpotential. That is, in seesaw type I we assume that the lepton number is strongly violated, which is a non widely acceptable assumption in the physicists community. As a result, another types of seesaw mechanisms that ‘respects’³ the lepton number arose. One of these mechanisms is the so called “Inverse Seesaw” mechanism. The construction of this mechanism requires the existence of another leptonic superfields other than the previously introduced right handed neutrino superfields. Explicitly, we have to add a superfield \hat{S} whose lepton number is opposite to that of \hat{N}^c . In this case, the most general neutrino part of the superpotential is given by

$$W^\nu = Y_\nu \hat{L}_L \hat{H}_u \hat{N}^c + M \hat{N}^c \hat{S} + Y_S \hat{L}_L \hat{H}_u \hat{S} + \mu_N \hat{N}^c \hat{N}^c + \mu_S \hat{S} \hat{S}, \quad (2.1.25)$$

where Y_S, μ_N and μ_S are naturally small because of the so called ’t Hooft criteria. Indeed, in the limit $Y_S, \mu_N, \mu_S \rightarrow 0$, the lepton number is restored as a conserved symmetry.

2.2 BLSSM Model

2.2.1 BLSSM Structure

The BLSSM is based on the gauge symmetry group $SU(3)_C \times SU(2)_L \times U(1)_Y \times U(1)_{B-L}$. This model is a natural extension of the MSSM, with: i) three chiral

³‘respects’ here in the sense that the violation of the lepton number must be weak.

2.2 BLSSM Model

singlet superfields \hat{N}_i introduced to cancel the $U(1)_{B-L}$ triangle anomaly and acting as RH neutrinos, thereby accounting for the measurements of light neutrino masses; ii) two chiral SM-singlet Higgs superfields $(\hat{\chi}_1, \hat{\chi}_2)$ with $B - L$ charge = ±2 for the spontaneously break the $U(1)_{B-L}$ gauge group; iii) a vector superfield, Z' , necessary to gauge $U(1)_{B-L}$.

The BLSSM model is a natural extension of the MSSM [214] with

- three RH neutrino chiral superfields (N_i), to account for measurements of light neutrino masses [27, 28, 167],
- two SM-singlet Higgs chiral superfields (χ_1, χ_2 with $B - L$ charges $Y_{BL} = -2, +2$, respectively). Their scalar components' vevs $v'_{1,2} = \langle \chi_{1,2} \rangle$ spontaneously break the $U(1)_{B-L}$,
- and a vector superfield necessary to gauge the $U(1)_{B-L}$.

The quantum numbers of the chiral superfields with respect to the SM gauge group ($\mathbb{G}_{\text{SM}} = SU(3)_C \otimes SU(2)_L \otimes U(1)_Y$) and $U(1)_{B-L}$ one are summarized in Table 3.1. The general expression for the covariant derivative D_μ is defined as

$$D_\mu = \partial_\mu - ig_s T^a G_\mu^a - ig \tau^i W_\mu^i - ig' Y B_\mu - ig'' Y_{B-L} B'_\mu, \quad (2.2.1)$$

where $T^a = \lambda^a/2$ and $\tau^i = \sigma^i/2$ and λ^a , ($a = 1 \cdots 8$) and σ^i , ($i = 1 \cdots 3$) are the Gell-mann and Pauli Matrices.

The full BLSSM superpotential is given by

$$W = Y_u^{ij} \hat{u}_i^c \hat{Q}_j \cdot \hat{H}_u - Y_d^{ij} \hat{d}_i^c \hat{Q}_j \cdot \hat{H}_d - Y_e^{ij} \hat{E}_i^c \hat{L}_j \cdot \hat{H}_d + Y_\nu^{ij} \hat{N}_i^c \hat{L}_j \cdot \hat{H}_u + \frac{1}{2} Y_N^{ij} \hat{N}_i^c \hat{\chi}_1 \hat{N}_j^c + \mu \hat{H}_u \cdot \hat{H}_d - \mu' \hat{\chi}_1 \hat{\chi}_2. \quad (2.2.2)$$

The superpotential of the BLSSM is given by [214]

$$W_{\text{BLSSM}} = (Y_u)_{ij} Q_i H_2 U_j^c + (Y_d)_{ij} Q_i H_1 D_j^c + (Y_e)_{ij} L_i H_1 E_j^c$$

Superfield	Spin-0	Spin- $\frac{1}{2}$	Generations	$\mathbb{G}_{\text{SM}} \otimes U(1)_{B-L}$
\hat{Q}	\tilde{Q}	Q	3	$(\mathbf{3}, \mathbf{2}, \frac{1}{6}, \frac{1}{6})$
\hat{d}^c	\tilde{d}^c	d^c	3	$(3, \mathbf{1}, \frac{1}{2}, -\frac{1}{6})$
\hat{u}^c	\tilde{u}^c	u^c	3	$(3, \mathbf{1}, -\frac{2}{3}, -\frac{1}{6})$
\hat{L}	\tilde{L}	L	3	$(\mathbf{1}, \mathbf{2}, -\frac{1}{2}, -\frac{1}{2})$
\hat{E}^c	\tilde{e}^c	e^c	3	$(\mathbf{1}, \mathbf{1}, 1, \frac{1}{2})$
\hat{N}^c	\tilde{N}^c	N^c	3	$(\mathbf{1}, \mathbf{1}, 0, \frac{1}{2})$
\hat{H}_d	H_d	\tilde{H}_d	1	$(\mathbf{1}, \mathbf{2}, -\frac{1}{2}, 0)$
\hat{H}_u	H_u	\tilde{H}_u	1	$(\mathbf{1}, \mathbf{2}, \frac{1}{2}, 0)$
$\hat{\chi}_1$	χ_1	$\tilde{\chi}_1$	1	$(\mathbf{1}, \mathbf{1}, 0, -1)$
$\hat{\chi}_2$	χ_2	$\tilde{\chi}_2$	1	$(\mathbf{1}, \mathbf{1}, 0, 1)$

Table 2.1: Chiral superfields and their quantum numbers in the BLSSM.

$$+ (Y_\nu)_{ij} L_i H_2 N_j^c + (Y_N)_{ij} N_i^c \chi_1 N_j^c + \mu H_1 H_2 + \mu' \chi_1 \chi_2. \quad (2.2.3)$$

The superpotential W_{BLSSM} can be decomposed into two parts

$$W_{\text{BLSSM}} = W_{\text{MSSM}} + W_{\text{BL}}, \quad (2.2.4)$$

where W_{MSSM} is the MSSM superpotential (1.2.6) and the extra part is due to the extra $B - L$ chiral and vector superfields

$$W_{\text{BL}} = (Y_\nu)_{ij} L_i H_2 N_j^c + (Y_N)_{ij} N_i^c \chi_1 N_j^c + \mu' \chi_1 \chi_2. \quad (2.2.5)$$

The BLSSM gauge invariant soft SUSY breaking terms are [31, 147]

- Gaugino masses for each gauge group (gluino, wino and bino):

$$-\frac{1}{2}(M_3 \tilde{g}^a \tilde{g}^a + M_2 \tilde{W}^a \tilde{W}^a + M_1 \tilde{B} \tilde{B} + M'_1 \tilde{B}' \tilde{B}') \quad (2.2.6)$$

- Squark mass terms:

$$-m_{\tilde{Q}_{ij}}^2 \tilde{Q}_i^\dagger \tilde{Q}_j - m_{\tilde{u}_{ij}}^2 \tilde{u}_{Li}^\dagger \tilde{u}_{Lj} - m_{\tilde{d}_{ij}}^2 \tilde{d}_{Li}^\dagger \tilde{d}_{Lj} \quad (2.2.7)$$

- Slepton mass terms:

$$-m_{\tilde{L}_{ij}}^2 \tilde{L}_i^\dagger \tilde{L}_j - m_{\tilde{e}_{ij}}^2 \tilde{\tilde{e}}_i^\dagger \tilde{\tilde{e}}_j - m_{\tilde{\nu}_{ij}}^2 \tilde{\tilde{\nu}}_i^\dagger \tilde{\tilde{\nu}}_j \quad (2.2.8)$$

- Higgs mass terms:

$$-m_{H_u}^2 H_u^\dagger H_u - m_{H_d}^2 H_d^\dagger H_d - (B_\mu H_u H_d + h.c.) - m_{\chi_1}^2 \chi_1^\dagger \chi_1 - m_{\chi_2}^2 \chi_2^\dagger \chi_2 - (B'_\mu \chi_1 \chi_2 + h.c.) \quad (2.2.9)$$

Triple scalar couplings

$$-a_u^{ij} \tilde{\tilde{u}}_{Li}^\dagger \tilde{Q}_j H_u - a_d^{ij} \tilde{\tilde{d}}_{Li}^\dagger \tilde{Q}_j H_d - a_e^{ij} \tilde{\tilde{e}}_{Li}^\dagger \tilde{L}_j H_d - a_\nu^{ij} \tilde{\tilde{\nu}}_{Li}^\dagger \tilde{L}_j H_u - a_n^{ij} \tilde{\tilde{\nu}}_{Ri}^\dagger \tilde{\nu}_j \chi_1 + h.c. \quad (2.2.10)$$

Accordingly, the BLSSM physical particle content has extra degrees of freedom than the MSSM, like: extra scalar and pseudoscalar Higgs $h'_{2,3}$, and A' , extra neutral gauge gauge boson Z' , extra RH Sneutrinos, extra gauginos (Zino prime) \tilde{Z}' , extra Higgsinos (the $B - L$ neutralinos) and, finally, extra Sneutrino and their Neutralinos. This way, the BLSSM has more supersymmetric particle, the lightest of which (LSP), expected in the MSSM to be stable, is a very attractive candidate for the nonbaryonic cold Dark Matter (DM) [147]. Also, the BLSSM suffers the same MSSM μ -problem but doubly due to the $B - L$ Higgs fields.

2.2.2 Gauge Kinetic Mixing in BLSSM

As already mentioned in the introduction, the presence of two Abelian gauge groups in combination with the given particle content gives rise to a new effect absent in the MSSM or other SUSY models with just one Abelian gauge group: the gauge kinetic mixing. To have simple forms of the tree level propagators, it is convenient to work in the basis in which the tree-level kinetic mixing is removed. By expressing the original $A_\mu^{1,2}$ fields in terms of the new fields denoted by A_μ^Y and A_μ^B (because they will play the roles of the weak hypercharge and extra $U(1)$ gauge bosons, respectively)

The most general kinetic term for two $U(1)$ gauge fields is invariant under any orthogonal transformation (rotation) of the gauge fields [102, 259].

$$\mathcal{L}_{U(1)}^{\text{kin}} = -\frac{1}{4}f_{\mu\nu}^1 f_{\mu\nu}^1 - \frac{1}{4}f_{\mu\nu}^2 f_{\mu\nu}^2 - \frac{\kappa}{2}f_{\mu\nu}^1 f_{\mu\nu}^2. \quad (2.2.11)$$

κ is a real constant constrained by the condition $|\kappa| < 1$. The most general covariant derivative of a matter field ψ_k is [102, 259]

$$\mathcal{D}_\mu = \partial_\mu + i \sum_{a,b=1}^2 Q_k^a g_{ab} A_\mu^b, \quad (2.2.12)$$

where the constants Q_k^a play the role of the $U(1)$ charges of ψ_k and g_{ab} are the coupling constants (running couplings in the $\overline{\text{MS}}$ renormalization scheme). The gauge transformations then are

$$A_\mu^a \rightarrow A_\mu^a + \partial_\mu \theta^a, \quad (2.2.13)$$

$$\psi_k \rightarrow \exp \left(-i \sum_{a,b=1}^2 Q_k^a g_{ab} \theta^b \right) \psi_k. \quad (2.2.14)$$

The existence of a whole matrix g_{ab} of couplings in place of only one gauge couplings per each $U(1)$ group factor is a peculiarity of the theory with multiple $U(1)$'s [259]. Even if not introduced in the original Lagrangian, the last term in (2.2.11) and the matrix g_{ab} of couplings are generated in the effective action by radiative corrections.

The kinetic Lagrangian (2.2.11), and the covariant derivative (2.2.12) can be written in matrix form as follows:

$$\mathcal{L}_{U(1)}^{\text{kin}} = -\frac{1}{4}f^T M f, \quad (2.2.15)$$

$$\mathcal{D}_\mu = \partial_\mu + i Q_k^T G A_\mu, \quad (2.2.16)$$

where $G = (g_{ab})$, and

$$f^T = (f_{\mu\nu}^1 \quad f_{\mu\nu}^2), \quad M = \begin{pmatrix} 1 & k \\ k & 1 \end{pmatrix} \quad (2.2.17)$$

$$Q_k^T = (Q_k^1 \quad Q_k^2), \quad A_\mu^T = (A_\mu^1 \quad A_\mu^2), \quad (2.2.18)$$

First, M can be diagonalized such that $M^{\text{diag}} = V^T M V = \text{diag}(\kappa_+, \kappa_-)$, where $\kappa_\pm = 1 \pm \kappa$, and

$$V = \frac{1}{\sqrt{2}} \begin{pmatrix} 1 & 1 \\ 1 & -1 \end{pmatrix} \quad (2.2.19)$$

This gives $f = V f'$ and

$$\mathcal{L}_{U(1)}^{\text{kin}} = -\frac{1}{4} f'^T M^{\text{diag}} f' = -\frac{\kappa_+}{4} f'_{\mu\nu} f'_{\mu\nu} - \frac{\kappa_-}{4} f'_{\mu\nu} f'_{\mu\nu} \quad (2.2.20)$$

For canonical kinetic terms, we normalize the field strengths such that

$$f'_{\mu\nu} = \frac{1}{\sqrt{\kappa_+}} f_{\mu\nu}^Y, \quad f'_{\mu\nu} = \frac{1}{\sqrt{\kappa_-}} f_{\mu\nu}^B \quad (2.2.21)$$

i.e., $f = V' f^{YB}$, where $f^{YB^T} = (f_{\mu\nu}^Y \quad f_{\mu\nu}^B)$, and $V' = V \text{diag}(\frac{1}{\sqrt{\kappa_+}}, \frac{1}{\sqrt{\kappa_-}})$. Thus

$$\mathcal{L}_{U(1)}^{\text{kin}} = -\frac{1}{4} f^{YB^T} f^{YB} = -\frac{1}{4} f_{\mu\nu}^Y f_{\mu\nu}^Y - \frac{1}{4} f_{\mu\nu}^B f_{\mu\nu}^B \quad (2.2.22)$$

This induces the transformation on the gauge fields $A = V' A^{YB}$. Explicitely,

$$A_\mu^1 = \frac{1}{\sqrt{2\kappa_+}} A_\mu^Y + \frac{1}{\sqrt{2\kappa_-}} A_\mu^B, \quad (2.2.23)$$

$$A_\mu^2 = \frac{1}{\sqrt{2\kappa_+}} A_\mu^Y - \frac{1}{\sqrt{2\kappa_-}} A_\mu^B, \quad (2.2.24)$$

and the redefinition of the couplings $G^{YB} = GV'$ such that

$$\mathcal{D}_\mu = \partial_\mu + i Q_k^T G A_\mu = \partial_\mu + i Q_k^T G^{YB} A_\mu^{YB}. \quad (2.2.25)$$

Upon removing the field strengths mixing in the Lagrangian, the gauge fields and couplings A^{YB} , G^{YB} are intended to be identified with the $U(1)_Y \times U(1)_E$ fields and couplings. However, more degree of freedom is available by rotating the gauge fields without changing the definitions of the charges. For this, the most general kinetic term

for two $U(1)$ gauge fields (2.2.22) is invariant under any orthogonal transformation (rotation) of the gauge fields [102, 259].

$$\tilde{A}^{YB} = \mathcal{O} A^{YB}, \quad A^{YB} = \begin{pmatrix} A_\mu^Y \\ A_\mu^B \end{pmatrix}, \quad \mathcal{O} = \begin{pmatrix} \cos \vartheta & -\sin \vartheta \\ \sin \vartheta & \cos \vartheta \end{pmatrix}. \quad (2.2.26)$$

This induces the redefinition of the couplings as

$$\mathcal{D}_\mu = \partial_\mu + iQ_k^T G^{YB} A^{YB} = \partial_\mu + iQ_k^T \tilde{G} \tilde{A}^{YB}, \quad (2.2.27)$$

where

$$\tilde{G} = G^{YB} \mathcal{O} = GV' \mathcal{O}, \quad (2.2.28)$$

and we notice that after all the gauge charges are untouched, and the rotation does not reintroduce the kinetic cross term [102, 259].

Appropriately, we choose ϑ such that at the EW scale the couplings have the form

$$G^{YB} = \begin{pmatrix} g_{YY} & g_{YB} \\ g_{BY} & g_{BB} \end{pmatrix} \rightarrow \tilde{G} = \begin{pmatrix} g_1 & \tilde{g} \\ 0 & g_{BL} \end{pmatrix} \quad (2.2.29)$$

This makes the appropriate choice

$$\tan \vartheta = -\frac{g_{BY}}{g_{BB}}. \quad (2.2.30)$$

where [102]:

$$\tilde{g}_{YY} = \frac{g_{YY}g_{BB} - g_{YB}g_{BY}}{\sqrt{g_{BB}^2 + g_{BY}^2}} = g_1 \quad (2.2.31)$$

$$\tilde{g}_{BB} = \sqrt{g_{BB}^2 + g_{BY}^2} = g_{BL} \quad (2.2.32)$$

$$\tilde{g}_{YB} = \frac{g_{YB}g_{BB} + g_{BY}g_{YY}}{\sqrt{g_{BB}^2 + g_{BY}^2}} = \tilde{g} \quad (2.2.33)$$

$$\tilde{g}_{BY} = 0 \quad (2.2.34)$$

With this convenient choice of basis, only the Higgs doublets contribute to the entries in the gauge boson mass matrix of the $U(1)_Y \otimes SU(2)_L$ sector and the impact of η and $\bar{\eta}$ is only in the off-diagonal elements as discussed later.

$$A^Y = \cos \vartheta \tilde{A}^Y - \sin \vartheta \tilde{A}^B, \quad (2.2.35)$$

$$A^B = \sin \vartheta \tilde{A}^Y + \cos \vartheta \tilde{A}^B. \quad (2.2.36)$$

where following combinations are the invariants of the rotation

$$\begin{aligned} g_{BB}g_{YY} - g_{BY}g_{YB}, & \quad g_{BB}^2 + g_{BY}^2, \\ g_{YB}g_{BB} + g_{BY}g_{YY}, & \quad g_{YY}^2 + g_{YB}^2. \end{aligned} \quad (2.2.37)$$

Immediate interesting consequences of the gauge kinetic mixing arise in various sectors of the model as discussed in the subsequent sections: (i) it induces mixing at tree level between the H_u , H_d and η , $\bar{\eta}$; (ii) additional D-terms contribute to the mass matrices of the squarks and sleptons; (iii) off-diagonal soft-SUSY breaking terms for the gauginos are induced via RGE evolution [92, 164] with important consequences for the neutralino sector as discussed in [259].

2.2.3 $B - L$ symmetry breaking

It is worth noting that the stability condition for

$$V(\chi_1, \chi_2) = \mu_1^2 |\chi_1|^2 + \mu_2^2 |\chi_2|^2 - \mu_3^2 (\chi_1 \chi_2 + h.c.) + \frac{1}{2} g_{BL}^2 (|\chi_2|^2 - |\chi_1|^2)^2, \quad (2.2.38)$$

is given by

$$2\mu_3^2 < \mu_1^2 + \mu_2^2. \quad (2.2.39)$$

Now to minimize such a potential, we equate $\frac{\partial V}{\partial \chi_i} = 0$, $i = 1, 2$. This leads to

$$\mu_1^2 = \mu_3^2 \cot \theta + \frac{M_{z'}^2}{4} \cos 2\theta, \quad (2.2.40)$$

$$\mu_2^2 = \mu_3^2 \tan \theta - \frac{M_{z'}^2}{4} \cos 2\theta. \quad (2.2.41)$$

From (2.2.40) and (2.2.41), we get

$$\sin 2\theta = \frac{2\mu_3^2}{m_{A'_0}^2}, \quad (2.2.42)$$

where $m_{A'_0}^2 := \mu_1^2 + \mu_2^2$. Also note that from (2.2.40),(2.2.41), we get

$$v'^2 = \frac{(\mu_1^2 - \mu_2^2) - (\mu_1^2 + \mu_2^2) \cos 2\theta}{2g_{BL}^2 \cos 2\theta} \quad (2.2.43)$$

Now we complete our analysis of symmetry breaking. We have

$$\begin{aligned} V_{11}(v'_1, v'_2) &= 2\mu_1^2 - 2g_{BL}^2(v'^2_2 - 3v'^2_1), \\ V_{12}(v'_1, v'_2) &= -2\mu_3^2 - 4g_{BL}^2v'_1v'_2, \\ V_{22}(v'_1, v'_2) &= 2\mu_2^2 + 2g_{BL}^2(3v'^2_2 - v'^2_1), \end{aligned}$$

where $V_{ij} := \frac{\partial^2 V(\chi_1, \chi_2)}{\partial \chi_i \partial \chi_j}$. Now, to be sure that the symmetry will be broken spontaneously, we must ensure that the point $(v'_1, v'_2) = (0, 0)$ is not a local minimum of the potential V . Since $(V_{11}V_{22} - V_{12}^2)(0, 0) = (2\mu_1^2)(2\mu_2^2) - (2\mu_3^2)^2$, and $V_{11}(0, 0) = 2\mu_1^2 > 0$, then we should impose a condition to make $(0, 0)$ a saddle point. This condition is

$$\mu_1^2 \mu_2^2 < \mu_3^4. \quad (2.2.44)$$

It is worth noting that it is impossible to simultaneously fulfill both the conditions (2.2.39) and (2.2.44) for positive values for μ_1^2 and μ_2^2 . To resolve this paradox, it must be clear that condition (2.2.39) is valid only at the GUT scale, while condition (2.2.44) is valid at the $B - L$ symmetry breaking scale. However, in the running of the RGEs, from the GUT scale down to the $B - L$ breaking scale, one finds that the masses of the Higgs singlets χ_1 and χ_2 run differently in the way that $m_{\chi_1}^2$ can become negative, whereas $m_{\chi_2}^2$ remains positive.

Indeed, let us consider the running of the scalar masses $m_{\chi_{1,2}}^2$ via the $B - L$ renormalization group equations. As is known, neglecting the Yukawa couplings of the first two generations for the SM quark and lepton is an acceptable approximation. This is because of the smallness of their masses, hence their Yukawas. However, for the Yukawa coupling Y_N , the situation is different because there is no constraints

2.2 BLSSM Model

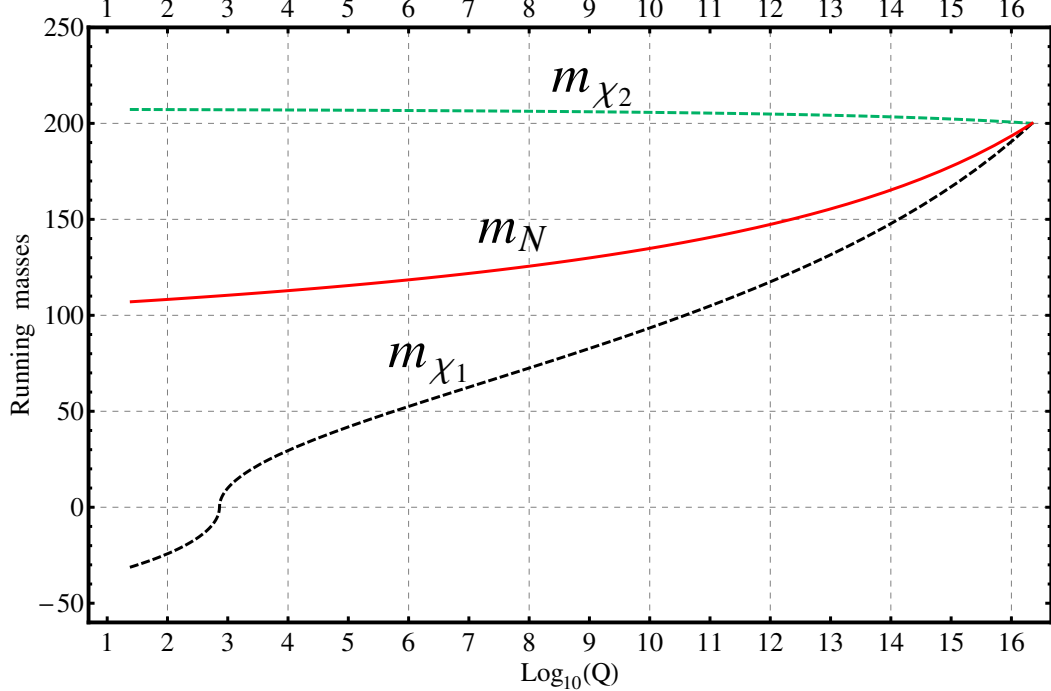


Figure 2.2: The evolution of the $B - L$ scalar masses from GUT to TeV scale for $m_0 = 200$ GeV, $M_{1/2} = A_0 = 100$ GeV and $Y_{N_3} \sim \mathcal{O}(1)$.

on the right handed neutrino Yukawa coupling to be hierarchical. In fact, we can assume, without loss of generality, that it is diagonal. Thus the RGEs of each $(Y_N)_{ii}$ is the same for $i = 1, 2, 3$. Also since there is no required hierarchy between the 3 RH neutrinos, we can assume a degenerate Yukawa coupling Y_N . That is we assume $(Y_N)_{ii} = (Y_N)_{33} =: Y_{N_3}$ for $i = 1, 2, 3$. In this respect, the RGEs for $\chi_{1,2}$ are given by [164, 290]

$$16\pi^2 \frac{dm_{\chi_1}^2}{dt} = -12g_{BL}^2 M_{BL}^2 + 12Y_{N_3}^2 (m_{\chi_1}^2 + 2m_{N_3}^2 + A_{N_3}^2), \quad (2.2.45)$$

$$16\pi^2 \frac{dm_{\chi_2}^2}{dt} = -12g_{BL}^2 M_{BL}^2, \quad (2.2.46)$$

and in order to solve these equations we should take into account the following RGEs

$$16\pi^2 \frac{dg_{BL}}{dt} = 9g_{BL}^3, \quad (2.2.47)$$

$$16\pi^2 \frac{dM_{BL}}{dt} = 18g_{BL}^2 M_{BL}, \quad (2.2.48)$$

$$16\pi^2 \frac{dY_{N_3}}{dt} = Y_{N_3} \left(-\frac{9}{2}g_{BL}^2 + 14Y_{N_3}^2 \right), \quad (2.2.49)$$

$$16\pi^2 \frac{dm_{N_3}^2}{dt} = -3g_{BL}^2 M_{BL}^2 + 8Y_{N_3}^2 (m_{\chi_1}^2 + 2m_{N_3}^2 + A_{N_3}^2), \quad (2.2.50)$$

$$16\pi^2 \frac{dA_{N_3}}{dt} = 28Y_{N_3}^2 A_{N_3} + 9g_{BL}^2 M_{BL}. \quad (2.2.51)$$

The evolution of these mass parameters depends on the boundary conditions at GUT scale. As mentioned before, we assume universal soft SUSY breaking at this scale. That is we have

$$m_{\chi_1}^2(\text{GUT}) = m_{\chi_2}^2(\text{GUT}) = m_{N_3}^2(\text{GUT}) = m_0^2, \quad (2.2.52)$$

$$M_{BL}(\text{GUT}) = M_{1/2}, \quad (2.2.53)$$

$$A_{N_3}(\text{GUT}) = A_0. \quad (2.2.54)$$

Fig. 2.2 reports the result of the running. In this figure, we set $m_0 = 200$ GeV, $M_{1/2} = A_0 = 100$ GeV and order one $Y_{N_3} \simeq M_{N_3}/v'$ is assumed. As can be seen from this figure, $m_{\chi_1}^2$ drops rapidly to negative region, while $m_{\chi_2}^2$ remains positive. Analogously to the radiative electroweak symmetry breaking, this mechanism works for large Yukawa coupling. Also in Fig. 2.2, we plot the scale evolution for the scalar mass $m_{N_3}^2$. Although $m_{N_3}^2$ decreases in the running from M_X , it remains positive at the TeV scale. Therefore, the $B - L$ breaking via a non-vanishing vacuum expectation value for right-handed sneutrino does not occur in the present framework.

2.2.4 BLSSM Spectrum

After $B - L$ symmetry breaking, the new gauge boson, Z' , acquires its mass from the kinetic term of the $B - L$ Higgs fields, $\chi_{1,2}$. Namely we have

$$M_{Z'}^2 = g_{BL}^2 \left([Y_{B-L}(\chi_1)]^2 v_1'^2 + [Y_{B-L}(\chi_2)]^2 v_2'^2 \right)$$

$$= g_{BL}^2 v'^2, \quad (2.2.55)$$

where

$$v' := \sqrt{v_1'^2 + v_2'^2}, \quad v'_i := \langle \chi_i \rangle, \quad \tan \theta := \frac{v'_1}{v'_2}. \quad (2.2.56)$$

It is worth mentioning that the mass of the Z' gauge boson has the experimental bound [48, 96]

$$M_{Z'}/g_{BL} > 6 \text{ TeV}. \quad (2.2.57)$$

The tree level mass matrix of the neutral CP-even Higgs bosons is given by

$$\begin{aligned} (M_V^2)_{ij} &= \frac{1}{2} \frac{\partial^2 V}{\partial \chi_i \partial \chi_j}(v'_1, v'_2) \\ &= \begin{pmatrix} \mu_1^2 - g_{BL}^2(v_2'^2 - 3v_1'^2) & -\mu_3^2 - 2g_{BL}^2 v'_1 v'_2 \\ -\mu_3^2 - 2g_{BL}^2 v'_1 v'_2 & \mu_2^2 + g_{BL}^2(3v_2'^2 - v_1'^2) \end{pmatrix}. \end{aligned}$$

Therefore, the eigenvalues of this mass matrix is given by

$$M_{h',H'}^2 = \frac{1}{2} \left[(m_{A'_0}^2 + M_{z'}^2) \mp \sqrt{(m_{A'_0}^2 + M_{z'}^2)^2 - 4m_{A'_0}^2 M_{z'}^2 \cos^2 2\theta} \right]. \quad (2.2.58)$$

It is worth noting that the $B - L$ extension does not affect the chargino mass matrix, that is, it will be exactly the same as that of MSSM. This is not the case in the neutralino mass matrix. It will be extended to be a 7×7 mass matrix. This happens as a consequence of the existence of the additional neutral states \tilde{Z}_{B-L} , $\tilde{\chi}_1$, $\tilde{\chi}_2$. Thus,

the neutralino mass matrix is given by

$$m_{\tilde{\chi}^0} = \left(\begin{array}{c|ccccccc} & \tilde{B} & \tilde{W}^0 & \tilde{H}_d^0 & \tilde{H}_u^0 & \tilde{Z}_{B-L} & \tilde{\chi}_1 & \tilde{\chi}_2 \\ \hline \tilde{B} & M_1 & 0 & -\frac{1}{2}g_1 v_d & \frac{1}{2}g_1 v_u & 0 & 0 & 0 \\ \tilde{W}^0 & 0 & M_2 & \frac{1}{2}g_2 v_d & -\frac{1}{2}g_2 v_u & 0 & 0 & 0 \\ \tilde{H}_d^0 & -\frac{1}{2}g_1 v_d & \frac{1}{2}g_2 v_d & 0 & -\mu & 0 & 0 & 0 \\ \tilde{H}_u^0 & \frac{1}{2}g_1 v_u & -\frac{1}{2}g_2 v_u & -\mu & 0 & 0 & 0 & 0 \\ \tilde{Z}_{B-L} & 0 & 0 & 0 & 0 & M_{B-L} & -g_{BL} v'_1 & g_{BL} v'_2 \\ \tilde{\chi}_1 & 0 & 0 & 0 & 0 & -g_{BL} v'_1 & 0 & -\mu' \\ \tilde{\chi}_2 & 0 & 0 & 0 & 0 & g_{BL} v'_2 & -\mu' & 0 \end{array} \right). \quad (2.2.59)$$

It is clear that this 7×7 matrix can be safely splitted into two mass matrices, the MSSM neutralino 4×4 mass matrix and an extra 3×3 mass matrix.

2.2.5 BLSSM Higgs Sector

The Higgs potential in terms of components is

$$\begin{aligned} V(H, \chi) = & |\mu|^2(|H_u^0|^2 + |H_d^0|^2) + |\mu'|^2(|\chi_1|^2 + |\chi_2|^2) + \frac{g^2}{8}(|H_u^0|^2 - |H_d^0|^2)^2 \\ & + \frac{g_{BL}^2}{2}(|\chi_1|^2 - |\chi_2|^2)^2 - \frac{\tilde{g}g_{BL}}{4}(|H_u^0|^2 - |H_d^0|^2)(|\chi_1|^2 - |\chi_2|^2) \\ & - m_u^2|H_u^0|^2 - m_d^2|H_d^0|^2 + B_\mu H_u^0 H_d^0 - m_1^2|\chi_1|^2 - m_2^2|\chi_2|^2 - B_{\mu'} \chi_1 \chi_2 \end{aligned} \quad (2.2.60)$$

where $g^2 = g_1^2 + g_2^2 + \tilde{g}^2$.

The relevant hypercharge and $B - L$ contributions to the scalar potential of the Higgs fields is of the gauge D -term. The $U(1)_Y \times U(1)_{B-L}$ kinetic mixing induces the following D -term mixing of both groups [259, 291]

$$V_D^{U(1)}(H) = \frac{1}{2} \sum_{i,j} (\phi_i^\dagger \phi_i) (Q_i^T G) (G^T Q_j) (\phi_j^\dagger \phi_j), \quad (2.2.61)$$

$$G = \begin{pmatrix} g_Y & \tilde{g} \\ 0 & g_{BL} \end{pmatrix}, \quad Q_i = \begin{pmatrix} Q_Y \\ Q_{BL} \end{pmatrix}_i, \quad \phi_i = H_u, H_d, \chi_1, \chi_2, \quad (2.2.62)$$

2.2 BLSSM Model

where the $U(1)_{B-L}$ charge is given by $Q_{BL} = (B - L)/2$. This form of G has the advantage that the new scalars do not contribute to the electroweak vev, and the entire impact of gauge kinetic mixing is encoded in one new coupling \tilde{g} [259, 291].

We expand the neutral components

$$H_{u,d}^0 = \frac{1}{\sqrt{2}}(v_{u,d} + \sigma_{u,d} + i\phi_{u,d}), \quad \chi_{1,2} = \frac{1}{\sqrt{2}}(x_{1,2} + \sigma_{1,2} + i\phi_{1,2}) \quad (2.2.63)$$

The scalar higgs mass matrix is the following block in the basis $(\sigma_u, \sigma_d, \sigma_1, \sigma_2)$:

$$M_H^2 = \begin{pmatrix} M_{HH}^2 & M_{H\chi}^2 \\ \cdot & M_{\chi\chi}^2 \end{pmatrix} \quad (2.2.64)$$

where the dot (\cdot) is for the symmetry of the full matrix and the off-diagonal block mixing of both the MSSM and $B - L$ sectors is

$$M_{H\chi}^2 = \frac{1}{2}\tilde{g}g_{BL} \begin{pmatrix} -v_u v_1 & v_u v_2 \\ v_d v_1 & -v_d v_2 \end{pmatrix} = \frac{vx}{2}\tilde{g}g_{BL} \begin{pmatrix} -s_\beta s_{\beta'} & s_\beta c_{\beta'} \\ c_\beta s_{\beta'} & -c_\beta c_{\beta'} \end{pmatrix} \quad (2.2.65)$$

The MSSM higgs mass matrix M_{HH}^2 is given by in the basis (σ_u, σ_d)

$$\begin{pmatrix} \frac{\tilde{g}g_{BL}}{4}x^2c_{2\beta'} + \frac{1}{8}g^2v^2(23s_\beta^2 - 7c_\beta^2) + \frac{B_\mu}{t_\beta} & -B_\mu - \frac{g^2}{4}v^2s_{2\beta} \\ \cdot & -\frac{\tilde{g}g_{BL}}{4}x^2c_{2\beta'} - \frac{1}{8}g^2v^2(7s_\beta^2 - 23c_\beta^2) + B_\mu t_\beta \end{pmatrix} \quad (2.2.66)$$

and the $B - L$ higgs mass matrix $M_{\chi\chi}^2$ is given by in the basis (σ_1, σ_2)

$$\begin{pmatrix} \frac{\tilde{g}g_{BL}}{4}v^2c_{2\beta} + \frac{1}{2}g_{BL}^2x^2(23s_{\beta'}^2 - 7c_{\beta'}^2) + \frac{B'_\mu}{t_{\beta'}} & -B_{\mu'} - g_{BL}^2x^2s_{2\beta'} \\ \cdot & -\frac{\tilde{g}g_{BL}}{4}v^2c_{2\beta} - \frac{1}{2}g_{BL}^2x^2(7s_{\beta'}^2 - 23c_{\beta'}^2) + B'_\mu t_{\beta'} \end{pmatrix} \quad (2.2.67)$$

$$B_\mu = t_{2\beta}(-\frac{1}{8}g^2v^2c_{2\beta} + \frac{1}{4}g_{BL}\tilde{g}x^2c_{2\beta'} - \frac{1}{2}(m_d^2 - m_u^2)) \quad (2.2.68)$$

$$B'_\mu = t_{2\beta'}(-\frac{1}{2}g_{BL}^2x^2c_{2\beta'} + \frac{1}{4}g_{BL}\tilde{g}v^2c_{2\beta} - \frac{1}{2}(m_2^2 - m_1^2)). \quad (2.2.69)$$

The heavy Higgs bosons tree-level mass eigenvalues are given in terms of the lightest SM-like Higgs boson $h \equiv h_1$ mass which is fixed at $m_h = 125$ GeV, and the next lightest Higgs boson $h' \equiv h_2$ mass $m_{h'} = 400$ GeV as follows

$$m_{H,H'}^2 = \frac{1}{2} \left[T_H - m_h^2 - m_{h'}^2 \pm \sqrt{(T_H - m_h^2 - m_{h'}^2)^2 - \frac{4D_H}{m_h^2 m_{h'}^2}} \right], \quad (2.2.70)$$

where the determinant $D_H = \text{Det}(M_H^2)$ and the trace $T_H = \text{Tr}(M_H^2)$ is given by

$$T_H = 2|\mu|^2 + m_d^2 + m_u^2 + 2g^2v^2 + 2|\mu'|^2 + m_2^2 + m_1^2 + 8g_{BL}^2x^2. \quad (2.2.71)$$

Tadpole Equations and Potential Minimization

The minimum of the Higgs potential (2.2.60) is

$$\begin{aligned} \langle V \rangle &= V(\langle H \rangle, \langle \chi \rangle) = |\mu|^2(v_u^2 + v_d^2) + |\mu'|^2(v_1^2 + v_2^2) \\ &\quad + \frac{g^2}{8}(v_u^2 - v_d^2)^2 - \frac{\tilde{g}g_{BL}}{4}(v_u^2 - v_d^2)(v_1^2 - v_2^2) + \frac{g_{BL}^2}{2}(v_1^2 - v_2^2)^2 \\ &\quad - m_u^2v_u^2 - m_d^2v_d^2 - 2v_u v_d B_\mu - m_1^2v_1^2 - m_2^2v_2^2 - 2v_1 v_2 B_{\mu'} \end{aligned} \quad (2.2.72)$$

where the vevs satisfy the following tadpole equations [259]

$$\frac{1}{2} \frac{\partial \langle V \rangle}{\partial v_u} = v_u \{ |\mu|^2 + m_u^2 - \frac{1}{8}g^2(v_d^2 - v_u^2) + \frac{1}{4}g_{BL}\tilde{g}(v_2^2 - v_1^2) \} - B_\mu v_d = 0, \quad (2.2.73)$$

$$\frac{1}{2} \frac{\partial \langle V \rangle}{\partial v_d} = v_d \{ |\mu|^2 + m_d^2 + \frac{1}{8}g^2(v_d^2 - v_u^2) - \frac{1}{4}g_{BL}\tilde{g}(v_2^2 - v_1^2) \} - B_\mu v_u = 0, \quad (2.2.74)$$

$$\frac{1}{2} \frac{\partial \langle V \rangle}{\partial v_1} = v_1 \{ |\mu'|^2 + m_1^2 - \frac{1}{2}g_{BL}^2(v_2^2 - v_1^2) + \frac{1}{4}g_{BL}\tilde{g}(v_d^2 - v_u^2) \} - B'_\mu v_2 = 0, \quad (2.2.75)$$

$$\frac{1}{2} \frac{\partial \langle V \rangle}{\partial v_2} = v_2 \{ |\mu'|^2 + m_2^2 + \frac{1}{2}g_{BL}^2(v_2^2 - v_1^2) - \frac{1}{4}g_{BL}\tilde{g}(v_d^2 - v_u^2) \} - B'_\mu v_1 = 0. \quad (2.2.76)$$

Before we solve them, we manipulate for some substitutions

$$|\mu|^2 + m_u^2 = \frac{1}{8}g^2(v_d^2 - v_u^2) - \frac{1}{4}g_{BL}\tilde{g}(v_2^2 - v_1^2) + \frac{B_\mu}{t_\beta}, \quad (2.2.77)$$

$$|\mu|^2 + m_d^2 = -\frac{1}{8}g^2(v_d^2 - v_u^2) + \frac{1}{4}g_{BL}\tilde{g}(v_2^2 - v_1^2) + B_\mu t_\beta, \quad (2.2.78)$$

$$|\mu'|^2 + m_1^2 = \frac{1}{2}g_{BL}^2(v_2^2 - v_1^2) - \frac{1}{4}g_{BL}\tilde{g}(v_d^2 - v_u^2) + \frac{B'_\mu}{t_{\beta'}}, \quad (2.2.79)$$

$$|\mu'|^2 + m_2^2 = -\frac{1}{2}g_{BL}^2(v_2^2 - v_1^2) + \frac{1}{4}g_{BL}\tilde{g}(v_d^2 - v_u^2) + B'_\mu t_{\beta'}. \quad (2.2.80)$$

We solve them for μ , μ' , B_μ and $B_{\mu'}$ as follows

$$\begin{aligned} |\mu|^2 &= \frac{g^2(v_d^4 - v_u^4) + 2g_{BL}\tilde{g}(v_d^2 - v_u^2)(v_2^2 - v_1^2) - 8(m_u^2 v_u^2 - m_d^2 v_d^2)}{8(v_u^2 - v_d^2)} \\ &= -\frac{1}{8}g^2 v^2 - \frac{1}{4}g_{BL}\tilde{g}x^2 c_{2\beta'} - \frac{1}{2}s c_{2\beta}(m_d^2 - m_u^2) - \frac{1}{2}(m_d^2 + m_u^2) \end{aligned} \quad (2.2.81)$$

$$\begin{aligned} |\mu'|^2 &= \frac{2g_{BL}^2(v_2^4 - v_1^4) + g_{BL}\tilde{g}(v_d^2 - v_u^2)(v_2^2 - v_1^2) - 4(m_1^2 v_1^2 - m_2^2 v_2^2)}{4(v_1^2 - v_2^2)} \\ &= -\frac{1}{2}g_{BL}^2 x^2 - \frac{1}{4}g_{BL}\tilde{g}v^2 c_{2\beta} - \frac{1}{2}s c_{2\beta'}(m_2^2 - m_1^2) - \frac{1}{2}(m_2^2 + m_1^2) \end{aligned} \quad (2.2.82)$$

$$\begin{aligned} B_\mu &= \frac{v_u v_d (g^2(v_d^2 - v_u^2) - 2g_{BL}\tilde{g}(v_2^2 - v_1^2) + 4(m_d^2 - m_u^2))}{4(v_u^2 - v_d^2)} \\ &= t_{2\beta}(-\frac{1}{8}g^2 v^2 c_{2\beta} + \frac{1}{4}g_{BL}\tilde{g}x^2 c_{2\beta'} - \frac{1}{2}(m_d^2 - m_u^2)) \end{aligned} \quad (2.2.83)$$

$$\begin{aligned} B'_\mu &= \frac{v_1 v_2 (2g_{BL}^2(v_2^2 - v_1^2) - g_{BL}\tilde{g}(v_d^2 - v_u^2) + 2(m_2^2 - m_1^2))}{2(v_1^2 - v_2^2)} \\ &= t_{2\beta'}(-\frac{1}{2}g_{BL}^2 x^2 c_{2\beta'} + \frac{1}{4}g_{BL}\tilde{g}v^2 c_{2\beta} - \frac{1}{2}(m_2^2 - m_1^2)). \end{aligned} \quad (2.2.84)$$

Similar to the MSSM, the BLSSM enjoys the radiative $B - L$ symmetry breaking as well. In BLSSM, it was shown that it is possible to link together the electroweak, $B - L$ and soft SUSY breakings at a scale of $\mathcal{O}(\text{TeV})$ [214]. Moreover, the BLSSM improves the heirarchy problem of the Higgs boson mass and the pushes the upper limits imposed by SUSY in MSSM to a higher value . It was shown that the upper bound on the Higgs mass can be enhanced to be around 200 GeV by from the one-loop radiative corrections due to the RH (s)neutrinos in a BLSSM with inverse seesaw mechanism [156, 212].

2.2.6 BLSSM Gauge Sector

Now we turn to the gauge sector of the BLSSM. The two scalars vevs $v_1 = \langle \chi_1 \rangle$ and $v_2 = \langle \chi_2 \rangle$ break the $U(1)_{BL}$ symmetry at the TeV scale and we get the $B - L$ heavy massive neutral boson Z_μ^{BL} with mass $g_{BL}x \sim \mathcal{O}(\text{TeV})$, with $v' = \sqrt{v_1^2 + v_2^2}$ for $v_1 = xs_\beta'$ and $v_2 = xc_\beta'$. After that, the electroweak symmetry $SU(2)_L \times U(1)_Y$ is broken down to $U(1)_{\text{em}}$ by the electroweak Higgs vevs $v_u = \langle H_u^0 \rangle$ and $v_d = \langle H_d^0 \rangle$ and the electroweak vev is given by $v = \sqrt{v_u^2 + v_d^2}$ with $v_u = vs_\beta$ and $v_d = vc_\beta$ and it is fixed such that $v = 246$ GeV and the Weinberg angle as $s_w^2 = 0.230$ [295]. As we did not extend the charged gauge boson sector, the electroweak charged W^\pm gauge bosons have a mass $M_W = g_2 v/2$. The neutral gauge bosons sector is more involved due to the extra Z' boson and the $U(1)$ -kinetic mixing. Thus, one can show that the (symmetric) mass matrix in the basis (W_μ^3, B_μ, B'_μ) , is given by [69, 259]

$$M_{WBB'}^2 = \frac{v^2}{4} \begin{pmatrix} g_2^2 & -g_2 g_1 & g_2 \tilde{g} \\ . & g_1^2 & -g_1 \tilde{g} \\ . & . & \tilde{g}^2 + 4\left(\frac{x}{v}\right)^2 g_{BL}^2 \end{pmatrix}. \quad (2.2.85)$$

After the first rotation we obtain the photon A_μ and the weak neutral gauge boson Z_μ^W . However, both Z_μ^W and $B - L$ neutral gauge boson Z_μ^{BL} mix via the $U(1)_Y \times U(1)_{BL}$ kinetic mixing, as mentioned above, and the physical light Z_μ and heavy Z'_μ neutral gauge bosons are given by

$$\begin{pmatrix} A_\mu \\ Z_\mu^W \end{pmatrix} = \begin{pmatrix} c_w & s_w \\ -s_w & c_w \end{pmatrix} \begin{pmatrix} B_\mu \\ W_\mu^3 \end{pmatrix}, \quad \begin{pmatrix} Z_\mu \\ Z'_\mu \end{pmatrix} = \begin{pmatrix} c_{w'} & s_{w'} \\ -s_{w'} & c_{w'} \end{pmatrix} \begin{pmatrix} Z_\mu^W \\ Z_\mu^{BL} \end{pmatrix}. \quad (2.2.86)$$

The weak and $B - L$ neutral gauge bosons (Z_μ^W, Z_μ^{BL}) mixing matrix is

$$M_{Z^W Z^{BL}}^2 = \frac{v^2}{4} \begin{pmatrix} g'^2 & -\tilde{g}g' \\ . & \tilde{g}^2 + 4\left(\frac{x}{v}\right)^2 g_{BL}^2 \end{pmatrix}. \quad (2.2.87)$$

where $g' = \sqrt{g_2^2 + g_1^2}$ and $M_0 = g'v/2$ is the Z boson mass without $Z - Z'$ mixing. This leads to the total mixing $(B_\mu, W_\mu^3, B'_\mu)^T = (U^0)^T (A_\mu, Z_\mu, Z'_\mu)^T$, where

$U^0 M_{WBB'}^2 (U^0)^T = \text{diag}(0, M_Z^2, M_{Z'}^2)$ and the rotation matrix U^0 is

$$U^0 = \begin{pmatrix} c_w & s_w & 0 \\ -c_{w'} s_w & c_{w'} c_w & s_{w'} \\ s_{w'} s_w & -s_{w'} c_w & c_{w'} \end{pmatrix}, \quad (2.2.88)$$

where $s_x = \sin x$, $c_x = \cos x$ and $t_x = \tan x$, and the Weinberg angle $s_w = e/g_2$. The $Z - Z'$ mixing angle is given by [69, 259]

$$t_{2w'} = \frac{2\tilde{g}g'}{4(\frac{x}{v})^2 g_{BL}^2 + \tilde{g}^2 - g'^2} \quad (2.2.89)$$

For the $Z - Z'$ mixing experimental constraints, one has $t_{2w'} \approx t_{w'} \approx s_{w'} \lesssim 10^{-3}$ [260, 261]. To the first order in the $Z - Z'$ mixing, the Z and Z' masses are given by

$$M_Z^2 \approx \frac{g'^2 v^2}{4} - \frac{\tilde{g}g' v^2}{8} t_{2w'}, \quad (2.2.90)$$

$$M_{Z'}^2 \approx \frac{(4(\frac{x}{v})^2 g_{BL}^2 + \tilde{g}^2)v^2}{4} + \frac{\tilde{g}g' v^2}{8} t_{2w'}. \quad (2.2.91)$$

It is worthy to mention that the $Z - Z'$ identically vanishes if and only if $\tilde{g} = 0$. However, for $x \gg v$ we have small mixing which is consistent with the experimental constraints, but with a quite large \tilde{g} such that the Z and Z' couplings with the Higgs bosons are not neglegible and consistent with the Z' searches as clarified first in Ref. [15].

3

PHENOMENOLOGY OF BLSSM

3.1 Introduction

The search for a heavy neutral CP-even Higgs boson at the current Run 3 of the LHC and a future HL-LHC is an active area of research [5, 6, 23, 64, 67, 107, 176, 188, 302]. This is so because virtually any extension of the Higgs sector beyond the single doublet structure of the SM, in which the only neutral CP-even state of it is identified with the particle that was discovered in 2012 at the LHC by the ATLAS and CMS experiments [3, 103], contains it. As a result, currently, probing such a heavy Higgs boson is one of the main goals of the LHC experiments, as it could well provide the first hint for BSM physics. Both ATLAS and CMS have searched for a heavy Higgs boson and the corresponding analyses typically involve looking for events in which the heavy Higgs boson is produced and then decays into SM particles, such as W^\pm or Z bosons, in turn decaying into leptons or jets [5], or into the SM Higgs boson itself [109], which then decays into, e.g., photons, b -quarks or τ leptons.

Supersymmetric extensions of the SM are one of the BSM frameworks that consistently predict the existence of several Higgs bosons, including a heavy neutral CP-even one. Such a Higgs boson mass can be significantly larger than the one of the SM Higgs state, potentially reaching several hundred GeV. For example, the MSSM

3.1 Introduction

contains five Higgs bosons: two CP-even (h and H , with $m_h < m_H$), one CP-odd (A) and two charged states (H^+ and H^-): for reviews, see, e.g., [145]. This is the simplest construct implementing supersymmetry, where the lightest CP-even Higgs boson, h , is designated as the SM Higgs boson, with a mass of 125 GeV, which, however, imposes a strenuous configuration on the MSSM parameter space, forcing the other CP-even Higgs boson, H , to be rather heavy and significantly decoupled. However, if supersymmetry is non-minimal, in either its gauge or Higgs sector or both, then the mass of additional CP-even Higgs states can become rather less constrained [254]. An example of this is the so-called BLSSM, which indeed offers the possibility of LHC signals for a CP-even Higgs state not only above the SM Higgs mass, e.g., in the range up to 500 GeV [188], but also afford one with a lighter mass spectrum, in turn able to explain past [15, 187] and present data anomalies [16].

The BLSSM is a theoretical extension of the MSSM that includes an additional $U(1)$ gauge symmetry known as $B - L$ (baryon number minus lepton number) [69, 70, 214, 259] as well as an extended Higgs sector. The $B - L$ symmetry is motivated by the observation that the difference between baryon and lepton number is conserved in many particle physics processes. In the BLSSM, the $B - L$ symmetry may be broken at the few TeV scale, giving rise to new particles such as two new extra neutral CP-even Higgs bosons. One of them, labeled h' , can have energies in the hundreds of GeV range. It is indeed the presence of such a h' state that causes the aforementioned new phenomenology to emerge in collider experiments, which can then be used to test the BLSSM hypothesis.

We emphasize that the SM-like Higgs state, henceforth labeled by h , is derived from the real parts of the neutral components of the Electro-Weak (EW) scalar doublets H_u and H_d whereas the (typically) next-to-lightest Higgs boson, h' , stems from the real parts of the neutral components of the $B - L$ scalar singlets χ_1 and χ_2 . Despite the fact that the mass mixing between these two types of Higgs bosons is

negligible, a non-vanishing kinetic mixing allows for relevant couplings between h' and the SM particles, resulting in a total cross section of h' production and decay into W^+W^- , ZZ or hh of $\mathcal{O}(1)$ fb. These signals are typically smaller than the associated backgrounds but, by using appropriate selection strategies, they can be probed with a reasonably high sensitivity. However, given that current experimental limits have significantly constrained also the BLSSM parameter space above and beyond what allowed for in Ref. [188], which targeted Run 2 sensitivities, we revisit here the scope of Run 3 and the HL-LHC in accessing the heavy neutral CP-even Higgs boson of the BLSSM, h' , in the mass region of 400 GeV or so. It is also worth mentioning that heavy Higgs boson searches have been conducted in many supersymmetric (and non-supersymmetric) extensions of the SM. Indeed, the BLSSM itself has been phenomenologically investigated rather widely in relation to Higgs, dark matter and heavy gauge boson physics due to its many degrees of freedom and its wide parameter space [13–16, 44, 53, 71, 79, 91, 143, 156, 160, 187, 188, 304]. Specifically, for heavy Higgs bosons, the situation in the BLSSM is significantly different from that of the MSSM, where the SM-like Higgs boson mass and couplings constrain the heavy Higgs boson phenomenology greatly. In contrast, in the BLSSM, while the Higgs bosons of MSSM origin are just as restricted as in the actual minimal model, the constraints on the other Higgs bosons from the $B - L$ sector are much relaxed in comparison.

The paper is organized as follows. We briefly review the BLSSM particle content, superpotential and gauge structure in Sec. 3.2, where we also discuss at some length its Higgs sector. Studies of h' signals at the LHC are then carried out in Sec. 3.3, wherein a detailed Monte Carlo (MC) analysis for h' production via (mostly) gluon-gluon fusion (ggF) and decay via $W^+W^- \rightarrow 2\ell + \cancel{E}_T$, $ZZ \rightarrow 4\ell$ and $hh \rightarrow b\bar{b}\gamma\gamma$ is performed. Our conclusions and final remarks are given in Sec. 6.4.

3.2 The BLSSM BPs and Spectrum

The BLSSM is based on the gauge symmetry group $SU(3)_C \otimes SU(2)_L \otimes U(1)_Y \otimes U(1)_{B-L}$. This model is a natural extension of the MSSM, with: i) three chiral singlet superfields \hat{N}_i introduced to cancel the $U(1)_{B-L}$ triangle anomaly and acting as right-handed neutrinos, thereby accounting for the measurements of light neutrino masses; ii) two chiral SM-singlet Higgs superfields $(\hat{\chi}_1, \hat{\chi}_2)$ with $B-L$ charge = ±2 to spontaneously break the $U(1)_{B-L}$ gauge group; iii) a vector superfield, Z' , necessary to gauge $U(1)_{B-L}$. The quantum numbers of the chiral superfields with respect to the SM gauge group ($\mathbb{G}_{SM} = SU(3)_C \otimes SU(2)_L \otimes U(1)_Y$) and the $U(1)_{B-L}$ one are summarized in Table 3.1, where the $U(1)_{Y,B-L}$ charges generators are given by $Q_Y = Y/2$, $Q_{BL} = B - L$ and the covariant derivative is $D_\mu \supset -i[g_1 Q_Y V_\mu + (\tilde{g} Q_Y + g_{BL} Q_{BL}) V'_\mu]$, where \tilde{g} is the gauge kinetic mixing, as discussed below, with V_μ and V'_μ are the $U(1)_Y$ being the $U(1)_{B-L}$ gauge fields, respectively.

Superfield	Spin-0	Spin- $\frac{1}{2}$	Generations	$\mathbb{G}_{SM} \otimes U(1)_{B-L}$
\hat{Q}	\tilde{Q}	Q	3	$(\mathbf{3}, \mathbf{2}, \frac{1}{6}, \frac{1}{3})$
\hat{d}^c	\tilde{d}^c	d^c	3	$(\mathbf{3}, \mathbf{1}, \frac{1}{3}, -\frac{1}{3})$
\hat{u}^c	\tilde{u}^c	u^c	3	$(\mathbf{3}, \mathbf{1}, -\frac{2}{3}, -\frac{1}{3})$
\hat{L}	\tilde{L}	L	3	$(\mathbf{1}, \mathbf{2}, -\frac{1}{2}, -1)$
\hat{E}^c	\tilde{e}^c	e^c	3	$(\mathbf{1}, \mathbf{1}, 1, 1)$
\hat{N}^c	\tilde{N}^c	N^c	3	$(\mathbf{1}, \mathbf{1}, 0, 1)$
\hat{H}_d	H_d	\tilde{H}_d	1	$(\mathbf{1}, \mathbf{2}, -\frac{1}{2}, 0)$
\hat{H}_u	H_u	\tilde{H}_u	1	$(\mathbf{1}, \mathbf{2}, \frac{1}{2}, 0)$
$\hat{\chi}_1$	χ_1	$\tilde{\chi}_1$	1	$(\mathbf{1}, \mathbf{1}, 0, -2)$
$\hat{\chi}_2$	χ_2	$\tilde{\chi}_2$	1	$(\mathbf{1}, \mathbf{1}, 0, 2)$

Table 3.1: Chiral superfields and their quantum numbers in the BLSSM.

The BLSSM superpotential is given by

$$W = Y_u^{ij} \hat{u}_i^c \hat{Q}_j \cdot \hat{H}_u - Y_d^{ij} \hat{d}_i^c \hat{Q}_j \cdot \hat{H}_d - Y_e^{ij} \hat{E}_i^c \hat{L}_j \cdot \hat{H}_d + Y_\nu^{ij} \hat{N}_i^c \hat{L}_j \cdot \hat{H}_u + \frac{1}{2} Y_N^{ij} \hat{N}_i^c \hat{\chi}_1 \hat{N}_j^c + \mu \hat{H}_u \cdot \hat{H}_d - \mu' \hat{\chi}_1 \hat{\chi}_2. \quad (3.2.1)$$

The relevant soft supersymmetry-breaking terms, adopting the usual universality assumptions at the Grand Unification Theory (GUT) scale, are given by

$$\begin{aligned} -\mathcal{L}_{\text{soft}} = & m_0^2 \sum_{\phi} |\phi|^2 + Y_u^A \tilde{Q} H_u \tilde{U}^c + Y_d^A \tilde{Q} H_d \tilde{D}^c + Y_e^A \tilde{L} H_d \tilde{E}^c + Y_\nu^A \tilde{L} H_u \tilde{\nu}^c + Y_N^A \tilde{N}^c \chi_1 \tilde{N}^c \\ & + \left[B (\mu H_u H_d + \mu' \chi_1 \chi_2) + \frac{1}{2} m_{1/2} \left(\tilde{g}^a \tilde{g}^a + \tilde{W}^a \tilde{W}^a + \tilde{B} \tilde{B} + \tilde{B}' \tilde{B}' \right) + h.c. \right], \end{aligned} \quad (3.2.2)$$

where the sum in the first term runs over the scalar fields $\phi = \tilde{Q}, \tilde{U}, \tilde{D}, \tilde{L}, \tilde{E}, \tilde{N}, H_{u,d}, \chi_{1,2}$ and $(Y_f^A)_{ij} \equiv A_0(Y_f)_{ij}$ ($f = u, d, e, \nu, N$) are the trilinear scalar interaction couplings associated with the fermion Yukawa couplings. The $B - L$ symmetry can be radiatively broken by the following non-vanishing Vacuum Expectation Values (VEVs): $\langle \chi_1 \rangle = v_1$ and $\langle \chi_2 \rangle = v_2$. We define $\tan \beta'$ as the ratio of these VEVs ($\tan \beta' = v_1/v_2$) in analogy to the MSSM case ($\tan \beta = v_u/v_d$) [213, 214].

After $B - L$ Spontaneous Symmetry Breaking (SSB), the new gauge boson, Z' , acquires its mass from the kinetic term of the $B - L$ Higgs fields, $\chi_{1,2}$. Namely, we have

$$M_{Z'}^2 = g_{BL}^2 v'^2 + \frac{1}{4} \tilde{g}^2 v^2, \quad (3.2.3)$$

where \tilde{g} is the gauge coupling mixing between $U(1)_Y$ and $U(1)_{B-L}$ and $v' = \sqrt{v_1^2 + v_2^2}$. Furthermore, the mixing angle between the SM Z and BLSSM Z' states is given by

$$\tan 2\theta' = \frac{2\tilde{g} \sqrt{g_1^2 + g_2^2}}{\tilde{g}^2 + 16(\frac{v'}{v})^2 g_{BL}^2 - g_2^2 - g_1^2}, \quad (3.2.4)$$

which should be $\lesssim 10^{-3}$.

We now turn to the neutral CP-even Higgs bosons in the BLSSM. The Higgs potential is

$$V(H, \chi) = |\mu|^2(|H_u^0|^2 + |H_d^0|^2) + |\mu'|^2(|\chi_1|^2 + |\chi_2|^2) + \frac{g^2}{8}(|H_u^0|^2 - |H_d^0|^2)^2 + \frac{g_{BL}^2}{2}(|\chi_1|^2 - |\chi_2|^2)^2$$

3.2 The BLSSM BPs and Spectrum

$$-\frac{\tilde{g}g_{BL}}{4}(|H_u^0|^2 - |H_d^0|^2)(|\chi_1|^2 - |\chi_2|^2) - m_1^2|\chi_1|^2 - m_2^2|\chi_2|^2 - B_\mu H_u^0 H_d^0 - B'_\mu \chi_1 \chi_2. \quad (3.2.5)$$

where $g^2 = g_1^2 + g_2^2 + \tilde{g}^2$. We expand the neutral components around their VEVs:

$$H_{u,d}^0 = \frac{1}{\sqrt{2}}(v_{u,d} + \sigma_{u,d} + i\phi_{u,d}), \quad \chi_{1,2} = \frac{1}{\sqrt{2}}(v_{1,2} + \sigma_{1,2} + i\phi_{1,2}). \quad (3.2.6)$$

The Higgs bosons (symmetric) mass matrix in the basis $(\sigma_u, \sigma_d, \sigma_1, \sigma_2)$ is given in block form by

$$M_H^2 = \begin{pmatrix} M_{HH}^2 & M_{H\chi}^2 \\ * & M_{\chi\chi}^2 \end{pmatrix}, \quad (3.2.7)$$

where the off-diagonal block mixing of both the MSSM and $B - L$ sectors is

$$M_{H\chi}^2 = \frac{vv'}{2}\tilde{g}g_{BL} \begin{pmatrix} -s_\beta s_{\beta'} & s_\beta c_{\beta'} \\ c_\beta s_{\beta'} & -c_\beta c_{\beta'} \end{pmatrix} \quad (3.2.8)$$

where we have used the shorthand notations $s_X \equiv \sin X$ and $c_X \equiv \cos X$. The MSSM Higgs mass matrix M_{HH}^2 in the basis (σ_u, σ_d) is given by

$$M_{HH}^2 = \begin{pmatrix} \frac{\tilde{g}g_{BL}}{4}v'^2 c_{2\beta'} + \frac{1}{8}g^2 v^2 (23s_\beta^2 - 7c_\beta^2) + \frac{B_\mu}{t_\beta} & -B_\mu - \frac{g^2}{4}v^2 s_{2\beta} \\ * & -\frac{\tilde{g}g_{BL}}{4}v'^2 c_{2\beta'} - \frac{1}{8}g^2 v^2 (7s_\beta^2 - 23c_\beta^2) + B_\mu t_\beta \end{pmatrix}, \quad (3.2.9)$$

where we have used the shorthand notation $t_X \equiv \tan X$ and the $B - L$ Higgs mass matrix $M_{\chi\chi}^2$ in the basis (σ_1, σ_2) is given by

$$M_{\chi\chi}^2 = \begin{pmatrix} \frac{\tilde{g}g_{BL}}{4}v^2 c_{2\beta} + \frac{1}{2}g_{BL}^2 v'^2 (23s_{\beta'}^2 - 7c_{\beta'}^2) + \frac{B'_\mu}{t_{\beta'}} & -B'_\mu - g_{BL}^2 v'^2 s_{2\beta'} \\ * & -\frac{\tilde{g}g_{BL}}{4}v^2 c_{2\beta} - \frac{1}{2}g_{BL}^2 v'^2 (7s_{\beta'}^2 - 23c_{\beta'}^2) + B'_\mu t_{\beta'} \end{pmatrix}, \quad (3.2.10)$$

where the tree-level tadpole equations solutions give

$$\begin{aligned} B_\mu &= -\frac{1}{8}t_{2\beta}[g^2 v^2 c_{2\beta} - 2g_{BL}\tilde{g}v'^2 c_{2\beta'} + 4(m_d^2 - m_u^2)], \\ B'_\mu &= -\frac{1}{4}t_{2\beta'}[2g_{BL}^2 v'^2 c_{2\beta'} - g_{BL}\tilde{g}v^2 c_{2\beta} + 2(m_2^2 - m_1^2)], \end{aligned} \quad (3.2.11)$$

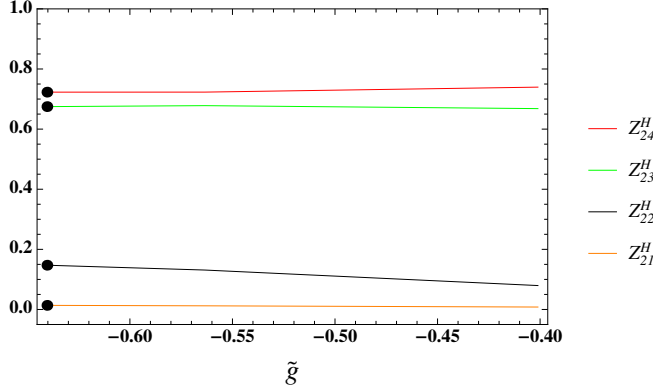


Figure 3.1: The Higgs mixing Z_{2i}^H ($i = 1, \dots, 4$) versus the gauge kinetic mixing coupling \tilde{g} . The values corresponding to the Benchmark Point (BP) of (forthcoming) Table 3.2a are labeled by ●.

where $m_{u,d}^2$, $m_{1,2}^2$ are the soft supersymmetry breaking Higgs $H_{u,d}, \chi_{1,2}$ mass parameters at the SSB scale(s).

The heavy Higgs boson tree-level mass eigenvalues are given in terms of the lightest SM-like Higgs boson $h \equiv h_1$ mass, which is fixed at $m_h = 125$ GeV, and the lightest $B - L$ Higgs boson $h' \equiv h_2$ mass, which we take to be $m_{h'} = 400$ GeV, as follows

$$m_{H,H'}^2 = \frac{1}{2} (T_H - m_h^2 - m_{h'}^2) \left[1 \pm \sqrt{1 - \frac{4D_H}{m_h^2 m_{h'}^2 (T_H - m_h^2 - m_{h'}^2)^2}} \right], \quad (3.2.12)$$

where $D_H = \text{Det}(M_H^2)$, and $T_H = \text{Tr}(M_H^2)$ are given by

$$T_H = (2 \cot 2\beta B_\mu + \frac{1}{4} g^2 v^2 \cos 2\beta) \sec 2\beta + (2 \cot 2\beta' B'_\mu + g_{BL}^2 v'^2 \cos 2\beta') \sec 2\beta' \quad (3.2.13)$$

$$D_H = (g^2 - \tilde{g}^2) v^2 v'^2 \cos 2\beta \cos 2\beta' \cot 2\beta \cot 2\beta' B_\mu B'_\mu. \quad (3.2.14)$$

The heavy Higgs bosons masses can be approximated by

$$m_{H'}^2 \sim \frac{D_H}{T_H m_h^2 m_{h'}^2}, \quad (3.2.15)$$

and $m_H^2 \sim T_H - m_h^2 - m_{h'}^2 - m_{H'}^2$. Also, the pseudoscalar Higgs bosons masses $m_{A^{(\prime)}}^2 = \frac{2B_\mu^{(\prime)}}{\sin 2\beta^{(\prime)}} \sim \mathcal{O}(\text{TeV})$. For $\sigma_i = \sigma_d, \sigma_u, \sigma_1, \sigma_2$, one has $\sigma_i = Z_{ji}^H h_j$, $h_j = h, h', H, H'$ and

3.2 The BLSSM BPs and Spectrum

conversely $h_j = Z_{ij}^H \sigma_i$. Further,

$$h' \approx Z_{22}^H \sigma_d + Z_{23}^H \sigma_1 + Z_{24}^H \sigma_2. \quad (3.2.16)$$

In Fig. 3.1, we display the mixing Z_{2i}^H versus the gauge kinetic mixing \tilde{g} . As it can be seen from this plot, h' is essentially generated from $\sigma_{1,2}$ with smaller contributions from the real components of σ_d which, however, connect it to the SM sector. The MSSM gauginos (bino, wino and gluino) soft masses are fixed to $M_{\tilde{B}} \sim 7.74 \times 10^2$ GeV, $M_{\tilde{W}} \sim 8.52 \times 10^2$ GeV and $M_{\tilde{g}} \sim 6.38 \times 10^2$ GeV at the SSB scale(s), respectively, while the $B - L$ gaugino (bino') soft mass $M_{\tilde{B}'}$, and the bino-bino' gauginos mixing soft mass $M_{\tilde{B}\tilde{B}'}$ are given in Table 3.2a.

The second lightest Higgs boson h' interaction couplings to quarks are given in terms of quark masses $M_{u,d}$ by

$$\Gamma_{\bar{u}u}^{h'} = -\frac{M_u}{vs_\beta} Z_{22}^H, \quad \Gamma_{\bar{d}d}^{h'} = -\frac{M_d}{vc_\beta} Z_{22}^H, \quad (3.2.17)$$

while its couplings to the SM gauge and Higgs bosons are given by

$$g_{h'WW} \approx g_2 M_W s_\beta Z_{22}^H, \quad (3.2.18)$$

$$g_{h'ZZ} \approx g_{h'WW} \left(\sec \theta_w - \frac{\tilde{g}}{g_2} s_{\theta_{w'}} \right)^2, \quad (3.2.19)$$

$$\begin{aligned} g_{h'h h} &\approx \frac{1}{4} Z_{22}^H \left[4\tilde{g} g_{BL} v' Z_{12}^H \left(Z_{13}^H s_{\beta'} - Z_{14}^H c_{\beta'} \right) - 3g^2 vs_\beta (Z_{12}^H)^2 \right] \\ &+ \frac{1}{2} Z_{23}^H \left[2g_{BL}^2 v' \left(3s_{\beta'} (Z_{13}^H)^2 - 2c_{\beta'} Z_{13}^H Z_{14}^H - s_{\beta'} (Z_{14}^H)^2 \right) - \tilde{g} g_{BL} \left(v' s_{\beta'} (Z_{12}^H)^2 + 2vs_\beta Z_{12}^H Z_{13}^H \right) \right] \\ &+ \frac{1}{2} Z_{24}^H \left[2g_{BL}^2 v' \left(c_{\beta'} (Z_{13}^H)^2 + 2s_{\beta'} Z_{13}^H Z_{14}^H - 3c_{\beta'} (Z_{14}^H)^2 \right) \right], \end{aligned} \quad (3.2.20)$$

where θ_w and $\theta_{w'}$ are the weak and $Z - Z'$ mixing angles, respectively. For $t_{\beta'} \sim 1$, $Z_{12}^H \sim 1$, $Z_{13}^H, Z_{14}^H \ll 1$, $Z_{23}^H, Z_{24}^H \sim \frac{1}{\sqrt{2}}$, the trilinear Higgs boson coupling $h'hh$ (relevant to our forthcoming analysis) is approximated by

$$g_{h'h h} \sim -\frac{1}{2} \left(\frac{3}{2} g^2 vs_\beta Z_{22}^H + \tilde{g} g_{BL} v' \right). \quad (3.2.21)$$

g_{BL}	\tilde{g}	t_β	$t_{\beta'}$	v'	m_u^2	m_d^2	m_1^2	m_2^2	$M_{\tilde{B}'}$	$M_{\tilde{B}\tilde{B}'}$	
0.675	-0.640	11.034	1.288	4875	-1.30×10^7	9.30×10^6	-5.75×10^5	4.02×10^6	1.49×10^3	-1.55×10^3	
(a) BP inputs (mass parameters are in GeV.)											
Z_{11}^H	Z_{12}^H	Z_{13}^H	Z_{14}^H	Z_{21}^H	Z_{22}^H	Z_{23}^H	Z_{24}^H	Z_{31}^H	Z_{32}^H	Z_{33}^H	
0.089	0.987	-0.100	-0.088	0.012	0.131	0.678	0.723	0.030	0.009	0.728	-0.685
											-0.995
											0.091
											0.021
											-0.019
(b) BP neutral CP-even Higgs mixing.											
m_{H^\pm}	m_A	$m_{A'}$	$m_{h_1 \equiv h}$	$m_{h_2 \equiv h'}$	$m_{h_3 \equiv H'}$	$m_{h_4 \equiv H}$	$M_{Z'}$				
4384	2587	4384	125	397	4241	4402	3300				

Table 3.2: BP and relevant outputs.

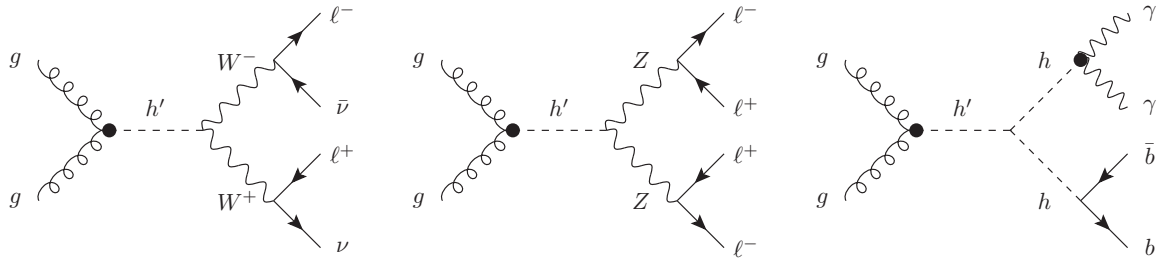


Figure 3.2: Feynman diagrams for h' production via ggF and decays via (from left to right) $W^+W^- \rightarrow 2\ell + \cancel{E}_T$, $h' \rightarrow ZZ \rightarrow 4\ell$ and $h' \rightarrow hh \rightarrow b\bar{b}\gamma\gamma$.

3.3 Search for a heavy neutral CP-even Higgs boson at the LHC

Many computational tools are used throughout this work, from building the model analytically to performing the numerical simulations at detector level. The BLSSM was first implemented into the SARAH package for Mathematica and the output was then passed to SPHENO [271, 290] for numerical calculations of the particle spectrum. After that, the ensuing UFO model was used in MADGRAPH [39] for MC event generation and Matrix Element (ME) calculations. After that, PYTHIA was used to simulate initial and final state radiation (through the Parton Shower (PS) formalism) as well as fragmentation/hadronization effects [287]. For detector simulation, the PYTHIA output was passed to DELPHES [135]. Finally, for data analysis, we used MADANALYSIS [117]. As for the BP used, we made sure that it was consistent with HIGGSBOUNDS and HIGGSIGNALS [76, 77] limits, as obtained from the latest LHC data.

The Feynman diagrams associated to the h' production and decay mechanisms discussed here are found in Fig. 3.2, wherein the \bullet symbol is meant to signify the exact loop function allowing for both b and t quark contributions. The Higgs production and decay rates are computed by factorising the h' propagator, so that the overall

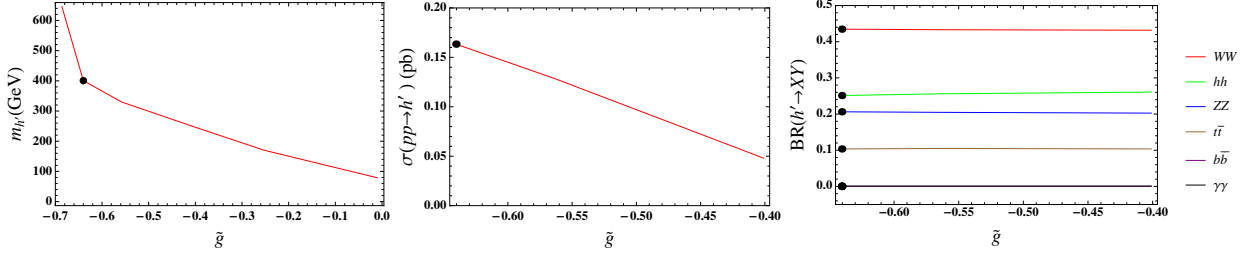


Figure 3.3: The dependence of (left) $m_{h'}$, (middle) the h' production cross section via ggF at $\sqrt{s} = 14$ TeV and (right) h' decay BRs (right) upon the gauge kinetic mixing coupling \tilde{g} . The values corresponding to the BP of Table 3.2a are labeled by \bullet .

event yield can be broken down into the h' production cross section and decay Branching Ratios (BRs). The MC event generation is done at Leading Order (LO) for both Signal (S) and Background (B), however, we include Next-to-Next-to-LO (NNLO) inclusive k -factors from Quantum Chromo-Dynamics (QCD) in computing our significances, specifically, we use 2.2 for the ggF signal and 1.2 for the Vector Boson Fusion (VBF) one (see below) as well as the EW backgrounds [63, 110, 193, 194, 276].

In Fig. 3.3 (left), we fix the SM-like Higgs boson mass to its measured value, i.e., $m_h \sim 125$ GeV, and show the change of $m_{h'}$ with the gauge kinetic mixing parameter \tilde{g} . However, one should be careful when reading this panel, as we only chose to show \tilde{g} and corresponding $m_{h'}$ values that give maximal values to the MSSM and $B - L$ Higgs sectors mixing represented in Z_{22}^H shown in Fig. 3.1, as desired for our study, where all BPs are validated by HIGGSBOUNDS and HIGGSIGNALS. Generally, this $m_{h'} - \tilde{g}$ subfigure would instead show a scattered pattern, as other BLSSM parameters could be tweaked such that any value of \tilde{g} can correspond to a broad range of $m_{h'}$. The cross section for ggF, properly convoluted with the default Parton Distribution Functions (PDFs) of our ME generator (namely, $\sigma(pp \rightarrow h')$), as function of \tilde{g} , is found in Fig. 3.3 (middle), for $\sqrt{s} = 14$ TeV. Also, in Fig. 3.3 (right) we show the h' decay BRs, again, as functions of \tilde{g} . In all three plots, the symbol \bullet refers to the BP adopted here, for which the corresponding σ and BR values are found in Table 3.3.

The production cross section of h' depends significantly on \tilde{g} , which is (as mentioned) the only source of mixing between the BLSSM Higgs $\chi_{1,2}$ singlets and the MSSM Higgs doublets $H_{u,d}$ that enables h' couplings with SM particles. However, the h' decay BRs are not significantly affected by it because both the partial and total decay widths of h' in each channel receive nearly the same contribution from \tilde{g} , which cancels out from the BRs. It is noteworthy that the three most significant decay channels are the bosonic ones in W^+W^- , ZZ and hh . In contrast, the fermionic decay channels into $t\bar{t}$ and $b\bar{b}$ are relatively less significant. Therefore, in the forthcoming MC analysis, we will concentrate on the former three decay channels.

For each channel, there are many corresponding background processes and all can be reduced by applying the cut-flows of Tables 3.4a, 3.4b and 3.4c, in correspondence of the three aforementioned channels, respectively. What remain in all cases, though, are the irreducible backgrounds $pp \rightarrow 2\ell + \cancel{E}_T$, $pp \rightarrow 4\ell$ and $pp \rightarrow \gamma\gamma b\bar{b}$. The following standard acceptance cuts on transverse momentum (P_T), pseudorapidity (η) and angular separation (ΔR) of the final state leptons, jets and photons are applied: $(P_T)_j \geq 20$, $(P_T)_a \geq 10$, $|\eta_j| \leq 5$, $|\eta_a| \leq 2.5$, $a = \gamma, \ell$ and $\Delta R_{ab} \geq 0.4$, $a, b = j, \gamma, \ell$.

In Tables 3.4a, 3.4b and 3.4c, the kinematical variables are defined such that M_{eff} is the effective mass being obtained as the sum of the transverse momentum of all final state objects and the transverse energy, while E_T is the scalar sum of the transverse energy of all (visible) final state objects in the plane transverse to the beam [117]. Furthermore, $M_{ab\dots}$ is an invariant mass and ΔR_{ab} is the separation between final state objects. (Note that an (opposite-sign) di-lepton mass reconstruction around one M_Z value in the 4ℓ channel is not useful, as the irreducible background is here dominated by $pp \rightarrow ZZ, Z\gamma^* \rightarrow 4\ell$.)

Quantity	Value
$\text{BR}(h' \rightarrow W^+W^-)$	0.432
$\text{BR}(h' \rightarrow ZZ)$	0.203
$\text{BR}(h' \rightarrow hh)$	0.261
$\sigma(pp \rightarrow h')$	163.400 (fb)
$\sigma(pp \rightarrow h' \rightarrow W^+W^- \rightarrow 2\ell + \cancel{E}_T)$	9.256 (fb)
$\sigma(pp \rightarrow h' \rightarrow ZZ \rightarrow 4\ell)$	0.406 (fb)
$\sigma(pp \rightarrow h' \rightarrow hh \rightarrow b\bar{b}\gamma\gamma)$	0.124 (fb)

Table 3.3: Production cross section σ (at $\sqrt{s} = 14$ TeV) and decay BRs into W^+W^- , ZZ and hh for the h' state (with $m_{h'} = 400$ GeV) of our BP, including the overall rates in the three final states $2\ell + \cancel{E}_T$, 4ℓ and $b\bar{b}\gamma\gamma$. Normalization is to LO for all σ 's.

3.3.1 The $h' \rightarrow W^+W^- \rightarrow 2\ell + \cancel{E}_T$ Channel

Table 3.4a provides the cut-flow for the h' production and decay analysis via the $2\ell + \cancel{E}_T$ signature, while event shapes and rates (the latter in correspondence to Run 3 luminosity) for

$$\sigma(pp \rightarrow h' \rightarrow W^+W^- \rightarrow 2\ell + \cancel{E}_T) \approx \sigma(pp \rightarrow h') \times \text{BR}(h' \rightarrow W^+W^- \rightarrow 2\ell + \cancel{E}_T) \quad (3.3.1)$$

are presented in Fig. 3.4. Herein, we also present the contributions of an additional signal channel, induced by (W^+W^- dominated) VBF with two additional (un>tagged) forward/backward jets, as it contributes not negligibly to the same ggF signal regions (so that it has been taken into account in extracting our final sensitivities). In this figure, the normalized (to 1) distributions used for the cut-flow (i.e., E_T , M_{eff} and $\Delta R_{\ell+\ell-}$) are presented, alongside the full transverse mass ($M_T^{\ell^+\ell^-} = \sqrt{(E_T^{\ell\ell} + \cancel{E}_T)^2 + |\vec{P}_T^{\ell\ell} + \vec{\cancel{E}}_T|^2}$, where $E_T^{\ell\ell} = \sqrt{|\vec{P}_T^{\ell\ell}|^2 + m_{\ell\ell}^2}$, and $\vec{\cancel{E}}_T$ is the negative vector sum of the transverse momenta of the reconstructed objects, including muons, electrons, photons, jets) of the final state (i.e., using both leptons in its definition), the latter integrating to the actual event numbers for Run 3 and also in presence of the background contribution. Altogether, from this last spectrum, it is clear that a

Cuts (select)	S	B	S/\sqrt{B}
Initial (no cut)	6120	8913654030	0.065
ID and Kin cuts	$2640^{\pm 39}$	$257832804^{\pm 14207}$	$0.164^{\pm 0.000}$
$E_T > 700 \text{ GeV}$	$338^{\pm 18}$	$70557^{\pm 256}$	$1.272^{\pm 0.004}$
$M_T^{\ell^+\ell^-} > 115 \text{ GeV}$	$267^{\pm 16}$	$3171^{\pm 56}$	$4.734^{\pm 0.004}$

(a) $pp \rightarrow h' \rightarrow W^+W^- \rightarrow 2\ell + \cancel{E}_T$ cut-flow at $L_{\text{int}} = 300 \text{ fb}^{-1}$.			
Cuts (select)	S	B	S/\sqrt{B}
Initial (no cut)	267	9712	2.72
$E_T > 300 \text{ GeV}$	$209^{\pm 7}$	$1680^{\pm 37}$	$5.09^{\pm 0.004}$
$M_{\ell^+\ell^-} > 50 \text{ GeV}$	$173^{\pm 8}$	$1395^{\pm 35}$	$4.63^{\pm 0.005}$

(b) $pp \rightarrow h' \rightarrow ZZ \rightarrow 4\ell$ cut-flow at $L_{\text{int}} = 300 \text{ fb}^{-1}$.			
Cuts (select)	S	B	S/\sqrt{B}
Initial (no cut)	951	19951560	0.213
$E_T > 200 \text{ GeV}$	$933^{\pm 4}$	$1476867^{\pm 1169}$	$0.768^{\pm 0.000}$
$M_{\gamma\gamma} > 120 \text{ GeV}$	$475^{\pm 15}$	$29023^{\pm 170}$	$2.787^{\pm 0.001}$
$M_{bb} > 50 \text{ GeV}$	$135^{\pm 11}$	$1945^{\pm 44}$	$3.055^{\pm 0.005}$
$\Delta R_{bb}^{\gamma\gamma} < 3.5$	$132^{\pm 11}$	$1746^{\pm 42}$	$3.156^{\pm 0.006}$
$M_{\gamma\gamma bb} > 360 \text{ GeV}$	$99^{\pm 10}$	$403^{\pm 20}$	$4.903^{\pm 0.017}$

(c) $pp \rightarrow h' \rightarrow hh \rightarrow b\bar{b}\gamma\gamma$ cut-flow at $L_{\text{int}} = 3000 \text{ fb}^{-1}$.

Table 3.4: S vs B rates for the three signals pursued in our analysis in correspondence of our BP: the $2\ell + \cancel{E}_T$ (a), 4ℓ and $b\bar{b}\gamma\gamma$ (c) final state. We adopt here $\sqrt{s} = 14 \text{ TeV}$ and integrated luminosity of Run 3 and HL-LHC. Inclusive NNLO k -factors from QCD are used here throughout.

high signal significance can be reached, however, it also shows that the shape does not promptly correlate to the h' mass value. Yet, the significant excess seen in this channel will clearly motivate a parallel search in the 4ℓ final state, which we are illustrating in the next subsection. However, before doing so, let us dwell more on the noise composition.

The dominant backgrounds in this channel are non-resonant W^+W^- , $t\bar{t}$, and $W^\pm t$ production, all of which have real W^+W^- pairs in the final state. Other important

backgrounds include Drell-Yan (DY) events ($pp \rightarrow Z/\gamma^{(*)} \rightarrow \ell^+\ell^-$) with \cancel{E}_T that may arise from mis-measurements, $W^\pm +$ jets events in which a jet produces an object reconstructed as the second electron and $W^\pm\gamma$ events in which the photon undergoes a conversion. Boson pair production $W^\pm\gamma^*/W^\pm Z^{(*)}/Wh^{(*)}$ and $ZZ^{(*)}$ can also produce opposite-charge lepton pairs with additional leptons that are not detected.

Demanding the following set of identification cuts (ID) with the number of b -jets $N(b) < 1$, the number of charged lepton pairs $N(\ell^+\ell^-) \leq 2$ and the number of jets $N(j) \leq 4$ in the kinematical (Kin) regions

3.3.1. for the leading lepton $P_\ell^T \geq 25$,

3.3.2. for the subleading lepton $P_\ell^T \geq 15$ and

3.3.3. for the two lepton $|\eta|_\ell < 2.5$

increases the S to B significance by a factor of about 2.5. The final analysis is included in Table 3.4a. After ID and Kin cuts, the DY, $W^\pm +$ jets, $W^\pm\gamma^{(*)}/Z^{(*)}$, $ZZ^{(*)}$ noises were eliminated so that in the end we kept only the irreducible backgrounds from W^+W^- , $t\bar{t}$ and $pp \rightarrow 2\ell + \cancel{E}_T$ events, which we stacked on top of each other in Fig. 3.4.

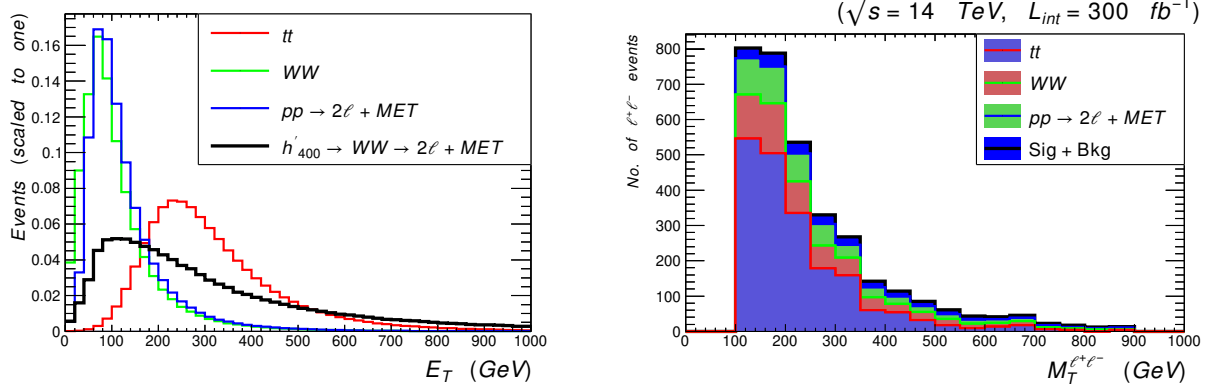


Figure 3.4: S and B distributions in E_T normalized to 1 before applying the cut-flow (left), and stacked normalized to the total event rate $M_T^{\ell^+\ell^-}$ after applying the cut-flow (right) for the integrated luminosity $L_{int} = 300 \text{ fb}^{-1}$. In both cases we show both the ggF contribution to the signal tt (red), WW (green), $2\ell + \cancel{E}_T$ (blue) backgrounds and for our BP signal (black).

3.3.2 The $h' \rightarrow ZZ \rightarrow 4\ell$ Channel

Table 3.4b provides the cut-flow for h' production and decay via the 4ℓ channel, while some relevant kinematics, in terms of event shapes and rates (the latter, again, in correspondence to Run 3 luminosity) for

$$\sigma(pp \rightarrow h' \rightarrow ZZ \rightarrow 4\ell) \approx \sigma(pp \rightarrow h') \times \text{BR}(h' \rightarrow ZZ \rightarrow 4\ell) \quad (3.3.2)$$

is presented in Fig. 3.5. Here, we concentrate on the normalized (to 1) distributions in transverse energy of all leptons (E_T) and opposite-sign di-lepton invariant mass ($M_{\ell^+\ell^-}$), both of which are used in our cut-flow. (Regarding the latter, notice that the loss of significance in applying the cut in invariant mass against the dominant irreducible background $pp \rightarrow ZZ, Z\gamma^* \rightarrow 4\ell$ is rather insignificant against the benefits of rejecting the irreducible one, e.g., from top-antitop quark production and fully leptonic W^+W^- decays (which has typically a harder distribution in this variable), so that the whole of the latter can be neglected.) In the end, the spectrum from which to extract the h' resonance, i.e., the final state invariant mass, $M_{4\ell}$, clearly reveals

a broad excess over a 400 GeV or so mass interval, altogether yielding significances in the discovery range. In fact, also a noticeable peak appear for $M_{4\ell} \approx 400$ GeV (which, as mentioned, can be correlated with the $M_T^{\ell^+\ell^-}$ distribution in the $2\ell + \cancel{E}_T$ final state), so that one can improve further the potential for h' discovery in the 4ℓ channel by optimizing a cut in this variable.

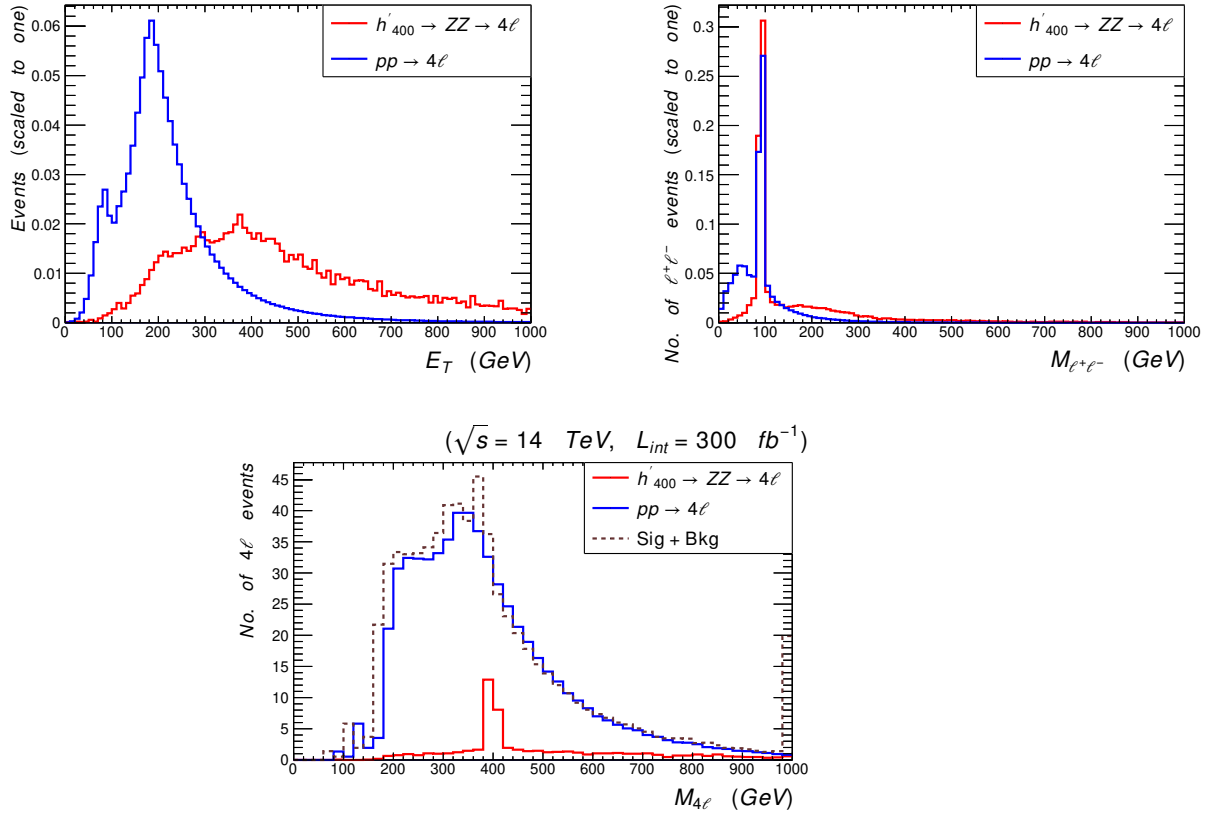


Figure 3.5: *S* and *B* distributions in E_T (top-left), $M_{\ell^+\ell^-}$ (top-right) and $M_{4\ell}$ (bottom), as defined in the text, the former two given before the cut-flow and normalized to 1 while the latter one given after it and normalized to the total event rate for the integrated luminosity $L_{\text{int}} = 300 \text{ fb}^{-1}$. In all cases we show only the ggF contribution to the 4ℓ signal for our BP while for the last spectrum we also show the (stacked) distribution.

3.3.3 The $h' \rightarrow hh \rightarrow b\bar{b}\gamma\gamma$ Channel

Table 3.4c provides the cut-flow for the h' production and decay analysis of the last channel we study,

$$\sigma(pp \rightarrow h' \rightarrow hh \rightarrow b\bar{b}\gamma\gamma) \approx \sigma(pp \rightarrow h') \times \text{BR}(h' \rightarrow hh \rightarrow b\bar{b}\gamma\gamma), \quad (3.3.3)$$

wherein we use HL-LHC luminosity, as this channel is not accessible during Run 3. The distributions used to inform our cut-flow herein (normalized to 1) are found in Fig. 3.6. These are the spectra in the transverse energy of the $b\bar{b}\gamma\gamma$ final state (E_T), $\gamma\gamma$ and $b\bar{b}$ invariant masses ($M_{\gamma\gamma}$ and $M_{b\bar{b}}$, respectively) and separations ($\Delta R_{\gamma\gamma}$ and $\Delta R_{b\bar{b}}$, respectively). Such a figure also presents the invariant mass of the final state ($M_{\gamma\gamma b\bar{b}}$), normalized to the HL-LHC luminosity. As seen from the signal and background responses to the cut-flow, it is clear that knowledge of the $m_{h'}$ value, gained during Run 3 of the LHC by exploiting the two previous signatures, is crucial in accessing this signal, which can ultimately be done at the 5σ level, despite the initially overwhelming background.

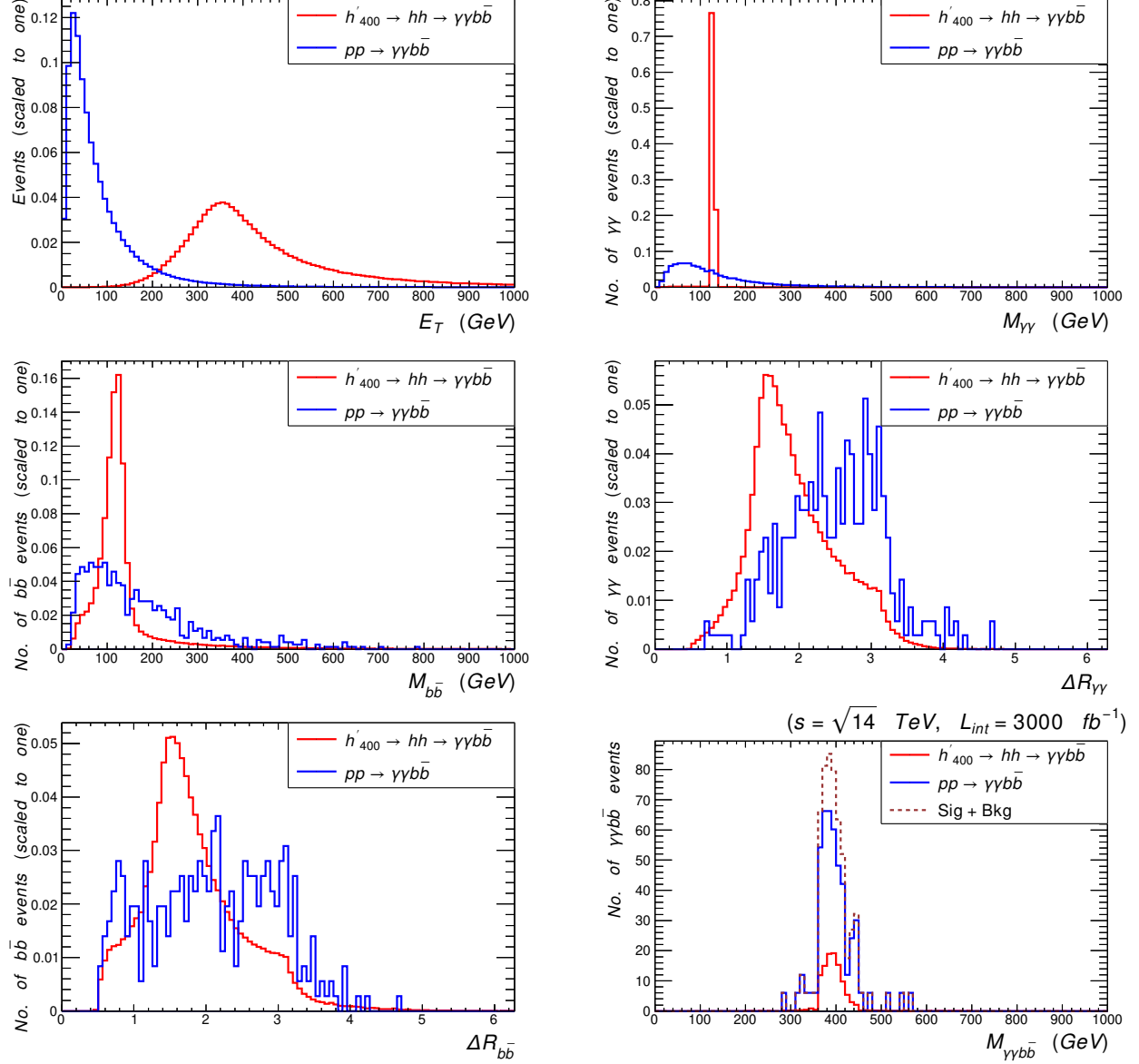


Figure 3.6: S and B distributions in E_T (top-left), $M_{\gamma\gamma}$ (top-right), $M_{b\bar{b}}$ (middle-left), $\Delta R_{\gamma\gamma}$ (middle-right) $\Delta R_{b\bar{b}}$ (bottom-left) and $M_{\gamma\gamma b\bar{b}}$ (bottom-right), as defined in the text, the former 5 given before the cut-flow and normalized to 1 while the latter one given after it and normalized to the total event rate for the integrated luminosity $L_{int} = 3000 \text{ fb}^{-1}$. In all cases we show only the ggF contribution to the $b\bar{b}\gamma\gamma$ signal for our BP while for the last spectrum we also show the (stacked) distribution.

3.3.4 Historical Significance

Before closing this section, we describe the patterns of significances in the three channels that we have studied, as they would evolve with luminosity, assuming fixed energy at $\sqrt{s} = 14$ TeV. These are shown in Fig. 3.7. It is evident that a full characterization of the h' state, involving its coupling to SM (massive) gauge and Higgs bosons is only possible through a combined effort of analyses to be entertained at both Run 3 of the LHC and HL-LHC. All used HEP tools here after are shown in Table 3.5.

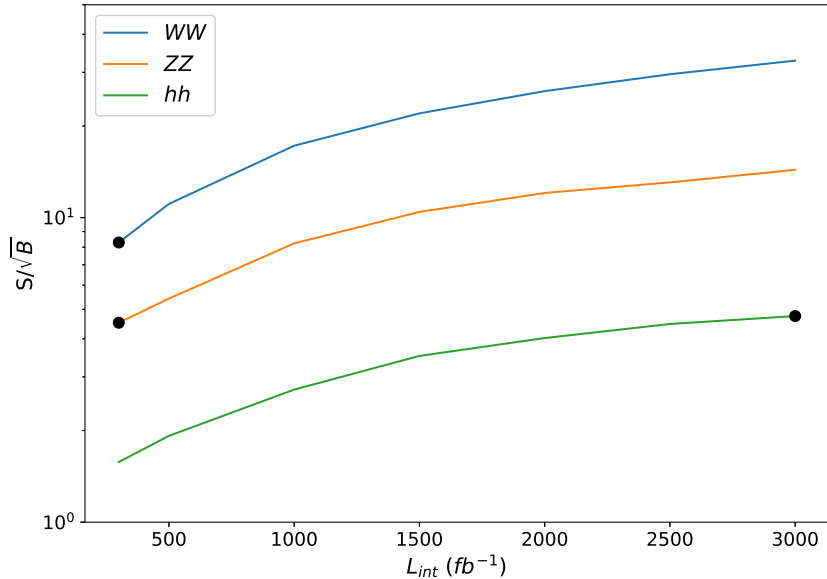


Figure 3.7: Significance of the $h' \rightarrow W^+W^-$, ZZ and hh signals that we have studied versus L_{int} for our BP. Data are produced at a center-of-mass energy of $\sqrt{s} = 14$ TeV. The rates are computed after applying the relevant kinematical analyses described in the text. The three \bullet points indicate the luminosity choices used in the MC simulations performed.

SARAH [290]	Model Building
SPHENO [270]	Spectrum calculator
HIGGSBOUNDS [76, 77]	Bounds on Higgs bosons couplings and masses
HIGGSIGNALS [76, 77]	Higgs observations peaks
FEYNARTS [185, 186, 289]	Loop diagrams
FEYNCALC [282]	Loop amplitude calculation
MADGRAPH [39]	Event MonteCarlo simulation
DELPHES [135]	Detector simulation
PYTHIA [288]	Parton shower and hadronization
MADANALYSIS [116]	Data analysis
TMVA [196, 297, 298]	Data analysis and Machine Learning Models

Table 3.5: Used HEP Tools

3.3.5 ML Analysis

Finally, we use machine learning (ML) algorithms to analyze the simulated signal and background events. In Fig. 3.8 , the upper left and lower left panels show the signal and background events separation in the $WW \rightarrow 2\ell + \cancel{E}_T$ and $hh \rightarrow b\bar{b}\gamma\gamma$ channels, respectively. In each of them, we notice that the ML algorithm learned efficiently from the training set and then classified the test set in both the signal (blue) and background (red). Also, we see that the signal and background events are well-separated with respect to the boosted decision tree (BDT) response. In the right upper and lower panels of Fig. 3.8, the significance $S/\sqrt{S+B}$ reaches its maximum value ~ 7.6 at a BDT response value ~ 0.4 for number of signal and background events $S = 267$ and $B = 3171$ in WW channel and $S = 99$ and $B = 403$ in hh channel, respectively, as in Table 3.4a and Table 3.4c. Moreover, Fig. 3.9 left panel shows the mutual uncorrelation of the kinematic variables $M_{\gamma\gamma}, \phi_{\gamma\gamma}$ and $\eta_{\gamma\gamma}$, while the right panel show the different ROC curves of the trained ML algorithms where the highest area under the curve (AUC) $\lesssim 1$ is the BDT ROC curve (dim gray) showing that BDT is the most efficient algorithm to use to separate the signal from the background events.

3.3 Search for a heavy neutral CP -even Higgs boson at the LHC

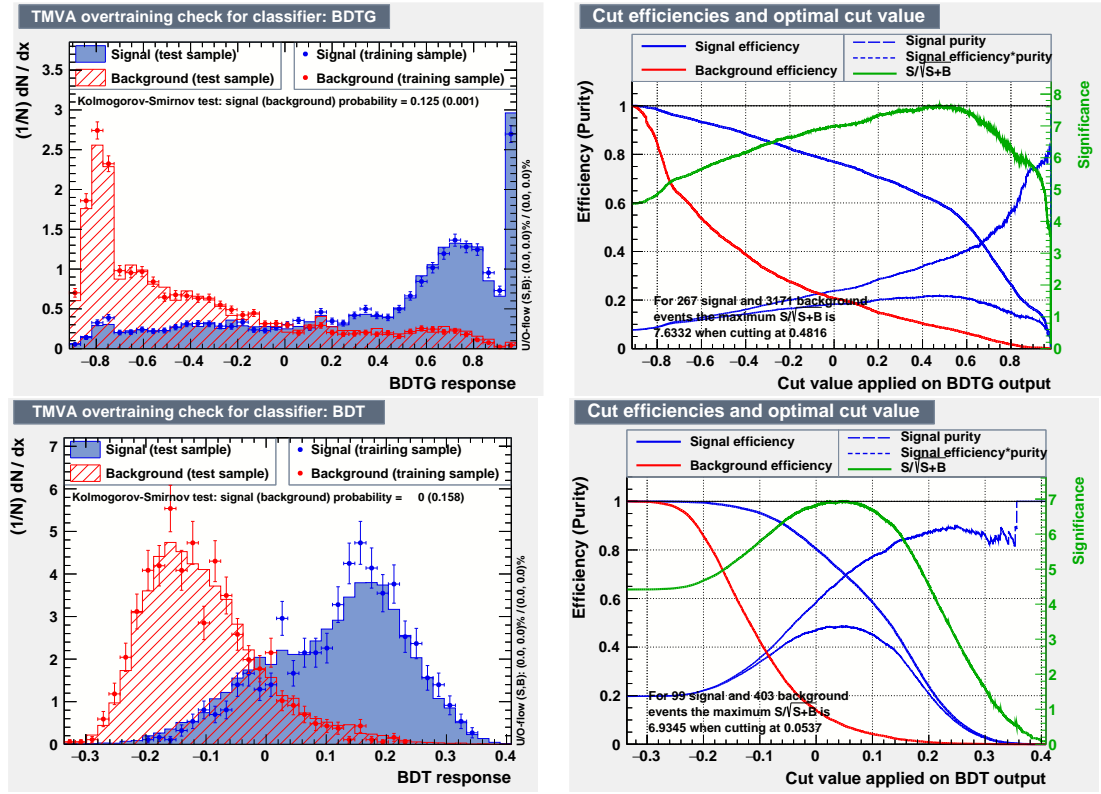


Figure 3.8: $H \rightarrow WW \rightarrow 2j + MET$ (up) and $H \rightarrow hh \rightarrow \gamma\gamma bb$ (down): S and B distributions, significance, correlation matrix and the receiver operating characteristic (ROC) curves for different ML algorithms at $m_{h'} = 400$ GeV, $L_{\text{int}} = 300/3000 \text{ fb}^{-1}$ [303].

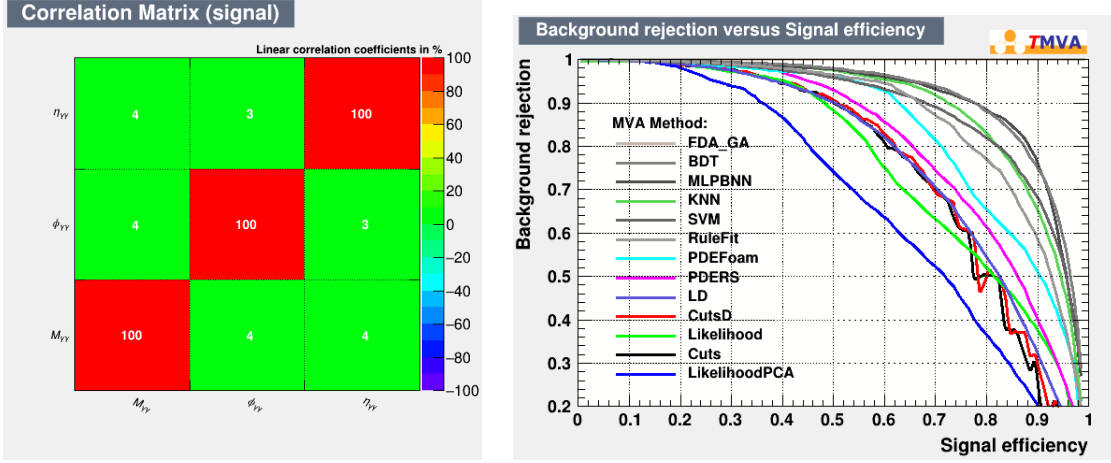


Figure 3.9: $H \rightarrow hh \rightarrow \gamma\gamma\bar{b}b$ S and B distributions, significance, correlation matrix and the ROC curves for different learning ML algorithms at $m_{h'} = 400$ GeV, $L_{\text{int}} = 300 \text{ fb}^{-1}$ [303].

3.4 Conclusion

In summary, we have shown that a theoretically well-motivated realization of supersymmetry, the so-called BLSSM, may yield detectable signals of a heavy neutral CP-even Higgs boson at the LHC, both during Run 3 and the HL-LHC phase. These emerge from the lightest (neutral) Higgs state of this scenario with prevalent $B - L$ composition, h' , while the lightest (neutral) Higgs state with predominant MSSM nature is identified with the discovered one, h (with $m_h = 125$ GeV). The subprocesses pursued to this effect, assuming a BP with an illustrative mass $m_{h'} = 400$ GeV, have been $gg \rightarrow h' \rightarrow W^+W^- \rightarrow 2\ell + \cancel{E}_T$, $gg \rightarrow h' \rightarrow ZZ \rightarrow 4\ell$ and $gg \rightarrow h' \rightarrow hh \rightarrow b\bar{b}\gamma\gamma$. The first one would be accessible during the early stages of Run 3 and the study of mass distributions would allow one to extract an indication of the h' mass. This information can then be used to optimize the selection of the second signal, which would reveal a clear pick centered around $m_{h'}$ by the end of Run 3. With the latter information available, one would then be able to establish the third

3.4 Conclusion

signal at the HL-LHC. All this will therefore enable one to fully characterize the h' state, not only through its mass, but also in terms of its couplings, as the W^+W^- , ZZ and hh decays are the dominant ones in the BLSSM while those to $t\bar{t}$ and $b\bar{b}$ pairs may be accessible at production level through the ggF channel. This finally opens up the possibility of eventually separating the BLSSM hypothesis from alternative ones also based on supersymmetry, since – thanks to the peculiar feature of (gauge) kinetic mixing appearing in the BLSSM (which incorporates an additional $U(1)_{B-L}$ group beyond the SM gauge symmetries) – competing signals stemming from, e.g., the MSSM would have rather different mass and coupling patterns.

We have come to these conclusions by performing a full MC analysis in presence of ME, PS, fragmentation/hadronization effects as well as detector modeling and upon devising dedicated cut-and-count cut-flows for each signature pursued. We are therefore confident that ATLAS and CMS would have sensitivity to this specific non-minimal realization of supersymmetry and advocate dedicate searches for the aforementioned signals.

4

LEFT RIGHT INVERSE SEESEW

4.1 Introduction

The SM of particle physics is in an excellent agreement with most of the confirmed experimental results. However, there exist several compelling arguments that indicate that the SM is only an effective low energy limit of a more fundamental underlying theory. Indeed, there are a number of theoretical and phenomenological outstanding issues in particle physics that can not be explained and the SM fails to address them adequately. Here, we may just mention the puzzles of dark matter and tiny neutrino masses [26, 29, 40, 151, 166], which can not be explained within the SM. One of the most popular extensions of the SM is the grand unified theory (GUT), where the SM gauge symmetry $SU(3)_C \times SU(2)_L \times U(1)_Y$ is extended to a bigger (simple or semisimple) group. Nonvanishing neutrino masses motivate the existence of right-handed neutrinos, and hence, all known fermions would have both left and right chirality. In this respect, the SM gauge group would be extended to the left-right (LR) symmetric gauge group, which is based on $SU(3)_C \times SU(2)_L \times SU(2)_R \times U(1)_{B-L}$, where left and right chirality are treated equally at high energy scales. In this class of models, the Majorana right-handed neutrinos are naturally heavy, and hence small left-handed neutrino masses are generated through seesaw mechanisms.

4.1 Introduction

In the conventional LR model proposed by Mohapatra *et al.* [249, 250, 279], the SM fermions (including the right-handed neutrino) are assigned in left- or right-handed doublets, and the following Higgs sector has been assumed: one bidoublet to construct the Yukawa couplings of quarks and leptons, in addition to a left- and right-handed scalar triplets for seesaw neutrino masses. The $SU(2)_R \times U(1)_{B-L}$ symmetry is broken down to $U(1)_Y$, at a high energy scale, by the VEV of the neutral component of the right-handed triplet, while the VEVs of neutral components of the bidoublet and the left-handed triplet contribute in breaking the electroweak symmetry, $SU(2)_L \times U(1)_Y$, down to $U(1)_{\text{em}}$. It was clear that the Higgs sector of this model is not minimal, with several neutral and singly and doubly charged components. Also, the left-handed triplet was introduced only to preserve LR symmetry, although its VEV must be fine-tuned to a very small value to avoid stringent constraints from the observed neutrino masses. Moreover, the Higgs triplets may induce tree level flavor violating processes that contradict the current experimental limits. Therefore, different variants of the conventional LR model have been considered [55, 58, 87, 141, 236, 256].

Here, we consider an example of a LR model, with a Higgs sector consisting of one scalar bidoublet and a scalar right-handed doublet. In this case and in order to generate light neutrino masses, we adopt the inverse-seesaw (IS) mechanism [93, 173, 247, 248, 306]. As known, this mechanism requires introducing other singlet fermions that couple with right-handed neutrinos and have a small mass [$\sim \mathcal{O}(1)$ KeV], which may be generated radiatively. The IS mechanism is quite motivated by having the TeV scale LR model that can be probed in current and future colliders, while in the conventional LR model, the GUT scale is the typical scale of breaking LR symmetry, where right-handed neutrino masses are generated. Moreover, in the limit of vanishing the above mentioned tiny mass, we will have massless left-handed neutrinos and the lepton number symmetry is restored. Thus, such a small scale can be considered, according to 't Hooft naturalness criteria [293],

as a natural scale of a global symmetry (lepton number) breaking. We also argue that in this class of models the tree-level flavor changing neutral current (FCNC) is under control. It turns out that the right-handed doublet is essentially decoupled from the two Higgs doublets, generated from the bidoublet; hence the Higgs sector of this model mimics the scenario of two the Higgs doublet model [128, 183, 184]. We show that the lightest CP -even Higgs boson, the SM-like Higgs boson, and the next lightest are generated from the neutral components of the bidoublet. For a wide range of the parameter space, one can show that the mass of the next lightest Higgs boson is of the order a few hundred GeVs.

4.2 Supersymmetric Left-Right Model

The Left-Right symmetry group restores Parity symmetry at high energy

$$G_{LR} = SU(3)_c \times SU(2)_L \times SU(2)_R \times U(1)_{B-L}. \quad (4.2.1)$$

However, parity violation at low energy weak interactions appears from the symmetry breaking:

$$SU(2)_L \times SU(2)_R \times U(1)_{B-L} \rightarrow SU(2)_L \times U(1)_Y \rightarrow U(1)_{\text{em}}. \quad (4.2.2)$$

where the hypercharge arises physically as a remnant symmetry with

$$\frac{Y}{2} = I_{3_R} + \frac{B - L}{2}, \quad Q = I_{3_L} + I_{3_R} + \frac{B - L}{2} = I_{3_L} + \frac{Y}{2}. \quad (4.2.3)$$

The Left-Right symmetry model can be attained from the breaking of GUTs: $SO(10) \rightarrow G_{LR}$ and $E_6 \rightarrow G_{LR}$. The LR symmetry solves the problem of neutrino masses naturally by considering right handed neutrino and seesaw mechanism [279]. The matter content of the Left-Right Symmetric Model (LRSM), where the right-handed neutrino ν_R forms an $SU(2)_R$ doublet with the right-handed charged leptons ℓ_R^\pm , is [250, 279]

$$q_L = \begin{pmatrix} u \\ d \end{pmatrix}_L \sim (3, 2, 1, \frac{1}{6}), \quad q_R = \begin{pmatrix} u \\ d \end{pmatrix}_R \sim (3, 1, 2, \frac{1}{6}),$$

$$\ell_L = \begin{pmatrix} \nu \\ e \end{pmatrix}_L \sim (1, 2, 1, \frac{-1}{2}), \quad \ell_R = \begin{pmatrix} \nu \\ e \end{pmatrix}_R \sim (1, 1, 2, \frac{-1}{2}). \quad (4.2.4)$$

The minimal set of the Higgs fields in the non-supersymmetric Left-Right model consists of a bidoublet Φ and $SU(2)_{L,R}$ triplets $\Delta_{L,R}$ respectively.

$$\Phi = \begin{pmatrix} \phi_1^0 & \phi_1^+ \\ \phi_2^- & \phi_2^0 \end{pmatrix} \sim (1, 2, 2^*, 0), \quad \Delta_{L,R} = \begin{pmatrix} \frac{1}{\sqrt{2}}\Delta_{L,R}^+ & \Delta_{L,R}^{++} \\ \Delta_{L,R}^0 & -\frac{1}{\sqrt{2}}\Delta_{L,R}^+ \end{pmatrix},$$

$$\Delta_L \sim (1, 3, 1, +2), \quad \Delta_R \sim (1, 1, 3, +2). \quad (4.2.5)$$

- **Minimal Supersymmetric Left-Right Model** The component-wise content of the scalar components of the Higgs superfields is as follows

$$\Phi_1 = \begin{pmatrix} \phi_{11}^0 & \phi_{11}^+ \\ \phi_{12}^- & \phi_{12}^0 \end{pmatrix}, \quad \Phi_2 = \begin{pmatrix} \phi_{21}^0 & \phi_{21}^+ \\ \phi_{22}^- & \phi_{22}^0 \end{pmatrix}, \quad (4.2.6)$$

$$\Phi_1 \sim (1, 2, 2, 0), \quad \Phi_2 \sim (1, 2, 2, 0), \quad (4.2.7)$$

$$\Delta = \begin{pmatrix} \frac{1}{\sqrt{2}}\delta_L^+ & \delta_L^{++} \\ \delta_L^0 & -\frac{1}{\sqrt{2}}\delta_L^+ \end{pmatrix}, \quad \bar{\Delta} = \begin{pmatrix} \frac{1}{\sqrt{2}}\Delta_L^- & \Delta_L^0 \\ \Delta_L^{--} & -\frac{1}{\sqrt{2}}\Delta_L^- \end{pmatrix}, \quad (4.2.8)$$

$$\Delta \sim (1, 3, 1, 2), \quad \bar{\Delta} \sim (1, 3, 1, -2), \quad (4.2.9)$$

$$\Delta_c = \begin{pmatrix} \frac{1}{\sqrt{2}}\Delta_R^- & \Delta_R^{--} \\ \Delta_R^0 & -\frac{1}{\sqrt{2}}\Delta_R^- \end{pmatrix}, \quad \bar{\Delta}_c = \begin{pmatrix} \frac{1}{\sqrt{2}}\delta_R^+ & \delta_R^0 \\ \delta_R^{++} & -\frac{1}{\sqrt{2}}\delta_R^+ \end{pmatrix}, \quad (4.2.10)$$

$$\Delta_c \sim (1, 1, 3, -2), \quad \bar{\Delta}_c \sim (1, 1, 3, 2). \quad (4.2.11)$$

- Under left-right symmetry the fields transform as

$$Q \leftrightarrow Q_c^*, \quad L \leftrightarrow L_c^*, \quad \Phi \leftrightarrow \Phi^\dagger, \quad \Delta \leftrightarrow \Delta_c^*, \quad \bar{\Delta} \leftrightarrow \bar{\Delta}_c^*. \quad (4.2.12)$$

- **Minimal Ω -Model:** To maintain the R -parity, two new triplet superfields were introduced [58] $\Omega(1, 3, 1, 0)$, $\Omega_c(1, 1, 3, 0)$ where under parity symmetry $\Omega \leftrightarrow \Omega_c$. The superpotential for this model is given by [57]

$$W_{LR\Omega} = h_l^{(i)} L^T \tau_2 \Phi_i \tau_2 L_c + h_q^{(i)} Q^T \tau_2 \Phi_i \tau_2 Q_c + i f L^T \tau_2 \Delta L + i f^* L_c^T \tau_2 \Delta_c L_c$$

$$+ m_\Delta \text{Tr } \Delta \bar{\Delta} + m_\Delta^* \text{Tr } \Delta_c \bar{\Delta}_c + \frac{m_\Omega}{2} \text{Tr } \Omega^2 + \frac{m_\Omega^*}{2} \text{Tr } \Omega_c^2$$

$$\begin{aligned}
 & + \mu_{ij} \text{Tr} \tau_2 \Phi_i^T \tau_2 \Phi_j + a \text{Tr} \Delta \Omega \bar{\Delta} + a^* \text{Tr} \Delta_c \Omega_c \bar{\Delta}_c \\
 & + \alpha_{ij} \text{Tr} \Omega \Phi_i \tau_2 \Phi_j^T \tau_2 + \alpha_{ij}^* \text{Tr} \Omega_c \Phi_i^T \tau_2 \Phi_j \tau_2.
 \end{aligned} \tag{4.2.13}$$

The structure of Ω vev gives $SU(2)_R \rightarrow U(1)_R$. Thus if $v_R < \omega_R$ then, the resulting symmetry breaking sequence is

$$\begin{aligned}
 & SU(2)_L \otimes SU(2)_R \otimes U(1)_{B-L} \xrightarrow{\langle \Omega_c \rangle} SU(2)_L \otimes U(1)_R \otimes U(1)_{B-L} \\
 & \qquad \qquad \qquad \xrightarrow{\langle \Delta_c \rangle} SU(2)_L \otimes U(1)_Y.
 \end{aligned} \tag{4.2.14}$$

- **Minimal Bitriplet Model:** Another possibility is to add a Higgs bitriplet $\eta(1, 3, 3, 0)$ and a parity odd singlet $\rho(1, 1, 1, 0)$ which also breaks parity spontaneously keeping R -parity conserved [263]. The superpotential with this Higgs content is

$$\begin{aligned}
 W_{\text{LRBitriplet}} = & f \eta_{\alpha i} \Delta_\alpha \Delta_i^c + f^* \eta_{\alpha i} \bar{\Delta}_\alpha \bar{\Delta}_i^c + \lambda_1 \eta_{\alpha i} \Phi_{am} \Phi_{bn} (\tau^\alpha \epsilon)_{ab} (\tau^i \epsilon)_{mn} \\
 & + m_\eta \eta_{\alpha i} \eta_{\alpha i} + M_\Delta (\Delta_\alpha \bar{\Delta}_\alpha + \Delta_i^c \bar{\Delta}_i^c) + \mu \epsilon_{ab} \Phi_{bm} \epsilon_{mn} \Phi_{an} \\
 & + m_\rho \rho^2 + \lambda_2 \rho (\Delta_\alpha \bar{\Delta}_\alpha - \Delta_i^c \bar{\Delta}_i^c).
 \end{aligned} \tag{4.2.15}$$

where α, a, b are $SU(2)_L$ and i, m, n are $SU(2)_R$ indices. The symmetry breaking pattern in this model is

$$\begin{aligned}
 & SU(2)_L \times SU(2)_R \times U(1)_{B-L} \times P \xrightarrow{\langle \eta \rangle} SU(2)_L \times SU(2)_R \times U(1)_{B-L} \\
 & \qquad \qquad \qquad \xrightarrow{\langle \Delta_c \rangle} SU(2)_L \times U(1)_Y \xrightarrow{\langle \Phi \rangle} U(1)_{\text{em}}.
 \end{aligned} \tag{4.2.16}$$

- **Only Bidoublet Model:** In this calss of models, the R -parity is spntaneously broken. The superpotential of this model is [163, 257]

$$\begin{aligned}
 W_{\text{LR}\Phi} = & Y_q Q^T \tau_2 \Phi_1 \tau_2 Q^c + Y'_q Q^T \tau_2 \Phi_2 \tau_2 Q^c + Y_e L^T \tau_2 \Phi_1 \tau_2 L^c \\
 & + Y'_e L^T \tau_2 \Phi_2 \tau_2 L^c + \mu_{ii} \text{Tr}(\Phi_i^T \tau_2 \Phi_i \tau_2).
 \end{aligned} \tag{4.2.17}$$

The symmetry is radiatively broken by the bidoublets as well as the right handed slepton [163, 257]:

4.3 Inverse Seesaw Mechanism

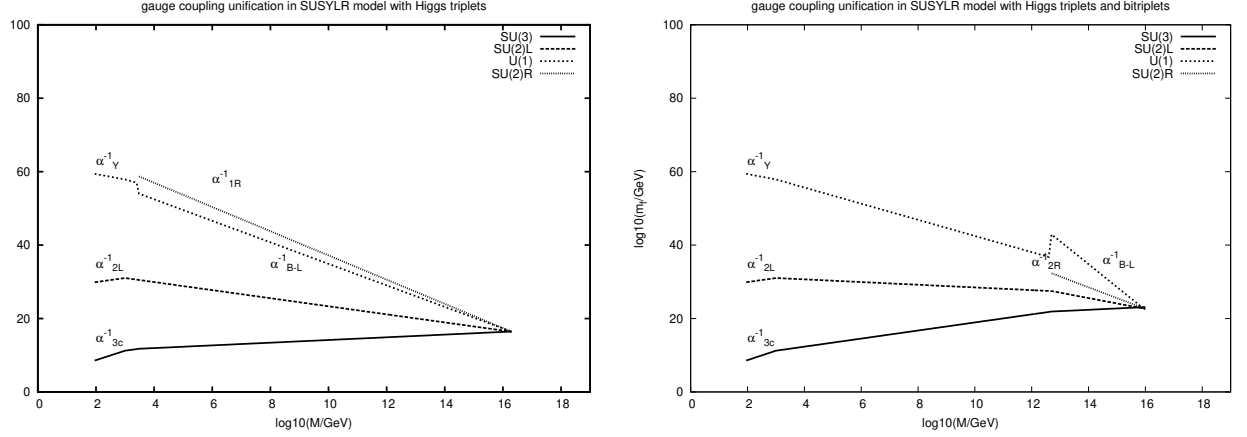


Figure 4.1: Gauge coupling unification [57, 88]

There are many varieties of supersymmetric left-right models with Higgs mass of order $\mathcal{O}(100)$ GeV [60]. But, here after, we only consider non-susy LR version for minimality.

4.3 Inverse Seesaw Mechanism

Despite neutrinos are considered to be massless in the SM, this assumption is contradicted with the neutrino oscillation observations, which indicate that the neutrinos are massive. They do not interact via electromagnetic and strong interaction because they have neither electric nor color charge. They interact via gravitational and weak interactions only as they have mass and isospin charge. Neutrinos are one type of the most abundant particles in the universe. However, they are incredibly difficult to detect. Now a lot of experimental like (Solar neutrinos, The super-Kamiokande experiment and The SNO experiment) proved neutrino have mass. So several way to try solve problem of neutrino massless in SM like Seesaw Mechanism type I, type II, type III and Inverse Seesaw (IS). Now, we focus on the in IS only.

In this scenario we add RH neutrino ν_R like type I and another Singlet fermions S with whose lepton number is opposite to that of ν_R where in this case the lepton

number is conservative. In this case, the most general IS neutrino Lagrangian is given by

$$\mathcal{L}_{\text{IS}}^\nu = y_\nu \bar{l}_L \tilde{\phi} \nu_R + M_R \overline{(\nu_R)^c} S + y_S \bar{l}_L \tilde{\phi} S + \mu_R \overline{(\nu_R)^c} \nu_R + \mu_S \overline{(S)^c} S + h.c., \quad (4.3.1)$$

where y_S, μ_R and μ_S are naturally small because of the so called 't Hooft criteria. Indeed, in the limit $y_S, \mu_R, \mu_S \rightarrow 0$, the lepton number is restored as a conserved symmetry.

After the electroweak symmetry breaking, the mass matrix of the neutrinos are given, for one generation, by

$$\mathcal{M}_\nu = \begin{pmatrix} 0 & M_D & M_S \\ M_D^T & \mu_R & M_R \\ M_S^T & M_R^T & \mu_S \end{pmatrix}. \quad (4.3.2)$$

where $M_D = y_\nu v$ and $M_S = y_S v$. As mentioned before, $M_S, \nu_R, \nu_S \ll M_D, M_R$, thus the neutrino masses can be given, with a very good approximation, by

$$m_{\nu_l} = \frac{M_D(M_D \mu_S - 2 M_R M_S)}{M_R^2 + M_D^2} \quad (4.3.3)$$

$$m_{\nu_h} = \frac{M_R(M_R \mu_S + 2 M_D M_S)}{2(M_R^2 + M_D^2)} + \frac{\mu_R}{2} \mp \sqrt{M_R^2 + M_D^2}. \quad (4.3.4)$$

It is worth mentioning that in the IS scenario, the neutrino Yukawa coupling can be of order $O(1)$ and the large scale M_R can be brought to be the TeV scale. This is because the suppression factor needed to account for light neutrino masses are played by the naturally small parameters M_S, μ_S instead of the Yukawa coupling y_ν . Indeed, If $y_\nu \sim O(1)$, $M_R \sim 1$ TeV and $\mu_S \sim 10 M_S \sim O(10^{-7})$ GeV, then a 1 eV neutrino mass can be obtained.

4.4 Left Right Model with Inverse Seesaw

Now we introduce a Left-Right Model with Inverse-Seesaw (LRIS), which is based on gauge symmetry $SU(3)_C \times SU(2)_L \times SU(2)_R \times U(1)_{B-L}$. The fermion content of

this model is as the same as its counterpart in the conventional left-right models [58, 87, 141, 236, 249, 250, 256, 279]. In addition, three SM singlet fermions S_1 with $B - L$ charge = +2 and three singlet fermions S_2 with $B - L$ charge = -2 are considered to implement the IS mechanism for neutrino masses. Note that we introduce pair of singlet fermions $S_{1,2}$ with opposite $B - L$ charges to keep the $U(1)_{B-L}$ anomaly free. The Higgs sector of the LRIS model consists of an $SU(2)_R$ scalar doublet χ_R to break $SU(2)_R \times U(1)_{B-L}$ to $U(1)_Y$ and a scalar bidoublet ϕ that breaks $SU(2)_L \times U(1)_Y$ down to $U(1)_{\text{em}}$, where the hypercharge Y is defined by $Y/2 = I_R^3 + (B - L)/2$, and I_R^3 is the third component of the right isospin. The detailed quantum numbers of the fermions and Higgs bosons are presented in Tab. 4.1.

Fields	$SU(3)_C \times SU(2)_L \times SU(2)_R \times U_{B-L}$
$Q_L = \begin{pmatrix} u_L \\ d_L \end{pmatrix}$	(3, 2, 1, $\frac{1}{3}$)
$Q_R = \begin{pmatrix} u_R \\ d_R \end{pmatrix}$	(3, 1, 2, $\frac{1}{3}$)
$L_L = \begin{pmatrix} \nu_L \\ e_L \end{pmatrix}$	(1, 2, 1, -1)
$L_R = \begin{pmatrix} \nu_R \\ e_R \end{pmatrix}$	(1, 1, 2, -1)
S_1	(1, 1, 1, -2)
S_2	(1, 1, 1, 2)
$\phi = \begin{pmatrix} \phi_1^0 & \phi_1^+ \\ \phi_2^- & \phi_2^0 \end{pmatrix}$	(1, 2, 2, 0)
$\chi_R = \begin{pmatrix} \chi_R^+ \\ \chi_R^0 \end{pmatrix}$	(1, 1, 2, 1)

Table 4.1: The LRIS particle Content and its representations and quantum numbers.

Also, in order to forbid a mixing mass term $M \bar{S}_1^c S_2$ that could spoil the IS mechanism, as discussed in [212], a Z_2 discrete symmetry is used, where all particles have even charges except S_1 which has an odd charge.

As in the SM, the strong interactions in the LRIS are based on the gauge group

$SU(3)_C$. The weak interactions of the LRIS are based on the gauge group $SU(2)_L \times SU(2)_R \times U(1)_{B-L}$. So we expect three extra gauge bosons, two of them are charged W_R^\pm analogous to the W^\pm boson, and another one neutral Z_R analogous to the Z boson (we will denote gauge bosons W^\pm and Z hereafter by W_L^\pm and Z_L , respectively). all RH component of fermion fields transform as doublets under $SU(2)_R$ symmetry in the LRIS and the corresponding gauge bosons of this new symmetry only couple to RH fermions. This idea of LR symmetry come from believe that physics law must be valid for RH as LH.

Like LRSM, The Lagrangian density of the LRIS can be summarized in; gauge, kinetic, scalar and Yukawa parts.

$$\mathcal{L}_{\text{LRIS}} = \mathcal{L}_{\text{Gauge}} + \mathcal{L}_{\text{Kinetic}} + \mathcal{L}_{\text{Scalar}} + \mathcal{L}_{\text{Yukawa}}, \quad (4.4.1)$$

where the gauge Lagrangian Contain the kinetic term of gauge boson and three and four-Point Interaction of Gauge field. Is given by;

$$\mathcal{L}_{\text{Gauge}} = -\frac{1}{4}G^{\mu\nu j}G_{\mu\nu}^j - \frac{1}{4}W_L^{\mu\nu i}W_{L\mu\nu}^i - \frac{1}{4}W_R^{\mu\nu i}W_{R\mu\nu}^i - \frac{1}{4}V^{\mu\nu}V_{\mu\nu} \quad (4.4.2)$$

Where G, W_L, W_R, V are strength tensors for gauge field respectively and satisfy following equation

$$G_{\mu\nu}^j = \partial_\mu G_\nu^j - \partial_\nu G_\mu^j - g_s f^{ijk} G_\nu^i G_\mu^k; \quad i, j, k = 1 \dots 8 \quad (4.4.3)$$

$$W_{L\mu\nu}^i = \partial_\mu W_{L\nu}^i - \partial_\nu W_{L\mu}^i - g_L \epsilon^{ijk} W_{L\nu}^j W_{L\mu}^k; \quad i, j, k = 1 \dots 3 \quad (4.4.4)$$

$$W_{R\mu\nu}^i = \partial_\mu W_{R\nu}^i - \partial_\nu W_{R\mu}^i - g_R \epsilon^{ijk} W_{R\nu}^j W_{R\mu}^k; \quad i, j, k = 1 \dots 3 \quad (4.4.5)$$

$$V_{\mu\nu} = \partial_\mu W_\nu - \partial_\nu W_\mu \quad (4.4.6)$$

where g_s, g_L, g_R are gauge couplings for $SU(3)_c, SU(2)_L, SU(2)_R$ Respectively and f^{ijk}, ϵ^{ijk} are structure constant defined by commutation relation of Lie Algebra for group. this field Transformation by following transformation

$$\Lambda.G_\mu \rightarrow U_c(\Lambda.G_\mu)U_c^\dagger - \frac{i}{g_s}(\partial_\mu U_c)U_c^\dagger \quad (4.4.7)$$

$$T_L \cdot W_{L_\mu} \rightarrow U_L (T_L \cdot W_{L_\mu}) U_L^\dagger - \frac{i}{g_L} (\partial_\mu U_L) U_L^\dagger \quad (4.4.8)$$

$$T_R \cdot W_{R_\mu} \rightarrow U_R (T_R \cdot W_{R_\mu}) U_R^\dagger - \frac{i}{g_R} (\partial_\mu U_R) U_R^\dagger \quad (4.4.9)$$

$$V_\mu \rightarrow V_\mu - \frac{1}{g_{BL}} \partial_\mu \alpha \quad (4.4.10)$$

where g_{BL} is gauge coupling for $U(1)_{B-L}$ and Λ are generator of $SU(3)$ group equal $\frac{1}{2}\lambda$ where λ is Gell-Man Matrices and satisfy liegroup commutation relation

$$[\Lambda^i, \Lambda^j] = i f^{ijk} \Lambda^k \quad (4.4.11)$$

and T_i are generator of $SU(2)$ group equal $\frac{1}{2}\sigma$ where σ is pauli Matrices and satisfy liegroup commutation relation

$$[T^i, T^j] = i \epsilon^{ijk} T^k \quad (4.4.12)$$

also we note that U_c, U_L, U_R are group $SU(3)_c, SU(2)_L, SU(2)_R$ can represent by

$$SU(3)_c \rightarrow e^{-i\gamma^a \Lambda_a}, \quad SU(2)_L \rightarrow e^{-i\beta_L^a T_L^a}, \quad SU(2)_R \rightarrow e^{-i\beta_R^a T_R^a}, \quad U(1)_{B_L} \rightarrow e^{-i\alpha(\frac{B-L}{2})}. \quad (4.4.13)$$

The kinetic term constitutes the kinetic term of fermions and interaction to gauge bosons;

$$\mathcal{L}_{\text{Kinetic}} = i \sum_{j=1}^3 (\bar{L}_{Lj} \gamma^\mu D_\mu L_{Lj} + \bar{L}_{Rj} \gamma^\mu D_\mu L_{Rj} + \bar{Q}_{Lj} \gamma^\mu D_\mu Q_{Lj} + \bar{Q}_{Rj} \gamma^\mu D_\mu Q_{Rj}) \quad (4.4.14)$$

The action of a group element of $SU(2)_L \times SU(2)_R$ on the fermion doublets by local matrix U_R is as follows

$$Q_R \rightarrow U_R Q_R = e^{-i\sigma \cdot \alpha_R(x)/2} Q_R, \quad (4.4.15)$$

$$L_R \rightarrow U_R L_R = e^{-i\sigma \cdot \alpha_R(x)/2} L_R, \quad (4.4.16)$$

and the transformation under $U(1)_{B-L}$ as

$$Q_R \rightarrow e^{-i\alpha(x)(B-L)/2} Q_R = e^{-i\alpha(x)/6} Q_R, \quad (4.4.17)$$

$$L_R \rightarrow e^{-i\alpha(x)(B-L)/2} L_R = e^{i\alpha(x)/2} L_R. \quad (4.4.18)$$

where quarks have $B - L = +1/3$ and the leptons -1

Accordingly, the covariant derivative takes the following forms for each term

$$\bar{L}_L \gamma^\mu D_\mu L_L = \bar{L}_L \gamma^\mu (\partial_\mu - \frac{ig_L}{2} \sigma \cdot W_{L,\mu} + \frac{ig_{BL}}{2} V_\mu) L_L, \quad (4.4.19)$$

$$\bar{L}_R \gamma^\mu D_\mu L_R = \bar{L}_R \gamma^\mu (\partial_\mu - \frac{ig_R}{2} \sigma \cdot W_{R,\mu} + \frac{ig_{BL}}{2} V_\mu) L_R, \quad (4.4.20)$$

$$\bar{Q}_L \gamma^\mu D_\mu Q_L = \bar{Q}_L^\alpha \gamma^\mu [(\partial_\mu - \frac{ig_L}{2} \sigma \cdot W_{L,\mu} - \frac{ig_{BL}}{6} V_\mu) \chi \alpha \beta - \frac{ig_s}{2} \lambda_{\alpha\beta} \cdot G_\mu] Q_L^\beta, \quad (4.4.21)$$

$$\bar{Q}_R \gamma^\mu D_\mu Q_R = \bar{Q}_R^\alpha \gamma^\mu [(\partial_\mu - \frac{ig_R}{2} \sigma \cdot W_{R,\mu} - \frac{ig_{BL}}{6} V_\mu) \chi \alpha \beta - \frac{ig_s}{2} \lambda_{\alpha\beta} \cdot G_\mu] Q_R^\beta, \quad (4.4.22)$$

where the strong and weak interactions of fermions and bosons are encoded in these kinetic terms.

The Higgs sector is added to make Breaking for Left-Right Model $SU(3)_c \times SU(2)_L \times SU(2)_R \times U_{B-L}(1)$ in hight energy to Standard Model $SU(3)_c \times SU(2)_L \times U_Y(1)$ by Right Higgs doublet χ_R then Breaking SM to electromagnetism U_{EM} by Bidoublet ϕ , also Higgs Sector have anther job which generating masses for Particles Standard Model as well as non Standard Model Particles Heavy Particle W_R, Z_R and neutrino,

now we will form scalar Lagrangian which given kinetic term for scalar field and self interaction. As all fermions in the LRIS are grouped in doublets under the $SU(2)$ groups, a gauge invariant Yukawa term -to give mass for this fermion- is $\bar{\psi}_L \phi \psi_R$ implies that the scalar field ϕ is a matrix of order 2×2 made out of two columns which are doublets of $SU(2)_L$ and at the same time the rows form two doublets of $SU(2)_R$ and has $B - L = 0$ because the leptons has $B_L = -1$. Hence $U(1)_{B-L}$ will be exact symmetry after Spontaneous Symmetry Breaking by ϕ only, So the first job of Higgs sector couldn't be achieved completely. So we have to add an extra Higgs field that transforms nontrivially under $SU(2)_R \times U(1)_{B-L}$ to break the LR symmetry to the SM one. In the LRIS we add anther Higgs doublet χ_R under the gauge group

$SU(2)_R$ to do the first job of Higgs completely.

Gauge invariance implies that the action of a group element of $SU(2)_L \times SU(2)_R$ on the Higgs multiplets is as follows

$$\phi \rightarrow U_L \phi U_R^\dagger, \quad \chi_R \rightarrow U_R \chi_R. \quad (4.4.23)$$

The bidoublet is a singlet under the $U(1)_{B-L}$ group. The doublet χ_R have $B-L = +1$ so that they transform under $U(1)_{B-L}$ as

$$\chi_R \rightarrow e^{-i\alpha(x)(B-L)/2} \chi_R = e^{-i\frac{\alpha(x)}{2}} \chi_R \quad (4.4.24)$$

Accordingly, the covariant derivative takes the following forms for each term

$$D_\mu \phi = \partial_\mu \phi - \frac{i g_L}{2} (\sigma \cdot W_{L,\mu}) \phi + \frac{i g_R}{2} \phi (\sigma \cdot W_{R,\mu}) \quad (4.4.25)$$

$$D_\mu \chi_R = \partial_\mu \chi_R - \frac{i g_R}{2} (\sigma \cdot W_{R,\mu}) \chi_R - i \frac{g_{BL}}{2} V_\mu \chi_R. \quad (4.4.26)$$

The scalar part of the Lagrangian contains the kinetic terms $\mathcal{L}_{\text{Scalar}}^{\text{Kin}}$ and potential $V(\phi, \chi_R)$ of Higgs multiplets

$$\mathcal{L}_{\text{Scalar}} = \mathcal{L}_{\text{Scalar}}^{\text{Kin}} - V(\phi, \chi_R) \quad (4.4.27)$$

where the kinetic Lagrangian of the scalars in the form

$$\mathcal{L}_{\text{Scalar}}^{\text{Kin}} = \text{Tr}[|D_\mu \phi|^2] + |D_\mu \chi_R|^2. \quad (4.4.28)$$

The most general Higgs potential that is invariant under the above mentioned symmetries (gauge and discrete) is given by [87]

$$\begin{aligned} V(\phi, \chi_R) = & \mu_1 \text{Tr}(\phi^\dagger \phi) + \mu_2 [\text{Tr}(\tilde{\phi} \phi^\dagger) + \text{Tr}(\phi^\dagger \tilde{\phi})] + \mu_3 (\chi_R^\dagger \chi_R) + \rho_1 (\chi_R^\dagger \chi_R)^2 \\ & + \lambda_1 (\text{Tr}(\phi^\dagger \phi))^2 + \lambda_2 [(\text{Tr}(\tilde{\phi} \phi^\dagger))^2 + (\text{Tr}(\phi^\dagger \tilde{\phi}))^2] + \lambda_3 \text{Tr}(\tilde{\phi} \phi^\dagger) \text{Tr}(\phi^\dagger \tilde{\phi}) \\ & + \lambda_4 \text{Tr}(\phi \phi^\dagger) (\text{Tr}(\tilde{\phi} \phi^\dagger) + \text{Tr}(\tilde{\phi}^\dagger \phi)) + \alpha_1 \text{Tr}(\phi^\dagger \phi) (\chi_R^\dagger \chi_R) + \alpha_2 (\chi_R^\dagger \phi^\dagger \tilde{\phi} \chi_R) \\ & + \alpha_3 (\chi_R^\dagger \tilde{\phi}^\dagger \tilde{\phi} \chi_R) + \alpha_4 (\chi_R^\dagger \phi^\dagger \tilde{\phi} \chi_R + h.c.). \end{aligned} \quad (4.4.29)$$

Here the conjugate Higgs bidoublet is defined as

$$\tilde{\phi} = \sigma_2 \phi^* \sigma_2 = \begin{pmatrix} \phi_2^{0*} & -\phi_2^+ \\ -\phi_1^- & \phi_1^{0*} \end{pmatrix} \quad (4.4.30)$$

and transforms in the same way as ϕ does.

The scalar potential contains the mass terms as well as the three and four-point self interactions for the Higgs fields. It is worth mentioning here that the potential parameters in (5.1.1) are constrained by the spectrum and minimization and boundedness from below conditions of the potential provided in the following.

To study the boundedness from below, and hence the stability, of the scalar potential (5.1.1) we use the co-positivity theorems of [204, 267] and follow the procedure used in [55] to ensure that the following symmetric matrix of the quartic terms, which are dominant at higher values of the fields, is co-positive:

$$\begin{pmatrix} \lambda_1 & \lambda_1 & \lambda_1 + 2\lambda_{23} & \lambda_1 & \frac{1}{2}\alpha_{13} & \frac{1}{2}\alpha_{12} \\ . & \lambda_1 & \lambda_1 & \lambda_1 + 2\lambda_3 & \frac{1}{2}\alpha_{12} & \frac{1}{2}\alpha_{13} \\ . & . & \lambda_1 & \lambda_1 & \frac{1}{2}\alpha_{12} & \frac{1}{2}\alpha_{13} \\ . & . & . & \lambda_1 & \frac{1}{2}\alpha_{13} & \frac{1}{2}\alpha_{12} \\ . & . & . & . & \rho_1 & \rho_1 \\ . & . & . & . & . & \rho_1 \end{pmatrix}. \quad (4.4.31)$$

Co-positivity of this matrix demands that $\lambda_1 > 0$, $\rho_1 > 0$, and either of the following cases

4.4.1. $\lambda_1 + 2\lambda_{23} > 0$, $\lambda_1 + 2\lambda_3 > 0$, $\alpha_{12} > 0$, $\alpha_{13} > 0$.

4.4.2. If $\lambda_1 + 2\lambda_{23} > 0$, $\lambda_1 + 2\lambda_3 < 0$, $\alpha_{12} > 0$, $\alpha_{13} > 0$, then $\lambda_3 < 0$ or $\lambda_1 + \lambda_3 > 0$ and $\lambda_2 > 0$.

4.4.3. If $\lambda_1 + 2\lambda_{23} < 0$, $\lambda_1 + 2\lambda_3 > 0$, $\alpha_{12} > 0$, $\alpha_{13} > 0$ then $\lambda_3 < 0$, $\lambda_2 < 0$ and $\lambda_1 + \lambda_{23} > 0$.

4.4.4. If $\lambda_1 + 2\lambda_{23} < 0$, $\lambda_1 + 2\lambda_3 < 0$, $\alpha_{12} > 0$, $\alpha_{13} > 0$, then $\lambda_3 < 0$.

4.4.5. If $\lambda_1 + 2\lambda_{23} > 0$, $\lambda_1 + 2\lambda_3 > 0$, $\alpha_{12} < 0$, $\alpha_{13} > 0$, then $\lambda_1\rho_1 > \frac{1}{4}\alpha_{13}^2$ and $\lambda_1\rho_1 > \frac{1}{2}(\alpha_{12} + \alpha_{13})^2$.

4.4.6. If $\lambda_1 + 2\lambda_{23} > 0$, $\lambda_1 + 2\lambda_3 > 0$, $\alpha_{12} > 0$, $\alpha_{13} < 0$, then $\lambda_1\rho_1 > \frac{1}{4}\alpha_{12}^2$ and $\lambda_1\rho_1 > \frac{1}{2}(\alpha_{12} + \alpha_{13})^2$.

4.4.7. If $\lambda_1 + 2\lambda_{23} > 0$, $\lambda_1 + 2\lambda_3 > 0$, $\alpha_{12} < 0$, $\alpha_{13} < 0$,
then $\lambda_1\rho_1 > \frac{1}{4}\alpha_{12}^2$ and $\lambda_1\rho_1 > \frac{1}{4}\alpha_{13}^2$ or $\lambda_1\rho_1 < \frac{1}{4}\alpha_{12}^2$ and $\lambda_1\rho_1 < \frac{1}{4}\alpha_{13}^2$.

4.4.8. If $\lambda_1 + 2\lambda_{23} < 0$, $\lambda_1 + 2\lambda_3 < 0$, $\alpha_{12} < 0$, $\alpha_{13} < 0$,
then $\lambda_3 < 0$ $\lambda_1\rho_1 > \frac{1}{4}\alpha_{12}^2$ and $\lambda_1\rho_1 > \frac{1}{4}\alpha_{13}^2$ or $\lambda_1\rho_1 < \frac{1}{4}\alpha_{12}^2$ and $\lambda_1\rho_1 < \frac{1}{4}\alpha_{13}^2$.

where we define $\alpha_{1i} = \alpha_1 + \alpha_i$, $i = 2, 3$, $\alpha_{32} = \alpha_3 - \alpha_2$ and $\lambda_{23} = 2\lambda_2 + \lambda_3$. Finally, field redifinition could be done to make quartic terms in potential like $\phi_1^0\phi_2^0\phi_R^+\phi_R^-$ nonnegative definite again as in [55].

The Gell-Mann-Nishijima formula of charges operators in LR models is

$$Q = T_L^3 + T_R^3 + Q_{BL}. \quad (4.4.32)$$

The Yukawa part contains mass terms for fermions and interaction between fermion and scalar field

$$\mathcal{L}_Y = \sum_{i,j=1}^3 y_{i,j}^L \bar{L}_{Li} \phi L_{Rj} + \tilde{y}_{i,j}^L \bar{L}_{Li} \tilde{\phi} L_{Rj} + y_{i,j}^Q \bar{Q}_{Li} \phi Q_{Rj} + \tilde{y}_{i,j}^Q \bar{Q}_{Li} \tilde{\phi} Q_{Rj} + y_{i,j}^s \bar{L}_{Ri} \tilde{\chi}_R S_{2j}^c + h.c., \quad (4.4.33)$$

where $y_{i,j}^L, \tilde{y}_{i,j}^L, y_{i,j}^Q, \tilde{y}_{i,j}^Q, y_{i,j}^s$, are 3×3 yukawa matrices which determine fermion masses. and $\tilde{\phi}$ is the dual bidoublet of the scalar bidoublet ϕ , defined as 4.4.30, and $\tilde{\chi}_R$ is the dual doublet of the scalar doublet χ_R , given by $\tilde{\chi}_R = i\tau_2 \chi_R^*$.

4.5 Spontaneous Symmetry Breaking in LRIS

Similar to SM and LRSM, all the fermions and gauge bosons must be massless. The symmetry Breaking of the LRIS is achieved in two stages first from LRIS to SM

with two Higgs doublet then breaking SM to EM, it occurs via VEV of scalar Higgs multiplets. The first symmetry breaking as following

$$SU(2)_L \times SU(2)_R \times U(1)_{B-L} \xrightarrow{\langle \chi_R \rangle} SU(2)_L \times U(1)_Y, \quad (4.5.1)$$

at this stage RH scalar Higgs doublet gets a VEV v_R and breaks LR symmetry to the SM symmetry. so Physical $W_{R,\mu}^\pm$ and Z_{R_μ} gauge bosons get their masses through interacting with RH Higgs doublet. After this stage, the hypercharge operator will appear as linear combination of the third component of the RH isospin operator T_R^3 and the $B - L$ operator Q_{BL} .

$$Y = T_R^3 + Q_{BL}. \quad (4.5.2)$$

The values of gauge couplings g_R and g_{BL} are related to the known coupling g_Y by:

$$\frac{1}{g_Y^2} = \frac{1}{g_R^2} + \frac{1}{g_{BL}^2} \quad (4.5.3)$$

then we can prove that hypercharge will be still symmetry after first breaking by effect Y to $\langle \chi_R \rangle$;

$$Y(\langle \chi_R \rangle) = T_R^3(\langle \chi_R \rangle) + Q_{B-L}(\langle \chi_R \rangle) = 0 \quad (4.5.4)$$

The next stage is the breaking of the SM symmetry by take VEV k_1, k_2 in the neutral components of the bidoublet Higgs for bidoublet ϕ .

$$SU(2)_L \times U(1)_Y \xrightarrow{\langle \phi \rangle, \langle \chi_L \rangle} U(1)_{EM}. \quad (4.5.5)$$

After this stage the physical $W_{L,\mu}^\pm$ and Z_{L_μ} gauge bosons acquire their masses. The values of the new gauge couplings g_R and g_{BL} are related to the EM charge e and the known coupling g_L by:

$$\frac{1}{e^2} = \frac{1}{g_L^2} + \frac{1}{g_R^2} + \frac{1}{g_{BL}^2} = \frac{1}{g_L^2} + \frac{1}{g_Y^2} \quad (4.5.6)$$

The VEVs of Higgs scalars are given to their neutral components

$$\langle \phi \rangle = \frac{1}{\sqrt{2}} \begin{pmatrix} k_1 & 0 \\ 0 & k_2 \end{pmatrix}, \quad \langle \chi_R \rangle = \frac{1}{\sqrt{2}} \begin{pmatrix} 0 \\ v_R \end{pmatrix} \quad (4.5.7)$$

where $v_R(\text{TeV}) \gg (k_1, k_2)(\text{GeV})$, and $\sqrt{k_1^2 + k_2^2} = v = 246 \text{ GeV}$ is the EW vacuum.

The scalar potential (5.1.1) leads to the following minimization condition(tadpole equation):

$$\lambda_1 k_1^3 + \lambda_4 k_2 (3k_1^2 + k_2^2) + k_1 \{k_2^2 (\lambda_1 + 2\lambda_{23}) + \mu_1 + \frac{1}{2}\alpha_{13}v_R^2\} + 2k_2\mu_2 + \frac{1}{2}\alpha_4 k_2 v_R^2 = 0, \quad (4.5.8)$$

$$\lambda_1 k_2^3 + \lambda_4 k_1 (k_1^2 + 3k_2^2) + k_2 \{k_1^2 (\lambda_1 + 2\lambda_{23}) + \mu_1 + \frac{1}{2}\alpha_{12}v_R^2\} + 2k_1\mu_2 + \frac{1}{2}\alpha_4 k_1 v_R^2 = 0, \quad (4.5.9)$$

$$\frac{1}{2}v_R \{\alpha_{13}k_1^2 + 2\alpha_4 k_1 k_2 + \alpha_{12}k_2^2 + 2(\mu_3 + \rho_1 v_R^2)\} = 0. \quad (4.5.10)$$

We solve them for μ_1 , μ_2 and μ_3 as follows

$$\mu_1 = -\lambda_1(k_1^2 + k_2^2) - 2\lambda_4 k_1 k_2 - \frac{\alpha_{12}k_2^2 - \alpha_{13}k_1^2}{2(k_2^2 - k_1^2)} v_R^2, \quad (4.5.11)$$

$$\mu_2 = -\frac{1}{2}\lambda_4(k_1^2 + k_2^2) - \lambda_{23}k_1 k_2 - \frac{1}{4}(\alpha_4 + \frac{\alpha_{32}k_1 k_2}{k_2^2 - k_1^2})v_R^2, \quad (4.5.12)$$

$$\mu_3 = -\frac{1}{2}(\alpha_{13}k_1^2 + 2\alpha_4 k_1 k_2 + \alpha_{12}k_2^2 + 2\rho_1 v_R^2). \quad (4.5.13)$$

4.5.1 Gauge Boson Masses

Now we turn to the gauge sector. The scalar bidoublet ϕ mixes the left and right gauge bosons. Thus, one can show that the symmetric mass matrix for neutral left, right and $B - L$ gauge bosons basis $(W_{R\mu}^3, V_\mu, W_{L\mu}^3)$, is given by

$$M_{ZZ'}^2 = \frac{1}{4} \begin{pmatrix} g_R^2(v_R^2 + v^2) & -g_{BL}g_R v_R^2 & -g_L g_R v^2 \\ . & g_{BL}^2 v_R^2 & 0 \\ . & . & g_L^2 v^2 \end{pmatrix}. \quad (4.5.14)$$

Notice that we exploit the symmetry of the matrix to write dots for the lower off diagonal elements instead of repeating them through the text. After the first stage of left-right symmetry breaking down to the SM symmetry, both the right and $B - L$ gauge bosons $W_{R\mu}^3$ and V_μ mix with an angle φ whose $s_\varphi = g_{BL}/\sqrt{g_R^2 + g_{BL}^2}$ to give the massless hypercharge $U(1)_Y$ gauge boson B_μ , while the right neutral gauge boson $Z_{R\mu}$ becomes massive. Then, the SM gauge symmetry is broken and $W_{L\mu}^3$, and B_μ mix with the Weinberg angle $\sin \theta_w \equiv s_w = e/g_L$ and give the photon A_μ and the left weak boson $Z_{L\mu}$. However, both $Z_{L\mu}$ and $Z_{R\mu}$ mix by the scalar bidoublet ϕ , as mentioned above, and give the physical states of Z_μ and Z'_μ bosons as follows

$$\begin{pmatrix} Z_{R\mu} \\ B_\mu \end{pmatrix} = \begin{pmatrix} c_\varphi & -s_\varphi \\ s_\varphi & c_\varphi \end{pmatrix} \begin{pmatrix} W_{R\mu}^3 \\ V_\mu \end{pmatrix}, \quad (4.5.15)$$

$$\begin{pmatrix} Z_{L\mu} \\ A_\mu \end{pmatrix} = \begin{pmatrix} c_w & -s_w \\ s_w & c_w \end{pmatrix} \begin{pmatrix} W_{L\mu}^3 \\ B_\mu \end{pmatrix}, \quad (4.5.16)$$

$$\begin{pmatrix} Z_\mu \\ Z'_\mu \end{pmatrix} = \begin{pmatrix} c_\vartheta & -s_\vartheta \\ s_\vartheta & c_\vartheta \end{pmatrix} \begin{pmatrix} Z_{L\mu} \\ Z_{R\mu} \end{pmatrix}. \quad (4.5.17)$$

This leads to the total mixing $(W_{R\mu}^3, V_\mu, W_{L\mu}^3)^T = U^0(Z'_\mu, Z_\mu, A_\mu)^T$, where $U^{0,T} M_Z^2 U^0 = \text{diag}(M_{Z'}^2, M_Z^2, 0)$ and the rotation matrix U^0 is

$$U^0 = \begin{pmatrix} c_\vartheta c_\varphi - s_\vartheta s_w s_\varphi & -s_\vartheta c_\varphi - c_\vartheta s_w s_\varphi & c_w s_\varphi \\ -c_\vartheta s_\varphi - s_\vartheta s_w c_\varphi & s_\vartheta s_\varphi - c_\vartheta s_w c_\varphi & c_w c_\varphi \\ s_\vartheta c_w & c_\vartheta c_w & s_w \end{pmatrix}, \quad (4.5.18)$$

where the $Z - Z'$ mixing angle ϑ is given by

$$\tan 2\vartheta = \frac{2M_{LR}}{M_{LL} - M_{RR}} = \frac{2g_2^3 \sqrt{g_2^2 + 2g_{BL}^2}}{(g_2^2 + g_{BL}^2)^2 (\frac{v_R}{v})^2 - 2g_2^2 g_{BL}^2}, \quad (4.5.19)$$

and the $(Z_{L\mu}, Z_{R\mu})$ symmetric mass matrix elements are

$$M_{LL} = \frac{g_2^2 v^2 (g_2^2 + 2g_{BL}^2)}{4(g_2^2 + g_{BL}^2)}, \quad (4.5.20)$$

$$M_{LR} = M_{RL} = \frac{-g_2^3 v^2 \sqrt{g_2^2 + 2g_{BL}^2}}{4(g_2^2 + g_{BL}^2)}, \quad (4.5.21)$$

$$M_{RR} = \frac{g_2^4 v^2 + (g_2^2 + g_{BL}^2)^2 v_R^2}{4(g_2^2 + g_{BL}^2)}. \quad (4.5.22)$$

The mass eigenvalues are given by

$$M_{Z,Z'}^2 = \frac{1}{2}(M_{LL} + M_{RR} \mp (M_{RR} - M_{LL})\sqrt{1 + \tan^2 2\vartheta}). \quad (4.5.23)$$

The LHC search for the Z' gauge boson is rather model dependent; in our case, we found that the following limits are imposed on $M_{Z'}$: $0.8 \lesssim M_{Z'} \lesssim 4.5$ TeV [1, 286].

The charged gauge boson symmetric mass matrix in basis $(W_{L\mu}^\pm, W_{R\mu}^\pm)$ is given by

$$M_{WW'}^2 = \frac{1}{4} \begin{pmatrix} g_L^2 v^2 & -g_L g_R v^2 s_{2\beta} \\ . & g_R^2 (v^2 + v_R^2) \end{pmatrix}. \quad (4.5.24)$$

Thus, the $W - W'$ diagonalization mixing angle ξ is

$$\tan 2\xi = \frac{2g_L g_R s_{2\beta}}{g_R^2 (1 + (\frac{v_R}{v})^2) - g_L^2}, \quad (4.5.25)$$

and the physical gauge bosons masses $M_{W,W'}$ are approximately

$$M_{W,W'}^2 = \frac{1}{8}(g_L^2 v^2 + g_R^2 (v^2 + v_R^2) \mp (g_R^2 (v^2 + v_R^2) - g_L^2 v^2)\sqrt{1 + \tan^2 2\xi}). \quad (4.5.26)$$

or approximately with $g_L = g_R$,

$$M_W = \frac{g_2 v}{2}, \quad M_{W'} = \frac{g_2 \sqrt{v^2 + v_R^2}}{2}. \quad (4.5.27)$$

The LHC's direct searches for W' impose stringent constraints on $M_{W'}$. These constraints, however, are model dependent, as they are determined by the assumptions imposed on the gauge couplings and the dominated channels of W' decays. In the LR model, the decay channel of W' to ν_R may be dominant, suppressing other decay channels to SM leptons or quarks. As a result, the bounds on $M_{W'}$ are relaxed, as highlighted in Ref. [165]. In this case, a conservative bound on the mass of the gauge boson W' is of order 2 TeV.

4.5.2 Fermion Masses

From yukawa terms one can get Dirac mass and neutrino mass from inverse seesaw for three generator of fermion

$$\mathcal{L}_Y = \sum_{i,j=1}^3 y_{i,j}^L \bar{L}_{Li} \phi L_{Rj} + \tilde{y}_{i,j}^L \bar{L}_{Li} \tilde{\phi} L_{Rj} + y_{i,j}^Q \bar{Q}_{Li} \phi Q_{Rj} + \tilde{y}_{i,j}^Q \bar{Q}_{Li} \tilde{\phi} Q_{Rj} + y_{ij}^s \bar{L}_{Ri} \tilde{\chi}_R S_2^c + h.c., \quad (4.5.28)$$

Dirac masses for fermions generated by couple ϕ and $\tilde{\phi}$ with both leptons and quarks, their Yukawa matrices are independent and allowing nontrivial quark and lepton mixings. χ_R only couple to leptons and new particle S_2 to generating Inverse seesaw matrix to get heavy neutrino masses.

After $B - L$ symmetry breaking, a small mass term $\mu_s \bar{S}_2^c S_2$ (and plausibly $\mu'_s \bar{S}_1^c S_1$) is generated from a non-renormalizable term (of dimension seven $\propto \chi_R^4 \bar{S}_2^c S_2 / M^3$), which implies that $\mu_s = \lambda_s v_R^4 / M^3 < \mathcal{O}(1) \text{ KeV}$ [11], where λ_s is an interaction effective dimensionless coupling. For $v_R \sim \mathcal{O}(10^3) \text{ GeV}$, one finds that $\mu_s \sim \mathcal{O}(10^{-7}) \text{ GeV}$ if $\lambda_s / M^3 \sim \mathcal{O}(10^{-19}) \text{ GeV}$. Thus, if $\lambda_s \sim \mathcal{O}(1)$, the non-renormalizable scale M is an intermediate scale, namely $M \sim \mathcal{O}(10^3) \text{ TeV}$. While for $\lambda_s \sim \mathcal{O}(10^{-3})$, one finds $M \sim \mathcal{O}(10) \text{ TeV}$. As a result, the Lagrangian of neutrino masses is given by

$$\mathcal{L}_m^\nu = M_D \bar{\nu}_L \nu_R + M_R \bar{\nu}_R^c S_2 + \mu_s \bar{S}_2^c S_2 + h.c., \quad (4.5.29)$$

where the 3×3 matrix $M_D = v(y^L s_\beta + \tilde{y}^L c_\beta) / \sqrt{2}$ is the Dirac neutrino mass matrix and the 3×3 matrix $M_R = y^s v_R / \sqrt{2}$. This is the standard neutrino IS matrices [173, 247, 248, 306]. Here, we have fixed the VEVs $k_{1,2}$ such that $v^2 = k_1^2 + k_2^2$ and $k_1 = v s_\beta$, $k_2 = v c_\beta$, where we define $s_x = \sin x$, $c_x = \cos x$ and $t_x = \tan x$, henceforth. In this regard, the following 9×9 neutrino mass matrix can be written as $\bar{\psi}^c \mathcal{M}_\nu \psi$ with

the flavour basis $\psi = (\nu_L^c, \nu_R, S_2)$ and

$$\mathcal{M}_\nu = \begin{pmatrix} 0 & M_D & 0 \\ M_D^T & 0 & M_R \\ 0 & M_R^T & \mu_s \end{pmatrix}. \quad (4.5.30)$$

The diagonalization of this mass matrix leads to the physical light and heavy neutrino states ν_{ℓ_i}, ν_{h_j} , $i = 1 \dots 3$, $j = 1 \dots 6$, with the following mass eigenvalues:

$$m_{\nu_{\ell_i}} = M_D M_R^{-1} \mu_s (M_R^T)^{-1} M_D^T, \quad i = 1 \dots 3, \quad (4.5.31)$$

$$m_{\nu_{h_j}}^2 = M_R^2 + M_D^2, \quad j = 1 \dots 6. \quad (4.5.32)$$

we note that this matrix in equation 4.5.30 can be diagonalization by 9×9 matrix V where

$$V^T M_\nu V = M_\nu^{diag} \quad (4.5.33)$$

On the other hand, after electroweak symmetry breaking, quarks and charged leptons acquire their masses via Higgs mechanism, as follows:

$$M_u = \frac{v}{\sqrt{2}} (y^Q s_\beta + \tilde{y}^Q c_\beta), \quad (4.5.34)$$

$$M_d = \frac{v}{\sqrt{2}} (y^Q c_\beta + \tilde{y}^Q s_\beta), \quad (4.5.35)$$

$$M_\ell = \frac{v}{\sqrt{2}} (y^L c_\beta + \tilde{y}^L s_\beta). \quad (4.5.36)$$

In contrast to the SM, fermions acquire their masses from different VEVs sources as shown in Eqs. (4.5.34-4.5.36). This allows the existence of a tree-level FCNC induced by neutral Higgs bosons exchange between different fermion families as we will see later. The physical fermions' masses are given after diagonalization by

$$M_u^{\text{diag}} = V_L^{u\dagger} M'^u V_R^u, \quad M_d^{\text{diag}} = V_L^{d\dagger} M'^d V_R^d, \quad M_\ell^{\text{diag}} = V_L^{\ell\dagger} M'^\ell V_R^\ell. \quad (4.5.37)$$

In this case, the quark Yukawa couplings can be written as

$$y^Q = -\frac{\sqrt{2}}{vc_{2\beta}} (s_\beta V_L^u M'^u V_R^{u\dagger} - c_\beta V_L^d M'^d V_R^{d\dagger}), \quad (4.5.38)$$

$$\tilde{y}^Q = -\frac{\sqrt{2}}{vc_{2\beta}}(c_\beta V_L^u M^u V_R^{u\dagger} - s_\beta V_L^d M^d V_R^{d\dagger}). \quad (4.5.39)$$

4.6 Higgs Sector in LRIS

As mentioned before, the Higgs sector of the LRIS consists of one bidoublet (ϕ) and one doublet (χ_R) complex scalar Higgs fields. The RH triplet (χ_R) is responsible for the first stage of symmetry breaking

$$SU(2)_L \times SU(2)_R \times U(1)_{B-L} \rightarrow SU(2)_L \times U(1)_Y \quad (4.6.1)$$

and the bidoublet (ϕ) accomplishes the second stage

$$SU(2)_L \times U(1)_Y \rightarrow U(1)_{\text{EM}} \quad (4.6.2)$$

Neutral component of Higgs fields are expanded around the vacuum as

$$\phi_1^0 = \frac{k_1 + h_1^0 + i\varphi_1^0}{\sqrt{2}}, \quad \phi_2^0 = \frac{k_2 + h_2^0 + i\varphi_2^0}{\sqrt{2}}, \quad \chi_R^0 = \frac{v_R + h_R^0 + i\varphi_R^0}{\sqrt{2}}. \quad (4.6.3)$$

It is worth noting that before symmetry breaking there were 12 scalar degrees of freedom: 8 of ϕ and 4 of χ_R . After symmetry breaking, two neutral components and four charged components of these degrees of freedom are eaten by the neutral gauge bosons: Z_μ and Z'_μ and the charged gauge bosons: W_μ^\pm and W'_μ^\pm to acquire their masses, respectively. Therefore in this class of models, six scalars remain as physical Higgs bosons, as we show, two of them are charged Higgs boson, one is a pseudoscalar Higgs boson, and the remaining three give CP -even neutral Higgs bosons.

4.6.1 Singly Charged Scalars

It can be easily seen that the symmetric mass matrix of the charged Higgs bosons in the basis $(\phi_1^\pm, \phi_2^\pm, \chi_R^\pm)$ is given by

$$M_{H^\pm}^2 = \frac{\alpha_{32}}{2} \begin{pmatrix} \frac{v_R^2 s_\beta^2}{c_{2\beta}} & \frac{v_R^2 s_{2\beta}}{2c_{2\beta}} & -vv_R s_\beta \\ \cdot & \frac{v_R^2 c_\beta^2}{c_{2\beta}} & -vv_R c_\beta \\ \cdot & \cdot & v^2 c_{2\beta} \end{pmatrix}. \quad (4.6.4)$$

Notice that since $s_\beta \ll 1$, the entries of the above matrix are of following orders: $(M_{H^\pm}^2)_{11} \ll v_R^2$, $(M_{H^\pm}^2)_{22} \approx v_R^2$ and $(M_{H^\pm}^2)_{33} \approx v^2$, while the off-diagonal are given by $(M_{H^\pm}^2)_{12} \ll v_R^2$, $(M_{H^\pm}^2)_{13} < vv_R$ and $(M_{H^\pm}^2)_{23} \approx vv_R$. The matrix $M_{H^\pm}^2$ can be diagonalized by a unitary matrix

$$Z^{H^\pm} = \begin{pmatrix} \frac{vc_{2\beta}}{\sqrt{v^2c_{2\beta}^2+v_R^2s_\beta^2}} & 0 & \frac{v_Rs_\beta}{\sqrt{v^2c_{2\beta}^2+v_R^2s_\beta^2}} \\ -\frac{\frac{1}{2}v_R^2s_{2\beta}}{\sqrt{(v^2c_{2\beta}^2+v_R^2s_\beta^2)(v^2c_{2\beta}^2+v_R^2)}} & \sqrt{\frac{v^2c_{2\beta}^2+v_R^2s_\beta^2}{v^2c_{2\beta}^2+v_R^2}} & \frac{vv_Rc_\beta c_{2\beta}}{\sqrt{(v^2c_{2\beta}^2+v_R^2s_\beta^2)(v^2c_{2\beta}^2+v_R^2)}} \\ -\frac{v_Rs_\beta}{\sqrt{v^2c_{2\beta}^2+v_R^2}} & -\frac{v_Rc_\beta}{\sqrt{v^2c_{2\beta}^2+v_R^2}} & \frac{vc_{2\beta}}{\sqrt{v^2c_{2\beta}^2+v_R^2}} \end{pmatrix}, \quad (4.6.5)$$

such that $Z^{H^\pm} M_{H^\pm}^2 Z^{H^\pm T} = \text{diag}(0, 0, m_{H^\pm}^2)$ and $(\phi_1^\pm, \phi_2^\pm, \chi_R^\pm)^T = Z^{H^\pm T} (G_1^\pm, G_2^\pm, H^\pm)^T$, where G_1^\pm and G_2^\pm are the charged Goldstone bosons eaten by the charged gauge bosons W_μ and W'_μ to acquire their masses via the Higgs mechanism. In addition, it remains one massive eigenstate of a physical charged Higgs boson H^\pm , with the following mass:

$$m_{H^\pm}^2 = \frac{\alpha_{32}}{2} \left(\frac{v_R^2}{c_{2\beta}} + v^2 c_{2\beta} \right), \quad (4.6.6)$$

where $\alpha_{32} = \alpha_3 - \alpha_2$. Thus, if $v_R \sim \mathcal{O}(\text{TeV})$ and $\alpha_{32} \sim \mathcal{O}(10^{-2})$, then the charged Higgs mass is in the order of hundreds GeV as in Tab. 5.1. The physical charged Higgs boson is given through the rotation matrix Z^{H^\pm} by

$$H^\pm = Z_{13}^{H^\pm} \phi_1^\pm + Z_{23}^{H^\pm} \phi_2^\pm + Z_{33}^{H^\pm} \chi_R^\pm, \quad (4.6.7)$$

where $Z_{13}^{H^\pm} \approx 1$, while $Z_{23}^{H^\pm} \approx v/(v_R t_\beta) < 1$ and $Z_{33}^{H^\pm} \approx v/v_R \ll 1$. Therefore, the charged Higgs is mainly made of ϕ_1^\pm . in fig 4.2 we can see plt of charged Higgs boson verses α_{32}

4.6.2 Neutral Pseudoscalars

Now, we consider the neutral scalar fields and their masses. This can be obtained if one fluctuates the neutral components of the bidoublet ϕ and the doublet χ_R around

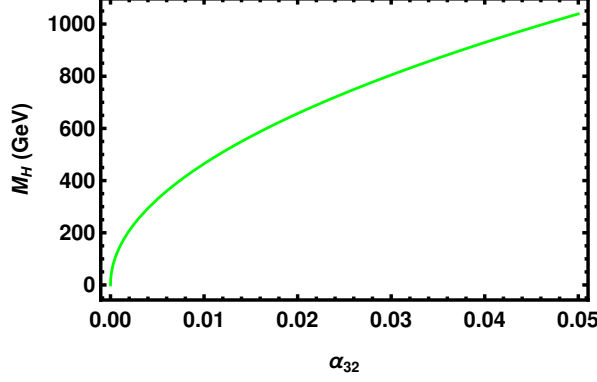


Figure 4.2: The Charged Higgs boson mass M_H as a function of the most relevant parameter α_{32} . The other involved parameters are varied as in Eq. (5.1.12).

their vacua as follows:

$$\phi_i^0 = \frac{1}{\sqrt{2}}(v_i + \phi_i^{0R} + i\phi_i^{0I}), \quad (4.6.8)$$

where $\phi_i = \phi_{1,2}, \chi_R$ and $v_i = k_{1,2}, v_R$. In this case, the symmetric mass matrix of the CP -odd Higgs bosons is given by

$$(M_A^2)_{ij} = \left. \frac{\partial^2 V(\phi, \chi_{L,R})}{\partial \phi_i^{0I} \partial \phi_j^{0I}} \right|_{\langle \phi_{i,j}^{0R} \rangle = \langle \phi_{i,j}^{0I} \rangle = 0}. \quad (4.6.9)$$

Therefore, in the basis $(\phi_1^{0I}, \phi_2^{0I}, \chi_R^{0I})$ the pseudoscalar Higgs mass matrix is given by

$$M_A^2 = \frac{1}{2} \left(\frac{v_R^2 \alpha_{32}}{c_{2\beta}} - 4v^2(2\lambda_2 - \lambda_3) \right) \begin{pmatrix} c_\beta^2 & s_\beta c_\beta & 0 \\ . & s_\beta^2 & 0 \\ . & . & 0 \end{pmatrix}, \quad (4.6.10)$$

which can be diagonalized by a unitary matrix

$$Z^A = \begin{pmatrix} 0 & 0 & 1 \\ -s_\beta & c_\beta & 0 \\ c_\beta & s_\beta & 0 \end{pmatrix}, \quad (4.6.11)$$

such that $Z^A M_A^2 Z^{AT} = \text{diag}(0, 0, m_A^2)$ and $(\phi_1^{0I}, \phi_2^{0I}, \chi_R^{0I})^T = Z^{AT} (G_1^0, G_2^0, A)^T$, where G_1^0 and G_2^0 are the neutral Goldstone bosons eaten by the two neutral gauge bosons Z_μ and Z'_μ to acquire their masses, and the following non-zero eigenvalue is the physical

mass of pseudoscalar boson A

$$m_A^2 = \frac{1}{2} \left(\frac{v_R^2}{c_{2\beta}} \alpha_{32} - 4v^2(2\lambda_2 - \lambda_3) \right). \quad (4.6.12)$$

Thus, for $v_R \sim \mathcal{O}(\text{TeV})$ and $\alpha_{32} \sim \mathcal{O}(10^{-2})$, the pseudoscalar Higgs mass is in the order of a few hundred GeVs, as well as in Tab. 5.1. The physical pseudoscalar Higgs boson is given through the rotation matrix Z^A by

$$A = c_\beta \phi_1^{0I} + s_\beta \phi_2^{0I}. \quad (4.6.13)$$

According to our choice $s_\beta \ll 1$ and $A \approx \phi_1^{0I}$.

In fig 4.3 we can see plt of charged Higgs boson verses α_{32} and λ_{23}

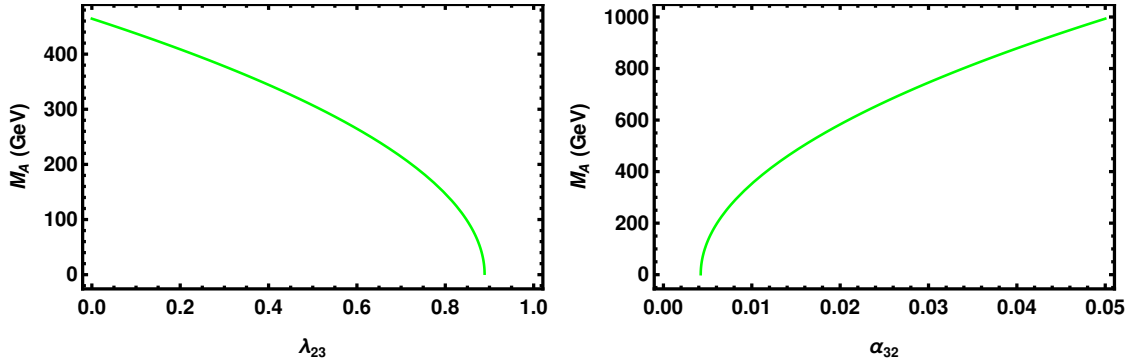


Figure 4.3: The CP-odd Higgs boson mass M_A as a function of the most relevant parameter α_{32} and λ_{23} . The other involved parameters are varied as in Eq. (5.1.12).

4.6.3 Neutral Scalars

Finally, we consider the CP -even Higgs bosons. Similar to the CP -odd Higgs, the (3×3) symmetric mass matrix of CP -even Higgs bosons is given by

$$(M_H^2)_{ij} = (m_{ij}) \frac{\partial^2 V(\phi, \chi_{L,R})}{\partial \phi_i^{0R} \partial \phi_j^{0R}} \Big|_{\langle \phi_{i,j}^{0R} \rangle = \langle \phi_{i,j}^{0I} \rangle = 0}, \quad (4.6.14)$$

with elements in basis $(\phi_1^{\text{Re}}, \phi_2^{\text{Re}}, \chi_R^{\text{Re}})$

$$m_{11} = 2v^2(\lambda_1 s_\beta^2 + \lambda_{23} c_\beta^2 + \lambda_4 s_{2\beta}) + \frac{1}{4} \left(\frac{1}{c_{2\beta}} + 1 \right) \alpha_{32} v_R^2, \quad (4.6.15)$$

$$m_{12} = m_{21} = v^2((\lambda_1 + \lambda_{23})s_{2\beta} + 2\lambda_4) - \frac{1}{4}\alpha_{32}v_R^2t_{2\beta}, \quad (4.6.16)$$

$$m_{13} = m_{31} = vv_R(\alpha_{13}s_\beta + \alpha_4c_\beta), \quad (4.6.17)$$

$$m_{22} = 2v^2(\lambda_1c_\beta^2 + \lambda_{23}s_\beta^2 + \lambda_4s_{2\beta}) + \frac{1}{4}(\frac{1}{c_{2\beta}} - 1)\alpha_{32}v_R^2, \quad (4.6.18)$$

$$m_{23} = m_{32} = vv_R(\alpha_{12}c_\beta + \alpha_4s_\beta), \quad (4.6.19)$$

$$m_{33} = 2\rho_1v_R^2, \quad (4.6.20)$$

where $\alpha_{1i} = \alpha_1 + \alpha_i$, $i = 2, 3$ and $\lambda_{23} = 2\lambda_2 + \lambda_3$. This matrix can be diagonalized by a unitary transformation matrix Z^H such that $Z^H M_H^2 Z^{HT} = \text{diag}(m_{H_1}^2, m_{H_2}^2, m_{H_3}^2)$ and $(\phi_1^{0R}, \phi_2^{0R}, \chi_R^{0R})^T = Z^{HT}(H_1, H_2, H_3)^T$. The coefficients of the rotation matrix Z^H are given explicitly below. After rotation we obtain three massive neutral Higgs bosons:

$$H_i = Z_{ij}^H \phi_j^{0R}. \quad (4.6.21)$$

As emphasized, the lightest eigenstate $H_1 \equiv h$ will be the SM-like Higgs boson that we fix its mass with $m_h = 125$ GeV [4, 105]. This condition can be used to fix the value of one of the involved parameters, λ_1 . The other two eigenvalues are given by

$$m_{H_{2,3}}^2 = \frac{1}{2} \left(T^h - m_h^2 \mp \sqrt{(T^h - m_h^2)^2 - \frac{4D^h}{m_h^2}} \right), \quad (4.6.22)$$

where the trace T^h of the Higgs matrix M_H^2 is

$$T^h = \text{Tr}(M_H^2) = 2v^2(\lambda_1 + \lambda_{23} + 2\lambda_4s_{2\beta}) + (\frac{\alpha_{32}}{2c_{2\beta}} + 2\rho_1)v_R^2, \quad (4.6.23)$$

and D^h is the determinant of M_H^2 , which is explicitly given in below.

before close this part of neutral scalar we can note some important remark from mass matrix of neutral Higgs. in order (for $t_\beta \ll 1$): (i) To obtain the SM-like Higgs boson h and another Higgs boson h' of order of a few GeVs we take $\lambda_1 \sim \mathcal{O}(10^{-1})$ and $\alpha_{32} \sim \mathcal{O}(10^{-2})$ so that $m_{11}, m_{22} \sim \mathcal{O}(\text{GeV}^2)$. (ii) Taking $\rho_1 \sim \mathcal{O}(10^{-1})$ alongside $\alpha_{32} \sim \mathcal{O}(10^{-2})$ leads to small mixing between χ_R^{0R} and the bidoublet components $\phi_{1,2}^{0R}$

such that $m_{13}^2/(m_{11}m_{33}) \ll 1$ and $m_{23}^2/(m_{22}m_{33}) \ll 1$. This leads to the small mixing of χ_R^{0R} and the light states h, h' and small mixing between the heaviest state H_3 and the bidoublet components $\phi_{1,2}^{0R}$, *i.e.* $Z_{13}^H, Z_{23}^H, Z_{31}^H, Z_{32}^H \sim \mathcal{O}(10^{-2} - 10^{-1}) \ll 1$, as in Table 5.1c. Thus, the heaviest Higgs boson $H_3 \sim \chi_R^{0R}$ with a mass $m_{H_3}^2 \approx m_{33}$. (iii) Moreover, if we assume that $\lambda_{23} \geq \lambda_1$, one finds that $m_{11} > m_{22}$ and $m_{12}^2/(m_{11}m_{22}) \ll 1$, which implies that the mixing $Z_{11}^H, Z_{22}^H \sim \mathcal{O}(10^{-2} - 10^{-1}) < 1$ as in Table 5.1c. Accordingly, the SM-like Higgs boson can be defined as $H_1 \sim \phi_2^{0R}$ and the next lightest Higgs boson is given by $H_2 \sim \phi_1^{0R}$, with masses $m_{H_1}^2 \approx m_{22} - m_{12}^2/(m_{11} - m_{22}) < m_{H_2}^2 \approx m_{11} + m_{12}^2/(m_{11} - m_{22})$. In addition, this keeps the SM-like Higgs couplings with the SM fermions and gauge bosons intact. (iv) For small values of λ_4 , one finds that H_1 could be the lightest while H_2 may represent the SM-like Higgs boson. However, for most of the parameter space ($\lambda_4, \alpha_{32}, t_\beta$) we have H_1 as the SM-like Higgs boson, and this is what we adopted here as in Eq. (5.1.12) below. (v) Due to the mass hierarchy considered here, values of $\alpha_{12,13}$ and α_4 are not constrained for the mass spectrum. But in our LHC analysis below, we see that large values of α_4 and λ_4 , as in Eq. (5.1.12) and Table 5.1, are preferable for large coupling $g_{h'hh}$ in Eq. (5.1.14), and hence for large $\sigma(h' \rightarrow hh)$. Lastly, we should mention here that all parameters are constrained by the copositivity conditions above.

The explicit rotation coefficients of the CP -even Higgs mass matrix (5.1.2) are [52, 278]

$$Z_{11}^H = \frac{f_{11}}{\sqrt{f_{11}^2 + f_{21}^2 + 1}}, \quad (4.6.24)$$

$$Z_{12}^H = \frac{f_{21}}{\sqrt{f_{11}^2 + f_{21}^2 + 1}}, \quad (4.6.25)$$

$$Z_{13}^H = \frac{1}{\sqrt{f_{11}^2 + f_{21}^2 + 1}}, \quad (4.6.26)$$

$$Z_{21}^H = \frac{f_{12}(1 + f_{21}^2) - f_{11}(1 + f_{21}f_{22})}{\sqrt{(1 + f_{11}^2 + f_{21}^2)\{(f_{11} - f_{12})^2 + (f_{21} - f_{22})^2 + (f_{12}f_{21} - f_{11}f_{22})^2\}}}, \quad (4.6.27)$$

$$Z_{22}^H = \frac{f_{22}(1 + f_{11}^2) - f_{21}(1 + f_{11}f_{12})}{\sqrt{(1 + f_{11}^2 + f_{21}^2)\{(f_{11} - f_{12})^2 + (f_{21} - f_{22})^2 + (f_{12}f_{21} - f_{11}f_{22})^2\}}}, \quad (4.6.28)$$

$$Z_{23}^H = \frac{f_{11}(f_{11} - f_{12}) + f_{21}(f_{21} - f_{22})}{\sqrt{(1 + f_{11}^2 + f_{21}^2)\{(f_{11} - f_{12})^2 + (f_{21} - f_{22})^2 + (f_{12}f_{21} - f_{11}f_{22})^2\}}}, \quad (4.6.29)$$

$$Z_{31}^H = \frac{(\text{sgn})(f_{22} - f_{21})}{\sqrt{(f_{11} - f_{12})^2 + (f_{21} - f_{22})^2 + (f_{12}f_{21} - f_{11}f_{22})^2}}, \quad (4.6.30)$$

$$Z_{32}^H = \frac{(\text{sgn})(f_{11} - f_{12})}{\sqrt{(f_{11} - f_{12})^2 + (f_{21} - f_{22})^2 + (f_{12}f_{21} - f_{11}f_{22})^2}}, \quad (4.6.31)$$

$$Z_{33}^H = \frac{(\text{sgn})(f_{12}f_{21} - f_{11}f_{22})}{\sqrt{(f_{11} - f_{12})^2 + (f_{21} - f_{22})^2 + (f_{12}f_{21} - f_{11}f_{22})^2}}, \quad (4.6.32)$$

where the sign term is

$$\text{sgn} = \text{sign}\{f_{11}(f_{23} - f_{22}) + f_{12}(f_{21} - f_{23}) + f_{13}(f_{22} - f_{21})\}, \quad (4.6.33)$$

and $f_{ij} = f_i(m_{H_j}^2)$, ($i = 1, 2$, $j = 1 \dots 3$) and the functions f_i 's are

$$f_1(x) = \frac{(m_{22} - x)(m_{33} - x) - m_{23}^2}{m_{12}m_{23} - m_{13}(m_{22} - x)}, \quad (4.6.34)$$

$$f_2(x) = -\frac{m_{12}(m_{33} - x) - m_{13}m_{23}}{m_{12}m_{23} - m_{13}(m_{22} - x)}. \quad (4.6.35)$$

The determinant of the CP -even Higgs mass matrix (5.1.2) is given by

$$\begin{aligned} D^h &= v^2 v_R^2 (-(\alpha_{12}c_\beta + \alpha_4s_\beta)((\alpha_{12}c_\beta + \alpha_4s_\beta)(v^2(c_{2\beta}(\lambda_{23} - \lambda_1) + 2\lambda_4s_{2\beta}) \\ &\quad - \frac{1}{4}\alpha_{32}v_R^2sc_{2\beta} + v^2(\lambda_1 + \lambda_{23}) - \frac{\alpha_{32}v_R^2}{4}) \\ &\quad - \frac{1}{4}(\alpha_{13}s_\beta + \alpha_4c_\beta)(4v^2(s_{2\beta}(\lambda_1 + \lambda_{23}) + 2\lambda_4) + \alpha_{32}v_R^2t_{2\beta})) \\ &\quad + (\alpha_{13}s_\beta + \alpha_4c_\beta)((\alpha_{12}c_\beta + \alpha_4s_\beta)(v^2s_{2\beta}(\lambda_1 + \lambda_{23}) \\ &\quad + \frac{1}{4}\alpha_{32}v_R^2t_{2\beta} + 2\lambda_4v^2) - (\alpha_{13}s_\beta + \alpha_4c_\beta)(v^2(c_{2\beta}(\lambda_1 - \lambda_{23}) + 2\lambda_4s_{2\beta}) \\ &\quad - \frac{1}{4}\alpha_{32}v_R^2sc_{2\beta} + v^2(\lambda_1 + \lambda_{23}) + \frac{\alpha_{32}v_R^2}{4})) \\ &\quad + \rho_1sc_{2\beta}(6v^2c_{2\beta}(\lambda_1\lambda_{23} - \lambda_4^2) + 2v^2c_{6\beta}(\lambda_1\lambda_{23} - \lambda_4^2) + \alpha_{32}\lambda_{23}v_R^2c_{4\beta} \\ &\quad - 4\alpha_{32}\lambda_4v_R^2s_{2\beta} - \alpha_{32}v_R^2(2\lambda_1 + \lambda_{23}))). \end{aligned} \quad (4.6.36)$$

5

PHENOMENOLOGY OF LRIS

5.1 Search for a heavy neutral Higgs boson in LRIS at the LHC

Here, we consider an example of a LR model, with a Higgs sector consisting of one scalar bidoublet and a scalar right-handed doublet. In this case and in order to generate light neutrino masses, we adopt the inverse-seesaw (IS) mechanism [93, 173, 247, 248, 306]. As known, this mechanism requires introducing other singlet fermions that couple with right-handed neutrinos and have a small mass [$\sim \mathcal{O}(1)$ KeV], which may be generated radiatively. The IS mechanism is quite motivated by having the TeV scale LR model that can be probed in current and future colliders, while in the conventional LR model, the GUT scale is the typical scale of breaking LR symmetry, where right-handed neutrino masses are generated. Moreover, in the limit of vanishing the above mentioned tiny mass, we will have massless left-handed neutrinos and the lepton number symmetry is restored. Thus, such a small scale can be considered, according to 't Hooft naturalness criteria [293], as a natural scale of a global symmetry (lepton number) breaking. We also argue that in this class of models the tree-level flavor changing neutral current (FCNC) is under control. It turns out that

the right-handed doublet is essentially decoupled from the two Higgs doublets, generated from the bidoublet; hence the Higgs sector of this model mimics the scenario of two the Higgs doublet model [128, 183, 184]. We show that the lightest CP -even Higgs boson, the SM-like Higgs boson, and the next lightest are generated from the neutral components of the bidoublet. For a wide range of the parameter space, one can show that the mass of the next lightest Higgs boson is of the order a few hundred GeVs.

In this section we analyze the discovery prospects of the next lightest CP -even neutral Higgs boson, h' , at the LHC. Our searches are performed by looking for resonant peaks in two processes, namely $h' \rightarrow hh \rightarrow b\bar{b}\gamma\gamma$ and $h' \rightarrow ZZ \rightarrow 4\ell$ ($\ell = e, \mu$). The analysis is pivoted on three benchmark points, with $m_{h'} = 250$ GeV, 400 GeV, and 600 GeV, for a center-of-mass energy $\sqrt{s} = 14$ TeV and $L_{\text{int}} = 300 \text{ fb}^{-1}$, and 3000 fb^{-1} , respectively. After imposing various sets of cuts to reduce backgrounds (B) and improve the statistical significance (S/\sqrt{B}), where S refers to the signal, we find that the SM-like Higgs boson pair production, with $b\bar{b}\gamma\gamma$ final states, is the most promising channel for probing our heavy Higgs boson at the LHC. The channel of the Z -pair production, decay to 4ℓ is less significant as its cross section is very small for $m_{h'} \gtrsim 300$ GeV, and the associated background is quite large for $m_{h'} \simeq 200$ GeV. We show that to probe h' through this channel, L_{int} must be increased up to $L_{\text{int}} = 3000 \text{ fb}^{-1}$.

5.1.1 Heavy Neutral CP-Even Higgs Boson in LRIS

As mentioned in the previous section, the Higgs sector of the LRIS consists of a bidoublet ϕ and a right doublet χ_R as in Table 4.1, and the gauge symmetries $SU(2)_R \times U(1)_{B-L}$ are spontaneously broken to $U(1)_Y$ through the VEV of χ_R , then the $SU(2)_L \times U(1)_Y$ symmetries are broken by VEVs of ϕ . The most general Higgs potential that is invariant under the above mentioned symmetries (gauge and discrete)

is given by [87]

$$\begin{aligned}
 V(\phi, \chi_R) = & \mu_1 \text{Tr}(\phi^\dagger \phi) + \mu_2 [\text{Tr}(\tilde{\phi} \phi^\dagger) + \text{Tr}(\tilde{\phi}^\dagger \phi)] + \mu_3 (\chi_R^\dagger \chi_R) + \rho_1 (\chi_R^\dagger \chi_R)^2 \\
 & + \lambda_1 (\text{Tr}(\phi^\dagger \phi))^2 + \lambda_2 [(\text{Tr}(\tilde{\phi} \phi^\dagger))^2 + (\text{Tr}(\tilde{\phi}^\dagger \phi))^2] + \lambda_3 \text{Tr}(\tilde{\phi} \phi^\dagger) \text{Tr}(\tilde{\phi}^\dagger \phi) \\
 & + \lambda_4 \text{Tr}(\phi \phi^\dagger) (\text{Tr}(\tilde{\phi} \phi^\dagger) + \text{Tr}(\tilde{\phi}^\dagger \phi)) + \alpha_1 \text{Tr}(\phi^\dagger \phi) (\chi_R^\dagger \chi_R) + \alpha_2 (\chi_R^\dagger \phi^\dagger \phi \chi_R) \\
 & + \alpha_3 (\chi_R^\dagger \tilde{\phi}^\dagger \tilde{\phi} \chi_R) + \alpha_4 (\chi_R^\dagger \phi^\dagger \tilde{\phi} \chi_R + h.c.).
 \end{aligned} \tag{5.1.1}$$

It is worth mentioning here that the potential parameters in (5.1.1) are constrained by the spectrum and minimization and boundedness from below conditions of the potential provided in Sec. 4.5.

It is worth noting that before symmetry breaking there were 12 scalar degrees of freedom: 8 of ϕ and 4 of χ_R . After symmetry breaking, two neutral components and four charged components of these degrees of freedom are eaten by the neutral gauge bosons: Z_μ and Z'_μ and the charged gauge bosons: W_μ^\pm and W'_μ^\pm to acquire their masses, respectively. Therefore in this class of models, six scalars remain as physical Higgs bosons; as we show, two of them are charged Higgs bosons, one is a pseudoscalar Higgs boson, and the remaining three give CP -even neutral Higgs bosons.

We consider the CP -even Higgs bosons. The (3×3) symmetric mass matrix of CP -even Higgs bosons is given by

$$(M_H^2)_{ij} = \frac{\partial^2 V(\phi, \chi_{L,R})}{\partial \phi_i^{0R} \partial \phi_j^{0R}} \Big|_{\langle \phi_{i,j}^{0R} \rangle = \langle \phi_{i,j}^{0I} \rangle = 0}, \tag{5.1.2}$$

with the elements

$$m_{11} = 2v^2(\lambda_1 s_\beta^2 + \lambda_{23} c_\beta^2 + \lambda_4 s_{2\beta}) + \frac{1}{4} \left(\frac{1}{c_{2\beta}} + 1 \right) \alpha_{32} v_R^2, \tag{5.1.3}$$

$$m_{12} = m_{21} = v^2((\lambda_1 + \lambda_{23}) s_{2\beta} + 2\lambda_4) - \frac{1}{4} \alpha_{32} v_R^2 t_{2\beta}, \tag{5.1.4}$$

$$m_{13} = m_{31} = v v_R (\alpha_{13} s_\beta + \alpha_4 c_\beta), \tag{5.1.5}$$

$$m_{22} = 2v^2(\lambda_1 c_\beta^2 + \lambda_{23} s_\beta^2 + \lambda_4 s_{2\beta}) + \frac{1}{4} \left(\frac{1}{c_{2\beta}} - 1 \right) \alpha_{32} v_R^2, \tag{5.1.6}$$

$$m_{23} = m_{32} = vv_R(\alpha_{12}c_\beta + \alpha_4s_\beta), \quad (5.1.7)$$

$$m_{33} = 2\rho_1v_R^2, \quad (5.1.8)$$

where $\alpha_{1i} = \alpha_1 + \alpha_i$, $i = 2, 3$ and $\lambda_{23} = 2\lambda_2 + \lambda_3$. This matrix can be diagonalized by a unitary transformation matrix Z^H such that $Z^H M_H^2 Z^{HT} = \text{diag}(m_{H_1}^2, m_{H_2}^2, m_{H_3}^2)$ and $(\phi_1^{0R}, \phi_2^{0R}, \chi_R^{0R})^T = Z^{HT}(H_1, H_2, H_3)^T$. The coefficients of the rotation matrix Z^H are given explicitly in Sec. 4.5. After rotation, we obtain three massive neutral Higgs bosons

$$H_i = Z_{ij}^H \phi_j^{0R}. \quad (5.1.9)$$

Here, a few remarks are in order (for $t_\beta \ll 1$): (i) To obtain the SM-like Higgs boson h and another Higgs boson h' of order of a few GeVs we take $\lambda_1 \sim \mathcal{O}(10^{-1})$ and $\alpha_{32} \sim \mathcal{O}(10^{-2})$ so that $m_{11}, m_{22} \sim \mathcal{O}(\text{GeV}^2)$. (ii) Taking $\rho_1 \sim \mathcal{O}(10^{-1})$ alongside $\alpha_{32} \sim \mathcal{O}(10^{-2})$ leads to small mixing between χ_R^{0R} and the bidoublet components $\phi_{1,2}^{0R}$ such that $m_{13}^2/(m_{11}m_{33}) \ll 1$ and $m_{23}^2/(m_{22}m_{33}) \ll 1$. This leads to the small mixing of χ_R^{0R} and the light states h, h' and small mixing between the heaviest state H_3 and the bidoublet components $\phi_{1,2}^{0R}$, *i.e.* $Z_{13}^H, Z_{23}^H, Z_{31}^H, Z_{32}^H \sim \mathcal{O}(10^{-2} - 10^{-1}) \ll 1$, as in Table 5.1c. Thus, the heaviest Higgs boson $H_3 \sim \chi_R^{0R}$ with a mass $m_{H_3}^2 \approx m_{33}$. (iii) Moreover, if we assume that $\lambda_{23} \geq \lambda_1$, one finds that $m_{11} > m_{22}$ and $m_{12}^2/(m_{11}m_{22}) \ll 1$, which implies that the mixing $Z_{11}^H, Z_{22}^H \sim \mathcal{O}(10^{-2} - 10^{-1}) < 1$ as in Table 5.1c. Accordingly, the SM-like Higgs boson can be defined as $H_1 \sim \phi_2^{0R}$ and the next lightest Higgs boson is given by $H_2 \sim \phi_1^{0R}$, with masses $m_{H_1}^2 \approx m_{22} - m_{12}^2/(m_{11} - m_{22}) < m_{H_2}^2 \approx m_{11} + m_{12}^2/(m_{11} - m_{22})$. In addition, this keeps the SM-like Higgs couplings with the SM fermions and gauge bosons intact. (iv) For small values of λ_4 , one finds that H_1 could be the lightest while H_2 may represent the SM-like Higgs boson. However, for most of the parameter space $(\lambda_4, \alpha_{32}, t_\beta)$ we have H_1 as the SM-like Higgs boson, and this is what we adopted here as in Eq. (5.1.12) below. (v) Due to the mass hierarchy considered here, values of $\alpha_{12,13}$ and α_4 are not constrained for

the mass spectrum. But in our LHC analysis below, we see that large values of α_4 and λ_4 , as in Eq. (5.1.12) and Table 5.1, are preferable for large coupling $g_{h'h h}$ in Eq. (5.1.14), and hence for large $\sigma(h' \rightarrow hh)$. Lastly, we should mention here that all parameters are constrained by the copositivity conditions of Sec. 4.5.

As emphasized, the lightest eigenstate $H_1 \equiv h$ will be the SM-like Higgs boson that we fix its mass with $m_h = 125$ GeV [4, 105]. This condition can be used to fix the value of one of the involved parameters, λ_1 . The other two eigenvalues are given by

$$m_{H_{2,3}}^2 = \frac{1}{2} \left(T^h - m_h^2 \mp \sqrt{(T^h - m_h^2)^2 - \frac{4D^h}{m_h^2}} \right), \quad (5.1.10)$$

where the trace T^h of the Higgs matrix M_H^2 is

$$T^h = \text{Tr}(M_H^2) = 2v^2(\lambda_1 + \lambda_{23} + 2\lambda_4 s_{2\beta}) + \left(\frac{\alpha_{32}}{2c_{2\beta}} + 2\rho_1 \right) v_R^2, \quad (5.1.11)$$

and D^h is the determinant of M_H^2 , which is explicitly given in Sec. 4.5. From Eq. (5.1.10), one can show that the next lightest CP -even neutral Higgs boson, $H_2 \equiv h'$, could have a mass of order a few hundred GeVs, as shown in Fig. 5.1 (left). In this figure, $m_{h'}$ is given as function of α_{32} , which is one of the relevant parameters in the scalar potential, with choosing $\lambda_{23} \in [-0.1, 3]$ and varying other parameters in the following ranges upon our discussion above:

$$\lambda_1 \in [0.18, 0.30], \lambda_4 \in [0.70, 0.99], \alpha_1 \in [0.06, 0.16], \alpha_4 \in [0.60, 0.99], \rho_1 \in [0.08, 0.14]. \quad (5.1.12)$$

Moreover, a huge scan over the parameter space of the LRIS was conducted taking into account the recent LHC constraints using integratively HIGGSBOUNDS and HIGGSIGNALS programs as explained below [76, 77]. The scan confirmed our previous discussions and ranges considered. We chose the three benchmark points in Table 5.1 with optimized cross sections in both signals of interest in our analysis below. We also considered our h' in the three mass ranges $m_{h'} = 250, 400$ GeV and 600 GeV. In Fig. 5.1 (left), we circled the three benchmark points of Table 5.1.

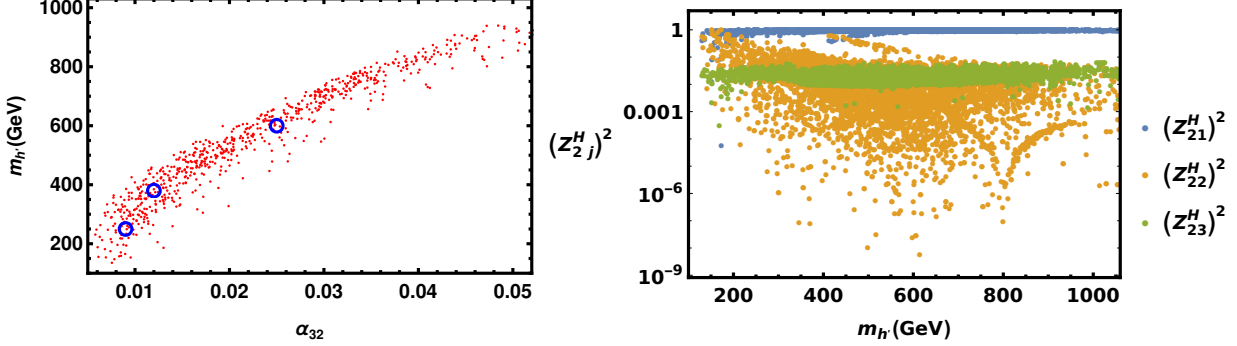


Figure 5.1: Left: The next lightest Higgs boson mass $m_{h'}$ as a function of the most relevant parameter α_{32} . The three benchmark points under consideration of Table 5.1 are surrounded by blue circles. Right: h' mixing versus its mass $m_{h'}$. The other involved parameters are varied as in Eq. (5.1.12).

The interactions of h' with the SM fermions and gauge bosons, which are quite relevant for its search at the LHC, are given in terms of the mixing coupling Z_{2i}^H . As explained above, the physical eigenstate h' is given by the superposition of real parts of neutral components of scalar doublets as follows:

$$h' = Z_{21}^H \phi_1^{0R} + Z_{22}^H \phi_2^{0R} + Z_{23}^H \chi_R^{0R}. \quad (5.1.13)$$

In Fig. 5.1 (right), we display the mixing Z_{2i}^H versus $m_{h'}$ for the same set of parameters considered in Fig. 5.1 (left). As can be seen from this plot, h' is essentially generated from ϕ_1 with smaller contributions from the real components of ϕ_2 and χ_R .

Now, we highlight the relevant interaction couplings of h' with Z_μ gauge boson, $g_{h'ZZ}$, and with the SM-like Higgs boson, $g_{h'hh}$. These interactions are generated from kinetic terms and the scalar potential terms, respectively, and they are dominantly given by

$$g_{h'hh} \approx -2i Z_{21}^H Z_{12}^H \{v((\lambda_1 - \lambda_{23})c_\beta + 3\lambda_4 s_\beta)Z_{12}^H + \alpha_4 v_R Z_{13}^H\}, \quad (5.1.14)$$

$$g_{h'ZZ} \approx \frac{i}{2} g_2^2 v (c_\beta Z_{21}^H + s_\beta Z_{22}^H)(U_{32}^0 - U_{12}^0)^2, \quad (5.1.15)$$

where U^0 is the neutral gauge bosons mixing matrix, given in Eq. (4.5.18). We fix the gauge couplings as follows: $g_L = g_R = g_2 = 0.663$, $g_{BL} = 0.422$, the electroweak VEV

as $v = 246$ GeV, and the Weinberg angle as $s_w^2 = 0.230$ [295]. In addition, the scale of LR symmetry breaking is fixed by $v_R = 6400$ GeV as given in Table 5.1. Finally, the scalar potential parameters α_i , λ_i and ρ_1 are varied within the above mentioned ranges in Eq. (5.1.12). Also, one can show that the coupling $g_{h'ZZ}$ is typically smaller than the coupling $g_{h'hh}$. Therefore, probing h' through its ZZ -decay channel may not be promising, as it will be illustrated in the next section. In Table 5.1, we fix the three benchmark points and their corresponding Higgs spectrum which are used in the LHC simulation analysis in Sec. 5.1.2, while Table 5.1c exhibits their corresponding neutral CP -even Higgs mixing. It is noticeable that there are three effective parameters:

Par	α_1	α_2	α_3	α_4	λ_1	λ_2	λ_3	λ_4	ρ_1	t_β
BP1	0.133	0.155	0.164	0.833	0.215	0.316	-0.155	0.997	0.104	0.134
BP2	0.229	0.090	0.102	0.620	0.198	0.230	-0.104	0.917	0.117	0.159
BP3	0.118	0.168	0.193	0.957	0.228	0.309	-0.116	0.985	0.138	0.055

(a) Benchmark points (BPs) of LRIS used in figures and analysis of Sec. 5.1.2.

Par	v_R	m_{H^\pm}	m_A	$m_{h'}$	m_{H_3}
BP1	6400	440	315	250	3000
BP2	6400	430	350	400	3100
BP3	6400	700	650	600	3400

(b) BPs Higgs mass spectrum (GeV) used in figures and analysis of Sec. 5.1.2.

Mixing	Z_{11}^H	Z_{12}^H	Z_{13}^H	Z_{21}^H	Z_{22}^H	Z_{23}^H	Z_{31}^H	Z_{32}^H	Z_{33}^H
BP1	-0.135	0.989	-0.051	0.978	0.125	-0.166	0.158	0.072	0.985
BP2	-0.155	0.987	-0.051	0.982	0.148	-0.119	0.110	0.068	0.992
BP3	-0.065	0.997	-0.038	0.988	0.059	-0.141	0.138	0.047	0.989

(c) Neutral Higgs mixing corresponding to the three BPs in Table 5.1.

Table 5.1: Benchmark points (BP) and corresponding Higgs spectrum (GeV) used in figures and analysis of Sec. 5.1.2.

α_{12} , α_{13} , and α_{23} involved in the above expressions. They are given in terms of the

three parameters: α_1 , α_2 , and α_3 , so there is not any redundancy. Also, the effective parameter $\lambda_{23} = 2\lambda_2 + \lambda_3$ and $2\lambda_2 - \lambda_3$ (in the pseudoscalar mass) in terms of the two parameters λ_2 and λ_3 , and hence we have two independent parameters and there is no redundancy again. Finally, to satisfy the W' and Z' mass constraints, we should take $v_R \sim \text{TeV}$.

5.1.2 Search for Heavy Higgs Bosons at the LHC

The heavy Higgs boson, h' , is mainly produced at the LHC from the gluon-gluon fusion (ggF) process, which induces about 90% of its total production cross section at the LHC. Other production mechanisms, like vector boson fusion (VBF), Higgs strahlung and Higgs production from top fusion associated with top quark, represent the remaining ratio of the h' production. In Fig. 5.2 (left), we show the h' ggF-production cross section versus $m_{h'}$ for the scanned values of parameters as in Eq. (5.1.12) and its preceding paragraph. It is noticeable from Fig. 5.2 (left) that the h' ggF production cross section $\sigma(pp \rightarrow h')$ can be of an order $\gtrsim 2 \text{ pb}$ for $m_{h'} \lesssim 400 \text{ GeV}$. In this regard, we consider $L_{\text{int}} = 300 \text{ fb}^{-1}$ for relatively light h' and $L_{\text{int}} = 3000 \text{ fb}^{-1}$ for heavy h' and in different decay channels, at $\sqrt{s} = 14 \text{ TeV}$.

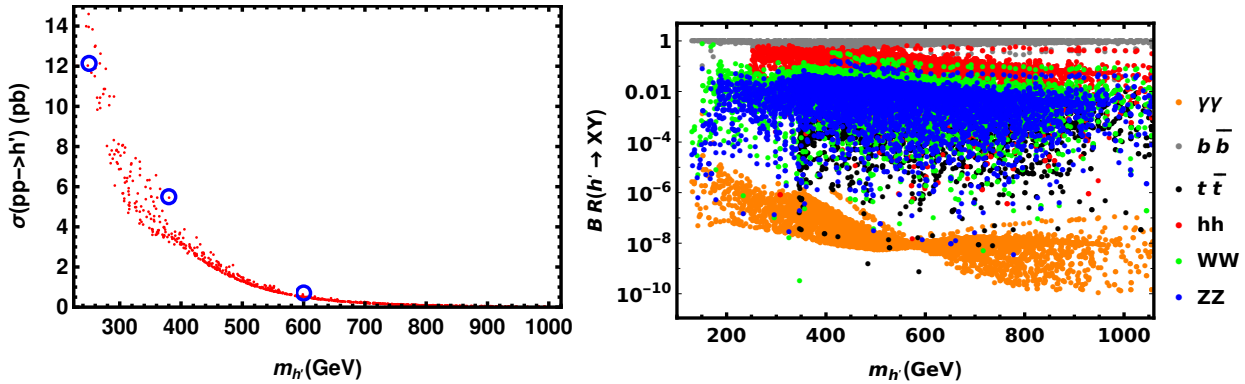


Figure 5.2: Left: The h' production cross section from ggF as a function of its mass $m_{h'}$. The three benchmark points under consideration of Table 5.1 are surrounded by blue circles. Right: Branching ratios (BR) of h' decays versus its mass $m_{h'}$. The relevant parameters values are used as in Fig. 5.1.

We checked that all our benchmark points, given in Table 5.1, are validated to satisfy the usual HIGGSBOUNDS and HIGGSSIGNALS limits confronted with the latest LHC data [76, 77]. Recall that HIGGSBOUNDS and HIGGSSIGNALS are testing Higgs sector both neutral and charged Higgs bosons of the model against the published exclusion bounds from Higgs searches at the LEP, Tevatron and LHC experiments. They are providing important tests for compatibility of any model beyond the SM.

Indeed, many HEP computational tools are used through this work from building the model analytically the way to the numerical manipulation. The LRIS model was first implemented into the SARAH package for building it, and it was then passed to SPHENO [271, 290] for numerical spectrum calculations. After that, the UFO model was used in MADGRAPH [39] for MONTECARLO events generation and matrix-element calculation. After that, PYTHIA was also used to simulate the initial and final state radiation, fragmentation, and hadronisation effects [287]. For detector simulation, the PYTHIA output was passed to DELPHES [135]. Finally, for data analysis, we used MADANALYSIS [117]. In Fig. 5.2 (right), we show the relevant h' decay branching ratios as functions of $m_{h'}$. It is remarkable to notice that for $m_{h'} \leq 600$ GeV, the h' decay branching ratio to two SM Higgs boson is not small, mainly $\text{BR}(h' \rightarrow hh) \geq 10\%$, which gives a hope for probing this heavy Higgs boson through this channel.

Search for h' Higgs boson in $h' \rightarrow hh \rightarrow b\bar{b}\gamma\gamma$

We began with the decay $h' \rightarrow hh \rightarrow b\bar{b}b\bar{b}$ for probing h' at the LHC, as the branching ratio $\text{BR}(h \rightarrow b\bar{b})$ is the largest of h decays. However, this process has a huge background and the signal is much lower than the relevant background, even for a quite heavy Higgs boson: $m_{h'} > 600$ GeV [2, 284] as in Fig. 5.3. We found that no set of cuts can be used to increase the statistical significance of the signal enough to overcome the corresponding background, as in Fig. 5.3. Specifically, we looked

at the selection cuts for the following events on the pseudorapidity, the transverse momentum and the invariant mass of any combination of the four final states' b jets, respectively: $|\eta_{bb}| < 2.4$, $(P_T)_{bb} > 30.0$ GeV and $100.0 \text{ GeV} < M_{bb} < 150.0 \text{ GeV}$. Because our signal contains four final states b jets from a pair of on shell SM Higgs bosons, it is expected that the majority of the signal events occur within a window centred on the SM Higgs mass $100.0 \text{ GeV} < M_{bb} < 150.0 \text{ GeV}$. The corresponding relevant background events b -jets final states, on the other hand, are produced from a variety of other sources, the vast majority of which fall outside the above window. As a result, selecting events in this window is more likely to exclude events from the background than it is to exclude events from the signal. We examined all relevant signal and background kinematics and noticed that the used kinematics of η_{bb} , $(P_T)_{bb}$, M_{bb} are the only discriminators that can be used to overweight signal over background and that our choices optimized their usage based on cut efficiencies and the relative signal-to-background significance S/\sqrt{B} . Also, we applied the cuts used in the experimental references [2, 284] on $|\eta_b| < 2.5$ (2.4) and $(P_T)_b > 40$ (30) GeV of each single b jet of the final states but we found no hope to enhance the significance and it gave results much less than we obtained by the cuts we used above. We also looked at the decay process $h' \rightarrow hh \rightarrow 2b + 2W \rightarrow b\bar{b}\ell\nu\ell\nu$, and we found that $\sigma(pp \rightarrow h' \rightarrow hh \rightarrow 2b + 2W \rightarrow b\bar{b}\ell\nu\ell\nu) \sim \mathcal{O}(10^{-15}) \text{ pb}$. This unusually small cross section is caused by various types of suppression for the corresponding amplitude. As a result, h' can not be probed through this channel even at high luminosity $L_{\text{int}} = 300, 3000 \text{ fb}^{-1}$ and small $m_{h'}$ [159, 283]. Therefore, in our analysis we are going to focus on the process $h' \rightarrow hh \rightarrow b\bar{b}\gamma\gamma$.

The on shell SM Higgs pair production from h' , followed by their decays $h' \rightarrow hh \rightarrow b\bar{b}\gamma\gamma$ is given by the Feynman diagram in Fig. 5.4. As mentioned, here we adapt the following different values of h' -mass: $m_{h'} = 250$ GeV, 400 GeV, and 600 GeV.

As the h' decay width $\Gamma_{h'}$ is much smaller than its mass, $\Gamma_{h'}/m_{h'} \ll 1$, the narrow

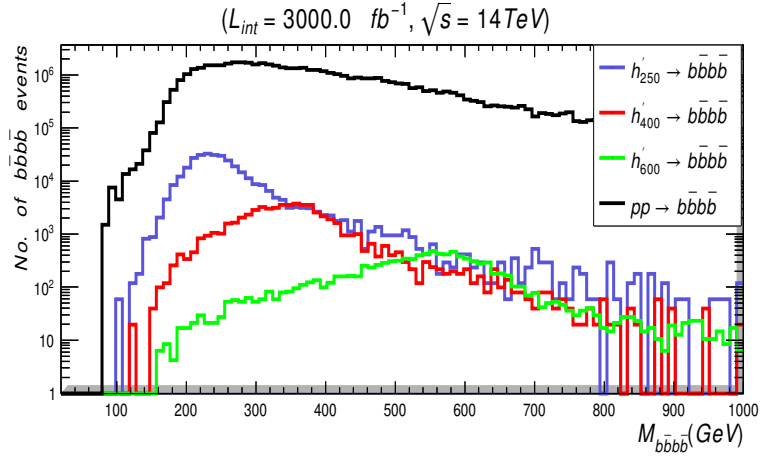


Figure 5.3: Number of signals events for $h' \rightarrow b\bar{b}b\bar{b}$ decays at mass $m_{h'} = 250$ GeV (blue), 400 GeV (red), and 600 GeV (green) induced by the ggF versus the invariant mass of the final states $b\bar{b}b\bar{b}$, at $\sqrt{s} = 14$ TeV and $L_{int} = 3000 \text{ fb}^{-1}$ alongside the relevant background events (black) after applying the cut flow $|\eta_{bb}| < 2.4$, $(P_T)_{bb} > 30.0$ and $100.0 < M_{bb} < 150.0$.

width approximation can be used and the total cross section $\sigma(pp \rightarrow h' \rightarrow hh \rightarrow b\bar{b}\gamma\gamma)$ can be approximated as

$$\sigma(pp \rightarrow h' \rightarrow hh \rightarrow b\bar{b}\gamma\gamma) \approx \sigma(pp \rightarrow h') \times \text{BR}(h' \rightarrow hh) \times \text{BR}(h \rightarrow b\bar{b}) \times \text{BR}(h \rightarrow \gamma\gamma), \quad (5.1.16)$$

where the $h' \rightarrow hh$ decay branching ratio $\text{BR}(h' \rightarrow hh)$ is given in terms of the coupling $g_{h'hh}$ of Eq. (5.1.14). In Table 5.2 the explicit values of the cross section and decay ratio of h' are presented for the three values of $m_{h'}$, under consideration. For

$m_{h'} \text{ (GeV)}$	$\sigma(pp \rightarrow h') \text{ (pb)}$	$\text{BR}(h' \rightarrow hh)$	$\sigma(pp \rightarrow h' \rightarrow hh \rightarrow b\bar{b}\gamma\gamma) \text{ (fb)}$
250	12.140	0.30	6.30
400	5.050	0.20	1.01
600	0.504	0.18	0.05

Table 5.2: $pp \rightarrow h'$ production cross section and its $h' \rightarrow hh$ decay branching ratio and the total cross section for its production and decay process $pp \rightarrow h' \rightarrow hh \rightarrow b\bar{b}\gamma\gamma$ for three different values of $m_{h'} = 250$ GeV, 400 GeV, and 600 GeV.

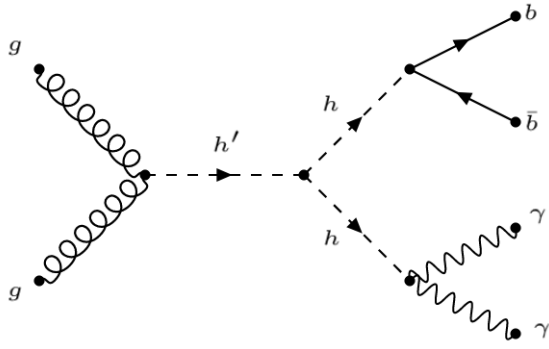


Figure 5.4: Feynman diagram for the h' ggF production and decay process $gg \rightarrow h' \rightarrow hh \rightarrow b\bar{b}\gamma\gamma$.

potential discovery of h' at the LHC, we analyze both its signal and the corresponding relevant background from the SM processes. There are many reducible background processes [101]

$$pp \rightarrow bbh\gamma\gamma/bbj\gamma/bbjj/cc\gamma\gamma/ccj\gamma/jj\gamma\gamma/ggh\gamma\gamma/tt/tt\gamma/tth\gamma\gamma/bbz\gamma\gamma/zh\gamma\gamma. \quad (5.1.17)$$

The following preselection cuts at parton level are imposed in order to avoid any divergence in the parton-level calculations [101, 296]:

5.1.1. The pseudorapidity η of the two photons must be in acceptance of the detector so $|\eta_{\gamma\gamma}| \leq 2.4$.

5.1.2. The pseudorapidity η of the two jets must be in acceptance of the detector so $|\eta_{jj}| \leq 2.4$.

5.1.3. The transverse momentum P_T of the two jets satisfies $(P_T)_{jj} \geq 20$ GeV.

5.1.4. The transverse momentum P_T of the two photon satisfies $(P_T)_{\gamma\gamma} \geq 25$ GeV.

All these backgrounds can be reduced by appropriate kinematical cuts on pseudorapidity η_{ab} , transverse momentum $(P_T)_{ab}$, invariant mass M_{ab} of two final states objects a, b , and the angular distance $(\Delta R)_{ab}$ between a, b in the transverse plane, as specified

in the cut flow tables below. The most relevant background processes which compete with our signal are the irreducible ones, $pp \rightarrow b\bar{b}\gamma\gamma$ and $pp \rightarrow zh \rightarrow b\bar{b}\gamma\gamma$. The later one can be also reduced down by the same set of cuts which are used in Table 5.3. In Fig. 5.5, we show the number of signal events distributions for $m_{h'} = 250$ GeV

Cuts (select)	Signal (S): $m_{h'} = 250$ GeV $(m_{h'} = 400$ GeV)	Background (B)	S/\sqrt{B}
Initial (no cut)	1904.00 (308.00)	25058.00	12.000 (1.950)
$M_{\gamma\gamma} > 119.5$ GeV	846.70 ± 21.70 (177.95 ± 8.82)	3015.10 ± 51.50	15.419 ± 0.00527 (3.241 ± 0.00272)
$M_{\gamma\gamma} < 130.5$ GeV	843.90 ± 19.30 (175.80 ± 8.36)	766.40 ± 19.20	30.430 ± 0.01500 (6.319 ± 0.01540)

- (a) Cut flow charts for the $h' \rightarrow hh \rightarrow b\bar{b}\gamma\gamma$ signal versus its relevant background and the corresponding number of events and significance at 300 fb^{-1} and $\sqrt{s} = 14$ TeV for $m_{h'} = 250$ GeV (400 GeV).

Cuts (select)	Signal (S): $m_{h'} = 600$ GeV	Background (B)	S/\sqrt{B}
Initial (no cut)	155.000	250650.00	0.310
$M_{bb} < 200.0$ GeV	52.250 ± 5.18	39823.60 ± 82.40	0.264 ± 0.0008
$M_{\gamma\gamma} > 119.5$ GeV	34.436 ± 5.91	4252.00 ± 64.70	0.530 ± 0.0010
$M_{\gamma\gamma} < 130.5$ GeV	33.542 ± 5.13	1084.10 ± 32.00	1.018 ± 0.0004
$(\Delta R)_{\gamma\gamma} < 2.0$	29.230 ± 4.35	200.50 ± 17.08	1.062 ± 0.0500
$(\Delta R)_{bb} < 2.0$	27.680 ± 4.46	132.83 ± 7.66	2.409 ± 0.0200
$(P_T)_{\gamma\gamma} > 200.0$ GeV	21.650 ± 4.36	57.65 ± 7.70	2.851 ± 0.0260

- (b) Cut flow charts for the $h' \rightarrow hh \rightarrow b\bar{b}\gamma\gamma$ signal versus its relevant background and the corresponding number of events and significance at $L_{\text{int}} = 3000 \text{ fb}^{-1}$ and $\sqrt{s} = 14$ TeV for $m_{h'} = 600$ GeV.

Table 5.3: Cut flow charts for the $h' \rightarrow hh \rightarrow b\bar{b}\gamma\gamma$ signal versus its relevant background and the corresponding number of events and significance at $\sqrt{s} = 14$ TeV for $m_{h'} = 250$ GeV (400 GeV) and (600 GeV).

and 400 GeV with the relevant irreducible background before (left) and after (right) applying cuts in Table 5.3, respectively. In our signal, the final states kinematics

are all boosted by the two on shell SM-like Higgs bosons and their distributions are narrowed and peaked around our h' windows. This behavior of signal events is unlike that of the background events where final states have many sources and their kinematics' distributions are usually broadened throughout the whole range of analysis. For this, we notice the high relative reduction of the background to our signal when we restrict our analysis on events of kinematics which are expected to be distributed about our h' as mentioned. We demand final state photons pairs of invariant masses as in Table 5.3 and this increases our signal significance in both cases of $m_{h'} = 250$ GeV, 400 GeV. This situation is shown in Fig. 5.5, where the signals are first much less than the relevant background (left) and choosing the certain cuts of Table 5.3 diminishes the background and makes the signals events finally dominate the background. The benchmark point with $m_{h'} = 600$ GeV is not included here as its cross section is quite tiny with the considered ($L_{\text{int}} = 300 \text{ fb}^{-1}$).

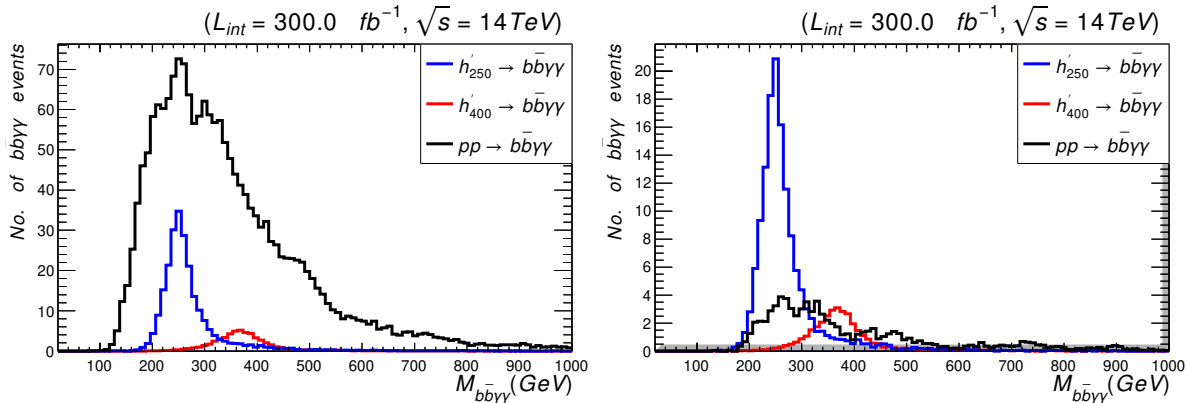


Figure 5.5: Number of signal events for $h' \rightarrow b\bar{b}\gamma\gamma$ decays at mass $m_{h'} = 250$ GeV (blue) and 400 GeV (red) induced by ggF versus the invariant mass of the final states $b\bar{b}\gamma\gamma$, at $\sqrt{s} = 14$ TeV and $L_{\text{int}} = 300 \text{ fb}^{-1}$ alongside the relevant background events (black) before (left) and after (right) applying the cut flow of Table 5.3. The corresponding values of cross sections and branching ratios are given in Table 5.2.

The cut flow in Table 5.3 is chosen upon full analysis of final state signal and background kinematics to optimize relative signal-to-background significance (S/\sqrt{B}). As

mentioned earlier, for $m_{h'} = 250$ GeV, 400 GeV with $L_{\text{int}} = 300 \text{ fb}^{-1}$ the most relevant cuts were taken around the two SM Higgs peaks in the two photon and two jets invariant mass distributions. Applying these cuts, a major part of the background events were excluded, as it has broad distributions because they were generated as elastic scattering rather than being from resonances at the regions of interest. Eventually, the backgrounds reduced relative to the signals at $m_{h'} = 250$ GeV, 400 GeV as in Fig. 5.5 (right).

From these results, it is clear that the SM-like Higgs boson pair production with $2\gamma + 2b\text{-jets}$ can be the smoking gun for probing the heavy CP -even neutral Higgs boson in this class of models that allows for a significant coupling between h' and the SM-like Higgs h boson, unlike several other extensions of the SM. The significance of the $h' \rightarrow b\bar{b}\gamma\gamma$ signal is presented in Fig. 5.6, for L_{int} values which vary from 100 fb^{-1} up to 3000 fb^{-1} at $\sqrt{s} = 14$ TeV, for the usual three values of $m_{h'}$. It is clear that the signal significance increases with considered L_{int} for each value of $m_{h'}$ giving better chances of h' discovery with higher L_{int} .

With $m_{h'} = 600$ GeV, one must consider higher $L_{\text{int}} \sim 3000 \text{ fb}^{-1}$, as the associated production and decay cross section are quite small. Here we apply the cut flow given in Table 5.3b. After applying all these cuts, the final distributions of this event are shown in Fig. 5.7. According to the plots shown in Fig. 5.6 and Fig. 5.7, it is clear that even h' with $m_{h'} \gtrsim 600$ GeV can still be discovered, but at the High-Luminosity Large Hadron Collider (HL-LHC), as it requires L_{int} of order $L_{\text{int}} = 3000 \text{ fb}^{-1}$.

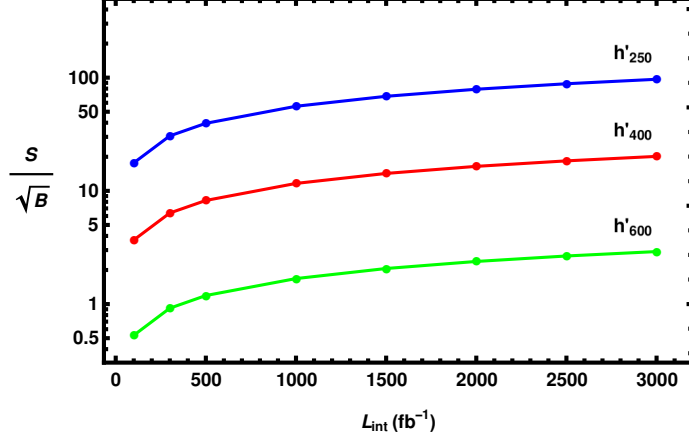


Figure 5.6: Significance of the $h' \rightarrow b\bar{b}\gamma\gamma$ signal of Fig. 5.5 relative to the corresponding background versus L_{int} at mass $m_{h'} = 250$ GeV (blue), 400 GeV (red) and 600 GeV (green). Data are produced at $\sqrt{s} = 14$ TeV, and points are interpolated between values of $L_{\text{int}} = 100, 300, 500, 1000, 1500, 2000, 2500 \text{ fb}^{-1}$ and $L_{\text{int}} = 3000 \text{ fb}^{-1}$. Notice that event rates are computed after the cuts described in Table 5.3, and the relative significance of the signals increases with L_{int} .

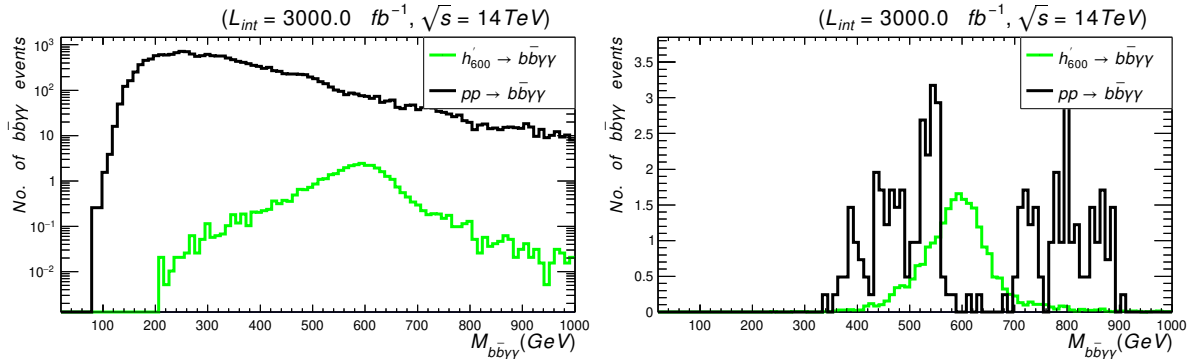


Figure 5.7: Number of signal events for $h' \rightarrow b\bar{b}\gamma\gamma$ decays at mass $m_{h'} = 600$ GeV (green) induced by ggF versus the invariant mass of the final states $b\bar{b}\gamma\gamma$, at $\sqrt{s} = 14$ TeV and $L_{\text{int}} = 3000 \text{ fb}^{-1}$ alongside the relevant background events background (black) before (left) and after (right) applying the cut flow set of Table 5.3b. The corresponding values of cross sections and branching ratios are given in Table 5.2. Left panel is plotted on log-scale vertical axis for the signal to show up relatively.

Search for h' Higgs boson in $h' \rightarrow ZZ \rightarrow 4\ell$

Here, we consider the possibility of probing h' through its final decay into four charged leptons, along the process $pp \rightarrow h' \rightarrow ZZ \rightarrow 4\ell$ ($\ell = e, \mu$) with the Feynman diagram in Fig. 5.8.

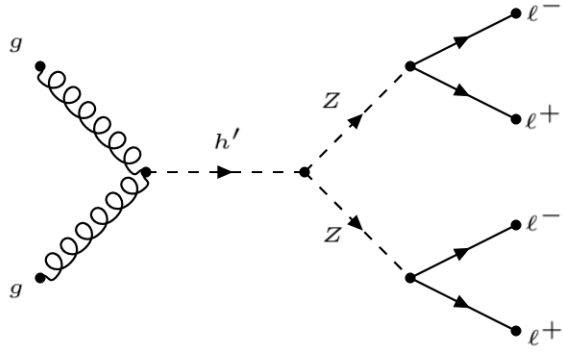


Figure 5.8: Feynman diagram for the h' ggF production and decay process $gg \rightarrow h' \rightarrow ZZ \rightarrow 4\ell$.

In the narrow width approximation, the total cross section can be written as

$$\sigma(pp \rightarrow h' \rightarrow ZZ \rightarrow 4\ell) \approx \sigma(pp \rightarrow h') \times \text{BR}(h' \rightarrow ZZ) \times (\text{BR}(Z \rightarrow 2\ell))^2, \quad (5.1.18)$$

and the $g_{h'ZZ}$ coupling is given in Eq. (5.1.15). As explained below Eq. (5.1.15), the $g_{h'ZZ}$ coupling can be as large as $\mathcal{O}(60)$ GeV causing the total cross section $\sigma(pp \rightarrow h' \rightarrow ZZ \rightarrow 4\ell)$ to drop quickly with the propagator mass $m_{h'}$ without any compensation from elsewhere, unlike the previous case of the $h' \rightarrow hh$ decay where the drop of $\sigma(pp \rightarrow h' \rightarrow hh \rightarrow b\bar{b}\gamma\gamma)$ due to the propagator mass $m_{h'}$ can be partially compensated for from the coupling $g_{h'h}$. Therefore, it is rather difficult to detect h' through this channel for heavy h' . In this aspect, we will focus our analysis on $m_{h'} = 250$ GeV. The h' production cross section, its decay branching ratio and the total cross section of $\sigma(pp \rightarrow h' \rightarrow ZZ \rightarrow 4\ell)$ are explicitly shown in Table 5.4a, for $m_{h'} = 250$ GeV and 400 GeV. It is clear from the results in Table 5.4a that with such small cross sections (fractions of fb), the number of associated events would be

$m_{h'} \text{ (GeV)}$	$\sigma(pp \rightarrow h') \text{ (pb)}$	$\text{BR}(h' \rightarrow ZZ)$	$\sigma(pp \rightarrow h' \rightarrow ZZ \rightarrow 4\ell) \text{ (fb)}$
250	12.140	0.050	0.2428
400	5.050	0.025	0.0579

(a) $pp \rightarrow h'$ production cross section and its $h' \rightarrow ZZ$ decay branching ratio and the total cross section for its production and decay process $pp \rightarrow h' \rightarrow ZZ \rightarrow 4\ell$ for three different values of $m_{h'} = 250 \text{ GeV}$ and 400 GeV .

Cuts (select)	Signal (S): $m_{h'} = 250 \text{ GeV}$ $(m_{h'} = 400 \text{ GeV})$	Background (B)	S/\sqrt{B}
Initial (no cut)	728.00 (174.00)	79890.00	2.58000 (0.43000)
$\cancel{H}_T > 150.0 \text{ GeV}$	58.65 ± 7.34 (38.20 ± 2.01)	247.70 ± 15.70	2.02457 ± 0.00790 (1.26340 ± 0.00597)

(b) Cut flow charts for the $h' \rightarrow ZZ \rightarrow 4\ell$ signal versus its relevant background and the corresponding number of events and significance at 3000 fb^{-1} and $\sqrt{s} = 14 \text{ TeV}$ for $m_{h'} = 250 \text{ GeV}, 400 \text{ GeV}$.

Table 5.4: $pp \rightarrow h'$ production cross section and its $h' \rightarrow ZZ$ decay branching ratio and the total cross section for its production and decay process $pp \rightarrow h' \rightarrow ZZ \rightarrow 4\ell$ and analysis for two different values of $m_{h'} = 250 \text{ GeV}$ and 400 GeV .

extremely smaller than the relevant background, as shown in Fig. 5.9 (left). Here, we consider larger $L_{\text{int}} = 3000 \text{ fb}^{-1}$ for the both cases of $m_{h'} = 250 \text{ GeV}$ and 400 GeV .

Again, as our signal is boosted away by the high mass value of the h' Higgs boson, an appropriate cut on the missing transverse hadronic energy $\cancel{H}_T = | - \sum_{\text{jet}} (\vec{P}_T)_{\text{jet}} |$ is applied as emphasized in Table 5.4b to enhance the relative significance of our signal to the corresponding irreducible background $pp \rightarrow 4\ell$. Accordingly, the background is reduced significantly as shown in Fig. 5.9 (right). However, the signal is also reduced and only a fraction of events would be available, which indicates that it is not possible to observe this signal via this channel. In Fig. 5.10, we present the significance of the $pp \rightarrow h' \rightarrow ZZ \rightarrow 4\ell$ signal to the corresponding background versus L_{int} , for mass $m_{h'} = 250 \text{ GeV}$ and 400 GeV , and $\sqrt{s} = 14 \text{ TeV}$. It is clear from this plot that this

5.1 Search for a heavy neutral Higgs boson in LRIS at the LHC

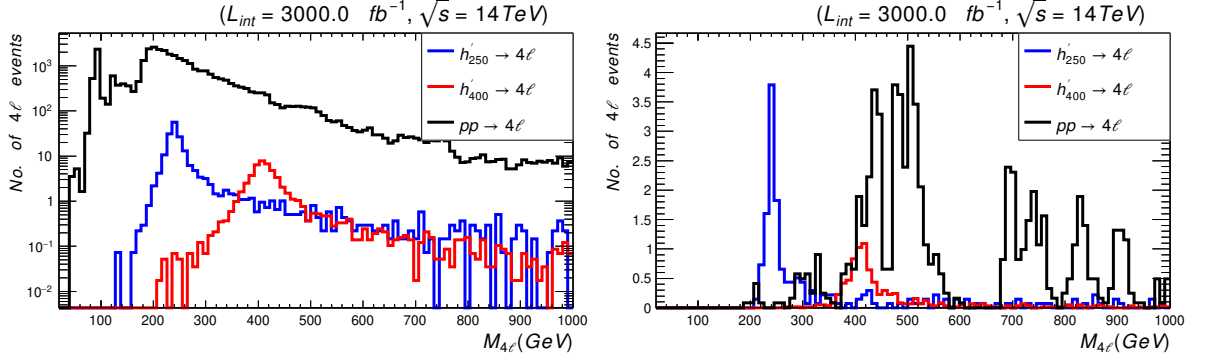


Figure 5.9: Number of signal events for $pp \rightarrow h' \rightarrow ZZ \rightarrow 4\ell$ decays at mass $m_{h'} = 250$ GeV (red) and 400 GeV (blue) induced by ggF versus the invariant mass of the final states 4ℓ , at $\sqrt{s} = 14$ TeV and $L_{\text{int}} = 3000 \text{ fb}^{-1}$ alongside the relevant background events background (black) before (left) and after (right) applying the cut flow of Table 5.4b. The corresponding values of cross sections and branching ratios are given in Table 5.4a.

signal can not be probed (*i.e.* $S/\sqrt{B} > 1$), unless we have $L_{\text{int}} \sim 3000 \text{ fb}^{-1}$.

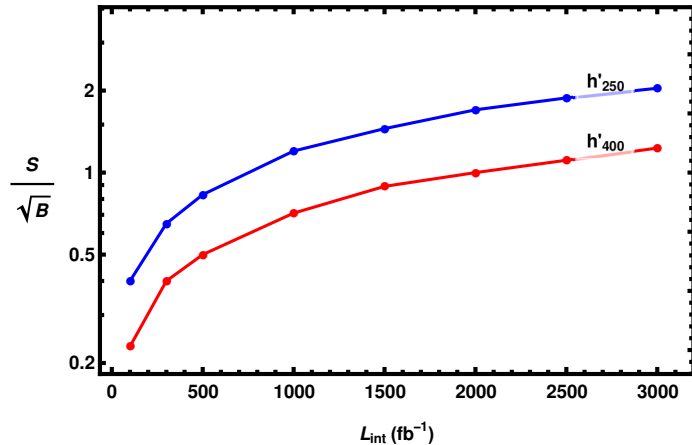


Figure 5.10: Significance of the $pp \rightarrow h' \rightarrow ZZ \rightarrow 4\ell$ signal of Fig. 5.9 relative to the corresponding background versus L_{int} at mass $m_{h'} = 250$ GeV (blue) and 400 GeV (red). Data are produced at $\sqrt{s} = 14$ TeV, and points correspond to $L_{\text{int}} = 100, 300, 500, 1000, 1500, 2000, 2500 \text{ fb}^{-1}$ and $L_{\text{int}} = 3000 \text{ fb}^{-1}$. Notice that event rates are computed after the cuts described in Table 5.4b and the relative significance of the signals increases with L_{int} .

5.1.3 Conclusion

We have proposed a simplified LR model, where $SU(2)_R \times U(1)_{B-L}$ symmetry is broken spontaneously by the VEV of a scalar doublet χ_R around TeV scale, and the electroweak symmetry $SU(2)_L \times U(1)_Y$ is broken by the VEVs of two Higgs doublets merged from a single bidoublet ϕ . We adopted IS mechanism to generate light neutrino masses. We also analyzed the Higgs sector in detail, in particular the three neutral CP -even Higgs bosons. We showed that the lightest of these particle can be assigned to the SM-like Higgs boson, with mass equals to 125 GeV. The next lightest Higgs boson, h' , which is stemmed from the bidoublet neutral component is of order a few hundred GeVs. We studied the LHC potential discovery for h' in this class of models. We performed analysis for searches for h' by looking for resonant peaks in the following two processes: $h' \rightarrow hh \rightarrow b\bar{b}\gamma\gamma$ and $h' \rightarrow ZZ \rightarrow 4\ell$ ($\ell = e, \mu$). We considered three benchmark points, with $m_{h'} = 250$ GeV, 400 GeV, and 600 GeV, at $\sqrt{s} = 14$ TeV and $L_{\text{int}} = 300 \text{ fb}^{-1}$ and $L_{\text{int}} = 3000 \text{ fb}^{-1}$. We emphasized that h' can be probed with good statistical significances in di-Higgs channel, with $2\gamma + 2b$ -jets final states. While the channel of Z -pair production and decays to 4ℓ is much less significant, it may be observed only at very high $L_{\text{int}} = 3000 \text{ fb}^{-1}$ and for light h' with mass less than 300 GeV.

5.2 Muon $g - 2$ anomaly in LRIS

Non-vanishing neutrino masses inferred from neutrino oscillation experiments [26, 29, 40, 151, 166], provided strong evidence for new BSM physics. The extensions of the SM to account for neutrino masses and mixing imply new sources of lepton flavor violation (LFV), which could explain the long-standing discrepancy between the SM prediction for the muon anomalous magnetic moment $a_\mu = (g_\mu - 2)/2$ and its experimental measurement.

Recent experimental results indicate a possible 4.2σ difference between the measured value of the anomalous magnetic moments of muons a_μ and the SM expectations [19, 162, 209, 215], namely

$$\delta a_\mu = a_\mu^{\text{exp}} - a_\mu^{\text{SM}} = (2.51 \pm 0.59) \times 10^{-9}. \quad (5.2.1)$$

We consider the explanation of the a_μ anomaly in the left-right (LR) model with inverse seesaw mechanism (LRIS) to generate light neutrino masses and mixing at low energy scale. The salient feature of this class of models is the large neutrino Yukawa couplings, which allow for significant nonuniversal leptonic contributions to the a_μ anomaly via diagrams mediated by charged Higgs bosons and right-handed neutrinos (RHNs). As constraints, we impose the experimental limits of the LFV $\mu \rightarrow e\gamma$, $\mu\text{-}e$ conversion, and the electron anomalous magnetic moment [22, 36, 99, 129].

The LR model is among the most natural extensions of the SM, which is motivated by grand unified theories (GUTs) and accounts for measured neutrino masses as well as providing an elegant explanation for the origin of parity violation in low-energy weak interactions. The LRIS has been analyzed in detail in Ref. [160]. We recall that it has a Higgs sector that consists of one scalar bidoublet and a scalar right-handed (RH) doublet only. In addition, the LRIS contains singlet fermions S_1, S_2 for adopting the IS mechanism of neutrino masses. Such a TeV scale LR model can be probed in current and future experiments as emphasized in Ref. [160]. In fact there are several new physics scenarios that have been proposed to accommodate δa_μ and δa_e results. See Refs. [61, 75, 80, 90, 106, 122, 123, 137, 138, 157, 180, 189, 201, 229, 230].

5.2.1 LRIS Couplings for a_μ

As previously advocated, we consider the LRIS model [160], which is based on the gauge group $\mathbb{G}_{\text{LR}} = SU(3)_C \times SU(2)_L \times SU(2)_R \times U(1)_{B-L}$. This model has the same fermion content as any other conventional left-right model [249, 250, 279], but

with two extra singlet fermions per family S_1 and S_2 with opposite $B - L$ charges $= -2, = +2$, respectively. The fermion singlet S_2 is presumed to implement the IS mechanism for neutrino masses, while the other, S_1 , is added to cancel the $U(1)_{B-L}$ anomaly caused by S_2 . The LRIS has a simple Higgs sector consisting of one RH doublet χ_R that breaks down left-right symmetry to the SM gauge symmetry and one bidoublet ϕ that is broken down into two SM Higgs doublets. Furthermore, a \mathbb{Z}_2 discrete symmetry is assumed, with all particles having even charges except S_1 , which has an odd charge. This symmetry prevents the mixing mass term $M \bar{S}_1^c S_2$ from being used to allow for the IS mechanism.

The most general LRIS Yukawa Lagrangian is given by

$$\mathcal{L}_Y = \sum_{i,j=1}^3 \bar{L}_{Li} (\phi y_{ij}^L + \tilde{\phi} \tilde{y}_{ij}^L) L_{Rj} + \bar{Q}_{Li} (\phi y_{ij}^Q + \tilde{\phi} \tilde{y}_{ij}^Q) Q_{Rj} + \bar{L}_{Ri} \tilde{\chi}_R y_{ij}^s S_{2j}^c + H.c., \quad (5.2.2)$$

where i, j are family indices, $\tilde{\phi}$ is the dual bidoublet of the scalar bidoublet ϕ , defined as $\tilde{\phi} = \tau_2 \phi^* \tau_2$, and $\tilde{\chi}_R$ is the dual doublet of the scalar doublet χ_R , given by $\tilde{\chi}_R = i\tau_2 \chi_R^*$. A nonvanishing VEV of χ_R , $\langle \chi_R \rangle = v_R/\sqrt{2}$ of order TeV breaks the RH EW sector together with $B - L$, namely $SU(2)_R \times U(1)_{B-L}$ down to the $U(1)_Y$ hypercharge symmetry. In addition, the VEVs of ϕ , $\langle \phi \rangle = \text{diag}(k_1/\sqrt{2}, k_2/\sqrt{2})$, are of order $\mathcal{O}(100)$ GeV, break the SM EW symmetry. The charged leptons acquire their masses via combinations of the lepton coupling Yukawa matrices y^L and \tilde{y}^L and t_β as defined below Eq. (5.2.3). Similarly, the quarks acquire their masses via combinations of the quark coupling Yukawa matrices y^Q and \tilde{y}^Q and t_β . The definition of the Yukawa couplings $y^{L,Q}$ and $\tilde{y}^{L,Q}$ in terms of physical fermion masses and mixing are recalled below from Ref. [160].

After $B - L$ symmetry breaking and EW symmetry breaking, the following 9×9

neutrino mass matrix is obtained in the basis (ν_L^c, ν_R, S_2)

$$\mathcal{M}_\nu = \begin{pmatrix} 0 & M_D & 0 \\ M_D^T & 0 & M_R \\ 0 & M_R^T & \mu^s \end{pmatrix}, \quad (5.2.3)$$

where the 3×3 matrix $M_D = v(y^L s_\beta + \tilde{y}^L c_\beta)/\sqrt{2}$ is the Dirac neutrino mass matrix and the 3×3 matrix $M_R = y^s v_R/\sqrt{2}$. Here, we have assumed that $k_1 = v s_\beta$, $k_2 = v c_\beta$, as constrained from the W boson mass $M_W \simeq g_L \sqrt{k_1^2 + k_2^2}/2$ in LRIS, where $v = 246$ GeV is the EW VEV, and $s_x = \sin x$, $c_x = \cos x$, and $t_x = \tan x$, henceforth. The neutrino mass matrix \mathcal{M}_ν can be diagonalized by 9×9 matrix U satisfying $U \mathcal{M}_\nu U^T = \mathcal{M}_\nu^{\text{diag}} = \text{diag}(m_{\nu_{\ell_i}}, m_{\nu_{h_j}})$, yielding the physical light and heavy neutrino states ν_{ℓ_i}, ν_{h_j} , $i = 1, 2, 3$, $j = 4, \dots, 9$, with the following light and heavy mass eigenvalues

$$m_{\nu_{\ell_i}} = M_D M_R^{-1} \mu^s (M_R^T)^{-1} M_D^T, \quad i = 1, 2, 3, \quad (5.2.4)$$

$$m_{\nu_{h_j}}^2 = M_R^2 \pm M_D^2, \quad j = 4, \dots, 9. \quad (5.2.5)$$

where $\mu^s \lesssim \mathcal{O}(10^{-5})$ GeV, $M_R \sim \mathcal{O}(\text{a few TeV})$ and $y^s \lesssim \mathcal{O}(10^{-1})$. For these values, Eq. (5.2.4) shows that the light neutrino masses can be of order eV. The S_1 fermions acquire radiative masses $m_{S_1} \sim \mu^s \sim \mathcal{O}(\text{KeV})$ and they do not mix with other neutrinos thanks to the \mathbb{Z}_2 discrete symmetry, so they are stable particles. As probable candidates of warm dark matter, one does not have to worry about the S_1 fermions to overclose the Universe. It was demonstrated in [153] that S_1 can account for the observed relic abundance and meanwhile it is not constrained by the constraints on sterile neutrino because its mixing with the active neutrinos vanishes identically in LRIS. On the other hand, the S_2 fermions also acquire radiative mass terms $\sim \mu^s$, but due to their large mixing with the RHN, which is $\sim M_R \sim \mathcal{O}(\text{a few TeV})$, they acquire masses $m_{S_2} \sim M_R$ as in Eq. (5.2.5).

The inverse relation of Eq. (5.2.4) is

$$M_D = U_{\text{PMNS}} \sqrt{m_\nu} \mathcal{R} \sqrt{(\mu^s)^{-1}} M_R, \quad (5.2.6)$$

where \mathcal{R} is an orthogonal matrix and U_{PMNS} is the 3×3 light neutrino mixing matrix [11, 98, 158].

In the following section, we will study the process a_μ , which is dominated by the charged Higgs boson contributions at the loop level; thus, we provide a brief analysis for charged Higgs bosons masses and interactions based on the detailed previous work of Ref. [160]. In the flavor basis $(\phi_1^\pm, \phi_2^\pm, \chi_R^\pm)$, the charged Higgs bosons symmetric mass matrix takes the form

$$M_{H^\pm}^2 = \frac{\alpha}{2} \begin{pmatrix} \frac{v_R^2 s_\beta^2}{c_{2\beta}} & \frac{v_R^2 s_{2\beta}}{2 c_{2\beta}} & -v v_R s_\beta \\ \cdot & \frac{v_R^2 c_\beta^2}{c_{2\beta}} & -v v_R c_\beta \\ \cdot & \cdot & v^2 c_{2\beta} \end{pmatrix}, \quad (5.2.7)$$

where the scalar potential parameter $\alpha = \alpha_3 - \alpha_2$ as in [160]. This matrix can be diagonalized by the unitary matrix

$$Z^{H^\pm} = \begin{pmatrix} \frac{v c_{2\beta}}{\sqrt{v^2 c_{2\beta}^2 + v_R^2 s_\beta^2}} & 0 & \frac{v_R s_\beta}{\sqrt{v^2 c_{2\beta}^2 + v_R^2 s_\beta^2}} \\ -\frac{\frac{1}{2} v_R^2 s_{2\beta}}{\sqrt{(v^2 c_{2\beta}^2 + v_R^2 s_\beta^2)(v^2 c_{2\beta}^2 + v_R^2)}} & \sqrt{\frac{v^2 c_{2\beta}^2 + v_R^2 s_\beta^2}{v^2 c_{2\beta}^2 + v_R^2}} & \frac{v v_R c_\beta c_{2\beta}}{\sqrt{(v^2 c_{2\beta}^2 + v_R^2 s_\beta^2)(v^2 c_{2\beta}^2 + v_R^2)}} \\ -\frac{v_R s_\beta}{\sqrt{v^2 c_{2\beta}^2 + v_R^2}} & -\frac{v_R c_\beta}{\sqrt{v^2 c_{2\beta}^2 + v_R^2}} & \frac{v c_{2\beta}}{\sqrt{v^2 c_{2\beta}^2 + v_R^2}} \end{pmatrix}. \quad (5.2.8)$$

Thus, the mass eigenstates are given by $(\phi_1^\pm, \phi_2^\pm, \chi_R^\pm)^T = (Z^{H^\pm})^T (G_1^\pm, G_2^\pm, H^\pm)^T$, where $Z^{H^\pm} M_{H^\pm}^2 (Z^{H^\pm})^T = \text{diag}(0, 0, m_{H^\pm}^2)$. Here G_1^\pm and G_2^\pm represent the charged massless Goldstone bosons that are eaten by the charged gauge bosons W_μ and W'_μ to acquire their masses and H^\pm is the physical massive charged Higgs boson. The charged Higgs boson mass is given by

$$m_{H^\pm}^2 = \frac{\alpha}{2} \left(\frac{v_R^2}{c_{2\beta}} + v^2 c_{2\beta} \right). \quad (5.2.9)$$

We notice from Eq. (5.2.9) that $\alpha > 0$ as long as $c_{2\beta} > 0$ (*i.e.*, $t_\beta < 1$) and vice versa. Moreover, for $v_R \sim \mathcal{O}(10 \text{ TeV})$ and $|\alpha| \sim \mathcal{O}(10^{-2})$, the charged Higgs boson mass can be of order hundreds GeV. The physical charged Higgs boson is defined as a linear combination of the flavor basis fields $\phi_1^\pm, \phi_2^\pm, \chi_R^\pm$, *i.e.*(corrected from [160]),

$$H^\pm = Z_{31}^{H^\pm} \phi_1^\pm + Z_{32}^{H^\pm} \phi_2^\pm + Z_{33}^{H^\pm} \chi_R^\pm. \quad (5.2.10)$$

It is worth noting that for $v_R \gg v$, $v_R \sim \mathcal{O}(\text{TeV})$ is enough, the mixing $Z_{33}^{H^\pm} \ll 1$ and the charged Higgs mass and combination reduce to the following approximations

$$m_{H^\pm} \simeq v_R \sqrt{\frac{\alpha}{2c_{2\beta}}}, \quad (5.2.11)$$

$$H^\pm \simeq -(s_\beta \phi_1^\pm + c_\beta \phi_2^\pm). \quad (5.2.12)$$

Finally, the charged Higgs boson couplings with fermion families are given by

$$\Gamma_{\bar{u}_i d_j}^{H^\pm} = - \left(\sum_{a=1}^3 V_{ja}^* (y_{ai}^{Q*} Z_{32}^{H^\pm} + \tilde{y}_{ai}^{Q*} Z_{31}^{H^\pm}) \right) P_L - \left(\sum_{a=1}^3 V_{ja} (y_{ia}^Q Z_{31}^{H^\pm} + \tilde{y}_{ia}^Q Z_{32}^{H^\pm}) \right) P_R, \quad (5.2.13)$$

$$\begin{aligned} \Gamma_{\bar{\nu}_k \ell}^{H^\pm} = & - \left(\sum_{i=1}^3 U_{k,i+3}^* (y_{i\ell}^{L*} Z_{31}^{H^\pm} - \tilde{y}_{i\ell}^{L*} Z_{32}^{H^\pm}) \right) P_L \\ & + \left(\sum_{i=1}^3 (U_{ki} (\tilde{y}_{i\ell}^L Z_{31}^{H^\pm} - y_{i\ell}^L Z_{32}^{H^\pm}) - U_{k,i+6} y_{i\ell}^{s*} Z_{33}^{H^\pm}) \right) P_R, \end{aligned} \quad (5.2.14)$$

where V is the 3×3 CKM quark mixing matrix and U is the 9×9 inverse seesaw neutrino mixing matrices defined after Eq. (5.2.3). The following parametrization will be used below

$$\Gamma_{\bar{u}_i d_j}^{H^\pm} = C_{ij} P_L + D_{ij} P_R, \quad (5.2.15)$$

$$\Gamma_{\bar{\nu}_k \ell}^{H^\pm} = \xi_{k\ell} P_L + \zeta_{k\ell} P_R. \quad (5.2.16)$$

We fix $v_R \sim \mathcal{O}(10 \text{ TeV})$ for the extra gauge bosons W', Z' experimental limits on their masses and mixing with the corresponding electroweak gauge bosons [160].

Hence, as noted before Eq. (5.2.12), $Z_{33}^{H^\pm} \ll 1$, and we can omit the third term $\sum_{i=1}^3 U_{k,i+6} y_{\ell i}^{s^*} Z_{33}^{H^\pm}$ from numerical calculations of the charged Higgs boson couplings with leptons $\zeta_{k\ell}$ in Eqs. (5.2.14) and (5.2.16). Moreover, The nonunitarity limits of the 3×3 light neutrino mixing matrix U_{PMNS} [11, 43, 142, 158, 199, 239] ensures that for the charged Higgs boson and lepton couplings in Eq. (5.2.16) $\xi_{k\ell} \ll 1$ for light neutrinos ($k = 1, 2, 3$) and $\zeta_{k\ell} \ll 1$ for heavy neutrinos ($k = 4, \dots, 9$). Thus, and according to Eq. (5.2.12), the relevant charged Higgs boson couplings with fermions can be approximated to

$$C_{ij} \simeq \sum_{a=1}^3 V_{ja}^* (y_{ai}^{Q^*} c_\beta + \tilde{y}_{ai}^{Q^*} s_\beta) \quad (5.2.17)$$

$$D_{ij} \simeq \sum_{a=1}^3 V_{ja} (y_{ia}^Q s_\beta + \tilde{y}_{ia}^Q c_\beta), \quad (5.2.18)$$

$$\xi_{k\ell} \simeq \sum_{i=1}^3 U_{k,i+3}^* (y_{\ell i}^{L^*} s_\beta - \tilde{y}_{\ell i}^{L^*} c_\beta), \quad k = 4, \dots, 9, \quad (5.2.19)$$

$$\zeta_{k\ell} \simeq \sum_{i=1}^3 U_{ki} (y_{i\ell}^L c_\beta - \tilde{y}_{i\ell}^L s_\beta), \quad k = 1, 2, 3. \quad (5.2.20)$$

It is clearly noticed that for $t_\beta \ll 1$ ($t_\beta \gg 1$) the couplings $\xi_{k\ell}$ ($\zeta_{k\ell}$) are \tilde{y}^L (y^L)-dominant, and hence the couplings $\xi_{k\ell}$ and $\zeta_{k\ell}$ are now uncorrelated. Moreover, if we closely investigate these couplings for $\ell = e, \mu$, we see that the family components $y_{\ell i}^L, \tilde{y}_{\ell i}^L$ can distinguish between the charged Higgs boson couplings to different lepton families. Successfully, this helps in explaining the a_μ anomaly and satisfying the LFV results as clarified below. This can be achieved via controlling the entries of y^s, μ^s and the orthogonal matrix \mathcal{R} in Eq. (5.2.6), where the quark and lepton Yukawa couplings can be written in terms of the fermion masses as follows [160]:

$$y^Q = \frac{\sqrt{2}}{v c_{2\beta}} (c_\beta V M_d V^\dagger - s_\beta M_u), \quad (5.2.21)$$

$$\tilde{y}^Q = \frac{\sqrt{2}}{v c_{2\beta}} (s_\beta V M_d V^\dagger - c_\beta M_u), \quad (5.2.22)$$

$$y^L = \frac{\sqrt{2}}{vc_{2\beta}}(c_\beta M_{\text{lp}} - s_\beta M_D), \quad (5.2.23)$$

$$\tilde{y}^L = \frac{-\sqrt{2}}{vc_{2\beta}}(s_\beta M_{\text{lp}} - c_\beta M_D), \quad (5.2.24)$$

where M_u, M_d, M_{lp} are the quarks and charged leptons diagonal mass matrices and M_D is the Dirac neutrino mass matrix defined after Eq. (5.2.3) and solved for it in Eq. (5.2.6). According to Eqs. (5.2.17) to (5.2.24), we can write the charged Higgs boson couplings to fermions in terms of the physical fermion masses as follows:

$$C_{ij} \simeq \frac{\sqrt{2}}{vc_{2\beta}} \sum_{a=1}^3 V_{ja}^* (VM_d V^\dagger - s_{2\beta} M_u)_{ai}^*, \quad (5.2.25)$$

$$D_{ij} \simeq \frac{\sqrt{2}}{vc_{2\beta}} \sum_{a=1}^3 V_{ja} (s_{2\beta} VM_d V^\dagger - M_u)_{ia}, \quad (5.2.26)$$

$$\xi_{k\ell} \simeq \frac{\sqrt{2}}{vc_{2\beta}} \sum_{i=1}^3 U_{k,i+3}^* (s_{2\beta} M_{\text{lp}} - M_D)_{ii}, \quad k = 4, \dots, 9, \quad (5.2.27)$$

$$\zeta_{k\ell} \simeq \frac{\sqrt{2}}{vc_{2\beta}} \sum_{i=1}^3 U_{ki} (M_{\text{lp}} - s_{2\beta} M_D)_{i\ell}, \quad k = 1, 2, 3, \quad (5.2.28)$$

where the conjugate “*” is omitted from the matrices when they are (taken) real. As noted after Eq. (5.2.20), for $t_\beta \ll 1$ ($t_\beta \gg 1$), the couplings $\xi_{k\ell}$ ($\zeta_{k\ell}$) are M_D (M_{lp})-dominant and uncorrelated, and the family components are discriminant. Similarly, the above discussion applies for the charged Higgs boson couplings with quarks as well.

Finally, we close this section by stating the scalar and pseudoscalar Higgs bosons sectors which were analyzed in detail with their couplings with charged leptons in [160]

$$\Gamma_{\ell\ell}^{hi} = \frac{v}{\sqrt{2}m_\ell} (Z_{i1}^H \tilde{y}_{\ell\ell}^L + Z_{i2}^H y_{\ell\ell}^L), \quad (5.2.29)$$

$$\Gamma_{\ell\ell}^A = \frac{v}{\sqrt{2}m_\ell} (Z_{31}^A \tilde{y}_{\ell\ell}^L - Z_{32}^A y_{\ell\ell}^L), \quad (5.2.30)$$

where Z^H, Z^A are the scalar and pseudoscalar Higgs mixing matrices, respectively [160, 278]. More details about the LRIS Higgs and gauge sectors couplings and mixing and their parameters and spectra can be found in our previous work in Ref. [160].

5.2.2 LRIS Contributions to a_μ

In this section we analyze new contributions from the LRIS to the muon anomalous magnetic moment, a_μ , induced by the light and heavy Z, W, Z', W' gauge bosons, as well as the neutral scalar and pseudoscalar and charged Higgs bosons h, A, H^\pm , as shown by their Feynman diagrams in Fig. 5.11. We will also consider the constraints on these contributions imposed by the experimental limits of the electron anomalous magnetic moment, a_e , and charged LFV processes, particularly, the $\mu \rightarrow e\gamma$ decay and the μ - e conversion. In this case, we can write $\delta a_\mu = a_\mu^{\text{LRIS}}$, where

$$a_\mu^{\text{LRIS}} = a_\mu^W + a_\mu^{W'} + a_\mu^Z + a_\mu^{Z'} + a_\mu^h + a_\mu^A + a_\mu^{H^\pm}. \quad (5.2.31)$$

The relevant amplitudes are, ignoring the $W - W'$ and $Z - Z'$ mixing, given by

$$a_\ell^W = G_F^\ell \sum_{k=1}^9 |U_{k,|\ell|}|^2 \left(\frac{10}{3} + \mathcal{F}_2(x_W^{\nu_k}) \right), \quad (5.2.32)$$

$$a_\ell^{W'} = G_F^\ell \sum_{k=1}^9 |U_{k,3+|\ell|}|^2 \left(\frac{10}{3} + \mathcal{F}_2(x_{W'}^{\nu_k}) \right) \left[\frac{1}{c_w} x_{W'}^W \right], \quad (5.2.33)$$

$$a_\ell^Z = G_F^\ell \left(c_{4w} - 5 \right) \left(\frac{1}{3} \right), \quad (5.2.34)$$

$$a_\ell^{Z'} = G_F^\ell \left(c_{4w'} - 12c_{2w'} - 5 \right) \left[\frac{t_w^2}{48s_{2w'}^2} x_{Z'}^W \right], \quad (5.2.35)$$

$$a_\ell^h = G_F^\ell \sum_{i=1}^3 x_{h_i}^\ell (\Gamma_{\ell\ell}^{h_i})^2 \left(\frac{7}{6} + \log(x_{h_i}^\ell) \right), \quad (5.2.36)$$

$$a_\ell^A = G_F^\ell \left(\frac{-1}{2} \right) x_A^\ell (\Gamma_{\ell\ell}^A)^2 \left(\frac{7}{6} + \log(x_A^\ell) \right), \quad (5.2.37)$$

where the lepton family order $|\ell| = 1, 2$ for $\ell = e, \mu$. The dimensionless coupling $G_F^\ell = \frac{G_F m_\ell^2}{8\sqrt{2}\pi^2}$ and the mass ratio parameters $x_b^a = \frac{m_a^2}{m_b^2}$, $a = \nu_k, W, \ell$, $b = W, W', Z', h_i, A, H^\pm$.

The neutral gauge bosons mixing angles $\theta_{w'}$ and the Weinberg angle θ_w are $s_{w'} = \frac{g_Y}{g_R}$, $s_w = \frac{e}{g_L}$, where g_Y is the hypercharge coupling. The $Z - Z'$ mixing angle $\theta_{w'}$ is constrained by $t_{w'} \lesssim 10^{-4}$ [260, 261]. Also, the W' mass is given by $m_{W'} = g_L \sqrt{v_R^2 + v^2}/2 \gtrsim \mathcal{O}(4 \text{ TeV})$ [260, 261].

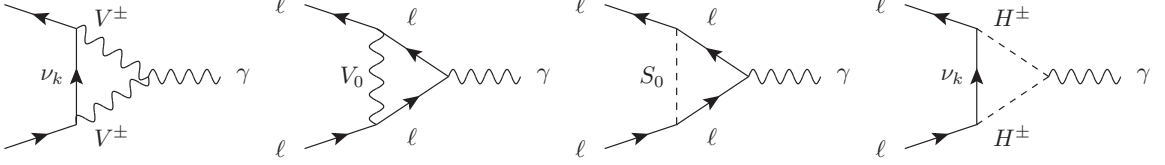


Figure 5.11: LRIS one-loop Feynman diagrams contributions to lepton $g_\ell - 2$ via massive neutrinos, $V^\pm = W, W'$, $V^0 = Z, Z'$, $S^0 = h_i, A$, and the charged Higgs boson H^\pm .

The analytical expressions of Eqs. (5.2.32)–(5.2.37) show that numerical values of the BSM contributions to a_μ mediated by W', Z', h_i, A are negligible due to the suppression of their masses ratios $x_{W',Z'}^W$ and $x_{h_i,A}^\ell$, and thus we exclude their minor contributions. Also, the second summation term $\sum_{k=1}^9 |U_{k,\ell}|^2 \mathcal{F}_2(x_W^{\nu_k}) \simeq \sum_{k=4}^9 |U_{k,\ell}|^2 \mathcal{F}_2(x_W^{\nu_k})$ of Eq. (5.2.32) which represents the W -RHN loops contributions of Fig. 5.11 is typically $\sim \mathcal{O}(10^{-2})$; only $\lesssim 0.4\%$ of the first term ($\frac{10}{3}$), and thus suppressed. This can be generally understood via the GIM cancellation mechanism [171] due to the unitarity of the full 9×9 neutrino mixing matrix U within the nonunitarity limits of the 3×3 U_{PMNS} light neutrino mixing matrix [11, 43, 142, 158, 199, 239]. In light of this, it can be generally concluded that any minimal BSM extension of the SM with RHN and with any adopted seesaw mechanism can not account for the measured a_μ anomaly and extra degrees of freedom are needed for this [11]. The LRIS with its extra degrees of freedom is a good candidate for such class of BSM models.

Finally, the charged Higgs boson H^\pm contribution to a_μ is given by

$$a_\ell^{H^\pm} = G_F^\ell \Gamma_\gamma^{H^\pm} \sum_{k=1}^9 \left(|\zeta'_{k\ell}|^2 \mathcal{F}_2(x_{H^\pm}^{\nu_k}) + 2\text{Re}[\zeta'_{k\ell} \xi'^*_{k\ell}] \mathcal{F}_1(x_{H^\pm}^{\nu_k}) \right), \quad (5.2.38)$$

where the charged Higgs boson interaction couplings with leptons $\xi_{k\ell}, \zeta_{k\ell}$ appear in Eq. (5.2.16), and $\zeta'_{k\ell} = \frac{v}{m_{\nu_k}} \zeta_{k\ell}$ and $\xi'_{k\ell} = \frac{v}{m_\ell} \xi_{k\ell}$. The charged Higgs boson interaction

coupling with photons is

$$\Gamma_{\gamma}^{H^{\pm}} = \frac{1}{6e} \left(g_L U_{21}^0 + g_R U_{31}^0 + (g_{BL} U_{11}^0 - g_L U_{21}^0) (Z_{33}^{H^{\pm}})^2 \right) \simeq \frac{1}{6e} \left(g_L U_{21}^0 + g_R U_{31}^0 \right), \quad (5.2.39)$$

where the last approximation is for $v_R \gg v$ where $Z_{33}^{H^{\pm}} \ll 1$, as noted before Eq. (5.2.12). The matrix U^0 is the neutral gauge bosons mixing matrix and g_R is the $SU(2)_R$ coupling [160]. The loop functions \mathcal{F}_k ($k = 1, 2$) in Eqs. (5.2.32), (5.2.33) and (5.2.38) are given by

$$\mathcal{F}_k(y) = \frac{y \mathcal{P}_k(y)}{(y-1)^{k+1}} - \frac{6y^{k+1} \log(y)}{(y-1)^{k+2}}, \quad k = 1, 2, \quad (5.2.40)$$

$$\mathcal{P}_1(y) = 3y + 3, \quad (5.2.41)$$

$$\mathcal{P}_2(y) = 2y^2 + 5y - 1. \quad (5.2.42)$$

It is understood that for $y \rightarrow 1$, the values of the loop functions \mathcal{F}_k ($k = 1, 2$) are given by their limits and $\mathcal{F}_1(1) = 1$ and $\mathcal{F}_2(1) = \frac{1}{2}$. This happens when some heavy neutrinos are degenerate in mass with the charged Higgs boson as in Fig. 5.12. Asymptotically, the ratio $\mathcal{F}_2(x)/\mathcal{F}_1(x)$ is increasing and bounded below and above, and $\mathcal{F}_2(x), \mathcal{F}_1(x) \rightarrow 0$ for $x \ll 1$ such that $\mathcal{F}_2(x)/\mathcal{F}_1(x) \rightarrow 1/3$ for $x \ll 1$, and $\mathcal{F}_2(x)/\mathcal{F}_1(x) \rightarrow 2/3$ for $x \gg 1$. Accordingly, the two loop functions \mathcal{F}_1 and \mathcal{F}_2 remain of the same order for all possible values of the argument x . Typically, the coupling $\Gamma_{\gamma}^{H^{\pm}} \sim 0.076$. Also, the first contribution term of Eq. (5.2.38) $\sum_{k=1}^9 |\zeta'_{k\ell}|^2 \mathcal{F}_2(x_{H^{\pm}}^{\nu_k}) \simeq \sum_{k=1}^3 |\zeta'_{k\ell}|^2 \mathcal{F}_2(x_{H^{\pm}}^{\nu_k})$ is $\sim \mathcal{O}(10^{-13})$. For light neutrinos, this term is suppressed by the loop function $\mathcal{F}_2(x_{H^{\pm}}^{\nu_k})$, while for heavy neutrinos, it is suppressed by their squared masses in the denominators of coefficients $|\zeta'_{k\ell}|^2$ ($k = 4, \dots, 9$). Indeed, the first term represents only 0.02% of the second term $\sum_{k=1}^9 2\text{Re}[\zeta'_{k\ell} \xi'^*_{k\ell}] \mathcal{F}_1(x_{H^{\pm}}^{\nu_k}) \simeq \sum_{k=4}^9 2\text{Re}[\zeta'_{k\ell} \xi'^*_{k\ell}] \mathcal{F}_1(x_{H^{\pm}}^{\nu_k})$, which is $\mathcal{O}(10^{-9})$, where this time, the second term is enhanced due to the charged lepton masses in the denominators of the coefficients $\zeta'_{k\ell} \xi'^*_{k\ell}$. Thus, the charged Higgs boson contribution to the a_{μ} anomaly Eq. (5.2.38)

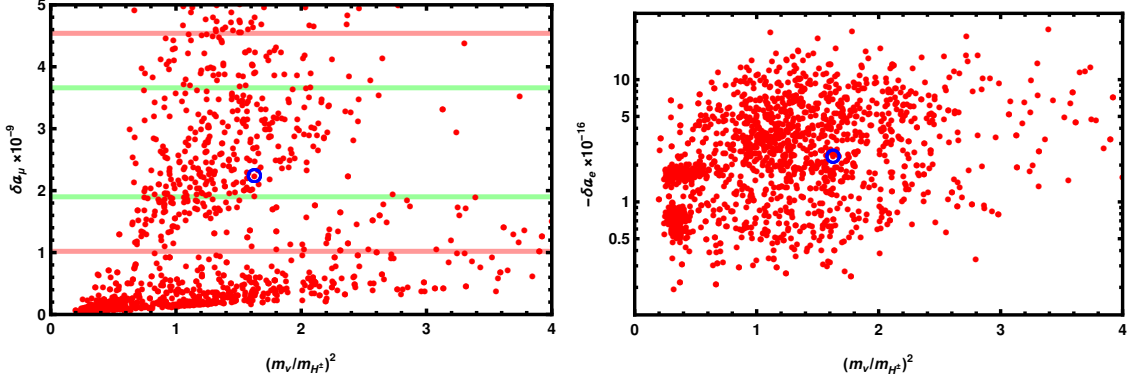


Figure 5.12: Left/right: the muon/electron magnetic moment anomalies $\delta a_\mu, -\delta a_e$ versus of the second heaviest neutrino and charged Higgs boson masses ratio parameter $x_{H^\pm}^{\nu_5} = m_{\nu_5}^2 / m_{H^\pm}^2$. The 1σ and 2σ standard errors of measurements of δa_μ are included in green and red borders, respectively. The BP of Table 5.5 is encircled.

can be approximated to

$$a_\ell^{H^\pm} \simeq 2G_F^\ell \Gamma_\gamma^{H^\pm} \sum_{k=4}^9 \text{Re}[\zeta'_{k\ell} \xi'_{k\ell}^*] \mathcal{F}_1(x_{H^\pm}^{\nu_k}) \lesssim \frac{3\Gamma_\gamma^{H^\pm}}{8\pi^2} m_\ell \sum_{k=4}^9 \frac{\zeta_{k\ell} \xi_{k\ell}}{m_{\nu_k}}, \quad (5.2.43)$$

where $\frac{3\Gamma_\gamma^{H^\pm}}{8\pi^2} \sim 3 \times 10^{-3}$ and the loop function \mathcal{F}_1 is increasing and bounded above such that $\mathcal{F}_1(x) \rightarrow 3$ for $x \gg 1$, and the complex notations “Re, *” are omitted as the couplings are (taken) real.

In the rest of this section, we analyze the parameter space of the LRIS for numerical scan for benchmark points (BPs). In the SM, all particles acquire their masses via the VEV of only one degree of freedom, the Higgs field, and each particle mass depends only on one parameter coupling, its coupling with the Higgs field. This feature almost fixes the SM parameters values, except maybe due to some measurements uncertainties. So, in the SM, couplings are fixed at the EW scale by particles masses. Conversely, in LRIS, there are many sources of VEVs and couplings for particles’ masses. So, in LRIS, VEVs, the Yukawa couplings and scalar potential parameters are in general free parameters (see Ref. [160]), and they can be varied while fermions and scalar masses are kept fixed. Also, in LRIS, the gauge couplings

are constrained by the gauge bosons masses at the EW scale and by their renormalization group equations (RGEs) evolution up to GUT scale, especially when we fix $v_R \sim \mathcal{O}(10 \text{ TeV})$ for the extra W', Z' experimental mixings and masses limits as discussed after Eq. (5.2.37).

The neutrinos masses Eqs. (5.2.4) and (5.2.5) and their mixing matrix U after Eq. (5.2.3) are given in terms of M_D, M_R , and μ^s (or equivalently $y^L, \tilde{y}^L, y^s, \mu^s, t_\beta$, and v_R). In our numerical analysis, we fix $v_R \sim \mathcal{O}(10 \text{ TeV})$. Also, we adopted the normal hierarchy of light neutrino masses m_{ν_ℓ} , as in Table 5.5. The chosen light neutrino masses values satisfy $\Delta m_{21}^2 = 7.224 \times 10^{-5} \text{ eV}^2$ and $\Delta m_{31}^2 = 2.500 \times 10^{-3} \text{ eV}^2$. They agree with the 1σ ranges of the observed solar and atmospheric mass splittings values $\Delta m_{\text{sol}}^2 = 7.420_{-0.200}^{+0.210} \times 10^{-5} \text{ eV}^2$, and $\Delta m_{\text{atm}}^2 = 2.517_{-0.028}^{+0.026} \times 10^{-3} \text{ eV}^2$ [158]. But, to satisfy the a_μ anomaly in the inverted hierarchy scenario of neutrino masses within the imposed LFV constraints, the nonunitarity limits of the U_{PMNS} matrix should be violated. In this case, one has to set relatively large ($\sim \mathcal{O}(10^{-10})$) and thus almost degenerate light neutrino masses to satisfy the inverted hierarchy scenario observed limits $\Delta m_{21}^2 = \Delta m_{\text{sol}}^2 = 7.420_{-0.200}^{+0.210} \times 10^{-5} \text{ eV}^2$, and $\Delta m_{32}^2 = \Delta m_{\text{atm}}^2 = -2.498_{-0.028}^{+0.028} \times 10^{-3} \text{ eV}^2$ [158]. Also, μ^s is enlarged for the a_μ anomaly and other relevant LFV constraints, and it mixes with other entries in the neutrino mass matrix (5.2.3), thus violating the nonunitarity limits of U_{PMNS} [158]. We chose to express M_D (and hence, in correlation, y^L, \tilde{y}^L) in terms of y^s, μ^s and t_β as in Eqs. (5.2.6), (5.2.23) and (5.2.24). Accordingly, substituting M_D and y^s in the heavy neutrino masses Eq. (5.2.5) determine them. So, in our numerical analysis below, we fix the normal hierarchy light neutrino masses and the entries of the U_{PMNS} matrix and scan over y^s and μ^s as in Eq. (5.2.44) for the neutrino sector [158]. It is also worth mentioning here that the consistency of all numerical calculations of Table 5.5 is verified. For example, the M_D matrix, when calculated from its main definition after Eq. (5.2.3) is found consistent with its values from Eq. (5.2.6). Also, the neutrino

masses in Table 5.5 are consistent with Table 5.6 and Eqs. (5.2.4), (5.2.5) and (5.2.45). Finally, the orthogonal matrix \mathcal{R} of Eq. (5.2.6) was fixed such that its nonvanishing components are $\mathcal{R}_{13} = \mathcal{R}_{21} = \mathcal{R}_{32} = 1$ as given in Table 5.6.

Also, the charged Higgs boson mass Eq. (5.2.9) is varied versus t_β and the scalar potential parameter α , and the charged Higgs mixing Z^{H^\pm} Eq. (5.2.8) is given in terms of t_β and v_R . For the charged Higgs boson mass and mixing, we scan over t_β and α as in Eq. (5.2.44). As detailed above, after Eqs. (5.2.5), (5.2.9) and (5.2.20), in our numerical analysis of the neutrino and charged Higgs sectors, we scanned over the following independent parameters' ranges [with $v_R \sim \mathcal{O}(10 \text{ TeV})$]

$$\alpha \sim [0.005, 0.050], t_\beta \sim [0.01, 0.99], (y^s)_{ij} \sim [0.01, 0.50] \delta_{ij}, (\mu^s)_{ij} \sim [10^{-9}, 10^{-5}] \delta_{ij} \text{ GeV}. \quad (5.2.44)$$

We checked that all of our BPs are validated to satisfy the usual HIGGSBOUNDS and HIGGSIGNALS limits confronted with the latest LEP, Tevatron, and LHC data [76, 77]. They provide important tests for compatibility of any BSM model. In our analysis, the LRIS model was first built in the SARAH package, then it was passed to SPHENO for numerical spectrum calculations [271, 290]. Specifically, we present one of our BPs in Table 5.5 with the corresponding observables in Table 5.7 and other parameters in Table 5.6 and Eq. (5.2.45).

The left (right) panel of Fig. 5.12 depicts the muon (electron) $g_{\mu(e)} - 2$ anomalies $\delta a_{\mu(e)}$ in LRIS, as given in Eqs. (5.2.32) and (5.2.38), resulting from the BSM contributions of the W -RHN loops and the charged Higgs boson contribution. We choose, without any loss of generality or independence, to show the distribution of $\delta a_{\mu(e)}$ versus the mass ratio $x_{H^\pm}^{\nu_5} = m_{\nu_5}^2 / m_{H^\pm}^2$ for its moderate and variable values, as it is clear from the masses values BP of Table 5.5, but any other of the independent or dependent parameters or any one of the heavy neutrinos ratios $x_{H^\pm}^{\nu_j}$ ($j = 4, \dots, 9$) would equally work for the same set of data. The green (red) borders indicate the 1σ (2σ) level of accuracy around the average δa_μ as in Eq. (5.2.1). The electron

α	t_β	v_R	$Z_{31}^{H^\pm}$	$Z_{32}^{H^\pm}$	$Z_{33}^{H^\pm}$	m_{H^\pm}
0.0058	0.1	10000	-0.099	-0.994	0.024	545

(a) BP and corresponding charged Higgs boson mixing and mass spectrum in GeVs.

m_{ν_1}	m_{ν_2}	m_{ν_3}	m_{ν_4}	m_{ν_5}	m_{ν_6}	m_{ν_7}	m_{ν_8}	m_{ν_9}
1.0×10^{-13}	8.5×10^{-12}	5.0×10^{-11}	108	695	1449	108	695	1449

(b) BP neutrino mass spectrum in GeVs.

Table 5.5: BP and corresponding charged Higgs boson and neutrino mass spectrum in GeVs.

anomaly δa_e is guaranteed to be within the allowed experimental uncertainty limits $|\delta a_e| \lesssim (10^{-15} - 10^{-13})$ [42, 170]. So, all BPs used in Figs. 5.12 and 5.13 satisfy the electron a_e anomaly limits. Furthermore, Fig. 5.13 shows that the LVF BR($\mu \rightarrow e\gamma$) in Eq. (5.2.49) satisfies the experimental bounds for the same set of parameters values as in Fig. 5.12.

The 9×9 neutrino mixing matrix U of the BP of Table 5.5, rounded to $\mathcal{O}(10^{-4})$, with the U_{PMNS} matrix [158], is

$$U = \begin{pmatrix} -0.8243 & 0.4535 & -0.3389 & 0 & 0 & 0 & 0 & 0.0000 & -0.0001 \\ 0.5465 & 0.4812 & -0.6853 & 0 & 0 & 0 & 0.0009 & 0.0002 & 0 \\ -0.1468 & -0.7453 & -0.6403 & 0 & 0 & 0 & 0 & -0.1137 & 0 \\ -0.0004 & -0.0003 & 0.0004 & -0.7071 & 0 & 0 & 0.7071 & 0 & 0 \\ -0.0120 & -0.0604 & -0.0517 & 0 & -0.7071 & 0 & 0 & 0.7025 & 0 \\ 0.0001 & 0.0000 & 0.0003 & 0 & 0 & 0.7071 & 0 & 0 & -0.7071 \\ -0.0004 & -0.0003 & 0.0004 & 0.7071 & 0 & 0 & 0.7071 & 0 & 0 \\ 0.0120 & 0.0604 & 0.0517 & 0 & -0.7071 & 0 & 0 & -0.7025 & 0 \\ -0.0001 & 0.0000 & 0.0000 & 0 & 0 & 0.7071 & 0 & 0 & 0.7071 \end{pmatrix}, \quad (5.2.45)$$

or in compact block form

$$U = \begin{pmatrix} U_{3 \times 3} & U_{3 \times 6} \\ U_{6 \times 3} & U_{6 \times 6} \end{pmatrix}^T, \quad (5.2.46)$$

where each block matrix is parametrized such that [11, 142]

$$U_{3 \times 6} \simeq [\mathbf{0}_{3 \times 3} | F]_{3 \times 6} U_{6 \times 6}, \quad (5.2.47)$$

Matrix	\mathcal{R}	y^s	μ^s	y^L	\tilde{y}^L	y^Q	\tilde{y}^Q	U_{PMNS}
1,1	0	1.53×10^{-2}	1.01×10^{-5}	-2.83×10^{-5}	3.13×10^{-4}	6.33×10^{-5}	-3.44×10^{-4}	0.8251
1,2	0	0	0	-6.86×10^{-3}	6.86×10^{-2}	-1.49×10^{-4}	1.48×10^{-3}	0.5449
1,3	1	0	0	-9.42×10^{-5}	9.42×10^{-4}	-3.53×10^{-4}	3.53×10^{-3}	0.1490
2,1	1	0	0	-2.75×10^{-5}	2.75×10^{-4}	1.38×10^{-4}	-1.38×10^{-3}	-0.4554
2,2	0	9.76×10^{-2}	3.82×10^{-9}	-3.39×10^{-2}	3.46×10^{-1}	2.27×10^{-5}	5.26×10^{-3}	0.4795
2,3	0	0	0	5.20×10^{-5}	-5.20×10^{-4}	-4.19×10^{-3}	4.19×10^{-2}	0.7513
3,1	0	0	0	3.93×10^{-4}	-3.93×10^{-3}	-6.08×10^{-4}	6.08×10^{-3}	0.3343
3,2	1	0	0	-2.96×10^{-2}	2.96×10^{-1}	4.16×10^{-3}	-4.16×10^{-2}	-0.6836
3,3	0	2.05×10^{-1}	5.49×10^{-6}	1.03×10^{-2}	-6.54×10^{-4}	-7.66×10^{-2}	9.99×10^{-1}	0.6427

Table 5.6: Yukawa and IS matrices BP of Table 5.5.

δa_μ	$-\delta a_e$	$\text{BR}(\mu \rightarrow e\gamma)$	$R_{\mu \rightarrow e}^{\text{Al}}$	$R_{\mu \rightarrow e}^{\text{Ti}}$	$R_{\mu \rightarrow e}^{\text{Au}}$
2.24×10^{-9}	2.30×10^{-16}	2.10×10^{-13}	4.10×10^{-51}	3.80×10^{-50}	4.10×10^{-49}

Table 5.7: Results of muon and electron $g_{\mu(e)} - 2$ and LFV processes $\text{BR}(\mu \rightarrow e\gamma)$ and $\mu\text{-}e$ conversion rates of the BP given in Table 5.5.

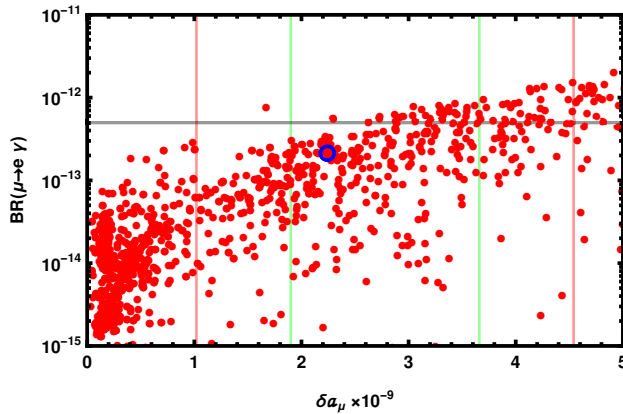


Figure 5.13: The branching ratio $\text{BR}(\mu \rightarrow e\gamma)$ versus the muon anomalous magnetic moment deviation δa_μ in LRIS. The green (red) borders are the 1σ (2σ) standard error of measurements of δa_μ , and the gray horizontal line is the upper bound on $\text{BR}(\mu \rightarrow e\gamma)$. The BP of Table 5.5 is encircled.

$$U_{3 \times 3} \simeq \left(\mathbf{1}_{3 \times 3} - \frac{1}{2} F F^T \right) U_{\text{PMNS}}, \quad (5.2.48)$$

where the nonunitarity limits of the U_{PMNS} is encoded in $F = M_D M_R^{-1}$ and the 3×6 extended matrix $\mathbb{F} = [\mathbf{0}_{3 \times 3} | F]_{3 \times 6}$ is $\mathbb{F}_{ij} = 0$ and $\mathbb{F}_{i,j+3} = F_{ij}$ for $i, j = 1, 2, 3$. Finally, $U_{6 \times 6}$ is the matrix which diagonalizes the $\{\nu_R, S_2\}$ mass matrix, and we have omitted the standard global phase matrix which gives the true positive values of neutrino masses.

5.2.3 LFV Constraints on a_μ

Now, we turn to the constraints on the charged Higgs boson contributions to LFV rare processes. The LRIS W -RHN and the charged Higgs boson contributions to the $\text{BR}(\mu \rightarrow e\gamma)$ and the $\mu\text{-}e$ conversion rates $R_{\mu \rightarrow e}$ are in order. Experiments set upper bounds to these quantities, and the stringent experimental limits on these processes should be regarded as constraints on the charged Higgs boson contribution

to a_μ [36, 129]. The LFV experiments set the upper limit $\text{BR}(\mu \rightarrow e\gamma) \lesssim 4.2 \times 10^{-13}$ with 90% confidence level [66]. In LRIS, the W -RHN and charged Higgs boson mediation for $\mu \rightarrow e\gamma$ leads to

$$\begin{aligned} \text{BR}(\mu \rightarrow e\gamma)_{\text{LRIS}} = & \frac{\alpha_w^3 s_w^2}{256\pi^2} \frac{m_\mu}{\Gamma_\mu} (x_W^\mu)^2 \sum_{k=1}^9 \left| U_{k,1} U_{k,2}^* \mathcal{F}_2(x_W^{\nu_k}) + \zeta'_{k,e} \zeta'^*_{k,\mu} \mathcal{F}_2(x_{H^\pm}^{\nu_k}) \right. \\ & \left. + (\zeta'_{k,e} \xi'^*_{k,\mu} + \xi'_{k,e} \zeta'^*_{k,\mu}) \mathcal{F}_1(x_{H^\pm}^{\nu_k}) \right|^2. \end{aligned} \quad (5.2.49)$$

As discussed after Eq. (5.2.37), the first term $\sum_{k=1}^9 U_{k,1} U_{k,2}^* \mathcal{F}_2(x_W^{\nu_k}) \simeq \sum_{k=1}^3 (U_{\text{PMNS}}^T)_{k,1} (U_{\text{PMNS}}^T)_{k,2} \mathcal{F}_2(x_W^{\nu_k})$ of Eq. (5.2.49) of the $W - \nu$ contribution is $\lesssim \mathcal{O}(10^{-29})$, and thus negligible by the GIM cancellation mechanism [171]. The remaining W -RHN contribution in the first term $\sum_{k=4}^9 U_{k,1} U_{k,2}^* \mathcal{F}_2(x_W^{\nu_k})$ vanishes due to contributions from the first two rows of the 3×6 upper-right block matrix in Eq. (5.2.45) which gives $U_{k,1} U_{k,2}^* \simeq 0$, $k = 4, \dots, 9$. Accordingly, we only constrain the charged Higgs boson contribution. For this, as discussed in the paragraph before Eq. (5.2.43), the second term $\sum_{k=1}^9 \zeta'_{k,e} \zeta'^*_{k,\mu} \mathcal{F}_2(x_{H^\pm}^{\nu_k}) \simeq \sum_{k=1}^3 \zeta'_{k,e} \zeta'^*_{k,\mu} \mathcal{F}_2(x_{H^\pm}^{\nu_k})$ is $\sim \mathcal{O}(10^{-9})$, and it is only about 0.004% of the third term $\sum_{k=1}^9 (\zeta'_{k,e} \xi'^*_{k,\mu} + \xi'_{k,e} \zeta'^*_{k,\mu}) \mathcal{F}_1(x_{H^\pm}^{\nu_k}) \simeq \sum_{k=4}^9 (\zeta'_{k,e} \xi'^*_{k,\mu} + \xi'_{k,e} \zeta'^*_{k,\mu}) \mathcal{F}_1(x_{H^\pm}^{\nu_k})$, which is $\sim \mathcal{O}(10^{-5})$ and need to be constrained. We can approximate Eq. (5.2.49) as

$$\begin{aligned} \text{BR}(\mu \rightarrow e\gamma)_{\text{LRIS}} \simeq & \frac{\alpha_w^3 s_w^2}{256\pi^2} \frac{m_\mu}{\Gamma_\mu} (x_W^\mu)^2 \sum_{k=4}^9 \left| (\zeta'_{k,e} \xi'^*_{k,\mu} + \xi'_{k,e} \zeta'^*_{k,\mu}) \mathcal{F}_1(x_{H^\pm}^{\nu_k}) \right|^2 \\ \lesssim & \frac{9\alpha_{\text{em}}}{256\pi^4} \frac{m_\mu^5}{\Gamma_\mu} \sum_{k=4}^9 \frac{1}{m_{\nu_k}^2} \left(\frac{\zeta_{k,e} \xi_{k,\mu}}{m_\mu} + \frac{\xi_{k,e} \zeta_{k,\mu}}{m_e} \right)^2, \end{aligned} \quad (5.2.50)$$

where the factor $\frac{9\alpha_{\text{em}}}{256\pi^4} \frac{m_\mu^5}{\Gamma_\mu} \sim 10^8$ and the loop function $\mathcal{F}_1(x) \lesssim 3$ for $x \gg 1$, as noted after Eq. (5.2.43), and again the complex notations are omitted as the couplings are (taken) real.

At the end, we check experimental limits on the charged Higgs boson contributions to the μ - e conversion on a nucleus with atomic weight A . The charged Higgs

contributes to the μ - e conversion rate as follows [36, 129]

$$R_{\mu \rightarrow e}^A = \frac{32G_F^2 m_\mu^5}{\Gamma_{\text{capt}}^A} \left[\left| \tilde{C}_{V,R}^{pp} V_A^{(p)} + \tilde{C}_{V,R}^{nn} V_A^{(n)} + \frac{1}{4} C_{D,L} D_A \right|^2 + \{L \leftrightarrow R\} \right], \quad (5.2.51)$$

where Γ_{capt}^A is the rate for the muon to transform to a neutrino by capture on the nucleus (A). Some numerical values of $\Gamma_{\text{capt}}^A \sim \mathcal{O}(1 - 10) \times 10^6 \text{ s}^{-1}$, and the nucleus and nucleon (n, p)-dependent “overlap integrals” $V_A^{(p)}, V_A^{(n)}, D_A \sim \mathcal{O}(10^{-2} - 10^{-1})$ for the nuclei $A = \text{Al}, \text{Ti}, \text{Au}$ are given in Ref. [216]. Experiments make the upper bounds $R_{\mu \rightarrow e}^{\text{Ti}} \leq 10^{-18}$, $R_{\mu \rightarrow e}^{\text{Al}} \leq 10^{-16}$, $R_{\mu \rightarrow e}^{\text{Au}} \leq 7 \times 10^{-13}$. In LRIS, the nucleon-dependent Wilson coefficients are given by

$$C_{D,L} = \frac{8G_F \alpha_{\text{em}}}{\pi s_w^2 \sqrt{2}} \sum_{k=1}^9 \sum_{j=1}^3 \sum_{q,q'=u,d,q \neq q'} (U_{k,e}^* U_{k,\mu} |V_{q',q_j}|^2) B_2(x_W^{\nu_k}, x_W^{q_j}), \quad (5.2.52)$$

$$\tilde{C}_{V,R}^{pp} = \frac{1}{8\pi^2 m_{H^\pm}^2} \sum_{k=1}^9 \sum_{j=1}^3 \sum_{q,q'=u,d,q \neq q'} (\zeta_{k,e} \xi_{k,\mu} + \zeta_{k,\mu} \xi_{k,e}) (C_{q',q_j}^2 + D_{q',q_j}^2) B_2(x_{H^\pm}^{\nu_k}, x_{H^\pm}^{q_j}), \quad (5.2.53)$$

$$\tilde{C}_{V,R}^{nn} = \frac{1}{4\pi^2 m_{H^\pm}^2} \sum_{k=1}^9 \sum_{j=1}^3 \sum_{q,q'=u,d,q \neq q'} (\zeta_{k,e} \xi_{k,\mu} + \xi_{k,e} \xi_{k,\mu}) (C_{q',q_j} D_{q',q_j}) B_1(x_{H^\pm}^{\nu_k}, x_{H^\pm}^{q_j}) \sqrt{x_{H^\pm}^{\nu_k} x_{H^\pm}^{q_j}}, \quad (5.2.54)$$

where in LRIS the interchange $\{L \leftrightarrow R\}$ does not change the coefficients. The parameters C_{ij}, D_{ij} , and $\zeta_{k\ell}, \xi_{k\ell}$ are the charged Higgs boson interaction couplings with quarks and leptons appearing in Eqs. (5.2.15) and (5.2.16), respectively, and the loop functions are

$$J_k(x) = \frac{1}{1-x} + \frac{x^k \log(x)}{(1-x)^2}, \quad (5.2.55)$$

$$B_k(x, y) = \frac{J_k(x) - J_k(y)}{x-y}, \quad k = 1, 2. \quad (5.2.56)$$

Asymptotically, $B_k(x, y) \rightarrow 0$ as $x \gg 1$ and $y \ll 1$. So the $W - \nu$ contribution Eq. (5.2.52) is clearly suppressed by the GIM cancellation mechanism [171]. The factor $\frac{32G_F^2 m_\mu^5}{\Gamma_{\text{capt}}^A} \sim \mathcal{O}(10^{-21} - 10^{-20})$ in Eq. (5.2.51), and all BPs are tested and found

to satisfy the μ - e conversion experimental limits mentioned after Eq. (5.2.51), and all of them are of order of the BP results in Table 5.7.

5.2.4 Conclusion

We have analyzed the muon anomalous magnetic moment a_μ in a minimal left-right symmetric model with neutrino masses inverse seesaw mechanism. We found that a reasonable region of the parameter space of the model is consistent with the observed muon $g - 2$ anomaly. We emphasized that, in this type of models, only the H^\pm loop explains a_μ significantly, in agreement with the $\text{BR}(\mu \rightarrow e\gamma)$, μ - e conversion and the electron $g_e - 2$ anomaly measured limits.

6

SEMI-VISIBLE DARK PHOTON IN A MODEL WITH VECTOR-LIKE LEPTONS FOR THE $(g - 2)_{e,\mu}$ AND W -BOSON MASS ANOMALIES

6.1 The VLSM model

We review the model proposed in Refs. [207, 208] in which the SM is extended by a $U(1)'$ gauge symmetry and a family of vector-like leptons. The matter contents of the model is summarized in Table 6.1.

6.1.1 Gauge boson sector

Unlike the studies in Refs. [207, 208], we explicitly introduce the gauge kinetic mixing of the $U(1)'$ and $U(1)_Y$ symmetries. The gauge kinetic terms are given by

$$\mathcal{L}_{\text{gauge}} = -\frac{1}{4}F_{\mu\nu}F^{\mu\nu} - \frac{1}{4}F'_{\mu\nu}F'^{\mu\nu} - \frac{\epsilon}{2}F'_{\mu\nu}F^{\mu\nu} - \frac{1}{4}G_{\mu\nu}^a G^{a\mu\nu}, \quad (6.1.1)$$

where $F_{\mu\nu}$, $F'_{\mu\nu}$ and $G_{\mu\nu}^a$ are the gauge field strengths of $U(1)_Y$, $U(1)'$ and $SU(2)_L$, respectively. Here, ϵ is the gauge kinetic mixing factor. We denote the neutral vector fields of $U(1)_Y$, $U(1)'$ and $SU(2)_L$ by B_μ , V_μ and W_μ^3 , respectively. After the symmetry

6.1 The VLSM model

Gauge Symmetry	ℓ_{L_i}	\bar{e}_{R_i}	H	L_L	\bar{E}_R	\bar{L}_R	E_L	\bar{N}_R	N_L	Φ
$SU(2)_L$	2	1	2	2	1	2	1	1	1	1
$U(1)_Y$	-1	2	-1	-1	2	1	-2	0	0	0
$U(1)'$	0	0	0	-1	1	1	-1	1	-1	-1

Table 6.1: Quantum numbers of the scalars and leptons in the model under the gauge symmetry $SU(2)_L \times U(1)_Y \times U(1)'$. The index $i = 1, 2, 3$ runs over the three generations of the SM leptons.

breaking by the SM Higgs boson and the $U(1)'$ breaking scalar Φ , the mass squared matrix for (W_μ^3, B_μ, V_μ) is given by

$$\mathcal{M}_V^2 = m_W^2 \begin{pmatrix} 1 & -t_W & 0 \\ -t_W & t_W^2 & 0 \\ 0 & 0 & t_V^2 \end{pmatrix}, \quad (6.1.2)$$

where $t_W := g_1/g_2$ and $t_V := m_V/m_W$ with $m_W := g_2 v_H/\sqrt{2}$ and $m_V = \sqrt{2}g'v_\Phi$.

Here, g_1 , g_2 and g' are respectively the gauge coupling constants of $U(1)_Y$, $SU(2)_L$ and $U(1)'$. The canonically normalized mass basis of the gauge bosons are defined as

$$\begin{pmatrix} W_\mu^3 \\ B_\mu \\ V_\mu \end{pmatrix} =: \begin{pmatrix} s_W & c_W C_{WA'} & c_W C_{WZ} \\ c_W & -s_W C_{BA'} & -s_W C_{BZ} \\ 0 & C_{VA'} & C_{VZ} \end{pmatrix} \begin{pmatrix} A_\mu \\ A'_\mu \\ Z_\mu \end{pmatrix}, \quad (6.1.3)$$

For $\epsilon, t_V \ll 1$, $C_{WA'}$, $C_{BA'}$, $C_{VZ} \sim \mathcal{O}(\epsilon)$ and C_{WZ} , C_{BZ} , $-C_{VA'} \sim 1 + \mathcal{O}(\epsilon^2)$. In this limit,

$$m_{A'}^2 \sim m_V^2(1 + c_W^2\epsilon^2), \quad m_Z^2 \sim \frac{m_W^2}{c_W^2}(1 + s_W^2\epsilon^2), \quad (6.1.4)$$

where $s_W := g_1/\sqrt{g_1^2 + g_2^2} =: t_W c_W$. The explicit form of these matrices are shown in Appendix C.1.

6.1.2 Fermion sector

In the gauge basis, the relevant part of the Lagrangian specifying the mass terms of the vector-like leptons and their Yukawa interactions are given by

$$\begin{aligned} \mathcal{L} \supset & m_L \bar{L}_R L_L + m_E \bar{E}_R E_L + m_N \bar{N}_R N_L \\ & + \bar{e}_{Ri} y_i^e \ell_{Lj} H + \Phi \lambda_i^L \bar{L}_R \ell_{Li} - \Phi^* \lambda_i^E \bar{e}_{Ri} E_L \\ & + \lambda_e \bar{E}_R L_L H - \lambda'_e \bar{L}_R \tilde{H} E_L + \lambda_n \bar{N}_R L_L \tilde{H} + \lambda'_n \bar{L}_R H N_L + h.c. \end{aligned} \quad (6.1.5)$$

Here, $\tilde{H} = i\sigma_2 H^*$ and $i, j = 1, 2, 3$ label the SM generations. After the symmetry breaking via non-zero vacuum expectation values (VEVs) of the scalar fields, v_Φ and v_H , the mass matrices for $e_L = (e_{L_i}^-, L_L^-, E_L^-)$, $e_R = (e_{R_i}^-, E_R^-, L_R^-)$ and $n_L = (\nu_{L_i}, L_L^0, N_L)$, $n_R = (N_R, L_R^0)$ are given by

$$\mathcal{M}_e = \begin{pmatrix} y_{ij} v_H & 0 & \lambda_{L_i} v_\Phi \\ 0 & \lambda_e v_H & m_L \\ \lambda_{E_j} v_\Phi & m_E & \lambda'_e v_H \end{pmatrix}, \quad \mathcal{M}_n = \begin{pmatrix} 0 & \lambda_{L_i} v_\Phi \\ \lambda_n v_H & m_L \\ m_N & \lambda'_n v_H \end{pmatrix}. \quad (6.1.6)$$

In this work, we do not explicitly introduce the right-handed neutrinos and treat neutrinos as massless particles. As shown in Ref. [208], the phenomenology will not be changed up to $\mathcal{O}(v_H/M_{\text{Maj}})$, when we introduce the heavy right-handed neutrinos with Majorana mass $M_{\text{Maj}} \sim 10^{10}$ GeV. The mass matrices are diagonalized as

$$U_{e_L}^\dagger \mathcal{M}_e U_{e_R} = \begin{pmatrix} m_{e_i} & 0 & 0 \\ 0 & m_{E_1} & 0 \\ 0 & 0 & m_{E_2} \end{pmatrix}, \quad U_{n_L}^\dagger \mathcal{M}_n U_{n_R} = \begin{pmatrix} 0 & 0 \\ m_{N_1} & 0 \\ 0 & m_{N_2} \end{pmatrix}, \quad (6.1.7)$$

where $U_{e_{L,R}}$ and U_{n_L} (U_{n_R}) are 5×5 (2×2) unitary matrices. The leptons in the mass basis are defined as

$$\hat{e}_A = U_{e_A}^\dagger e_A, \quad \hat{n}_A = U_{n_A}^\dagger n_A, \quad A = L, R. \quad (6.1.8)$$

The Dirac fermions are defined as

$$[\psi_\ell]_J := \begin{pmatrix} [\hat{\ell}_L]_J \\ [\hat{\ell}_R]_J \end{pmatrix}, \quad \ell = e, n, \quad J = 1, 2, 3, 4, 5, \quad (6.1.9)$$

6.1 The VLSM model

where $[\hat{n}_R]_j = 0$ for $j = 1, 2, 3$.

Throughout this work, we assume that the $U(1)'$ breaking scalar Φ exclusively couples to the first generation, i.e.

$$\lambda_{L_i} =: \lambda_L \delta_{1i}, \quad \lambda_{E_i} =: \lambda_E \delta_{1i}, \quad \lambda_{N_i} =: \lambda_N \delta_{1i}, \quad (6.1.10)$$

so that the lepton flavor violations are not induced from the mixing. As we shall study the dark photon of $\mathcal{O}(1)$ GeV, the VEV of Φ is expected to be in this order, which is much smaller than that studied in Refs. [207, 208]. In this regime, with omitting the mixing with the second and third generations, the diagonalization matrices are approximately given by

$$U_{e_L} = \begin{pmatrix} 1 & 0 & 0 \\ 0 & c_{e_L} & s_{e_L} \\ 0 & -s_{e_L} & c_{e_L} \end{pmatrix} \begin{pmatrix} 1 - (\eta_{L_1}^2 + \eta_{L_2}^2)/2 & \eta_{L_1} & -\eta_{L_2} \\ -\eta_{L_1} & 1 & 0 \\ \eta_{L_2} & 0 & 1 \end{pmatrix},$$

$$U_{e_R} = \begin{pmatrix} 1 & 0 & 0 \\ 0 & s_{e_R} & c_{e_L} \\ 0 & c_{e_R} & -s_{e_L} \end{pmatrix} \begin{pmatrix} 1 - (\eta_{R_1}^2 + \eta_{R_2}^2)/2 & -\eta_{R_1} & \eta_{R_2} \\ \eta_{R_1} & 1 & 0 \\ -\eta_{R_2} & 0 & 1 \end{pmatrix}, \quad (6.1.11)$$

where

$$\eta_{L_1} := c_{e_R} \lambda_L \frac{v_\Phi}{m_{E_1}}, \quad \eta_{L_2} := s_{e_R} \lambda_L \frac{v_\Phi}{m_{E_2}}, \quad \eta_{R_1} := s_{e_L} \lambda_E \frac{v_\Phi}{m_{E_1}}, \quad \eta_{R_2} := c_{e_L} \lambda_E \frac{v_\Phi}{m_{E_2}}. \quad (6.1.12)$$

The first matrices diagonalize the right-lower 2×2 block of \mathcal{M}_e and their analytical forms, as well as the diagonalization of the neutrino mass matrix, are shown in Appendix C.1. The second matrices approximately diagonalize the small off-diagonal elements of the electron and the vector-like leptons up to the second order in $\eta := \mathcal{O}(\eta_{L_{1,2}}, \eta_{R_{1,2}})$.

6.1.3 Fermion interactions

The gauge interactions of the leptons with the neutral gauge bosons in the mass basis are given by

$$\begin{aligned} \mathcal{L}_{VF} = & \sum_{\ell=e,n} \bar{\psi}_\ell \gamma_\mu \sum_{A=L,R} \left[e A^\mu Q_\ell \right. \\ & \left. + \sum_{X=A',Z} \frac{g_2}{c_W} X^\mu \left\{ I_{\ell_A} (c_W^2 C_{WX} + s_W^2 C_{BX}) - s_W^2 Q_\ell C_{BX} + \frac{c_W g'}{g_2} Q'_{\ell_A} C_{VX} \right\} \right] P_A \psi_\ell \\ =: & -e A^\mu \bar{\psi}_e \gamma^\mu \psi_e + \sum_{X=A',Z} \sum_{A=L,R} \sum_{\ell=e,n} X^\mu \bar{\psi}_\ell \gamma_\mu g_{\ell_A}^X P_A \psi_\ell, \end{aligned} \quad (6.1.13)$$

where

$$I_{e_A} = -\frac{1}{2} U_{e_A}^\dagger \mathcal{P}_A U_{e_A} =: -\frac{1}{2} \mathcal{E}_A, \quad I_{n_A} = +\frac{1}{2} U_{n_A}^\dagger \mathcal{P}_A U_{n_A} =: \frac{1}{2} \mathcal{N}_A, \quad Q'_{\ell_A} = -U_{\ell_A}^\dagger \mathcal{P}' U_{\ell_A}, \quad (6.1.14)$$

with $\mathcal{P}_R := \text{diag}(0, 0, 0, 0, 1) =: 1 - \mathcal{P}_L$ and $\mathcal{P}' := \text{diag}(0, 0, 0, 1, 1)$. The electric coupling constant is defined as $e = g_1 g_2 / \sqrt{g_1^2 + g_2^2}$, and the electric charged are $Q_e = -1$ and $Q_n = 0$. The W -boson couplings are given by

$$\mathcal{L}_W = \frac{g_2}{\sqrt{2}} W_\mu^- \bar{\psi}_n \gamma^\mu \sum_{A=L,R} h_A P_A \psi_e + h.c. = \sum_{A=L,R} W_\mu^- \bar{\psi}_n \gamma^\mu g_A^W P_A \psi_e + h.c., \quad (6.1.15)$$

where

$$h_A := U_{n_A}^\dagger \mathcal{P}_A U_{e_A}. \quad (6.1.16)$$

The $U(1)'$ Higgs boson Φ is expanded as

$$\Phi = v_\Phi + \frac{1}{\sqrt{2}} (\chi + i a_\chi), \quad (6.1.17)$$

where a_χ is the Nambu-Goldstone boson absorbed by the dark photon A' . The Yukawa interactions of the CP-even Higgs χ are given by

$$-\mathcal{L}_\chi = \frac{\chi}{\sqrt{2}} \sum_{\ell=e,n} \bar{\psi}_\ell Y_\ell^\chi P_L \psi_\ell + h.c., \quad (6.1.18)$$

6.1 The VLSM model

where

$$Y_e^\chi = U_{e_L}^\dagger \begin{pmatrix} 0 & 0 & \lambda_{L_i} \\ 0 & 0 & 0 \\ \lambda_{E_j} & 0 & 0 \end{pmatrix} U_{e_R}, \quad Y_n^\chi = U_{n_L}^\dagger \begin{pmatrix} 0 & \lambda_{L_i} \\ 0 & 0 \\ 0 & 0 \end{pmatrix} U_{n_R}. \quad (6.1.19)$$

Up to $\mathcal{O}(\epsilon^2)$, the gauge couplings are given by

$$g_{\ell_A}^Z \sim \frac{g_2}{c_W} (I_{\ell_A} - s_W^2 Q_\ell) + \epsilon s_W g' Q'_{\ell_A} + \epsilon^2 g_2 t_W c_W \left\{ \frac{1}{2} I_{\ell_A} - Q_\ell \left(1 - \frac{s_W^2}{2} \right) \right\}, \quad (6.1.20)$$

$$g_{\ell_A}^{A'} \sim -g' Q'_{\ell_A} \left(1 + \frac{c_W^2}{2} \epsilon^2 \right) + \epsilon c_W s_W g_2 Q_\ell. \quad (6.1.21)$$

As explicitly shown in Appendix C.1, we find

$$\mathcal{E}_L \sim \begin{pmatrix} 1 - \eta_e^2/\lambda_E^2 & s_{e_L} \eta_e/\lambda_E & -c_{e_L} \eta_e/\lambda_E \\ s_{e_L} \eta_e/\lambda_E & c_{e_L}^2 & c_{e_L} s_{e_L} \\ -c_{e_L} \eta_e/\lambda_E & c_{e_L} s_{e_L} & s_{e_L}^2 \end{pmatrix}, \quad \mathcal{E}_R \sim \begin{pmatrix} \eta_e^2/\lambda_L^2 & c_{e_R} \eta_e/\lambda_L & -s_{e_R} \eta_e/\lambda_L \\ c_{e_R} \eta_e/\lambda_L & c_{e_R}^2 & -c_{e_R} s_{e_R} \\ -s_{e_R} \eta_e/\lambda_L & -s_{e_R} c_{e_R} & s_{e_R}^2 \end{pmatrix}, \quad (6.1.22)$$

where

$$\eta_e := \lambda_L \lambda_E v_\Phi \left(\frac{s_{e_L} c_{e_R}}{m_{E_1}} + \frac{c_{e_L} s_{e_R}}{m_{E_2}} \right), \quad (6.1.23)$$

will appear in Δa_e expression in Sec. 6.2. For the $U(1)'$ boson couplings,

$$Q'_{e_L} \sim \begin{pmatrix} \eta_{L_1}^2 + \eta_{L_2}^2 & -\eta_{L_1} & \eta_{L_2} \\ -\eta_{L_1} & 1 & 0 \\ \eta_{L_2} & 0 & 1 \end{pmatrix}, \quad Q'_{e_R} \sim \begin{pmatrix} \eta_{R_1}^2 + \eta_{R_2}^2 & \eta_{R_1} & -\eta_{R_2} \\ \eta_{R_1} & 1 & 0 \\ -\eta_{R_2} & 0 & 1 \end{pmatrix}. \quad (6.1.24)$$

Hence, the Z -boson couplings to the SM leptons are shifted at $\mathcal{O}(\epsilon^2, \eta^2)$ and those of the dark photon A' appears at ϵ with the sub-dominant contributions at $\mathcal{O}(\epsilon^2, \eta^2)$. The off-diagonal couplings of the SM leptons and the vector-like ones are induced at $\mathcal{O}(\eta)$. The structures are similar for the couplings involving the neutral leptons. The Yukawa couplings of the χ boson is approximately given by

$$Y_e^\chi \sim \begin{pmatrix} 2\eta_e & c_{e_R} \lambda_L & -s_{e_R} \lambda_L \\ -s_{e_L} \lambda_E & \mathcal{O}(v_\Phi/m_{E_1}) & \mathcal{O}(v_\Phi/m_{E_1}) \\ c_{e_L} \lambda_E & \mathcal{O}(v_\Phi/m_{E_1}) & \mathcal{O}(v_\Phi/m_{E_2}) \end{pmatrix}. \quad (6.1.25)$$

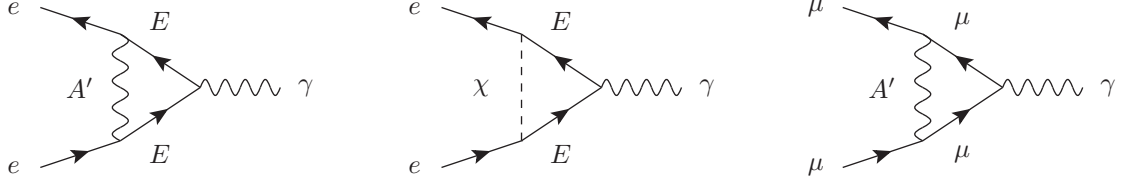


Figure 6.1: The Feynman diagrams dominantly contribute to the Δa_e (left and middle) and Δa_μ (right).

6.2 Anomalous magnetic moments and W -boson mass

6.2.1 Anomalous magnetic moments

The 1-loop contribution to the anomalous magnetic moment of the lepton $\ell = e, \mu$ via the neutral gauge boson $X = Z, A'$ and the charged leptons is given by

$$\delta_X a_\ell = -\frac{m_\ell}{8\pi^2 m_X^2} \sum_{B=1}^5 \left[\left(\left| [g_{eL}^X]_{i_\ell B} \right|^2 + \left| [g_{eR}^X]_{i_\ell B} \right|^2 \right) m_\ell F_Z(x_{e_B}^X) + \text{Re} \left([g_{eL}^X]_{i_\ell B} [g_{eR}^X]_{i_\ell B}^* \right) m_{e_B} G_Z(x_{e_B}^X) \right], \quad (6.2.1)$$

where $x_{e_B}^X = m_{e_B}^2/m_X^2$. Here, m_{e_B} is the mass of the B -th generation charged lepton, with flavor index $B = 1, \dots, 5$. The index $i_\ell = 1, 2$ for $\ell = e, \mu$. The loop functions $F_Z(x), G_Z(x)$ are defined in Appendix C.2. The 1-loop contribution from the χ scalar to Δa_ℓ is given by [140, 202]

$$\delta_\chi a_\ell = -\frac{m_\ell}{32\pi^2 m_\chi^2} \sum_{B=1}^5 \left[\left(\left| [Y_e^\chi]_{i_\ell B} \right|^2 + \left| [Y_e^\chi]_{Bi_\ell} \right|^2 \right) m_\ell F_S(y_{e_B}^\chi) + \text{Re} \left([Y_e^\chi]_{i_\ell B} [Y_e^\chi]_{Bi_\ell} \right) m_{e_B} G_S(y_{e_B}^\chi) \right], \quad (6.2.2)$$

where, $y_{e_B}^\chi := m_{e_B}^2/m_\chi^2$. Also, the loop functions $F_S(x), G_S(x)$ are defined in Appendix C.2. Altogether, the new physics contribution to the anomalous magnetic moment is given by

$$\Delta a_\ell = \delta_{A'} a_\ell + \delta_Z a_\ell + \delta_\chi a_\ell - \delta_Z^{\text{SM}} a_\ell, \quad (6.2.3)$$

6.2 Anomalous magnetic moments and W -boson mass

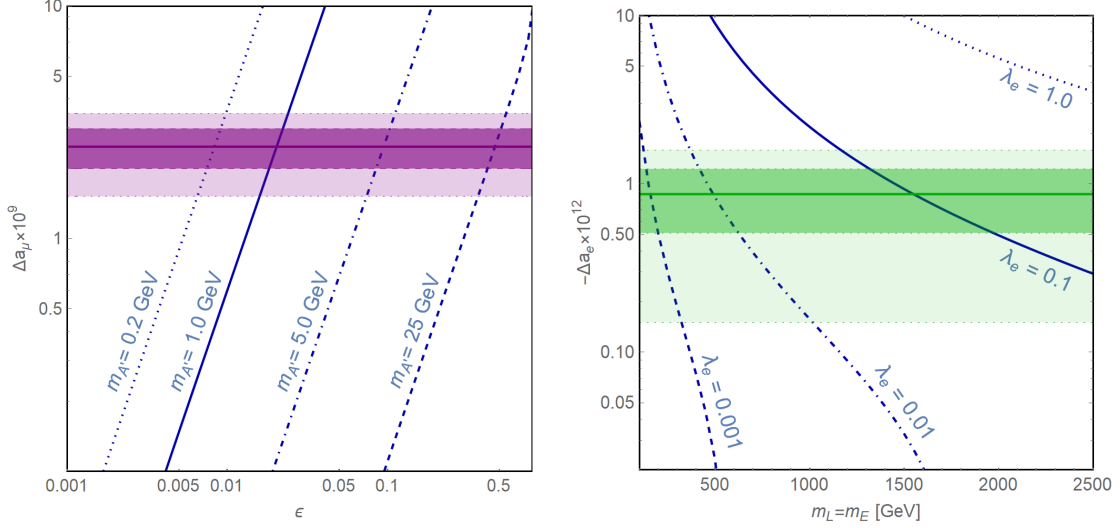


Figure 6.2: The left panel shows ϵ versus Δa_μ with $m_{A'} = 0.2, 1, 5, 25 \text{ GeV}$. The dark (light) purple region is the 1σ (2σ) range. The right panel shows $m_L = m_E$ versus $-\Delta a_e$ with $\lambda_e = 0.001, 0.01, 0.1, 1.0$. The dark (light) green region is the 1σ (2σ) range. The input parameters other than $m_L = m_E$ are chosen as the BP-A shown in Table 6.2.

where the SM contribution via the Z -boson loop,

$$\delta_Z^{\text{SM}} a_\ell = -\frac{g_2^2 m_\ell^2}{8\pi^2 m_W^2} \left[\left(\frac{1}{4} - s_W^2 + 2s_W^4 \right) F_Z(x_\ell^Z) + s_W^2 \left(-\frac{1}{2} + s_W^2 \right) G_Z(x_\ell^Z) \right] \quad (6.2.4)$$

is subtracted. The contributions from the Z , W and Higgs bosons are negligible because the off-diagonal couplings in the mass basis are suppressed. The Feynman diagrams dominantly contribute to Δa_e and Δa_μ are shown in Fig. 6.1.

Let us estimate the sizes of Δa_ℓ in our model. From Eq. (6.1.20), the dark photon contribution to Δa_μ is approximately given by

$$\Delta a_\mu \sim \delta_{A'} a_\mu \simeq -\frac{c_W^2 s_W^2 g_2^2 m_\mu^2 \epsilon^2}{8\pi^2 m_{A'}^2} \left(2F_Z(x_\mu^{A'}) + G_Z(x_\mu^{A'}) \right) \quad (6.2.5)$$

$$\sim 2.8 \times 10^{-9} \times \left(\frac{\epsilon}{0.02} \right)^2 \left(\frac{1 \text{ GeV}}{m_{A'}} \right)^2 \left(\frac{2F_Z(x_\mu^{A'}) + G_Z(x_\mu^{A'})}{-2/3} \right). \quad (6.2.6)$$

Note that $2F_Z + G_Z$ is negative for $m_{A'} > m_\mu$.

It is turned out that Δa_e is dominantly from the 1-loop diagrams involving the vector-like leptons along with the dark photon or the χ boson, because of the chiral enhancement proportional to the vector-like lepton masses. From Eqs. (6.1.20) and (6.1.24), we find

$$\Delta a_e \sim -\frac{m_e \eta_e}{16\pi^2 v_\Phi} \sim -3.2 \times 10^{-13} \times \left(\frac{1 \text{ GeV}}{v_\Phi} \right) \left(\frac{\eta_e}{10^{-7}} \right), \quad (6.2.7)$$

and η_e is approximately given by

$$\eta_e \sim \lambda_L \lambda_E \frac{\lambda_e v_H v_\Phi}{m_L m_E} \sim 1.7 \times 10^{-7} \times \left(\frac{\lambda_e \lambda_L \lambda_E}{10^{-3}} \right) \left(\frac{v_\Phi}{1 \text{ GeV}} \right) \left(\frac{10^3 \text{ GeV}}{\sqrt{m_L m_E}} \right)^2, \quad (6.2.8)$$

for $v_H \ll m_E$. Thus, the vector-like mass around the TeV-scale can explain the deviation in Δa_e for the Yukawa coupling constants of $\mathcal{O}(0.1)$ and $v_\Phi \sim \mathcal{O}(1)$ GeV. Note that the contribution from the gauge kinetic mixing will be sub-dominant when Δa_μ is explained because the coupling induced by the kinetic mixing is flavor universal and it is estimated as

$$\delta_{A'} a_e \Big|_\epsilon = \frac{m_e^2}{m_\mu^2} \Delta a_\mu \simeq 5.8 \times 10^{-14} \times \left(\frac{\Delta a_\mu}{2.51 \times 10^{-9}} \right). \quad (6.2.9)$$

For $\eta_e \sim 10^{-7}$, the Z -boson couplings of the SM leptons are very close to the SM one since the deviation is at $\mathcal{O}(\eta_e^2)$, see Eq. (6.1.22).

Fig. 6.2 shows the values of Δa_μ (left) and Δa_e (right) based on our numerical analysis. We see that Δa_μ is explained for $\epsilon \sim 0.02$ for the 1 GeV dark photon as expected from Eq. (6.2.5). For $(\epsilon, m_{A'}) = (0.02, 1 \text{ GeV})$, Δa_e is explained by the vector-like lepton loops if the vector-like lepton masses are 1.5 TeV (500 GeV) with $\lambda_e = 0.1$ (0.01), as expected from Eqs. (6.2.7) and (6.2.8). Thus, our model provides a unified explanation for both Δa_e and Δa_μ without introducing lepton flavor violations.

6.2.2 W -boson mass

As shown in Refs. [205, 206], the W -boson mass shift can be explained by the 1-loop effects of the fourth family vector-like leptons. The T parameter [265, 266] has a dominant contribution to this shift compared to the S, U parameters and the T parameter is given by [139, 223]

$$\begin{aligned} 16\pi s_W^2 c_W^2 T = & \sum_{a,\beta} \left\{ \left(|h_{a\beta}^L|^2 + |h_{a\beta}^R|^2 \right) \theta_+(y_a, y_\beta) + 2\text{Re} (h_{a\beta}^L h_{a\beta}^{R*}) \theta_-(y_a, y_\beta) \right\} \\ & - \sum_{a < b} \left\{ \left(|\mathcal{N}_{ab}^L|^2 + |\mathcal{N}_{ab}^R|^2 \right) \theta_+(y_a, y_b) + 2\text{Re} (\mathcal{N}_{ab}^L \mathcal{N}_{ab}^{R*}) \theta_-(y_a, y_b) \right\} \\ & - \sum_{\alpha < \beta} \left\{ \left(|\mathcal{E}_{\alpha\beta}^L|^2 + |\mathcal{E}_{\alpha\beta}^R|^2 \right) \theta_+(y_\alpha, y_\beta) + 2\text{Re} (\mathcal{E}_{\alpha\beta}^L \mathcal{E}_{\alpha\beta}^{R*}) \theta_-(y_\alpha, y_\beta) \right\}, \end{aligned} \quad (6.2.10)$$

where the indices a, b (α, β) run over the neutral (charged) leptons, and $y_a := m_{e_a}^2/m_Z^2$, $y_\alpha := m_{n_\alpha}^2/m_Z^2$. Here, $h_{a\beta}^A = [h_A]_{a\beta}$, $\mathcal{E}_{\alpha\beta}^A = [\mathcal{E}_A]_{\alpha\beta}$ and $\mathcal{N}_{ab}^A = [\mathcal{N}_A]_{ab}$ for $A = L, R$. The formula of $2\pi S$ can be obtained by replacing $\theta_\pm \rightarrow \psi_\pm$ ($\theta_\pm \rightarrow \chi_\pm$) in the first line (the second and third lines), while by replacing $\theta_\pm \rightarrow \chi_\pm$ the formula of $-2\pi U$ can be obtained. The loop functions are defined in Appendix C.2. The W -boson mass is given by [174, 238]

$$\hat{m}_W^2 = m_W^2 \Big|_{\text{SM}} \left[1 + \frac{\alpha}{c_W^2 - s_W^2} \left(-\frac{S}{2} + c_W^2 T + \frac{c_W^2 - s_W^2}{4s_W^2} U \right) + \Delta_W \right], \quad (6.2.11)$$

where

$$\Delta_W = \frac{c_W^2}{c_W^2 - s_W^2} \left(-\frac{\Delta m_Z^2}{m_Z^2} + t_W^2 \Delta h_{e\nu}^L \right), \quad (6.2.12)$$

is the tree-level contribution from the Z -boson mass squared shift $\Delta m_Z^2/m_Z^2 := m_Z^2/m_Z^2|_{\text{SM}} - 1 \simeq s_W^2 \epsilon^2$ due to the kinetic mixing and the W -boson coupling to the SM leptons $\Delta h_{e\nu}^L := 1 - [h_L]_{11} \sim \mathcal{O}(\eta^2)$ ¹. The tree-level contributions are too

¹The tree-level contributions can be absorbed into the oblique parameters [59, 192], but our oblique parameters only include the loop effects from the vector-like leptons which are expected to be dominant.

small to explain the shift in the W -boson mass, and hence $T \sim \mathcal{O}(0.1)$ is necessary to explain the CDF II measurement. In fact, the limit on the dark-photon contributions to the EW precision data is $\epsilon < 2.7 \times 10^{-2}$ for $m_{A'} \ll 10$ GeV [124], where the most important effect is from the shift of the Z -boson mass which results the shift of the W -boson mass.

The T parameter is approximately given by

$$16\pi^2 c_W^2 s_W^2 T \simeq \frac{4(\lambda'_n v_H)^4}{3m_L^2 m_Z^2} \left[1 + \frac{1}{4} \left(\frac{\lambda'_e m_L}{\lambda'_n m_E} \right)^2 \left\{ 2 - 6 \log \frac{m_E^2}{m_L^2} + 3 \left(\frac{\lambda'_e}{\lambda'_n} \right)^2 \right\} \right], \quad (6.2.13)$$

where we assume $m_N \ll v_H \ll m_L \ll m_E$ and $\lambda_e, \lambda_n \ll \lambda'_e, \lambda'_n$. The first term in the parenthesis comes from the W -boson contributions involving N_2 and E_1 which are sensitive to the mass difference in the doublet-like states. Since the second term is negative due to the logarithmic term, the T parameter slightly increases as it is suppressed by m_E . For $m_L \ll m_E$, the T parameter is estimated as

$$T \sim 0.1 \times \lambda'_n^4 \left(\frac{230 \text{ GeV}}{m_L} \right)^2. \quad (6.2.14)$$

Thus, the shift of the W -boson mass suggested by the CDF II measurement can be explained if $100 \lesssim m_L \lesssim 300$ GeV and $\lambda'_n \sim 1$, so that the mass split between the neutral and charged doublet-like states is sizable ².

On the left panel of Fig. 6.3, we plot the region where the W -boson mass is shifted due to the vector-like lepton loops. The values favored by the CDF II and PDG are explained in the 1σ (2σ) range in the darker (lighter) red and blue regions, respectively. In this plot, the input parameters except m_L , m_E and $\lambda_L = \lambda_E$ are set to the values at the BP-B shown in Table 6.2. The value of $\lambda_L = \lambda_E$ are chosen to explain $\Delta a_e \simeq -8.7 \times 10^{-13}$ based on the approximated formula in Eq. (6.2.7), and hence both Δa_e and Δa_μ are explained everywhere on the (m_L, m_E) plane. The

²In models without the singlet vector-like neutrino N , the split should be originated from the charged leptons, and thus the charged vector-like lepton should be lighter than 200 GeV to explain the CDF II result [205].

6.2 Anomalous magnetic moments and W -boson mass

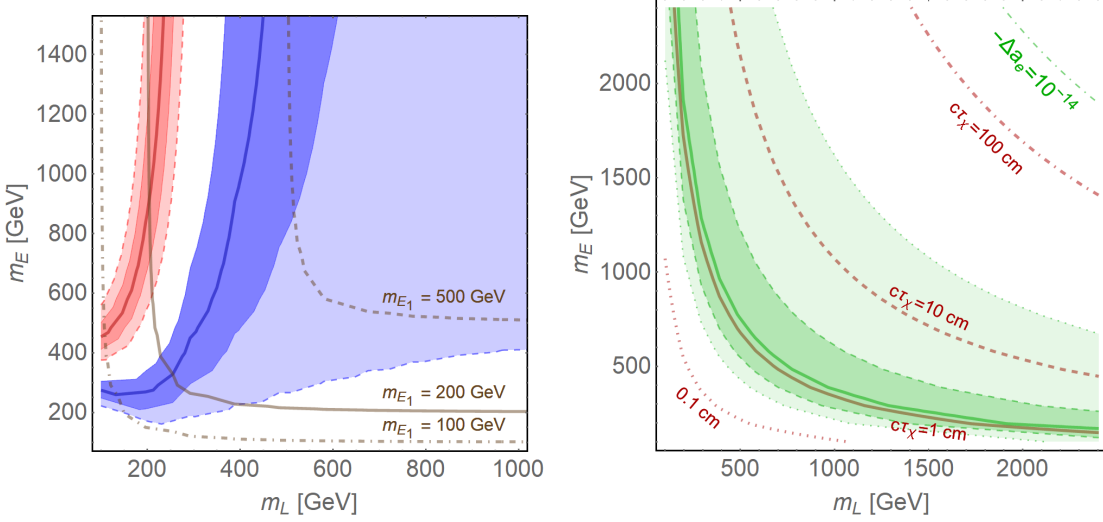


Figure 6.3: On the left panel, m_W is explained the CDF II and PDG result within the 1σ (2σ) range in the darker (lighter) red and blue regions, respectively. The solid line are the masses of the lightest charged exotic lepton $m_{E_1} = 100, 200$ and 500 GeV from bottom to top (left to right). The value of $\lambda_L = \lambda_E$ chosen to explain Δa_e . On the right panel, $\Delta a_e = -8.7 \times 10^{-13}$ on the green line, and it is within the 1σ (2σ) range in the darker (lighter) green region. The red lines are the length of flight of χ . The inputs are those at the BP-B in Table 6.2 except (m_L, m_E) (and $\lambda_L = \lambda_E$) on the left (right) panel.

CDF II value is explained if the doublet-like vector-like lepton is about 200 GeV, while that of the PDG is explained at $m_L \sim 500$ GeV depending on the singlet mass m_E . We shall briefly discuss about the LHC signals of the light vector-like charged leptons in the next section.

Table 6.2 shows the three benchmark points (BPs) which explain both Δa_e and Δa_μ . At the all points, $\epsilon = 0.02$ and $m_{A'} = 1$ GeV for $\Delta a_\mu \sim 2 \times 10^{-9}$. The Yukawa couplings and vector-like masses are set to explain Δa_e . As discussed in the next section, we assume the spectrum $m_\chi < m_{N_1}/2 < m_{A'}$ to realize the semi-visible dark photon compatible with the current limits. We also assume $\lambda_n \sim 0$ to keep m_{N_1} of $\mathcal{O}(1)$ GeV. At the BP-A, the vector-like leptons are about 1.5 TeV, and hence the W -boson mass is very close to the SM value. At the BP-B (BP-C), the lightest

*Chapter 6: SEMI-VISIBLE DARK PHOTON IN A MODEL WITH
VECTOR-LIKE LEPTONS FOR THE $(g - 2)_{e,\mu}$ AND W -BOSON MASS
ANOMALIES*

Table 6.2: Values of the inputs and the outputs at the benchmark points. At the all points, the other inputs not shown in the table are set to $\epsilon = 0.0203$, $\lambda_n = 0$, $(m_V, m_\chi, m_{N_1}) = (1.0, 0.3, 0.4)$ GeV and $v_\Phi = 2\sqrt{2}$ GeV. The mass parameters are in the unit of GeV unless it is specified.

inputs	A	B	C
(m_L, m_E)	(1500., 1500.)	(300., 1400.)	(500., 1400.)
$\lambda_L = \lambda_E$	0.2	0.25	0.3
λ_e	0.1	0.01	0.01
$\lambda'_e = \lambda'_n$	0.5	1.	1.
outputs	A	B	C
(m_{E_1}, m_{E_2})	(1448., 1553.)	(297.4, 1411.)	(495.4, 1412.)
(m_{N_1}, m_{N_2})	(0.399, 1503.)	(0.346, 346.8)	(0.378, 529.4)
$-\Delta a_e \times 10^{13}$	9.326	7.698	6.557
$\Delta a_\mu \times 10^9$	2.488	2.488	2.488
m_W	80.3558	80.4046	80.3726
(S, T, U)	$(2.388, 2.039, -0.260) \times 10^{-4}$	(0.012, 0.111, 0.009)	(0.007, 0.041, 0.002)
$\Gamma_{A'} [\text{MeV}]$	1.318	1.486	1.399
$\text{Br}(A' \rightarrow N_1 N_1)$	0.9988	0.9989	0.9988
$c\tau_{N_1} [\text{cm}]$	2.754	0.004444	0.006934
$\text{Br}(N_1 \rightarrow \chi \nu)$	1.	1.	1.
$c\tau_\chi [\text{cm}]$	1.078	1.541	2.065
$\text{Br}(E_1 \rightarrow W N_1)$	0.7525	0.9216	0.9079
$\text{Br}(E_1 \rightarrow A'e)$	0.1237	0.03918	0.04606
$\text{Br}(E_1 \rightarrow \chi e)$	0.1237	0.03918	0.04606

charged lepton mass is about 300 (500) GeV, so that the W -boson mass favored by the CDF II (PDG) data is explained. We see that the W mass shift is dominantly explained by the T parameter, and the other oblique parameters, S and U , are much smaller.

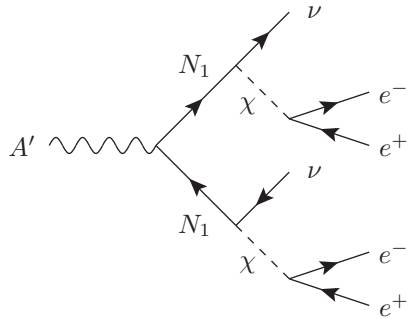


Figure 6.4: Dominant dark photon semi-visible decay.

6.3 Signals of light particles

6.3.1 Semi-visible dark photon

The experiments exclude the dark photon responsible for the muon anomalous magnetic moment if it decays to a pair of electrons or invisible particles [7, 42, 74, 226, 227]. The invisible dark photons are also searched in meson decays [51, 119–121]. There are limits from deep inelastic scatterings independently to decays of the dark photon, and the current limit for $\mathcal{O}(1)$ GeV dark photon is $\epsilon \lesssim 0.035$ [97, 218, 242, 299, 300], which is larger than our benchmark points $\epsilon = 0.02$. However, the experiments lose sensitivity for the other semi-visible dark photon decay modes, as discussed in Refs. [17, 148, 149, 252]. There is the experimental analysis searching for such dark photon at the fixed-target experiment NA64 [100]. According to Refs. [17, 100], the dark photon explanation for Δa_μ is viable for $m_{A'} \sim \mathcal{O}(0.1 - 1)$ GeV if the decay of heavy neutral fermion is fast enough. In our model, the dark photon will dominantly decay to a pair of vector-like neutrinos N_1 if $2m_N < m_{A'}$. Then the vector-like neutrino N_1 will decay to the CP-even Higgs boson χ in the $U(1)'$ breaking scalar Φ . The scalar χ subsequently decays to a pair of electrons. Altogether, the decay chain

of the dark photon is shown in Fig. 6.4:

$$A' \rightarrow N_1 N_1, \quad N_1 \rightarrow \nu \chi, \quad \chi \rightarrow ee, \quad (6.3.1)$$

which is kinematically allowed if $m_{A'}/2 > m_{N_1} > m_\chi > 2m_e$. There are two pairs of electrons in the final state accompanied with two neutrinos. Thus, the signal at the experiments will be semi-visible if these decays happen inside detectors whose size is $\mathcal{O}(1\text{ m})$.

The first decay $A' \rightarrow N_1 N_1$ occurs promptly because $N_1 \sim N$ has the $U(1)'$ charge and there is the coupling without suppression from η . The second decay $N_1 \rightarrow \chi \nu$ is relatively long, but is enough short since the coupling is suppressed only by v_H/m_L . Note that the decay width of N_1 is too small if the scalar χ is much heavier than N_1 so that there is only three-body decays via A' or the SM bosons. The decay width of the scalar χ is approximately given by

$$\Gamma(\chi \rightarrow ee) = \frac{m_\chi}{16\pi} |[Y_e^\chi]_{ee}|^2 \left(1 - \frac{4m_e^2}{m_\chi^2}\right)^{3/2} \sim \frac{m_\chi}{4\pi} \eta_e^2 \quad (6.3.2)$$

Interestingly, this is directly related to the approximated formula of Δa_e in Eq. (6.2.7), so that the length of flight of χ is estimated as

$$c\tau_\chi \sim 1 \text{ cm} \times \left(\frac{8.8 \times 10^{-13}}{|\Delta a_e|}\right)^2 \left(\frac{0.4 \text{ GeV}}{m_\chi}\right) \left(\frac{2\sqrt{2} \text{ GeV}}{v_\Phi}\right)^2. \quad (6.3.3)$$

Thus, the scalar χ decays before reaching or inside the detectors if $|\Delta a_e| \sim \mathcal{O}(10^{-13})$, whereas the decay can not be detected and thus the signal is invisible if $|\Delta a_e| \ll 10^{-13}$. The decay widths of A' , N_1 and χ as well as the corresponding branching fractions at the BPs are shown in Table 6.2. We see that the lifetime of A' and N_1 are (much) less than $\mathcal{O}(\text{cm})$ and these dominantly decay to $N_1 N_1$ and $\chi \nu$, respectively. Here, we calculated the two-body decays of A' to two leptons and that of N_1 to $\nu \chi$ on top of the three body-decays via the gauge bosons which are negligibly small because of the suppressed couplings and the kinetic suppression. Thus, we confirmed that the dark

photon decay can be dominated by $A' \rightarrow N_1 N_1$, $N_1 \rightarrow \chi \nu$. If χ only decays to two electrons, the length of flight is $\mathcal{O}(1)$ cm, and hence this will be detected as prompt decay or displaced vertices depending on the detector design. It is also possible that the χ scalar decays to two pions if there are couplings in the quark sector as for the electrons. In this case, the lifetime would be shorter. In Ref. [17], the dark photon decay proceeds as

$$A' \rightarrow \psi_i \psi_j, \psi_i \rightarrow \psi_{i-1} e^+ e^-, \psi_j \rightarrow \psi_{j-1} e^+ e^-, \dots, \psi_2 \rightarrow \psi_1 e^+ e^-, \quad (6.3.4)$$

where ψ_i 's are neutral exotic fermion and ψ_1 is considered to be stable, so that it can be the dark matter. In this scenario, the neutral fermion ψ_i decays to three particles via off-shell dark photon, and thus their lifetimes tend to be longer than our case in which the decay chain $N_1 \rightarrow \nu \chi, \chi \rightarrow ee$ proceeds via only two-body decays. Furthermore, the energy deposits from the χ decay will be larger than those from the decays of ψ_i because of the larger phase space. Therefore, the signals from our dark photon will more easily evade from the experimental limits searching for invisible dark photons. We expect that the dark photon of $\mathcal{O}(0.1 - 1)$ GeV in our case will not be excluded by the current data. The simulation as done in Ref. [17] is beyond the scope of this work, but the simulation would confirm that the semi-visible dark photon responsible for the lepton magnetic moments would not be excluded by the experiments.

6.3.2 The light vector-like neutrino and $U(1)'$ scalar

In the realization of the semi-visible dark photon, the vector-like neutrino N_1 and the $U(1)'$ scalar χ should also be $\mathcal{O}(0.1 \text{ GeV})$. The light vector-like neutrino N_1 mixes with the SM neutrinos through the mixing induced by v_Φ and v_H . Using the results in Appendix C.1, the mixing between the light vector-like neutrino and the electron

neutrino is approximately given by

$$[h_L]_{eN_1} \sim \frac{\lambda_L \lambda_e'^2 v_\Phi v_H^2}{2m_L m_E^2} \sim 4 \times 10^{-6} \times \lambda_e'^2 \left(\frac{\lambda_L}{0.3} \right) \left(\frac{v_\Phi}{1 \text{ GeV}} \right) \left(\frac{500 \text{ GeV}}{m_L} \right) \left(\frac{1500 \text{ GeV}}{m_E} \right)^2, \quad (6.3.5)$$

where h_L is defined in Eq. (6.1.15), and thus this mixing is $\mathcal{O}(10^{-6})$ for our model. This is safely below the current experimental limits on the active-sterile mixing for $m_{N_1} \sim \mathcal{O}(0.1 \text{ GeV})$, see Fig. 6 in Ref. [85].

In our model, the light scalar χ of mass $\sim \mathcal{O}(0.1 \text{ GeV})$ is coupled to e^+e^- with a coupling strength estimated to be $2\eta_e \sim \mathcal{O}(10^{-7})$ from Eq. (6.2.8). Such a light scalar is constrained by the collider experimental limits searching for $e^+e^- \rightarrow \gamma\chi(\rightarrow e^+e^-)$ at BaBar [73, 226], KLOE [41], Belle-II projection [18, 38, 72] and the electron beam dump experiments [72, 234]. Relevant to the light scalar mass range under consideration, these experiments impose an upper bound on its coupling with an e^+e^- pair, $Y_e^\chi \lesssim 10^{-3}$. The limit of $Y_e^\chi \lesssim 10^{-3}$ is obtained for $m_\chi \gtrsim 20 \text{ MeV}$ from BaBar [226] and Belle-II [18, 38, 72]. The beam dump experiments [83, 132, 275] have sensitivities for $m_\chi \sim 1-200 \text{ MeV}$ with $Y_e^\chi \sim 10^{-2}-10^{-6}$, and no limits for heavier masses [234]. Therefore, our values are comfortably below this upper bound.

6.3.3 Vector-like lepton search at the LHC

We briefly discuss the LHC limits for the charged vector-like lepton E_1 , which is expected to be light particularly to explain the W -boson mass shift. The vector-like leptons might be excluded by the LHC limits. For the doublet-like leptons, the mass below 800 GeV is excluded if it decays to the SM particles [285, 301]. In our model, however, the vector-like lepton E_1 decays to WN_1 , $A'e$ and/or χe , as discussed in Refs. [206]. The branching fractions of these decay modes of our BPs are shown in Table 6.2. For the BPs, the dominant decay mode $E_1 \rightarrow WN_1$, followed by $N_1 \rightarrow \chi\nu \rightarrow ee\nu$, has at least two electrons in the final states. This case might be

covered by the same search studied in Ref. [206], but there is no study for searching for the cascade decay. Thus, we can not exclude this possibility. In addition, due to the many-body decay cascade, the phase space of the decay $E_1 \rightarrow WN_1$ is small and thus the many leptons in the final state are relatively soft. The sub-dominant decay modes $E_1 \rightarrow \chi e \rightarrow eee$ and $E_1 \rightarrow A'e \rightarrow eee$ have three electrons in the final state. These signals are similar to those from $E_1 \rightarrow Z'\mu \rightarrow \mu\mu\mu$, studied in Ref. [206], which excludes the vector-like lepton masses up to 500 GeV for $\text{Br}(E_1 \rightarrow eee) \sim 10\%$. For our BP-A, $\text{Br}(E_1 \rightarrow eee) \simeq 12\%$ and $m_{E_1} \simeq 1.5$ TeV, which is safely above this limit. On the other hand, the limit for branching fractions less than 10% are not visible, therefore the BP-B and BP-C whose $\text{Br}(E_1 \rightarrow eee) \simeq 5\%$, may be allowed. We also note that this will not be the case if χ dominantly decays to quarks³.

6.4 Conclusions

In this work, we proposed a scenario in which both anomalies in electron and muon anomalous magnetic moments are explained without extending the model proposed in Refs. [207, 208]. The discrepancy for electron, Δa_e , is explained by the 1-loop diagrams involving the dark photon and the vector-like leptons, whereas that for muon, Δa_μ is explained by the 1-loop diagrams induced by the gauge kinetic mixing with photons. Since the latter effect is always positive, we can not consider the opposite case in which $\Delta a_e < 0$ is explained by the gauge kinetic mixing. Since two discrepancies are explained by the different origins, there is no lepton flavor violations induced by the new particles in the model. We also showed that the W -boson mass measured at the CDF II can be explained if the vector-like lepton is below 300 GeV. Such a light vector-like lepton would be excluded by the high-multiplicity lepton channels at the

³If χ couples with quarks, the precision measurements of kaon decays will constrain the χ as discussed in Ref. [232], depending on the flavor structure of the quark couplings. Also, the relation of the lifetime to Δa_e , in Eq. (6.3.3) is changed by the mixing with quarks. A concrete study is beyond the scope of this paper.

LHC, depending on its decay modes, as discussed in Sec. 6.3.3. If the light vector-like lepton is not excluded by the LHC, this model can address the three anomalies simultaneously.

The dark photon explanation of Δa_μ is severely constrained by the experiments in the simplest setups. In our model, however, the dark photon can decay to a pair of vector-like neutrinos, $A' \rightarrow N_1 N_1$, followed by the decays $N_1 \rightarrow \chi (\rightarrow ee) \nu$, so that the dark photon becomes semi-visible which is not excluded by the dark photon searches. We also find that the lifetime of the χ field is directly related to the new physics contribution to Δa_e , and thus our resolution to avoid the invisible dark photons search works only if $|\Delta a_e| \gtrsim 10^{-14}$. This scenario would be probed by the direct searches for the semi-visible dark photons, or pair productions of the charged vector-like leptons at the LHC, which are subjects of our future works. Our model provides an explicit example of the semi-visible dark photon relying only on two-body decays which are qualitatively different from those considered in the literature.

7

Conclusion

In this thesis, we have analyzed some phenomenological aspects of some well motivated nonminimal extensions of the SM. These extensions includes both SUSY and non-SUSY models.

In summary, we have shown that a theoretically well-motivated realization of supersymmetry, the so-called BLSSM, may yield detectable signals of a heavy neutral CP-even Higgs boson at the LHC, both during Run 3 and the HL-LHC phase. These emerge from the lightest (neutral) Higgs state of this scenario with prevalent $B - L$ composition, h' , while the lightest (neutral) Higgs state with predominant MSSM nature is identified with the discovered one, h (with $m_h = 125$ GeV). The subprocesses pursued to this effect, assuming a BP with an illustrative mass $m_{h'} = 400$ GeV, have been $gg \rightarrow h' \rightarrow W^+W^- \rightarrow 2\ell + \cancel{E}_T$, $gg \rightarrow h' \rightarrow ZZ \rightarrow 4\ell$ and $gg \rightarrow h' \rightarrow hh \rightarrow b\bar{b}\gamma\gamma$. The first one would be accessible during the early stages of Run 3 and the study of mass distributions would allow one to extract an indication of the h' mass. This information can then be used to optimize the selection of the second signal, which would reveal a clear pick centered around $m_{h'}$ by the end of Run 3. With the latter information available, one would then be able to establish the third signal at the HL-LHC. All this will therefore enable one to fully characterize the h' state,

not only through its mass, but also in terms of its couplings, as the W^+W^- , ZZ and hh decays are the dominant ones in the BLSSM while those to $t\bar{t}$ and $b\bar{b}$ pairs may be accessible at production level through the ggF channel. This finally opens up the possibility of eventually separating the BLSSM hypothesis from alternative ones also based on supersymmetry, since – thanks to the peculiar feature of (gauge) kinetic mixing appearing in the BLSSM (which incorporates an additional $U(1)_{B-L}$ group beyond the SM gauge symmetries) – competing signals stemming from, e.g., the MSSM would have rather different mass and coupling patterns.

We have come to these conclusions by performing a full MC analysis in presence of ME, PS, fragmentation/hadronization effects as well as detector modeling and upon devising dedicated cut-and-count cut-flows for each signature pursued. We are therefore confident that ATLAS and CMS would have sensitivity to this specific non-minimal realization of supersymmetry and advocate dedicate searches for the aforementioned signals.

We have proposed a simplified LR model, where $SU(2)_R \times U(1)_{B-L}$ symmetry is broken spontaneously by the VEV of a scalar doublet χ_R around TeV scale, and the electroweak symmetry $SU(2)_L \times U(1)_Y$ is broken by the VEVs of two Higgs doublets merged from a single bidoublet ϕ . We adopted IS mechanism to generate light neutrino masses. We also analyzed the Higgs sector in detail, in particular the three neutral CP -even Higgs bosons. We showed that the lightest of these particle can be assigned to the SM-like Higgs boson, with mass equals to 125 GeV. The next lightest Higgs boson, h' , which is stemmed from the bidoublet neutral component is of order a few hundred GeVs. We studied the LHC potential discovery for h' in this class of models. We performed analysis for searches for h' by looking for resonant peaks in the following two processes: $h' \rightarrow hh \rightarrow b\bar{b}\gamma\gamma$ and $h' \rightarrow ZZ \rightarrow 4\ell$ ($\ell = e, \mu$). We considered three benchmark points, with $m_{h'} = 250$ GeV, 400 GeV, and 600 GeV, at $\sqrt{s} = 14$ TeV and $L_{\text{int}} = 300 \text{ fb}^{-1}$ and $L_{\text{int}} = 3000 \text{ fb}^{-1}$. We emphasized that h'

can be probed with good statistical significances in di-Higgs channel, with $2\gamma + 2b$ -jets final states. While the channel of Z -pair production and decays to 4ℓ is much less significant, it may be observed only at very high $L_{\text{int}} = 3000 \text{ fb}^{-1}$ and for light h' with mass less than 300 GeV.

We have analyzed the muon anomalous magnetic moment a_μ in a minimal left-right symmetric model with neutrino masses inverse seesaw mechanism. We found that a reasonable region of the parameter space of the model is consistent with the observed muon $g - 2$ anomaly. We emphasized that, in this type of models, only the H^\pm loop explains a_μ significantly, in agreement with the $\text{BR}(\mu \rightarrow e\gamma)$, μ - e conversion and the electron $g_e - 2$ anomaly measured limits.

In this work, we proposed a scenario in which both anomalies in electron and muon anomalous magnetic moments are explained without extending the model proposed in Refs. [207,208]. The discrepancy for electron, Δa_e , is explained by the 1-loop diagrams involving the dark photon and the vector-like leptons, whereas that for muon, Δa_μ is explained by the 1-loop diagrams induced by the gauge kinetic mixing with photons. Since the latter effect is always positive, we can not consider the opposite case in which $\Delta a_e < 0$ is explained by the gauge kinetic mixing. Since two discrepancies are explained by the different origins, there is no lepton flavor violations induced by the new particles in the model. We also showed that the W -boson mass measured at the CDF II can be explained if the vector-like lepton is below 300 GeV. Such a light vector-like lepton would be excluded by the high-multiplicity lepton channels at the LHC, depending on its decay modes, as discussed in Sec. 6.3.3. If the light vector-like lepton is not excluded by the LHC, this model can address the three anomalies simultaneously.

The dark photon explanation of Δa_μ is severely constrained by the experiments in the simplest setups. In our model, however, the dark photon can decay to a pair of vector-like neutrinos, $A' \rightarrow N_1 N_1$, followed by the decays $N_1 \rightarrow \chi(\rightarrow ee)\nu$, so that the

dark photon becomes semi-visible which is not excluded by the dark photon searches. We also find that the lifetime of the χ field is directly related to the new physics contribution to Δa_e , and thus our resolution to avoid the invisible dark photons search works only if $|\Delta a_e| \gtrsim 10^{-14}$. This scenario would be probed by the direct searches for the semi-visible dark photons, or pair productions of the charged vector-like leptons at the LHC, which are subjects of our future works. Our model provides an explicit example of the semi-visible dark photon relying only on two-body decays which are qualitatively different from those considered in the literature.

A

LRIS Appendix

A.0.1 Tadpole Equations and Potential Minimization

The minimum of the scalar potential (5.1.1) is

$$\begin{aligned} \langle V \rangle = V(\langle \phi \rangle, \langle \chi_R \rangle) = & \frac{1}{4} \left[\lambda_1(k_1^4 + k_2^4) + 4\lambda_4 k_1 k_2 (k_1^2 + k_2^2) + 2(\lambda_1 + 2\lambda_{23}) k_1^2 k_2^2 \right. \\ & + 2\mu_1(k_1^2 + k_2^2) + (\alpha_{13} k_1^2 + \alpha_{12} k_2^2) v_R^2 \\ & \left. + 2k_1 k_2 (4\mu_2 + \alpha_4 v_R^2) + 2\mu_3 v_R^2 + \rho_1 v_R^4 \right], \end{aligned} \quad (\text{A.0.1})$$

where the VEVs satisfy the following tadpole equations

$$\begin{aligned} \frac{\partial \langle V \rangle}{\partial k_1} = & \lambda_1 k_1^3 + \lambda_4 k_2 (3k_1^2 + k_2^2) + k_1 \{ k_2^2 (\lambda_1 + 2\lambda_{23}) + \mu_1 + \frac{1}{2} \alpha_{13} v_R^2 \} \\ & + 2k_2 \mu_2 + \frac{1}{2} \alpha_4 k_2 v_R^2 = 0, \end{aligned} \quad (\text{A.0.2})$$

$$\begin{aligned} \frac{\partial \langle V \rangle}{\partial k_2} &= \lambda_1 k_2^3 + \lambda_4 k_1 (k_1^2 + 3k_2^2) + k_2 \{ k_1^2 (\lambda_1 + 2\lambda_{23}) + \mu_1 + \frac{1}{2} \alpha_{12} v_R^2 \} \\ &\quad + 2k_1 \mu_2 + \frac{1}{2} \alpha_4 k_1 v_R^2 = 0, \end{aligned} \quad (\text{A.0.3})$$

$$\frac{\partial \langle V \rangle}{\partial v_R} = \frac{1}{2} v_R \{ \alpha_{13} k_1^2 + 2\alpha_4 k_1 k_2 + \alpha_{12} k_2^2 + 2(\mu_3 + \rho_1 v_R^2) \} = 0. \quad (\text{A.0.4})$$

We solve them for μ_1 , μ_2 and μ_3 as follows:

$$\mu_1 = -\lambda_1(k_1^2 + k_2^2) - 2\lambda_4 k_1 k_2 - \frac{\alpha_{12} k_2^2 - \alpha_{13} k_1^2}{2(k_2^2 - k_1^2)} v_R^2, \quad (\text{A.0.5})$$

$$\mu_2 = -\frac{1}{2} \lambda_4 (k_1^2 + k_2^2) - \lambda_{23} k_1 k_2 - \frac{1}{4} (\alpha_4 + \frac{\alpha_{32} k_1 k_2}{k_2^2 - k_1^2}) v_R^2, \quad (\text{A.0.6})$$

$$\mu_3 = -\frac{1}{2} (\alpha_{13} k_1^2 + 2\alpha_4 k_1 k_2 + \alpha_{12} k_2^2 + 2\rho_1 v_R^2). \quad (\text{A.0.7})$$

where we define $\alpha_{1i} = \alpha_1 + \alpha_i$, $i = 2, 3$, $\alpha_{32} = \alpha_3 - \alpha_2$ and $\lambda_{23} = 2\lambda_2 + \lambda_3$.

A.0.2 Copositivity Conditions of the Higgs Potential

To study the boundedness from below and hence, the stability, of the scalar potential (5.1.1) we use the copositivity theorems of [204, 267] and follow the procedure used in [55] to ensure that the following symmetric matrix of the quartic terms, which are dominant at higher values of the fields, is copositive:

$$\begin{pmatrix} \lambda_1 & \lambda_1 & \lambda_1 + 2\lambda_{23} & \lambda_1 & \frac{1}{2}\alpha_{13} & \frac{1}{2}\alpha_{12} \\ . & \lambda_1 & \lambda_1 & \lambda_1 + 2\lambda_3 & \frac{1}{2}\alpha_{12} & \frac{1}{2}\alpha_{13} \\ . & . & \lambda_1 & \lambda_1 & \frac{1}{2}\alpha_{12} & \frac{1}{2}\alpha_{13} \\ . & . & . & \lambda_1 & \frac{1}{2}\alpha_{13} & \frac{1}{2}\alpha_{12} \\ . & . & . & . & \rho_1 & \rho_1 \\ . & . & . & . & . & \rho_1 \end{pmatrix}. \quad (\text{A.0.8})$$

Copositivity of this matrix demands that $\lambda_1 > 0$, $\rho_1 > 0$, and either of the following cases

A.0.1. $\lambda_1 + 2\lambda_{23} > 0$, $\lambda_1 + 2\lambda_3 > 0$, $\alpha_{12} > 0$, $\alpha_{13} > 0$.

A.0.2. If $\lambda_1 + 2\lambda_{23} > 0$, $\lambda_1 + 2\lambda_3 < 0$, $\alpha_{12} > 0$, $\alpha_{13} > 0$, then $\lambda_3 < 0$ or $\lambda_1 + \lambda_3 > 0$ and $\lambda_2 > 0$.

A.0.3. If $\lambda_1 + 2\lambda_{23} < 0$, $\lambda_1 + 2\lambda_3 > 0$, $\alpha_{12} > 0$, $\alpha_{13} > 0$ then $\lambda_3 < 0$, $\lambda_2 < 0$ and $\lambda_1 + \lambda_{23} > 0$.

A.0.4. If $\lambda_1 + 2\lambda_{23} < 0$, $\lambda_1 + 2\lambda_3 < 0$, $\alpha_{12} > 0$, $\alpha_{13} > 0$, then $\lambda_3 < 0$.

A.0.5. If $\lambda_1 + 2\lambda_{23} > 0$, $\lambda_1 + 2\lambda_3 > 0$, $\alpha_{12} < 0$, $\alpha_{13} > 0$, then $\lambda_1\rho_1 > \frac{1}{4}\alpha_{13}^2$ and $\lambda_1\rho_1 > \frac{1}{2}(\alpha_{12} + \alpha_{13})^2$.

A.0.6. If $\lambda_1 + 2\lambda_{23} > 0$, $\lambda_1 + 2\lambda_3 > 0$, $\alpha_{12} > 0$, $\alpha_{13} < 0$, then $\lambda_1\rho_1 > \frac{1}{4}\alpha_{12}^2$ and $\lambda_1\rho_1 > \frac{1}{2}(\alpha_{12} + \alpha_{13})^2$.

A.0.7. If $\lambda_1 + 2\lambda_{23} > 0$, $\lambda_1 + 2\lambda_3 > 0$, $\alpha_{12} < 0$, $\alpha_{13} < 0$,
then $\lambda_1\rho_1 > \frac{1}{4}\alpha_{12}^2$ and $\lambda_1\rho_1 > \frac{1}{4}\alpha_{13}^2$ or $\lambda_1\rho_1 < \frac{1}{4}\alpha_{12}^2$ and $\lambda_1\rho_1 < \frac{1}{4}\alpha_{13}^2$.

A.0.8. If $\lambda_1 + 2\lambda_{23} < 0$, $\lambda_1 + 2\lambda_3 < 0$, $\alpha_{12} < 0$, $\alpha_{13} < 0$,
then $\lambda_3 < 0$ $\lambda_1\rho_1 > \frac{1}{4}\alpha_{12}^2$ and $\lambda_1\rho_1 > \frac{1}{4}\alpha_{13}^2$ or $\lambda_1\rho_1 < \frac{1}{4}\alpha_{12}^2$ and $\lambda_1\rho_1 < \frac{1}{4}\alpha_{13}^2$.

Finally, field redefinition could be done to make quartic terms in potential like $\phi_1^0\phi_2^0\phi_R^+\phi_R^-$ nonnegative definite again as in [55].

A.0.3 Neutral CP -even Higgs Rotations and Determinant

The explicit rotation coefficients of the CP -even Higgs mass matrix (5.1.2) are [52,278]

$$Z_{11}^H = \frac{f_{11}}{\sqrt{f_{11}^2 + f_{21}^2 + 1}}, \quad (\text{A.0.9})$$

$$Z_{12}^H = \frac{f_{21}}{\sqrt{f_{11}^2 + f_{21}^2 + 1}}, \quad (\text{A.0.10})$$

$$Z_{13}^H = \frac{1}{\sqrt{f_{11}^2 + f_{21}^2 + 1}}, \quad (\text{A.0.11})$$

$$Z_{21}^H = \frac{f_{12}(1 + f_{21}^2) - f_{11}(1 + f_{21}f_{22})}{\sqrt{(1 + f_{11}^2 + f_{21}^2)\{(f_{11} - f_{12})^2 + (f_{21} - f_{22})^2 + (f_{12}f_{21} - f_{11}f_{22})^2\}}}, \quad (\text{A.0.12})$$

$$Z_{22}^H = \frac{f_{22}(1 + f_{11}^2) - f_{21}(1 + f_{11}f_{12})}{\sqrt{(1 + f_{11}^2 + f_{21}^2)\{(f_{11} - f_{12})^2 + (f_{21} - f_{22})^2 + (f_{12}f_{21} - f_{11}f_{22})^2\}}}, \quad (\text{A.0.13})$$

$$Z_{23}^H = \frac{f_{11}(f_{11} - f_{12}) + f_{21}(f_{21} - f_{22})}{\sqrt{(1 + f_{11}^2 + f_{21}^2)\{(f_{11} - f_{12})^2 + (f_{21} - f_{22})^2 + (f_{12}f_{21} - f_{11}f_{22})^2\}}}, \quad (\text{A.0.14})$$

$$Z_{31}^H = \frac{(\text{sgn})(f_{22} - f_{21})}{\sqrt{(f_{11} - f_{12})^2 + (f_{21} - f_{22})^2 + (f_{12}f_{21} - f_{11}f_{22})^2}}, \quad (\text{A.0.15})$$

$$Z_{32}^H = \frac{(\text{sgn})(f_{11} - f_{12})}{\sqrt{(f_{11} - f_{12})^2 + (f_{21} - f_{22})^2 + (f_{12}f_{21} - f_{11}f_{22})^2}}, \quad (\text{A.0.16})$$

$$Z_{33}^H = \frac{(\text{sgn})(f_{12}f_{21} - f_{11}f_{22})}{\sqrt{(f_{11} - f_{12})^2 + (f_{21} - f_{22})^2 + (f_{12}f_{21} - f_{11}f_{22})^2}}, \quad (\text{A.0.17})$$

where the sign term is

$$\text{sgn} = \text{sign}\{f_{11}(f_{23} - f_{22}) + f_{12}(f_{21} - f_{23}) + f_{13}(f_{22} - f_{21})\}, \quad (\text{A.0.18})$$

and $f_{ij} = f_i(m_{H_j}^2)$, ($i = 1, 2$, $j = 1 \dots 3$) and the functions f_i 's are

$$f_1(x) = \frac{(m_{22} - x)(m_{33} - x) - m_{23}^2}{m_{12}m_{23} - m_{13}(m_{22} - x)}, \quad (\text{A.0.19})$$

$$f_2(x) = -\frac{m_{12}(m_{33} - x) - m_{13}m_{23}}{m_{12}m_{23} - m_{13}(m_{22} - x)}. \quad (\text{A.0.20})$$

The determinant of the CP -even Higgs mass matrix (5.1.2) is given by

$$\begin{aligned} D^h &= v^2 v_R^2 (-(\alpha_{12}c_\beta + \alpha_4 s_\beta)((\alpha_{12}c_\beta + \alpha_4 s_\beta)(v^2(c_{2\beta}(\lambda_{23} - \lambda_1) + 2\lambda_4 s_{2\beta}) \\ &\quad - \frac{1}{4}\alpha_{32}v_R^2 sc_{2\beta} + v^2(\lambda_1 + \lambda_{23}) - \frac{\alpha_{32}v_R^2}{4})) \\ &\quad - \frac{1}{4}(\alpha_{13}s_\beta + \alpha_4 c_\beta)(4v^2(s_{2\beta}(\lambda_1 + \lambda_{23}) + 2\lambda_4) + \alpha_{32}v_R^2 t_{2\beta})) \\ &\quad + (\alpha_{13}s_\beta + \alpha_4 c_\beta)((\alpha_{12}c_\beta + \alpha_4 s_\beta)(v^2 s_{2\beta}(\lambda_1 + \lambda_{23}) \\ &\quad + \frac{1}{4}\alpha_{32}v_R^2 t_{2\beta} + 2\lambda_4 v^2) - (\alpha_{13}s_\beta + \alpha_4 c_\beta)(v^2(c_{2\beta}(\lambda_1 - \lambda_{23}) + 2\lambda_4 s_{2\beta}) \\ &\quad - \frac{1}{4}\alpha_{32}v_R^2 sc_{2\beta} + v^2(\lambda_1 + \lambda_{23}) + \frac{\alpha_{32}v_R^2}{4})) \\ &\quad + \rho_1 sc_{2\beta}(6v^2 c_{2\beta}(\lambda_1 \lambda_{23} - \lambda_4^2) + 2v^2 c_{6\beta}(\lambda_1 \lambda_{23} - \lambda_4^2) + \alpha_{32}\lambda_{23}v_R^2 c_{4\beta} \\ &\quad - 4\alpha_{32}\lambda_4 v_R^2 s_{2\beta} - \alpha_{32}v_R^2(2\lambda_1 + \lambda_{23}))). \end{aligned} \quad (\text{A.0.21})$$

B

The muon anomalous magnetic moment a_μ in QED and the EW Theory

In quantum field theories of particles, real particles are like birds and virtual particles are more like fish in the vacuum sea. Like a fish, the mean lifetime of a virtual particle when it emerges from vacuum is much shorter than the natural mean lifetime of its corresponding real particle. It is the uncertainty principle which allows such blobs in vacuum. Virtual particles interact with each other and with real particles. They also mediate interactions among real particles. Their intermediate contributions may strengthen or weaken some direct interactions among real particles or even enable kinds of indirect interactions among them. Kinematics of virtual particles interactions

are only ruled by the sacred conservation laws of energy, momentum and internal charges, not by intrinsic properties of their corresponding real ones.

When a spinning charged particle is placed in a magnetic field, its spin precesses about the axis of the magnetic field. In quantum mechanics, this precession speed is quantized by $g \frac{e\hbar}{2m}$. The g -factor is measured by both Stern-Gerlach and Einstein-de Haas experiments to be $g = 2$. Dirac equation predicts the exact value of g as a product of the relativistic symmetry of the spacetime. Later high levels precision of experiments showed that g is a bit larger than 2. Feynman, Shwinger and Tomanaga promoted the classical field theory of electrodynamics into QED and showed that a major part of the anomalous excess in g is due to the interaction with the unconstrained magnetic field of the QED vacuum mediated by virtual photons and muons.

In this manuscript, we are going to check how QED contributions coming from virtual photons and muons strengthen the magnetic moment of muons giving the main part of the anomalous corrections to its g -factor of $a_\mu^{\text{QED}} = \frac{g-2}{2} = \frac{\alpha}{2\pi} \sim \mathcal{O}(10^{-3})$ on the one-loop level. Moreover, extra contributions from virtual neutrinos, W, Z and Higgs bosons give corrections of order $a_\mu^{\text{EW}} \sim \mathcal{O}(10^{-9})$ in the electroweak theory on the one-loop level.

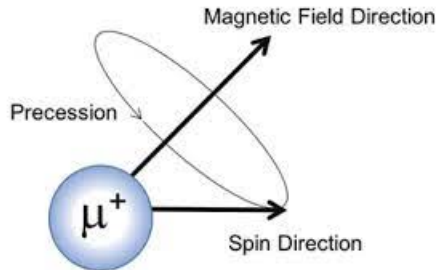


Figure B.1: spin precession about a magnetic field.

B.1 Algebra and Useful Relations

$$\text{B.1.1. } p = q_2 - q_1, \quad q = q_2 + q_1, \quad u_1 = u(q_1), \quad \bar{u}_2 = \bar{u}(q_2), \quad q_1^2 = m_1^2, \quad q_2^2 = m_2^2$$

$$\text{B.1.2. } \{\gamma^\mu, \gamma^\nu\} = 2g^{\mu\nu}, \quad \gamma^\mu \gamma_\mu = 4$$

$$\text{B.1.3. } \{\gamma^\mu, \gamma_5\} = 0, \quad \gamma_5^2 = 1$$

$$\text{B.1.4. } P_L = \frac{1}{2}(1 - \gamma_5), \quad P_R = \frac{1}{2}(1 + \gamma_5), \quad P_L^2 = P_L, \quad P_R^2 = P_R, \quad P_L P_R = P_R P_L = 0$$

$$\text{B.1.5. } \sigma^{\mu\nu} = \frac{i}{2}[\gamma^\mu, \gamma^\nu]$$

B.1.6. Notation:

$$\begin{aligned} \Gamma^\mu &= \bar{u}_2 \gamma^\mu u_1, & \Gamma_5^\mu &= \bar{u}_2 \gamma^\mu \gamma_5 u_1, & \Gamma_{L,R}^\mu &= \bar{u}_2 \gamma^\mu P_{L,R} u_1 = \frac{1}{2}(\Gamma^\mu \mp \Gamma_5^\mu), \\ p_\nu \Sigma^{\mu\nu} &= \bar{u}_2 p_\nu \sigma^{\mu\nu} u_1, & p_\nu \Sigma_5^{\mu\nu} &= \bar{u}_2 p_\nu \sigma^{\mu\nu} \gamma_5 u_1, & P^\mu &= \bar{u}_2 p^\mu u_1, & P_5^\mu &= \bar{u}_2 p^\mu \gamma_5 u_1, \\ Q_1^\mu &= \bar{u}_2 q_1^\mu u_1, & Q_{1,5}^\mu &= \bar{u}_2 q_1^\mu \gamma_5 u_1, & Q_2^\mu &= \bar{u}_2 q_2^\mu u_1, & Q_{2,5}^\mu &= \bar{u}_2 q_2^\mu \gamma_5 u_1 \end{aligned}$$

$$\text{B.1.7. } \gamma^\mu \gamma^\nu = \frac{1}{2}(\{\gamma^\mu, \gamma^\nu\} + [\gamma^\mu, \gamma^\nu]) = \frac{1}{2}(2g^{\mu\nu} - 2i\sigma^{\mu\nu}) = g^{\mu\nu} - i\sigma^{\mu\nu}$$

$$\text{B.1.8. } \gamma^\nu \gamma^\mu \gamma_\nu = -2\gamma^\mu, \quad \gamma^\nu \gamma_5 \gamma_\nu = 4\gamma_5$$

$$\text{B.1.9. } \gamma^\nu \gamma^\rho \gamma^\mu \gamma_\nu = 4g^{\rho\mu}$$

$$\text{B.1.10. } \gamma^\nu \gamma^\rho \gamma^\mu \gamma^\sigma \gamma_\nu = -2\gamma^\sigma \gamma^\mu \gamma^\rho$$

$$\text{B.1.11. } \mathcal{A}\gamma^\mu = A_\nu \gamma^\nu \gamma^\mu = A_\nu (2g^{\mu\nu} - \gamma^\mu \gamma^\nu) = 2A^\mu - \gamma^\mu \mathcal{A}$$

$$\text{B.1.12. } \mathcal{A}\mathcal{B} = A_\mu B_\nu \gamma^\mu \gamma^\nu = A_\mu B_\nu (2g^{\mu\nu} - \gamma^\mu \gamma^\nu) = 2A \cdot B - \mathcal{B}\mathcal{A}$$

$$\text{B.1.13. } \mathcal{A}^2 = 2A^2 - \mathcal{A}^2 \rightarrow \mathcal{A}^2 = A^2$$

$$\text{B.1.14. } (\not{q}_1 - m_1)u_1 = \bar{u}_2(\not{q}_2 - m_2) = 0$$

$$\text{B.1.15. } (\not{q}_1 - m_1)P_L u_1 = (P_R \not{q}_1 - m_1 P_L)u_1 = m_1(P_R - P_L)u_1 = m_1 \gamma_5 u_1,$$

$$\bar{u}_2 P_L (\not{q}_2 - m_2) = \bar{u}_2(\not{q}_2 P_R - m_2 P_L) = m_2 \bar{u}_2(P_R - P_L) = m_2 \bar{u}_2 \gamma_5$$

B.1.16. $\not{q}_1 u_1 = m_1 u_1 \rightarrow \gamma^\mu \gamma^\nu q_1^\nu u_1 = m_1 \gamma^\mu u_1 \rightarrow (g^{\mu\nu} - i\sigma^{\mu\nu}) q_{1\nu} u_1 = m_1 \gamma^\mu u_1.$

i.e., $q_1^\mu u_1 = (m_1 \gamma^\mu + i q_{1\nu} \sigma^{\mu\nu}) u_1$ and

$$\bar{u}_2 q_1^\mu u_1 = \bar{u}_2 (m_1 \gamma^\mu + i q_{1\nu} \sigma^{\mu\nu}) u_1$$

$$\bar{u}_2 q_1^\mu \gamma_5 u_1 = \bar{u}_2 (-m_1 \gamma^\mu + i q_{1\nu} \sigma^{\mu\nu}) \gamma_5 u_1$$

B.1.17. Similarly, $\bar{u}_2 q_2^\mu = \bar{u}_2 (m_2 \gamma^\mu - i q_{2\nu} \sigma^{\mu\nu})$ or

$$\bar{u}_2 q_2^\mu u_1 = \bar{u}_2 (m_2 \gamma^\mu - i q_{2\nu} \sigma^{\mu\nu}) u_1$$

$$\bar{u}_2 q_2^\mu \gamma_5 u_1 = \bar{u}_2 (m_2 \gamma^\mu - i q_{2\nu} \sigma^{\mu\nu}) \gamma_5 u_1$$

B.1.18. Gordon identity for the total momentum $q = q_1 + q_2$ (by summing the corresponding identities in above two items)

$$\bar{u}_2 (q_2^\mu + q_1^\mu) u_1 = (m_1 + m_2) \bar{u}_2 \gamma^\mu u_1 - i \bar{u}_2 p_\nu \sigma^{\mu\nu} u_1 \quad (\text{B.1.1})$$

$$\bar{u}_2 (q_2^\mu + q_1^\mu) \gamma_5 u_1 = (m_2 - m_1) \bar{u}_2 \gamma^\mu \gamma_5 u_1 - i \bar{u}_2 p_\nu \sigma^{\mu\nu} \gamma_5 u_1 \quad (\text{B.1.2})$$

B.1.19. Using the above Gordon identities, we can deduce the following Gordon identities for the ingoing and outgoing momenta q_1, q_2

$$\bar{u}_2 q_1^\mu u_1 = \frac{1}{2} \bar{u}_2 \{(q_2^\mu + q_1^\mu - p^\mu) u_1 = \frac{1}{2} (m_1 + m_2) \bar{u}_2 \gamma^\mu u_1 - \frac{i}{2} \bar{u}_2 p_\nu \sigma^{\mu\nu} u_1 - \frac{1}{2} \bar{u}_2 p^\mu u_1 \quad (\text{B.1.3})$$

$$\bar{u}_2 q_2^\mu u_1 = \frac{1}{2} \bar{u}_2 \{(q_2^\mu + q_1^\mu + p^\mu) u_1 = \frac{1}{2} (m_1 + m_2) \bar{u}_2 \gamma^\mu u_1 - \frac{i}{2} \bar{u}_2 p_\nu \sigma^{\mu\nu} u_1 + \frac{1}{2} \bar{u}_2 p^\mu u_1 \quad (\text{B.1.4})$$

$$\bar{u}_2 q_1^\mu \gamma_5 u_1 = \frac{1}{2} (m_2 - m_1) \bar{u}_2 \gamma^\mu \gamma_5 u_1 - \frac{i}{2} \bar{u}_2 p_\nu \sigma^{\mu\nu} \gamma_5 u_1 - \frac{1}{2} \bar{u}_2 p^\mu \gamma_5 u_1 \quad (\text{B.1.5})$$

$$\bar{u}_2 q_2^\mu \gamma_5 u_1 = \frac{1}{2} (m_2 - m_1) \bar{u}_2 \gamma^\mu \gamma_5 u_1 - \frac{i}{2} \bar{u}_2 p_\nu \sigma^{\mu\nu} \gamma_5 u_1 + \frac{1}{2} \bar{u}_2 p^\mu \gamma_5 u_1 \quad (\text{B.1.6})$$

B.1.20. $\bar{u}_2 \not{p} u_1 = \bar{u}_2 (\not{q}_2 - \not{q}_1) u_1 = (m_2 - m_1) \bar{u}_2 u_1$

B.1.21. $\bar{u}_2 \not{p} \gamma_5 u_1 = \bar{u}_2 (\not{q}_2 - \not{q}_1) \gamma_5 u_1 = \bar{u}_2 (\not{q}_2 \gamma_5 + \gamma_5 \not{q}_1) u_1 = (m_2 + m_1) \bar{u}_2 \gamma_5 u_1$

$$\text{B.1.22. } p^2 = (q_2 - q_1)^2 = q_1^2 + q_2^2 - 2q_1 \cdot q_2 = m_1^2 + m_2^2 - 2q_1 \cdot q_2$$

$$\text{B.1.23. } 2q_1 \cdot q_2 = m_1^2 + m_2^2 - p^2$$

$$\text{B.1.24. } p \cdot q_1 = (q_2 - q_1) \cdot q_1 = q_2 \cdot q_1 - q_1^2 = \frac{1}{2}(m_2^2 - m_1^2) - \frac{1}{2}p^2$$

$$\text{B.1.25. } p \cdot q_2 = m_2^2 - q_1 \cdot q_2 = \frac{1}{2}(m_2^2 - m_1^2) + \frac{1}{2}p^2$$

$$\text{B.1.26. } p \cdot (q_2 + q_1) = q_2^2 - q_1^2 = m_2^2 - m_1^2$$

$$\text{B.1.27. } \bar{u}_2 \not{p} \gamma^\mu \not{p} u_1 = \bar{u}_2 (2p^\mu - \gamma^\mu \not{p}) \not{p} u_1 = 2(m_2 - m_1) \bar{u}_2 p^\mu u_1 - p^2 \bar{u}_2 \gamma^\mu u_1$$

$$\text{B.1.28. } \bar{u}_2 \not{q}_1 \gamma^\mu \not{q}_1 u_1 = m_1 \bar{u}_2 (2q_1^\mu - \gamma^\mu \not{q}_1) u_1 = 2m_1 \bar{u}_2 q_1^\mu u_1 - m_1^2 \bar{u}_2 \gamma^\mu u_1 = m_1 m_2 \bar{u}_2 \gamma^\mu u_1 - im_1 \bar{u}_2 p_\nu \sigma^{\mu\nu} u_1 - m_1 \bar{u}_2 p^\mu u_1$$

$$\text{B.1.29. } \bar{u}_2 \not{q}_2 \gamma^\mu \not{q}_2 u_1 = m_2 \bar{u}_2 (2q_2^\mu - \not{q}_2 \gamma^\mu) u_1 = 2m_2 \bar{u}_2 q_2^\mu u_1 - m_2^2 \bar{u}_2 \gamma^\mu u_1 = m_1 m_2 \bar{u}_2 \gamma^\mu u_1 - im_2 \bar{u}_2 p_\nu \sigma^{\mu\nu} u_1 + m_2 \bar{u}_2 p^\mu u_1$$

$$\text{B.1.30. } \bar{u}_2 \not{q}_2 \gamma^\mu \not{q}_1 u_1 = m_1 m_2 \bar{u}_2 \gamma^\mu u_1$$

$$\text{B.1.31. } \bar{u}_2 \not{p} \gamma^\mu \not{q}_1 u_1 = m_1 \bar{u}_2 (\not{q}_2 \gamma^\mu - \not{q}_1 \gamma^\mu) u_1 = m_1(m_1 + m_2) \bar{u}_2 \gamma^\mu u_1 - 2m_1 \bar{u}_2 q_1^\mu u_1 = im_1 \bar{u}_2 p_\nu \sigma^{\mu\nu} u_1 + m_1 \bar{u}_2 p^\mu u_1$$

B.1.32. Also, and using Gordon identity,

$$\begin{aligned} \bar{u}_2 \not{q}_1 \gamma^\mu \not{q}_2 u_1 &= \bar{u}_2 (2q_1^\mu - \gamma^\mu \not{q}_1) \not{q}_2 u_1 = 2m_2 \bar{u}_2 q_1^\mu u_1 - \bar{u}_2 \gamma^\mu (2q_1 \cdot q_2 - \not{q}_2 \not{q}_1) u_1 \\ &= 2m_2 \bar{u}_2 q_1^\mu u_1 - (m_1^2 + m_2^2 - p^2) \bar{u}_2 \gamma^\mu u_1 + m_1 \bar{u}_2 (2q_2^\mu - \not{q}_2 \gamma^\mu) u_1 \\ &= 2\bar{u}_2 (m_2 q_1^\mu + m_1 q_2^\mu) u_1 - (m_1^2 + m_2^2 + m_1 m_2 - p^2) \bar{u}_2 \gamma^\mu u_1 \\ &= (3m_1 m_2 - m_1^2 - m_2^2 + p^2) \bar{u}_2 \gamma^\mu u_1 - 2i \bar{u}_2 (m_1 q_{2\nu} - m_2 q_{1\nu}) \sigma^{\mu\nu} u_1 \end{aligned} \tag{B.1.7}$$

$$\begin{aligned} \bar{u}_2 \not{q}_1 \gamma^\mu \not{q}_2 u_1 &= \bar{u}_2 (2q_1^\mu - \gamma^\mu \not{q}_1) \not{q}_2 u_1 \\ &= 2m \bar{u}_2 (q_1^\mu + q_2^\mu) u_1 - (3m^2 - p^2) \bar{u}_2 \gamma^\mu u_1 \\ &= (m^2 + p^2) \bar{u}_2 \gamma^\mu u_1 - 2im \bar{u}_2 p_\nu \sigma^{\mu\nu} u_1 \end{aligned} \tag{B.1.8}$$

B.1.33. Finally, and using Gordon identity,

$$\begin{aligned}\bar{u}_2 \not{q}_1 \gamma^\mu \not{p} u_1 &= \bar{u}_2 (\not{q}_1 \gamma^\mu \not{q}_2 - \not{q}_1 \gamma^\mu \not{q}_1) u_1 \\ &= (2m^2 + p^2) \bar{u}_2 \gamma^\mu u_1 - 2im \bar{u}_2 p_\nu \sigma^{\mu\nu} u_1 - 2m \bar{u}_2 q_1^\mu u_1 \\ &= p^2 \bar{u}_2 \gamma^\mu u_1 - im \bar{u}_2 p_\nu \sigma^{\mu\nu} u_1 + m \bar{u}_2 p^\mu u_1\end{aligned}\quad (\text{B.1.9})$$

$$\begin{aligned}\bar{u}_2 \not{q}_1 \gamma^\mu \not{p} u_1 &= \bar{u}_2 (\not{q}_1 \gamma^\mu \not{q}_2 - \not{q}_1 \gamma^\mu \not{q}_1) u_1 \\ &= (3m_1 m_2 - m_2^2 + p^2) \bar{u}_2 \gamma^\mu u_1 - 2i \bar{u}_2 (m_1 q_{2\nu} - m_2 q_{1\nu}) \sigma^{\mu\nu} u_1 - 2m_1 \bar{u}_2 q_1^\mu u_1\end{aligned}\quad (\text{B.1.10})$$

B.1.34. Ward identity in QED is the (abelian gauge) QFT version of the classical field theory Noether current conservation $\partial_\mu j^\mu = 0$ in momentum space. It holds for all orders of perturbation for the photon momentum p^μ and any QED amplitude \mathcal{M}

$$p_\mu \mathcal{M}^\mu = 0. \quad (\text{B.1.11})$$

B.1.35. Feynman parametrization combines the factors in the denominator

$$\frac{1}{ABC} = 2 \int_0^1 dz dy dx \delta(1 - x - y - z) \frac{1}{[xA + yB + zC]^3} \quad (\text{B.1.12})$$

B.2 Theory of Magnetic Moment

B.2.36. [82, 277] Nonrelativistic Hamiltonian of Schrödinger-Pauli equation

$$H - e\phi = \frac{(\vec{p} - e\vec{A})^2}{2m} - g \frac{e}{2m} \vec{B} \cdot \vec{S} = \frac{\vec{p}^2}{2m} - \frac{e}{2m} \vec{B} \cdot (\vec{L} + g\vec{S}) \quad (\text{B.2.1})$$

The g -factor is a free parameter for which both Stern-Gerlach and Einstein-de Haas experiments set $g = 2$. The spin operator $\vec{S} = \frac{\hbar}{2}\vec{\sigma}$.

B.2.37. The orbital and spin magnetic moments are

$$\vec{\mu}_\ell = \frac{e}{2m} \vec{L}, \quad \vec{\mu}_s = g \frac{e}{2m} \vec{S} = \frac{e}{m} \vec{S} = \frac{e\hbar}{2m} \vec{\sigma} \quad (\text{B.2.2})$$

B.2.38. [82, 277] (Relativistic) Dirac equation

$$(i\cancel{D} - m)\psi = (i\cancel{\partial} - e\cancel{A} - m)\psi = 0 \rightarrow (i\cancel{D} + m)(i\cancel{D} - m)\psi = 0 \rightarrow (\cancel{D}^2 + m^2)\psi = 0 \quad (\text{B.2.3})$$

But

$$\begin{aligned} \cancel{D}^2 &= \gamma^\mu \gamma^\nu D_\mu D_\nu = \frac{1}{4}(\{\gamma^\mu, \gamma^\nu\}\{D_\mu, D_\nu\} + [\gamma^\mu, \gamma^\nu][D_\mu, D_\nu]) \\ &= \frac{1}{4}(2g^{\mu\nu}\{D_\mu, D_\nu\} - 2i\sigma^{\mu\nu}ieF^{\mu\nu}) = D_\mu^2 + \frac{e}{2}F_{\mu\nu}\sigma^{\mu\nu}. \end{aligned} \quad (\text{B.2.4})$$

Thus

$$(\cancel{D}^2 + m^2)\psi = (D_\mu^2 + \frac{e}{2}F_{\mu\nu}\sigma^{\mu\nu} + m^2)\psi = 0, \quad (\text{B.2.5})$$

or explicitly

$$\frac{(H - eA_0)^2}{2m}\psi = \left\{ \frac{m}{2} + \frac{(\vec{p} - e\vec{A})^2}{2m} - 2\frac{e}{2m}\vec{B} \cdot \vec{S} \pm i\frac{e}{m}\vec{E} \cdot \vec{S} \right\}\psi \quad (\text{B.2.6})$$

B.2.39. The extra term $g\frac{e}{4}F_{\mu\nu}\sigma^{\mu\nu}$ is the source of $g\frac{e}{2m}\vec{B} \cdot \vec{S}$ with $g = 2$.

B.2.40. In QFT, thus, a general and relativistic way to extract corrections to g is to look for loops that have the same effect as an additional $F_{\mu\nu}\sigma^{\mu\nu}$ term.

B.2.41. A generally useful way to think about corrections to the way photons interact with spinors, such as corrections to g , is to consider off-shell S -matrix elements.

B.2.42. [277] QED Lagrangian

$$\mathcal{L}_{\text{QED}} = -\frac{1}{4}F_{\mu\nu}^2 + \bar{\psi}(i\cancel{D} - m)\psi = -\frac{1}{4}F_{\mu\nu}^2 + \bar{\psi}(i\cancel{\partial} - m)\psi - eA_\mu\bar{\psi}\gamma^\mu\psi \quad (\text{B.2.7})$$

B.2.43. The main vertex of QED is $-eA_\mu\bar{\psi}\gamma^\mu\psi$. The tree-level QED amplitude is

$$i\mathcal{M}_0^\mu = A_\mu p \sim \begin{cases} q_1 \\ q_2 \end{cases} = -ie \bar{u}(q_2)\gamma^\mu u(q_1) \quad (\text{B.2.8})$$

B.2.44. The term equivalent to $\bar{\psi}F_{\mu\nu}\sigma^{\mu\nu}\psi$ has the form $A_\mu \bar{u}(q_2)p_\nu\sigma^{\mu\nu}u(q_1)$ in momentum space, where $p = q_2 - q_1$ is the photon momentum.

B.2.45. Using Gordon identity, we see that the tree level amplitude decomposes in two terms. In the first interaction term the photon couples to the momentum of the field. The second term is spin dependent and gives the magnetic moment, and $g = \frac{4m}{e} \times$ the coefficient of $ip_\nu\bar{u}_2\sigma^{\mu\nu}u_1$.

$$\mathcal{M}_0^\mu = -e\left(\frac{q_1^\mu + q_2^\mu}{2m}\right) \bar{u}_2 u_1 - \frac{e}{2m} i\bar{u}_2 p_\nu \sigma^{\mu\nu} u_1 \quad (\text{B.2.9})$$

B.2.46. In general, a reducible four vector bilinear covariant can be expanded in the 16-dim Dirac irreducible basis of scalar (1 component), pseudoscalar (1 component), vector (4 components), axial vector (4 components), and the antisymmetric 2nd-rank tensor (6 components) whose matrix basis

$$\Gamma = \{\Gamma^S = 1, \Gamma^P = \gamma_5, \Gamma_\mu^V = \gamma_\mu, \Gamma_\mu^A = \gamma_5\gamma_\mu, \Gamma_{\mu\nu}^T = \sigma_{\mu\nu}\}. \quad (\text{B.2.10})$$

B.2.47. With the momentum basis either of the ingoing and outgoing momenta (q_1^μ, q_2^μ) or the total momentum and the momentum transfer (q^μ, p^μ), the amplitude can be written as follows (q_1^μ, q_2^μ or q^μ, p^μ) $\bar{u}_2 u_1$, (q_1^μ, q_2^μ or q^μ, p^μ) $\bar{u}_2 \gamma_5 u_1$, $\bar{u}_2 \gamma^\mu u_1$, $\bar{u}_2 \gamma_5 \gamma^\mu u_1$, $\bar{u}_2 p_\nu \sigma^{\mu\nu} u_1$, or explicitly

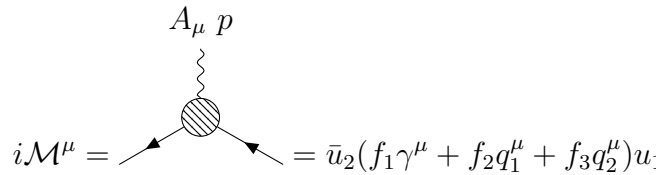
$$\mathcal{M}^\mu = \bar{u}_2 [q_1^\mu (C_1^S + C_1^P \gamma_5) + q_2^\mu (C_2^S + C_2^P \gamma_5) + (C^V + C^A \gamma_5) \gamma^\mu + C^T p_\nu \sigma^{\mu\nu}] u_1, \quad (\text{B.2.11})$$

or equivalently,

$$\mathcal{M}^\mu = \bar{u}_2 [q^\mu (C_+^S + C_+^P \gamma_5) + p^\mu (C_-^S + C_-^P \gamma_5) + (C^V + C^A \gamma_5) \gamma^\mu + C^T p_\nu \sigma^{\mu\nu}] u_1. \quad (\text{B.2.12})$$

B.2.48. In achiral theories which do not violate parity, like QED, only scalar, vectors and tensors are expanded to. Moreover, Ward identity in QED relates scalar, vector and tensor components and makes the independence of only two of them.

- B.2.49. It is better to work in the momentum basis of the total momentum and momentum transfer (q^μ, p^μ), and to use Gordon identity so that we can write all dimensionful parameters in terms of the mass parameter m and momentum transfer p^2 . This way, we intend eventually to bring all operators in the scalar, vectors and tensors forms $\bar{u}_2 p^\mu u_1$, $\bar{u}_2 \gamma^\mu u_1$, and $\bar{u}_2 p_\nu \sigma^{\mu\nu} u_1$.
- B.2.50. In the momentum basis (q_1^μ, q_2^μ), the general QED loop amplitude in the scalar-vector basis has the form



$$i\mathcal{M}^\mu = \text{---} \nearrow \text{---} = \bar{u}_2(f_1 \gamma^\mu + f_2 q_1^\mu + f_3 q_2^\mu)u_1 \quad (\text{B.2.13})$$

- B.2.51. [264,277] Using Ward identity $p_\mu \mathcal{M}^\mu = \bar{u}_2(f_1 p + f_2 p \cdot q_1 + f_3 p \cdot q_2)u_1 = \frac{1}{2}p^2 \bar{u}_2(f_3 - f_2)u_1 = 0$ sets $f_2 = f_3$. Also, using Gordon identity, which substitutes the resultant $\bar{u}_2(q_1^\mu + q_2^\mu)u_1$ in terms of $\bar{u}_2 \gamma^\mu u_1$ and $\bar{u}_2 p_\nu \sigma^{\mu\nu} u_1$, the general amplitude can be normalized to put in the form

$$\mathcal{M}^\mu = (-ie) \bar{u}_2[F_1(\frac{p^2}{m^2})\gamma^\mu + \frac{i\sigma^{\mu\nu}}{2m}p_\nu F_2(\frac{p^2}{m^2})]u_1. \quad (\text{B.2.14})$$

- B.2.52. At low energy, the g -factor and the anomalous magnetic moment read off

$$g = 2 + 2F_2(0), \quad a_\mu = \frac{g-2}{2} = F_2(0). \quad (\text{B.2.15})$$

B.3 a_μ in QED

- B.3.53. **Aim:** Obtaining the QED contribution to the anomalous magnetic moment of muon a_μ , and obtaining the renormalization constant δ_1 .
- B.3.54. For the two muons we use the above identities and relations with $m = m_1 = m_2$.

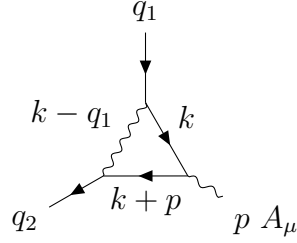


Figure B.2: One-loop QED contributions to a_μ .

B.3.55. Vertex $\bar{u}_2 \not{A} u_1$ loop amplitude

$$\begin{aligned} i\mathcal{M}^\mu &= (-ie)^3 \bar{u}_2 \int \frac{d^4k}{(2\pi)^4} \gamma^\nu \frac{i(\not{k} + \not{p} + m)}{(k+p)^2 - m^2 + i\epsilon} \gamma^\mu \frac{i(\not{k} + m)}{k^2 - m^2 + i\epsilon} \gamma^\alpha \frac{-ig_{\nu\alpha}}{(k-q_1)^2 + i\epsilon} u_1 \\ &= -e^3 \int \frac{d^4k}{(2\pi)^4} \frac{\bar{u}_2 \gamma^\nu (\not{k} + \not{p} + m) \gamma^\mu (\not{k} + m) \gamma_\nu u_1}{(k^2 - m^2 + i\epsilon)((k+p)^2 - m^2 + i\epsilon)((k-q_1)^2 + i\epsilon)} \end{aligned} \quad (\text{B.3.1})$$

B.3.56. Feynman parametrization combines the factors in the denominator

$$\frac{1}{ABC} = 2 \int_0^1 dz dy dx \delta(1-x-y-z) \frac{1}{[xA + yB + zC]^3}$$

B.3.57. The denominator ($x + y + z = 1$)

$$\begin{aligned} xA + yB + zC &= x(k^2 - m^2) + y((k+p)^2 - m^2) + z(k-q_1)^2 \\ &= k^2 + 2k \cdot (yp - zq_1) + yp^2 + zq_1^2 - (x+y)m^2 \\ &= (k + yp - zq_1)^2 - (yp - zq_1)^2 + yp^2 + zq_1^2 - (x+y)m^2 \\ &= (k + yp - zq_1)^2 + y(1-y)p^2 + 2yzp \cdot q_1 + [z(1-z) - (1-z)]m^2 \\ &= (k + yp - zq_1)^2 + y(1-y)p^2 - yzp^2 - (1-z)^2m^2 \\ &= (k + yp - zq_1)^2 + y(1-y-z)p^2 - (1-z)^2m^2 \\ &= (k + yp - zq_1)^2 + xyp^2 - (1-z)^2m^2 \\ &= (k + yp - zq_1)^2 - \Delta(x, y, z; p^2) \end{aligned} \quad (\text{B.3.2})$$

B.3.58. $\Delta(x, y, z; p^2) \equiv \Delta(p^2) \equiv \Delta = (1-z)^2m^2 - xyp^2 = (x-y)^2m^2 - xyp^2$ is symmetric in x, y .

B.3.59. Shift $k \rightarrow k - yp + zq_1$ in the loop integral. Then $[xA + yB + zC]^3 \rightarrow [k^2 - \Delta]^3$.

B.3.60. After shifting the loop momentum $k \rightarrow k - yp + zq_1$ we drop the linear terms in the loop momentum k , as they vanish by the symmetry $\int d^4k k^\mu f(k^2) = \int d^3k \int_{-\infty}^{\infty} k^\mu f(k^2) = 0$. Consequently, the numerator processes as follows

$$\begin{aligned}
N^\mu &= \bar{u}_2[\gamma^\nu(\not{k} + \not{p} + m)\gamma^\mu(\not{k} + m)\gamma_\nu]u_1 \\
&= \bar{u}_2[\gamma^\nu\{\not{k}\gamma^\mu\not{k} + \not{p}\gamma^\mu\not{k} + m^2\gamma^\mu + m((\not{k} + \not{p})\gamma^\mu + \gamma^\mu\not{k})\}\gamma_\nu]u_1 \\
&= -2 \bar{u}_2[\not{k}\gamma^\mu\not{k} + \not{k}\gamma^\mu\not{p} + m^2\gamma^\mu - 2m(2k^\mu + p^\mu)]u_1 \\
&\quad (\text{shift } k \text{ and drop } k\text{-linear terms}) \\
&\rightarrow -2 \bar{u}_2[\not{k}\gamma^\mu\not{k} + \Sigma_2^\mu + \Sigma_1^\mu + m^2\gamma^\mu - 2m((1 - 2y)p^\mu + 2zq_1^\mu)]u_1 \\
&= -2 \bar{u}_2[\not{k}\gamma^\mu\not{k} + \Sigma_2^\mu + \Sigma_1^\mu + m^2(1 - 4z)\gamma^\mu + 2imz p_\nu\sigma^{\mu\nu} - 2m(1 - 2y - z)p^\mu]u_1 \\
&\quad (x + y + z = 1, 1 - 2y - z = x - y) \\
&= -2 \bar{u}_2[\not{k}\gamma^\mu\not{k} + \Sigma_2^\mu + \Sigma_1^\mu + m^2(1 - 4z)\gamma^\mu + 2imz p_\nu\sigma^{\mu\nu} - 2m(x - y)p^\mu]u_1
\end{aligned} \tag{B.3.3}$$

$$\bar{u}_2\Sigma_1^\mu u_1 = \bar{u}_2[(-y\not{p} + z\not{q}_1)\gamma^\mu\not{p}]u_1$$

$$\bar{u}_2\Sigma_2^\mu u_1 = \bar{u}_2[(-y\not{p} + z\not{q}_1)\gamma^\mu(-y\not{p} + z\not{q}_1)]u_1 \tag{B.3.4}$$

B.3.61. Beside dropping the k -linear terms, we notice that for $\mu \neq \nu$,

$$\int d^4k k^\mu k^\nu f(k^2) = \int d^2k \int_{-\infty}^{\infty} dk^\mu k^\mu \int_{-\infty}^{\infty} dk^\nu k^\nu f(k^2) = 0 = \int d^4k g^{\mu\nu}(k^\mu)^2 f(k^2) \tag{B.3.5}$$

and thus for the loop integral we can replace $k^\mu k^\nu \rightarrow g^{\mu\nu}(k^\mu)^2$ for $\mu \neq \nu$.

B.3.62. Moreover, since $k^2 = (k^0)^2 - (\vec{k})^2$ is symmetric in k^i, k^j ($i, j = 1, 2, 3$), then the integration

$$\int d^4k (k^i)^2 f(k^2) = \frac{1}{3} \int d^4k (\vec{k})^2 f(k^2). \tag{B.3.6}$$

Also, since k^2 is antisymmetric in $(k^0)^2$ and $(\vec{k})^2$, then

$$\int d^4k (k^0)^2 f(k^2) = \frac{-1}{3} \int d^4k (\vec{k})^2 f(k^2). \quad (\text{B.3.7})$$

B.3.63. Hence, we have

$$\int d^4k (k^0)^2 f(k^2) = \frac{g^{00}}{4} \int d^4k k^2 f(k^2), \quad (\text{B.3.8})$$

$$\int d^4k (k^i)^2 f(k^2) = \frac{g^{ii}}{4} \int d^4k k^2 f(k^2). \quad (\text{B.3.9})$$

i.e., we always can replace $\int d^4k k^\mu k^\nu f(k^2) \rightarrow \frac{1}{4}g^{\mu\nu} \int d^4k k^2 f(k^2)$ or simply $k^\mu k^\nu \rightarrow \frac{1}{4}g^{\mu\nu}k^2$ in the loop integrand for the loop momentum k (only for the loop momentum k , not for any of the external momenta q_1, q_2, p as well.)

$$\int d^4k k^\mu k^\nu f(k^2) = \frac{g^{\mu\nu}}{4} \int d^4k k^2 f(k^2). \quad (\text{B.3.10})$$

B.3.64. The above loop momentum replacement makes the numerator

$$-\frac{1}{2}N^\mu = \bar{u}_2 \left[-\frac{1}{2}k^2 \gamma^\mu + \Sigma_2^\mu + \Sigma_1^\mu + m^2(1-4z) \gamma^\mu + 2imz p_\nu \sigma^{\mu\nu} - 2m(x-y) p^\mu \right] u_1 \quad (\text{B.3.11})$$

B.3.65. We have

$$\begin{aligned} \bar{u}_2 \Sigma_1^\mu u_1 &= \bar{u}_2 (-y \not{p} + z \not{q}_1) \gamma^\mu \not{p} u_1 = -y \bar{u}_2 \not{p} \gamma^\mu \not{p} u_1 + z \bar{u}_2 \not{q}_1 \gamma^\mu \not{p} u_1 \\ &= yp^2 \bar{u}_2 \gamma^\mu u_1 + z [p^2 \bar{u}_2 \gamma^\mu u_1 - im \bar{u}_2 p_\nu \sigma^{\mu\nu} u_1 + m \bar{u}_2 p^\mu u_1] \\ &= (y+z)p^2 \bar{u}_2 \gamma^\mu u_1 - imz \bar{u}_2 p_\nu \sigma^{\mu\nu} u_1 + mz \bar{u}_2 p^\mu u_1 \end{aligned} \quad (\text{B.3.12})$$

$$\begin{aligned} \bar{u}_2 \Sigma_2^\mu u_1 &= \bar{u}_2 (-y \not{p} + z \not{q}_1) \gamma^\mu (-y \not{p} + z \not{q}_1) u_1 \\ &= -y \bar{u}_2 \Sigma_1^\mu u_1 - yz \bar{u}_2 \not{p} \gamma^\mu \not{q}_1 u_1 + z^2 \bar{u}_2 \not{q}_1 \gamma^\mu \not{q}_1 u_1 \\ &= -y [(y+z)p^2 \bar{u}_2 \gamma^\mu u_1 - imz \bar{u}_2 p_\nu \sigma^{\mu\nu} u_1 + mz \bar{u}_2 p^\mu u_1] \\ &\quad - yz [im \bar{u}_2 p_\nu \sigma^{\mu\nu} u_1 + m \bar{u}_2 p^\mu u_1] \\ &\quad + z^2 [m^2 \bar{u}_2 \gamma^\mu u_1 - im \bar{u}_2 p_\nu \sigma^{\mu\nu} u_1 - m \bar{u}_2 p^\mu u_1] \end{aligned}$$

$$= [z^2 m^2 - y(y+z)p^2] \bar{u}_2 \gamma^\mu u_1 - imz^2 \bar{u}_2 p_\nu \sigma^{\mu\nu} u_1 - mz(2y+z) \bar{u}_2 p^\mu u_1 \quad (\text{B.3.13})$$

For $x+y+z = 1$, $1-2y-z = x-y$ and

$$\bar{u}_2 [\Sigma_1^\mu + \Sigma_2^\mu] u_1 = \bar{u}_2 [(z^2 m^2 + (1-y)(y+z)p^2) \gamma^\mu - imz(1+z) p_\nu \sigma^{\mu\nu} + mz(x-y) p^\mu] u_1 \quad (\text{B.3.14})$$

B.3.66. The numerator reduces to

$$\begin{aligned} N^\mu &= -2\bar{u}_2 [-\frac{1}{2}k^2 \gamma^\mu + \Sigma_1^\mu + \Sigma_2^\mu + m^2(1-4z) \gamma^\mu + 2imz p_\nu \sigma^{\mu\nu} - 2m(x-y) p^\mu] u_1 \\ &= [k^2 - 2(1-x)(1-y)p^2 - 2(1-4z+z^2)m^2] \bar{u}_2 \gamma^\mu u_1 \\ &\quad - 2imz(1-z) p_\nu \bar{u}_2 \sigma^{\mu\nu} u_1 - 2m(z-2)(x-y)p^\mu \bar{u}_2 u_1 \end{aligned} \quad (\text{B.3.15})$$

B.3.67. From Ward identity $p_\mu N^\mu = 0$ because

$$\begin{aligned} p_\mu N^\mu &= [k^2 - 2(1-x)(1-y)p^2 - 2(1-4z+z^2)m^2] \bar{u}_2 \not{p} u_1 \\ &\quad - 2imz(1-z) p_\mu p_\nu \bar{u}_2 \sigma^{\mu\nu} u_1 - 2m(z-2)(x-y)p^2 \bar{u}_2 u_1 \end{aligned} \quad (\text{B.3.16})$$

But $\bar{u}_2 \not{p} u_1 = 0$. Also $p_\mu p_\nu \bar{u}_2 \sigma^{\mu\nu} u_1 = 0$ from symmetry issue of μ, ν . Finally, the last term $m(z-2)(x-y)p^2 \bar{u}_2 u_1$ is antisymmetric in x, y while Δ is symmetric in x, y and the contribution of this term vanishes identically by integration over x, y .

B.3.68. From Ward identity, drop the last term of N^μ and use

$$N^\mu = [k^2 - 2(1-x)(1-y)p^2 - 2(1-4z+z^2)m^2] \bar{u}_2 \gamma^\mu u_1 - 2imz(1-z) p_\nu \bar{u}_2 \sigma^{\mu\nu} u_1 \quad (\text{B.3.17})$$

B.3.69. Define the following integral in the complex domain as an analytic function in the D -dim

$$\mathcal{I}(r, s; M^2) = \int \frac{d^D k}{(2\pi)^D} \frac{(k^2)^r}{(k^2 - M^2 + i\epsilon)^s} = \frac{i(-1)^{r+s}}{16\pi^2 \Gamma(s)} \frac{(4\pi)^{2-\frac{D}{2}}}{(M^2)^{s-r-\frac{D}{2}}} \frac{\Gamma(r+\frac{D}{2})}{\Gamma(\frac{D}{2})} \Gamma(s-r-\frac{D}{2}) \quad (\text{B.3.18})$$

B.3.70. For $D = 4 - \varepsilon$, $\Gamma(2 - \frac{D}{2}) = \Gamma(\frac{\varepsilon}{2}) = \frac{2}{\varepsilon} - \gamma + \mathcal{O}(\varepsilon)$

B.3.71. In QED, replace the coupling $e \rightarrow e\mu^{2-\frac{D}{2}}$ for dimensional regularization.

$$\begin{aligned}\mathcal{I}(1, 3; \Delta) &= \frac{i}{32\pi^2} \left(\frac{4\pi\mu^2}{\Delta} \right)^{2-\frac{D}{2}} \frac{D}{2} \Gamma(2 - \frac{D}{2}) \\ &= \frac{i}{16\pi^2} \left(\frac{4\pi\mu^2}{\Delta} \right)^{\frac{\varepsilon}{2}} (1 - \frac{\varepsilon}{4}) \Gamma(\frac{\varepsilon}{2}) \\ &= \frac{i}{16\pi^2} [1 + \frac{\varepsilon}{2} \ln(\frac{4\pi\mu^2}{\Delta}) + \mathcal{O}(\varepsilon^2)] (1 - \frac{\varepsilon}{4}) [\frac{2}{\varepsilon} - \gamma + \mathcal{O}(\varepsilon)] \\ &= \frac{i}{16\pi^2} [\frac{2}{\varepsilon} - \gamma - \frac{1}{2} + \ln(\frac{4\pi\mu^2}{\Delta}) + \mathcal{O}(\varepsilon)] \\ &= \frac{i}{16\pi^2} [\frac{2}{\varepsilon} + \ln(\frac{\tilde{\mu}^2}{\Delta}) + \mathcal{O}(\varepsilon)], \quad \tilde{\mu}^2 = 4\pi\mu^2 \exp(-\gamma - \frac{1}{2}) \\ &\rightarrow \frac{i}{16\pi^2} \ln(\frac{\tilde{\mu}^2}{\Delta}),\end{aligned}\tag{B.3.19}$$

$$\begin{aligned}\mathcal{I}(0, 3; \Delta) &= \frac{-i}{32\pi^2} \frac{1}{\Delta} \left(\frac{4\pi\mu^2}{\Delta} \right)^{2-\frac{D}{2}} \Gamma(3 - \frac{D}{2}) \\ &= \frac{-i}{32\pi^2} \frac{1}{\Delta} \left(\frac{4\pi\mu^2}{\Delta} \right)^{2-\frac{D}{2}} (2 - \frac{D}{2}) \Gamma(2 - \frac{D}{2}) \\ &= \frac{-i}{32\pi^2} \frac{1}{\Delta} [1 + \frac{\varepsilon}{2} \ln(\frac{4\pi\mu^2}{\Delta}) + \mathcal{O}(\varepsilon^2)] (\frac{\varepsilon}{2}) [\frac{2}{\varepsilon} - \gamma + \mathcal{O}(\varepsilon)] \\ &= \frac{-i}{32\pi^2} \frac{1}{\Delta} [1 + \mathcal{O}(\varepsilon)] = \frac{-i}{32\pi^2} \frac{1}{\Delta}\end{aligned}\tag{B.3.20}$$

B.3.72. $F_2^{\text{QED}}(0) = \frac{2m}{e} \times \text{coefficient of } \bar{u}_2 p_\nu \sigma^{\mu\nu} u_1 \text{ in } i\mathcal{M}^\mu \text{ at } p^2 = 0$ (with $\alpha = \frac{e^2}{4\pi}$)

$$\begin{aligned}F_2^{\text{QED}}(0) &= \frac{2m}{e} (-e^3) (-2im)(2) \int_0^1 dz dy dx \delta(1 - x - y - z) z(1 - z) \mathcal{I}(0, 3; \Delta(x, y, z; p^2 = 0)) \\ &= \frac{m^2 e^2}{4\pi^2} \int_0^1 dz dy dx \delta(1 - x - y - z) \frac{z(1 - z)}{\Delta(x, y, z; p^2 = 0)} \\ &= \frac{\alpha m^2}{\pi} \int_0^1 dz dy dx \delta(1 - x - y - z) \frac{z(1 - z)}{(1 - z)^2 m^2} \\ &= \frac{\alpha}{\pi} \int_0^1 dz \frac{z}{1 - z} \int_0^{1-z} dy = \frac{\alpha}{\pi} \int_0^1 z dz = \frac{\alpha}{2\pi}\end{aligned}\tag{B.3.21}$$

B.3.73. Eventually, in QED, to $\mathcal{O}(\alpha^2)$, and with $\alpha = \frac{1}{137}$,

$$g = 2 + 2F_2^{\text{QED}}(0) = 2 + \frac{\alpha}{\pi} = 2.00232,\tag{B.3.22}$$

$$a_\mu^{\text{QED}} = \frac{\alpha}{2\pi} = 116171491.308 \times 10^{-11}. \quad (\text{B.3.23})$$

This is the main result of this part!

B.3.74. Higher order QED corrections to a_μ gives the perturbation expansion

$$a_\mu^{\text{QED}} = \sum_{n=1}^{\infty} C_n \left(\frac{\alpha}{\pi}\right)^n = \frac{1}{2} \left(\frac{\alpha}{\pi}\right) + C_2 \left(\frac{\alpha}{\pi}\right)^2 + C_3 \left(\frac{\alpha}{\pi}\right)^3 + \dots \quad (\text{B.3.24})$$

B.3.75. [21] Experimentally,

$$a_\mu^{\text{Exp}} = 116592061(41) \times 10^{-11}, \quad (\text{B.3.25})$$

$$a_\mu^{\text{Exp}} - a_\mu^{\text{SM}} = (251 \pm 59) \times 10^{-11}. \quad (\text{B.3.26})$$

B.4 a_μ in EW Theory

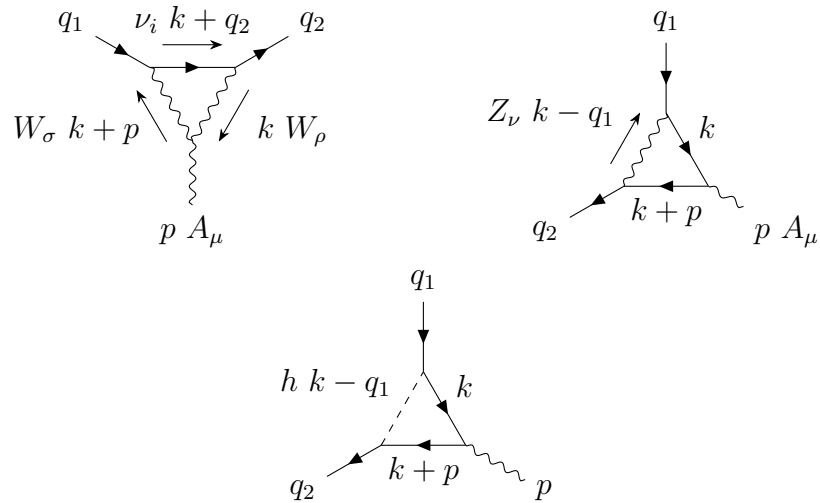


Figure B.3: One-loop EW W, Z, H contributions to a_μ .

B.4.1 $W - \nu$ -loop

B.4.76. [108] In the general R_ξ gauge the, $W - \nu$ -loop contribution to the vertex $\bar{u}_2 \not{A} u_1$ loop amplitude

$$\begin{aligned}
i\mathcal{M}^\mu &= \left(\frac{ig}{\sqrt{2}}\right)^2 \bar{u}_2 \int \frac{d^4k}{(2\pi)^4} \gamma^\alpha P_L \frac{i(k + \not{q}_2)}{(k + q_2)^2 + i\epsilon} \gamma^\nu P_L \\
&\quad \times \frac{-i[g_{\alpha\rho} + \frac{(\xi-1)k_\alpha k_\rho}{k^2 - \xi M_W^2}]}{k^2 - M_W^2 + i\epsilon} \frac{-i[g_{\sigma\nu} + \frac{(\xi-1)(k+p)_\sigma (k+p)_\nu}{(k+p)^2 - \xi M_W^2}]}{(k+p)^2 - M_W^2 + i\epsilon} \\
&\quad \times (-ie)[(p - k)^\sigma g^{\mu\rho} + (2k + p)^\mu g^{\rho\sigma} - (k + 2p)^\rho g^{\sigma\mu}] \\
&\quad (\xi = 1 \text{ 't Hooft-Feynman gauge}) \\
&= \frac{eg^2}{2} \int \frac{d^4k}{(2\pi)^4} \frac{g_{\alpha\rho} g_{\sigma\nu} [(p - k)^\sigma g^{\mu\rho} + (2k + p)^\mu g^{\rho\sigma} - (k + 2p)^\rho g^{\sigma\mu}]}{(k^2 - M_W^2 + i\epsilon)((k + p)^2 - M_W^2 + i\epsilon)((k + q_2)^2 + i\epsilon)} \\
&\quad \times \bar{u}_2 \gamma^\alpha P_L (k + \not{q}_2) \gamma^\nu P_L u_1 \\
&= \frac{eg^2}{2} \int \frac{d^4k}{(2\pi)^4} \frac{[(p - k)_\nu \delta_\alpha^\mu + (2k + p)^\mu g_{\nu\alpha} - (k + 2p)_\alpha \delta_\nu^\mu] \bar{u}_2 \gamma^\alpha (k + \not{q}_2) \gamma^\nu P_L u_1}{(k^2 - M_W^2 + i\epsilon)((k + p)^2 - M_W^2 + i\epsilon)((k + q_2)^2 + i\epsilon)} \tag{B.4.1}
\end{aligned}$$

B.4.77. Feynman parametrization combines the factors in the denominator

$$\frac{1}{ABC} = 2 \int_0^1 dz dy dx \delta(1 - x - y - z) \frac{1}{[xA + yB + zC]^3}$$

B.4.78. The denominator ($x + y + z = 1$)

$$\begin{aligned}
xA + yB + zC &= x(k^2 - M_W^2) + y((k + p)^2 - M_W^2) + z((k + q_2)^2) \\
&= (k + yp + zq_2)^2 - \Delta(x, y, z; p^2) \tag{B.4.2}
\end{aligned}$$

B.4.79. $\Delta(x, y, z; p^2) \equiv \Delta(p^2) \equiv \Delta = (1 - z)M_W^2 - z(1 - z)m^2 - xyp^2$ is symmetric in x, y

B.4.80. Shift $k \rightarrow k - yp - zq_2$ in the loop integral. Then $[xA + yB + zC]^3 \rightarrow [k^2 - \Delta]^3$.

B.4.81. After shifting the loop momentum $k \rightarrow k - yp - zq_2$ and dropping the linear terms in the loop momentum k , which vanish by the symmetry $\int d^4k k^\mu f(k^2) = 0$, the numerator processes as follows

$$\begin{aligned}
N^\mu &= [(p - k)_\nu \delta_\alpha^\mu + (2k + p)^\mu g_{\nu\alpha} - (k + 2p)_\alpha \delta_\nu^\mu] \bar{u}_2 \gamma^\alpha (\not{k} + \not{q}_2) \gamma^\nu P_L u_1 \\
&\quad (\text{shift } k \text{ and drop } k\text{-linear terms}) \\
&= [(p - k + yp + zq_2)_\nu \delta_\alpha^\mu + (2k - 2yp - 2zq_2 + p)^\mu g_{\nu\alpha} - (k - yp - zq_2 + 2p)_\alpha \delta_\nu^\mu] \\
&\quad \times \bar{u}_2 \gamma^\alpha (\not{k} - \not{y} \not{p} + (1 - z) \not{q}_2) \gamma^\nu P_L u_1 \\
&= [-k_\nu \delta_\alpha^\mu + 2k^\mu g_{\nu\alpha} - k_\alpha \delta_\nu^\mu] \bar{u}_2 \gamma^\alpha \not{k} \gamma^\nu P_L u_1 \\
&\quad + [((1 + y)p + zq_2)_\nu \delta_\alpha^\mu + ((1 - 2y)p - 2zq_2)^\mu g_{\nu\alpha} - ((2 - y)p - zq_2)_\alpha \delta_\nu^\mu] \\
&\quad \times \bar{u}_2 \gamma^\alpha (-y \not{p} + (1 - z) \not{q}_2) \gamma^\nu P_L u_1 \\
&\quad (\text{symmetry of } \alpha, \nu \text{ and replacing } k^\mu k^\nu \rightarrow \frac{1}{4} g^{\mu\nu} k^2 \text{ in the first line}) \\
&= \bar{u}_2 [-2k_\nu \gamma^\mu + 2k^\mu \gamma_\nu] \not{k} \gamma^\nu P_L u_1 \\
&\quad + \bar{u}_2 \gamma^\mu (-y \not{p} + (1 - z) \not{q}_2) ((1 + y) \not{p} + z \not{q}_2) P_L u_1 \\
&\quad + ((1 - 2y)p - 2zq_2)^\mu \bar{u}_2 \gamma_\nu (-y \not{p} + (1 - z) \not{q}_2) \gamma^\nu P_L u_1 \\
&\quad - \bar{u}_2 ((2 - y) \not{p} - z \not{q}_2) (-y \not{p} + (1 - z) \not{q}_2) \gamma^\mu P_L u_1 \\
&\supset -3k^2 \bar{u}_2 \gamma^\mu P_L u_1 \\
&\quad + \bar{u}_2 \gamma^\mu (-yz \not{p} \not{q}_2 + (1 - z)(1 + y) \not{q}_2 \not{p}) P_L u_1 + (-y(1 + y)p^2 + z(1 - z)m^2) \bar{u}_2 \gamma^\mu P_L u_1 \\
&\quad - 2((1 - 2y)p - 2zq_2)^\mu \bar{u}_2 (-y \not{p} + (1 - z) \not{q}_2) P_L u_1 \\
&\quad - \bar{u}_2 ((2 - y)(1 - z) \not{p} \not{q}_2 + yz \not{q}_2 \not{p}) \gamma^\mu P_L u_1 - (-y(2 - y)p^2 - z(1 - z)m^2) \bar{u}_2 \gamma^\mu P_L u_1 \\
&\supset -3k^2 \bar{u}_2 \gamma^\mu P_L u_1 \\
&\quad + (1 + y - z) \bar{u}_2 \gamma^\mu \not{q}_2 \not{p} P_L u_1 + (-y(1 + y + z)p^2 + z(1 - z)m^2) \bar{u}_2 \gamma^\mu P_L u_1
\end{aligned}$$

$$\begin{aligned}
& -2((1-2y-2z)q_2 - (1-2y)q_1)^\mu \bar{u}_2(m(1-y-z) + y\gamma_1)P_L u_1 \\
& + m(2-y-2z) \bar{u}_2 \not{p} \gamma^\mu P_L u_1 - ((2-y)(1-y-z)p^2 - z(1-z)m^2) \bar{u}_2 \gamma^\mu P_L u_1 \\
& \supset -3k^2 \bar{u}_2 \gamma^\mu P_L u_1 \\
& + m^2(1+y-z) \bar{u}_2 \gamma^\mu P_L u_1 - (1+y-z) \bar{u}_2 \gamma^\mu \not{q}_2 \not{q}_1 P_L u_1 \\
& + (-y(1+y+z)p^2 + z(1-z)m^2) \bar{u}_2 \gamma^\mu P_L u_1 \\
& - 2((1-2y-2z)q_2 - (1-2y)q_1)^\mu \bar{u}_2(m(1-y-z) + y\gamma_1)P_L u_1 \\
& + m^2(2-y-2z) \bar{u}_2 \gamma^\mu P_L u_1 - m(2-y-2z) \bar{u}_2 \not{q}_1 \gamma^\mu P_L u_1 \\
& - ((2-y)(1-y-z)p^2 - z(1-z)m^2) \bar{u}_2 \gamma^\mu P_L u_1
\end{aligned}$$

$$\begin{aligned}
N^\mu = & -3k^2 \bar{u}_2 \gamma^\mu P_L u_1 \\
& + m^2(1+y-z) \bar{u}_2 \gamma^\mu P_L u_1 - 2m(1+y-z) \bar{u}_2 q_2^\mu P_R u_1 + m^2(1+y-z) \bar{u}_2 \gamma^\mu P_R u_1 \\
& + (-y(1+y+z)p^2 + z(1-z)m^2) \bar{u}_2 \gamma^\mu P_L u_1 \\
& - 2m((1-2y-2z)q_2 - (1-2y)q_1)^\mu \bar{u}_2((1-y-z)P_L + yP_R)u_1 \\
& + m^2(2-y-2z) \bar{u}_2 \gamma^\mu P_L u_1 - 2m(2-y-2z) \bar{u}_2 q_1^\mu P_L u_1 + m^2(2-y-2z) \bar{u}_2 \gamma^\mu P_R u_1 \\
& - ((2-y)(1-y-z)p^2 - z(1-z)m^2) \bar{u}_2 \gamma^\mu P_L u_1 \\
& \supset -3k^2 \bar{u}_2 \gamma^\mu P_L u_1 + m^2(1-z)(3+z) \bar{u}_2 \gamma^\mu u_1 - m^2 z(1-z) \bar{u}_2 \gamma^\mu \gamma_5 u_1 \\
& - m(1+y(1-2z)-z) \bar{u}_2 q_1^\mu u_1 + m(1+y(3-4y-2z)-z) \bar{u}_2 q_1^\mu \gamma_5 u_1 \\
& + m(y(1-2z)-2(1-z)^2) \bar{u}_2 q_2^\mu u_1 + m(y(-5+4y+6z)-2z(1-z)) \bar{u}_2 q_2^\mu \gamma_5 u_1 \\
& - 2(1-z-y(1-y-z))p^2 \bar{u}_2 \gamma^\mu P_L u_1 \\
& \supset -3k^2 \bar{u}_2 \gamma^\mu P_L u_1 \\
& + m^2(-3+8z-5z^2) \bar{u}_2 \gamma^\mu u_1 - \frac{1}{2}m^2(8y^2 + 8y(-1+z) + (-1+z)(1+4z)) \bar{u}_2 \gamma^\mu \gamma_5 u_1 \\
& - 2p^2(1-z-y(1-y-z)) \bar{u}_2 \gamma^\mu P_L u_1 \\
& + \frac{im}{2}\{2z^2-5z+3\} \bar{u}_2 p_\nu \sigma^{\mu\nu} u_1 - \frac{im}{2}(1-2z)(1-2y-z) \bar{u}_2 p_\nu \sigma^{\mu\nu} \gamma_5 u_1
\end{aligned}$$

$$\begin{aligned}
& -m\{x(1-2x) - y(1-2y)\} \bar{u}_2 p^\mu u_1 + \frac{1}{2}m\{8y^2 - (1-z)(1+8y+2z)\} \bar{u}_2 p^\mu \gamma_5 u_1 \\
& \supset -m(1+y-z) \bar{u}_2 q_2^\mu u_1 + 2mz(1-z) \bar{u}_2 q_2^\mu u_1 - m(2-y-2z) \bar{u}_2 q_1^\mu u_1 + \dots \\
& \supset \frac{im}{2}\{2z^2 - 5z + 3\} \bar{u}_2 p_\nu \sigma^{\mu\nu} u_1
\end{aligned} \tag{B.4.3}$$

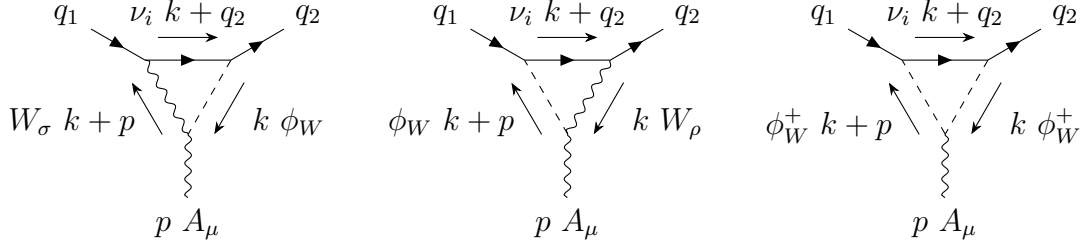
B.4.82. As before, and as $\frac{G_F}{\sqrt{2}} = \frac{g^2}{8M_W^2}$

$$\begin{aligned}
F_2(0) &= \frac{2m}{e} \left(\frac{eg^2}{2}\right) \left(\frac{im}{2}\right) (2) \int_0^1 dz dy dx \delta(1-x-y-z) \{2z^2 - 5z + 3\} \mathcal{I}(0, 3; \Delta(x, y, z; p^2 = 0)) \\
&= \frac{m^2 g^2}{32\pi^2} \int_0^1 dz dy dx \delta(1-x-y-z) \frac{2z^2 - 5z + 3}{\Delta(x, y, z; p^2 = 0)} \\
&= \frac{m^2 g^2}{32\pi^2} \int_0^1 dz dy dx \delta(1-x-y-z) \frac{2z^2 - 5z + 3}{(1-z)M_W^2 - z(1-z)m^2} \\
&= \frac{G_F m^2}{4\pi^2 \sqrt{2}} \int_0^1 dz \int_{y=0}^{1-z} dy \frac{2z^2 - 5z + 3}{1-z-z(1-z)\frac{m^2}{M_W^2}} \\
&= \frac{G_F m^2}{4\pi^2 \sqrt{2}} \int_0^1 dz \{(3-2z)(1-z)^2\} \\
&\quad \times \left[\frac{1}{1-z} + \frac{z}{1-z} \frac{m^2}{M_W^2} + \mathcal{O}\left(\frac{m^4}{M_W^4}\right) \right] \\
&\approx \frac{G_F m^2}{4\pi^2 \sqrt{2}} \int_0^1 dz (3-2z)[1-z+z(1-z)\frac{m^2}{M_W^2}] \\
&= \frac{G_F m^2}{4\pi^2 \sqrt{2}} \left[\frac{7}{6} + \frac{1}{3} \frac{m^2}{M_W^2} \right] \approx \frac{7}{3} \cdot \frac{G_F m^2}{8\pi^2 \sqrt{2}}
\end{aligned} \tag{B.4.4}$$

B.4.83. As we chose working in the $\xi = 1$ 't Hooft-Feynman gauge, we have to include the W -Goldston bosons loops contributions as well to obtain the physicksal gauge invariant result. Now, we calculate these Goldston contributions.

B.4.84. [108] (**Left diagram**) In the general R_ξ gauge, the amplitude is

$$\begin{aligned}
i\mathcal{M}^\mu &= \left(\frac{ig}{\sqrt{2}}\right) \left(\frac{-igm}{\sqrt{2}M_W}\right) \bar{u}_2 \int \frac{d^4 k}{(2\pi)^4} P_L \frac{i(\not{k} + \not{q}_2)}{(k+q_2)^2 + i\epsilon} \gamma^\nu P_L \\
&\quad \times \frac{i}{k^2 - \xi M_W^2 + i\epsilon} (ie) M_W g^{\mu\sigma} \frac{-i[g_{\sigma\nu} + \frac{(\xi-1)(k+p)_\sigma(k+p)_\nu}{(k+p)^2 - \xi M_W^2}]}{(k+p)^2 - M_W^2 + i\epsilon}
\end{aligned}$$


 Figure B.4: The Goldston ϕ_W contributions to a_μ .

($\xi = 1$ 't Hooft-Feynman gauge)

$$= -\frac{eg^2m}{2} \int \frac{d^4k}{(2\pi)^4} \frac{\bar{u}_2(\not{k} + \not{q}_2)\gamma^\mu P_L u_1}{(k^2 - M_W^2 + i\epsilon)((k+p)^2 - M_W^2 + i\epsilon)((k+q_2)^2 + i\epsilon)} \quad (\text{B.4.5})$$

B.4.85. The numerator processes as follows

$$\begin{aligned} N^\mu &= \bar{u}_2(\not{k} + \not{q}_2)\gamma^\mu P_L u_1 \\ &\quad (\text{shift } k \text{ and drop } k\text{-linear terms}) \\ &\rightarrow \bar{u}_2(-y\not{p} + (1-z)\not{q}_2)\gamma^\mu P_L u_1 \\ &= \bar{u}_2(m(1-y-z) + y\not{q}_1)\gamma^\mu P_L u_1 \\ &= m(1-y-z) \bar{u}_2\gamma^\mu P_L u_1 + y \bar{u}_2(2q_1^\mu - \gamma^\mu \not{q}_1)P_L u_1 \\ &\supset -\frac{i}{2}y \bar{u}_2 p_\nu \sigma^{\mu\nu} u_1 \end{aligned} \quad (\text{B.4.6})$$

B.4.86. As before, and as $\frac{G_F}{\sqrt{2}} = \frac{g^2}{8M_W^2}$

$$\begin{aligned} F_2(0) &= \frac{2m}{e} \left(\frac{-eg^2m}{2} \right) \left(-\frac{i}{2} \right) (2) \int_0^1 dz dy dx \delta(1-x-y-z) y \mathcal{I}(0, 3; \Delta(x, y, z; p^2 = 0)) \\ &= \frac{m^2 g^2}{32\pi^2} \int_0^1 dz dy dx \delta(1-x-y-z) \frac{y}{\Delta(x, y, z; p^2 = 0)} \\ &= \frac{m^2 g^2}{32\pi^2} \int_0^1 dz dy dx \delta(1-x-y-z) \frac{y}{(1-z)M_W^2 - z(1-z)m^2} \end{aligned}$$

$$\begin{aligned}
&= \frac{G_F m^2}{4\pi^2 \sqrt{2}} \int_0^1 dz \frac{1}{1-z - z(1-z)\frac{m^2}{M_W^2}} \int_{y=0}^{1-z} y dy \\
&= \frac{G_F m^2}{8\pi^2 \sqrt{2}} \int_0^1 dz (1-z)^2 \left[\frac{1}{1-z} + \frac{z}{1-z} \frac{m^2}{M_W^2} + \mathcal{O}\left(\frac{m^4}{M_W^4}\right) \right] \\
&\approx \frac{G_F m^2}{8\pi^2 \sqrt{2}} \int_0^1 dz [1-z + z(1-z)\frac{m^2}{M_W^2}] \\
&= \frac{G_F m^2}{8\pi^2 \sqrt{2}} \left[\frac{1}{2} + \frac{1}{6} \frac{m^2}{M_W^2} \right] \approx \frac{1}{2} \cdot \frac{G_F m^2}{8\pi^2 \sqrt{2}}
\end{aligned} \tag{B.4.7}$$

B.4.87. [108] (**Middle diagram**) In the general R_ξ gauge, the amplitude is

$$\begin{aligned}
i\mathcal{M}^\mu &= \left(\frac{ig}{\sqrt{2}}\right) \left(\frac{igm}{\sqrt{2}M_W}\right) \bar{u}_2 \int \frac{d^4k}{(2\pi)^4} \gamma^\alpha P_L \frac{i(\not{k} + \not{q}_2)}{(k+q_2)^2 + i\epsilon} P_R \\
&\quad \times \frac{-i[g_{\alpha\rho} + \frac{(\xi-1)k_\alpha k_\rho}{k^2 - \xi M_W^2}]}{k^2 - M_W^2 + i\epsilon} (ie) M_W g^{\mu\rho} \frac{i}{(k+p)^2 - \xi M_W^2 + i\epsilon} \\
&\quad (\xi = 1 \text{ 't Hooft-Feynman gauge}) \\
&= -\frac{eg^2 m}{2} \int \frac{d^4k}{(2\pi)^4} \frac{\bar{u}_2 \gamma^\mu (\not{k} + \not{q}_2) P_R u_1}{(k^2 - M_W^2 + i\epsilon)((k+p)^2 - M_W^2 + i\epsilon)((k+q_2)^2 + i\epsilon)},
\end{aligned} \tag{B.4.8}$$

which is very clear that this loop gives the same contribution as the previous one

$$\frac{1}{2} \cdot \frac{G_F m^2}{8\pi^2 \sqrt{2}} \tag{B.4.9}$$

B.4.88. [108] (**Right diagram**) In the general R_ξ gauge, the amplitude is

$$\begin{aligned}
i\mathcal{M}^\mu &= \left(\frac{-igm}{\sqrt{2}M_W}\right) \left(\frac{igm}{\sqrt{2}M_W}\right) \bar{u}_2 \int \frac{d^4k}{(2\pi)^4} P_L \frac{i(\not{k} + \not{q}_2)}{(k+q_2)^2 + i\epsilon} P_R \\
&\quad \times \frac{i}{k^2 - \xi M_W^2 + i\epsilon} (-ie)(-2k-p)^\mu \frac{i}{(k+p)^2 - \xi M_W^2 + i\epsilon} \\
&\quad (\xi = 1 \text{ 't Hooft-Feynman gauge}) \\
&= -\frac{eg^2 m^2}{2M_W^2} \int \frac{d^4k}{(2\pi)^4} \frac{(-2k-p)^\mu \bar{u}_2 (\not{k} + \not{q}_2) P_R u_1}{(k^2 - M_W^2 + i\epsilon)((k+p)^2 - M_W^2 + i\epsilon)((k+q_2)^2 + i\epsilon)}
\end{aligned} \tag{B.4.10}$$

B.4.89. The numerator processes as follows

$$\begin{aligned}
 N^\mu &= (-2k - p)^\mu \bar{u}_2(\not{k} + \not{q}_2) P_R u_1 \\
 &\quad (\text{shift } k \text{ and drop } k\text{-linear terms}) \\
 &= (-2k + 2yp + 2zq_2 - p)^\mu \bar{u}_2(\not{k} - y\not{p} - z\not{q}_2 + \not{q}_2) P_R u_1 \\
 &= -2k^\mu \bar{u}_2 \not{k} P_R u_1 + (2yp + 2zq_2 - p)^\mu \bar{u}_2(-y\not{p} - z\not{q}_2 + \not{q}_2) P_R u_1 \\
 &\supset -\frac{1}{2}k^2 \bar{u}_2 \gamma^\mu P_R u_1 + mz(1-z) \bar{u}_2 q_2^\mu u_1 \\
 &\supset -\frac{im}{2}z(1-z) \bar{u}_2 p_\nu \sigma^{\mu\nu} u_1
 \end{aligned} \tag{B.4.11}$$

B.4.90. As before, and as $\frac{G_F}{\sqrt{2}} = \frac{g^2}{8M_W^2}$

$$\begin{aligned}
 F_2(0) &= \frac{2m}{e} \left(-\frac{eg^2 m^2}{2M_W^2}\right) \left(-\frac{im}{2}\right) (2) \int_0^1 dz dy dx \delta(1-x-y-z) z(1-z) \\
 &\quad \times \mathcal{I}(0, 3; \Delta(x, y, z; p^2 = 0)) \\
 &= \frac{m^4 g^2}{32\pi^2 M_W^2} \int_0^1 dz dy dx \delta(1-x-y-z) \frac{z(1-z)}{\Delta(x, y, z; p^2 = 0)} \\
 &= \frac{G_F m^4}{4\pi^2 \sqrt{2}} \int_0^1 dz dy dx \delta(1-x-y-z) \frac{z(1-z)}{(1-z)M_W^2 - z(1-z)m^2} \\
 &= \frac{G_F m^2}{4\pi^2 \sqrt{2}} \frac{m^2}{M_W^2} \int_0^1 dz \int_{y=0}^{1-z} dy \frac{z(1-z)}{1-z-z(1-z)\frac{m^2}{M_W^2}} \\
 &= \frac{G_F m^2}{4\pi^2 \sqrt{2}} \frac{m^2}{M_W^2} \int_0^1 dz z(1-z)^2 \\
 &\quad \times \left[\frac{1}{1-z} + \frac{z}{1-z} \frac{m^2}{M_W^2} + \mathcal{O}\left(\frac{m^4}{M_W^4}\right) \right] \\
 &= \frac{G_F m^2}{4\pi^2 \sqrt{2}} \frac{m^2}{M_W^2} \int_0^1 dz z[1-z+z(1-z)\frac{m^2}{M_W^2}] \\
 &= \frac{G_F m^2}{4\pi^2 \sqrt{2}} \frac{m^2}{M_W^2} \left[\frac{1}{6} + \frac{1}{12} \frac{m^2}{M_W^2}\right] \approx \frac{1}{3} \cdot \frac{G_F m^2}{8\pi^2 \sqrt{2}} \frac{m^2}{M_W^2} \sim \mathcal{O}\left(\frac{m^4}{M_W^4}\right)
 \end{aligned} \tag{B.4.12}$$

B.4.91. The final $W - \nu$ loop contribution to $\mathcal{O}(\frac{m^2}{M_W^2})$ is the sum of the W -loop and its corresponding Goldston ϕ_W -loops. For $G_F = 1.1663787 \times 10^{-5}$ GeV $^{-2}$ and

$m = 0.1056583755$ GeV this contribution is

$$a_\mu^{W-\nu} = \frac{10}{3} \cdot \frac{G_F m^2}{8\pi^2 \sqrt{2}} = 388.706 \times 10^{-11} \quad (\text{B.4.13})$$

B.4.2 Z-loop

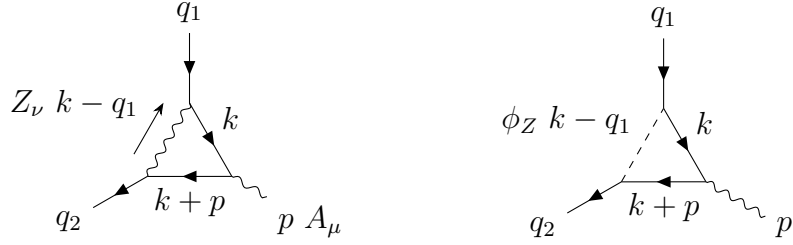


Figure B.5: One-loop EW Z and its corresponding Goldston boson ϕ_Z -loops contributions to a_μ .

B.4.92. [108] In the general R_ξ gauge the, Z -loop contribution to the vertex $\bar{u}_2 \not{A} u_1$ loop amplitude is

$$\begin{aligned} i\mathcal{M}^\mu &= \left(\frac{ig}{2c_w}\right)^2 \bar{u}_2 \int \frac{d^4k}{(2\pi)^4} \frac{-i[g_{\rho\nu} + \frac{(\xi-1)(k-q_1)_\rho(k-q_1)_\nu}{(k-q_1)^2 - \xi M_Z^2}]}{(k-q_1)^2 - M_Z^2 + i\epsilon} \\ &\quad \times \gamma^\rho (2s_w^2 - P_L) \frac{i(\not{k} + \not{p} + m)}{(k+p)^2 - m^2 + i\epsilon} (-ie\gamma^\mu) \frac{i(\not{k} + m)}{k^2 - m^2 + i\epsilon} \gamma^\nu (2s_w^2 - P_L) u_1 \\ &\quad (\xi = 1 \text{ 't Hooft-Feynman gauge}) \\ &= \frac{-eg^2}{4c_w^2} \int \frac{d^4k}{(2\pi)^4} \frac{\bar{u}_2 \gamma_\nu (2s_w^2 - P_L) [(\not{k} + \not{p} + m)\gamma^\mu (\not{k} + m)] \gamma^\nu (2s_w^2 - P_L) u_1}{(k^2 - m^2 + i\epsilon)((k+p)^2 - m^2 + i\epsilon)((k-q_1)^2 - M_Z^2 + i\epsilon)} \end{aligned} \quad (\text{B.4.14})$$

B.4.93. Feynman parametrization combines the factors in the denominator

$$\frac{1}{ABC} = 2 \int_0^1 dz dy dx \delta(1 - x - y - z) \frac{1}{[xA + yB + zC]^3}$$

B.4.94. The denominator ($x + y + z = 1$)

$$\begin{aligned} xA + yB + zC &= x(k^2 - m^2) + y((k+p)^2 - m^2) + z((k-q_1)^2 - M_Z^2) \\ &= (k + yp - zq_1)^2 - \Delta(x, y, z; p^2) \end{aligned} \quad (\text{B.4.15})$$

B.4.95. $\Delta(x, y, z; p^2) \equiv \Delta(p^2) \equiv \Delta = zM_Z^2 + (1-z)^2m^2 - xyp^2$ is symmetric in x, y

B.4.96. Shift $k \rightarrow k - yp + zq_1$ in the loop integral. Then $[xA + yB + zC]^3 \rightarrow [k^2 - \Delta]^3$.

B.4.97. After shifting the loop momentum $k \rightarrow k - yp + zq_1$ and dropping the linear terms in the loop momentum k , which vanish by the symmetry $\int d^4k k^\mu f(k^2) = 0$, the numerator processes as follows

$$\begin{aligned} N^\mu &= \bar{u}_2 \gamma_\nu (2s_w^2 - P_L) [(\not{k} + \not{p} + m) \gamma^\mu (\not{k} + m)] \gamma^\nu (2s_w^2 - P_L) u_1 \\ &\quad (\text{shift } k \text{ and drop all } k \text{ terms}) \\ &= \bar{u}_2 \gamma_\nu (2s_w^2 - P_L) [(\not{k} + (1-y)\not{p} + z\not{q}_1 + m) \gamma^\mu (\not{k} - y\not{p} + z\not{q}_1 + m)] \gamma^\nu (2s_w^2 - P_L) u_1 \\ &= \bar{u}_2 \gamma_\nu (2s_w^2 - P_L) [((1-y)\not{p} + z\not{q}_1 + m) \gamma^\mu (-y\not{p} + z\not{q}_1 + m)] \gamma^\nu (2s_w^2 - P_L) u_1 \\ &= \bar{u}_2 (2s_w^2 - P_R) \gamma_\nu [((1-y)\not{p} + z\not{q}_1) \gamma^\mu (-y\not{p} + z\not{q}_1)] \gamma^\nu (2s_w^2 - P_L) u_1 \\ &\quad + m \bar{u}_2 (2s_w^2 - P_R) \gamma_\nu [((1-y)\not{p} + z\not{q}_1) \gamma^\mu + \gamma^\mu (-y\not{p} + z\not{q}_1)] \gamma^\nu (2s_w^2 - P_L) u_1 \\ &\quad + m^2 \bar{u}_2 (2s_w^2 - P_R) \gamma_\nu \gamma^\mu \gamma^\nu (2s_w^2 - P_L) u_1 \\ &= -2 \bar{u}_2 [(-y\not{p} + z\not{q}_1) \gamma^\mu ((1-y)\not{p} + z\not{q}_1)] (2s_w^2 - P_L)^2 u_1 \\ &\quad + 4m \bar{u}_2 [((1-y)p + zq_1)^\mu + (-yp + zq_1)^\mu] (2s_w^2 - P_R) (2s_w^2 - P_L) u_1 \\ &\quad - 2m^2 \bar{u}_2 \gamma^\mu (2s_w^2 - P_L)^2 u_1 \\ &\supset -2 \bar{u}_2 [\Sigma_1^\mu + \Sigma_2^\mu] (2s_w^2 - P_L)^2 u_1 + 2mz \{(4s_w^2 - 1)^2 - 1\} \bar{u}_2 q_1^\mu u_1 \\ &\supset imz(1-y) \{(4s_w^2 - 1)^2 + 1\} \bar{u}_2 p_\nu \sigma^{\mu\nu} u_1 - imz \{(4s_w^2 - 1)^2 - 1\} \bar{u}_2 p_\nu \sigma^{\mu\nu} u_1 \\ &\supset imz[y \{(4s_w^2 - 1)^2 - 1\} + 2] \bar{u}_2 p_\nu \sigma^{\mu\nu} u_1 \end{aligned} \quad (\text{B.4.16})$$

B.4.98. As before, and as $\frac{G_F}{\sqrt{2}} = \frac{g^2}{8M_W^2}$ and $M_W^2 = c_w^2 M_Z^2$

$$\begin{aligned}
 F_2(0) &= \frac{2m}{e} \left(\frac{-eg^2}{4c_w^2} \right) (im)(2) \int_0^1 dz dy dx \delta(1-x-y-z) z[y\{(4s_w^2 - 1)^2 - 1\} + 2] \\
 &\quad \times \mathcal{I}(0, 3; \Delta(x, y, z; p^2 = 0)) \\
 &= -\frac{m^2 g^2}{32\pi^2 c_w^2} \int_0^1 dz dy dx \delta(1-x-y-z) \frac{z[y\{(4s_w^2 - 1)^2 - 1\} + 2]}{\Delta(x, y, z; p^2 = 0)} \\
 &= \frac{m^2 g^2}{32\pi^2 c_w^2} \int_0^1 dz \int_{y=0}^{1-z} dy \frac{z[y\{(4s_w^2 - 1)^2 - 1\} + 2]}{z M_Z^2 + (1-z)^2 m^2} \\
 &= \frac{m^2 g^2}{32\pi^2 c_w^2 M_Z^2} \int_0^1 dz \int_{y=0}^{1-z} dy \frac{z[y\{(4s_w^2 - 1)^2 - 1\} + 2]}{z + (1-z)^2 \frac{m^2}{M_Z^2}} \\
 &= \frac{m^2 g^2}{32\pi^2 M_W^2} \int_0^1 dz \int_0^{1-z} dy z[y\{(4s_w^2 - 1)^2 - 1\} + 2] \left[\frac{1}{z} - (1 - \frac{2}{z} + \frac{1}{z^2}) \frac{m^2}{M_Z^2} + \mathcal{O}(\frac{m^4}{M_Z^4}) \right] \\
 &\approx \frac{1}{3} \cdot \frac{G_F m^2}{8\pi^2 \sqrt{2}} \{(4s_w^2 - 1)^2 - 5\}
 \end{aligned} \tag{B.4.17}$$

B.4.99. As we chose working in the $\xi = 1$ 't Hooft-Feynman gauge, we have to include the Z -Goldston boson loops contributions as well to obtain the physicksal result. However, the Z -Goldston contributes only at $\mathcal{O}(\frac{m^4}{M_Z^4})$ and it is ommitted. The final Z -loop contribution to $\mathcal{O}(\frac{m^2}{M_Z^2})$ and for $G_F = 1.1663787 \times 10^{-5} \text{ GeV}^{-2}$, $m = 0.1056583755 \text{ GeV}$ and $s_w^2 = 0.23$ is

$$a_\mu^Z = \frac{1}{3} \cdot \frac{G_F m^2}{8\pi^2 \sqrt{2}} \{(4s_w^2 - 1)^2 - 5\} = -194.104 \times 10^{-11} \tag{B.4.18}$$

Nevertheless, we calculate the Goldston ϕ_Z -loop for completeness.

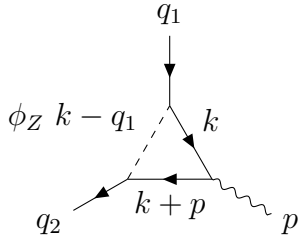


Figure B.6: One-loop Goldston boson ϕ_Z -loops contribution to a_μ .

B.4.100. [108] (ϕ_Z -loop) In the general R_ξ gauge, the ϕ_Z -loop amplitude is

$$\begin{aligned}
 i\mathcal{M}^\mu &= \left(\frac{gm}{2M_W}\right)^2 \bar{u}_2 \int \frac{d^4k}{(2\pi)^4} \frac{i}{(k - q_1)^2 - M_Z^2 + i\epsilon} \\
 &\quad \times \gamma_5 \frac{i(\not{k} + \not{p} + m)}{(k + p)^2 - m^2 + i\epsilon} (-ie\gamma^\mu) \frac{i(\not{k} + m)}{k^2 - m^2 + i\epsilon} \gamma_5 u_1 \\
 &\quad (\xi = 1 \text{ 't Hooft-Feynman gauge}) \\
 &= \frac{-eg^2m^2}{4M_W^2} \int \frac{d^4k}{(2\pi)^4} \frac{\bar{u}_2 \gamma_5[(\not{k} + \not{p} + m)\gamma^\mu(\not{k} + m)]\gamma_5 u_1}{(k^2 - m^2 + i\epsilon)((k + p)^2 - m^2 + i\epsilon)((k - q_1)^2 - M_Z^2 + i\epsilon)} \tag{B.4.19}
 \end{aligned}$$

B.4.101. Feynman parametrization combines the factors in the denominator

$$\frac{1}{ABC} = 2 \int_0^1 dz dy dx \delta(1 - x - y - z) \frac{1}{[xA + yB + zC]^3}$$

B.4.102. The denominator ($x + y + z = 1$)

$$\begin{aligned}
 xA + yB + zC &= x(k^2 - m^2) + y((k + p)^2 - m^2) + z((k - q_1)^2 - M_Z^2) \\
 &= (k + yp - zq_1)^2 - \Delta(x, y, z; p^2) \tag{B.4.20}
 \end{aligned}$$

B.4.103. $\Delta(x, y, z; p^2) \equiv \Delta(p^2) \equiv \Delta = zM_Z^2 + (1 - z)^2m^2 - xyp^2$ is symmetric in x, y

B.4.104. Shift $k \rightarrow k - yp + zq_1$ in the loop integral. Then $[xA + yB + zC]^3 \rightarrow [k^2 - \Delta]^3$.

B.4.105. After shifting the loop momentum $k \rightarrow k - yp + zq_1$ and dropping the linear terms in the loop momentum k , which vanish by the symmetry $\int d^4k k^\mu f(k^2) = 0$, the numerator processes as follows

$$\begin{aligned}
 N^\mu &= \bar{u}_2 \gamma_5[(\not{k} + \not{p} + m)\gamma^\mu(\not{k} + m)]\gamma_5 u_1 \\
 &\quad (\text{shift } k \text{ and drop all } k \text{ terms}) \\
 &\rightarrow \bar{u}_2 \gamma_5[(\not{k} + (1 - y)\not{p} + z\not{q}_1 + m)\gamma^\mu(\not{k} - y\not{p} + z\not{q}_1 + m)]\gamma_5 u_1 \\
 &\rightarrow \bar{u}_2 \gamma_5[((1 - y)\not{p} + z\not{q}_1 + m)\gamma^\mu(-y\not{p} + z\not{q}_1 + m)]\gamma_5 u_1
 \end{aligned}$$

$$\begin{aligned}
&= \bar{u}_2 \gamma_5 [((1-y)\not{p} + z\not{q}_1) \gamma^\mu (-y\not{p} + z\not{q}_1)] \gamma_5 u_1 \\
&\quad + m \bar{u}_2 \gamma_5 [((1-y)\not{p} + z\not{q}_1) \gamma^\mu + \gamma^\mu (-y\not{p} + z\not{q}_1)] \gamma_5 u_1 \\
&\quad + m^2 \bar{u}_2 \gamma_5 \gamma^\mu \gamma_5 u_1 \\
&= -\bar{u}_2 [((1-y)\not{p} + z\not{q}_1) \gamma^\mu (-y\not{p} + z\not{q}_1)] u_1 + m \bar{u}_2 [((1-y)\not{p} + z\not{q}_1) \gamma^\mu + \gamma^\mu (-y\not{p} + z\not{q}_1)] u_1 \\
&\quad - m^2 \bar{u}_2 \gamma^\mu u_1 \\
&\supset -\bar{u}_2 [-y\not{p} \gamma^\mu \not{p} + z\not{p} \gamma^\mu \not{q}_1 + \Sigma_2^\mu] u_1 - 2m \bar{u}_2 [(1-y-z) q_1^\mu + y q_2^\mu] u_1 \\
&\supset -2mz \bar{u}_2 q_1^\mu u_1 - 2imyz \bar{u}_2 p_\nu \sigma^{\mu\nu} u_1 - 2m(2yz + z^2) \bar{u}_2 q_1^\mu u_1 \\
&\quad - 2m \bar{u}_2 [(1-y-z) q_1^\mu + y q_2^\mu] u_1 \\
&\supset im[z - 2yz + 2yz + z^2 + 1 - y - z + y] \bar{u}_2 p_\nu \sigma^{\mu\nu} u_1 \\
&\supset im[1 + z^2] \bar{u}_2 p_\nu \sigma^{\mu\nu} u_1
\end{aligned} \tag{B.4.21}$$

B.4.106. As before, and as $\frac{G_F}{\sqrt{2}} = \frac{g^2}{8M_W^2}$ and $M_W^2 = c_w^2 M_Z^2$

$$\begin{aligned}
F_2(0) &= \frac{2m}{e} \left(\frac{-eg^2 m^2}{4M_W^2} \right) (im)(2) \int_0^1 dz dy dx \delta(1-x-y-z) (1+z^2) \mathcal{I}(0, 3; \Delta(x, y, z; p^2=0)) \\
&= -\frac{m^2 g^2}{32\pi^2} \frac{m^2}{M_W^2} \int_0^1 dz dy dx \delta(1-x-y-z) \frac{1+z^2}{\Delta(x, y, z; p^2=0)} \\
&= -\frac{m^2 g^2}{32\pi^2} \frac{m^2}{M_W^2} \int_0^1 dz \frac{1+z^2}{z M_Z^2 + (1-z)^2 m^2} \int_{y=0}^{1-z} dy \\
&= -\frac{m^2 g^2}{32\pi^2 M_Z^2} \frac{m^2}{M_W^2} \int_0^1 dz \frac{(1+z^2)(1-z)}{z + (1-z)^2 \frac{m^2}{M_Z^2}} \\
&= -\frac{m^2 g^2}{32\pi^2 M_Z^2} \frac{m^2}{M_W^2} \int_0^1 dz (1+z^2)(1-z) \left[\frac{1}{z} - (1 - \frac{2}{z} + \frac{1}{z^2}) \frac{m^2}{M_Z^2} + \mathcal{O}(\frac{m^4}{M_Z^4}) \right] \\
&\approx -\frac{1}{4} \cdot \frac{G_F m^2}{8\pi^2 \sqrt{2}} \cdot \mathcal{O}(\frac{m^2}{M_Z^2}) \sim \mathcal{O}(\frac{m^4}{M_Z^4})
\end{aligned} \tag{B.4.22}$$

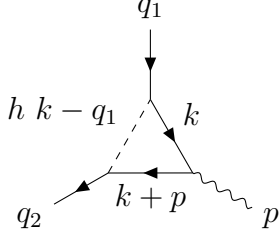


Figure B.7: One-loop EW Higgs-loop contribution to a_μ .

B.4.3 Higgs loop

- B.4.107. [108] In the general R_ξ gauge, the Higgs-loop contribution to the vertex $\bar{u}_2 \not{A} u_1$ amplitude is

$$\begin{aligned} i\mathcal{M}^\mu &= \left(\frac{-igm}{2M_W}\right)^2 \bar{u}_2 \int \frac{d^4k}{(2\pi)^4} \frac{i}{(k-q_1)^2 - m_h^2 + i\epsilon} \frac{i(\not{k} + \not{p} + m)}{(k+p)^2 - m^2 + i\epsilon} (-ie\gamma^\mu) \frac{i(\not{k} + m)}{k^2 - m^2 + i\epsilon} \\ &= \frac{eg^2m^2}{4M_W^2} \int \frac{d^4k}{(2\pi)^4} \frac{\bar{u}_2[(\not{k} + \not{p} + m)\gamma^\mu(\not{k} + m)]u_1}{(k^2 - m^2 + i\epsilon)((k+p)^2 - m^2 + i\epsilon)((k-q_1)^2 - m_h^2 + i\epsilon)} \end{aligned} \quad (\text{B.4.23})$$

- B.4.108. Feynman parametrization combines the factors in the denominator

$$\frac{1}{ABC} = 2 \int_0^1 dz dy dx \delta(1-x-y-z) \frac{1}{[xA+yB+zC]^3}$$

- B.4.109. The denominator ($x+y+z=1$)

$$\begin{aligned} xA + yB + zC &= x(k^2 - m^2) + y((k+p)^2 - m^2) + z((k-q_1)^2 - m_h^2) \\ &= (k+yp-zq_1)^2 - \Delta(x, y, z; p^2) \end{aligned} \quad (\text{B.4.24})$$

- B.4.110. $\Delta(x, y, z; p^2) \equiv \Delta(p^2) \equiv \Delta = zm_h^2 + (1-z)^2m^2 - xyp^2$ is symmetric in x, y

- B.4.111. Shift $k \rightarrow k - yp + zq_1$ in the loop integral. Then $[xA+yB+zC]^3 \rightarrow [k^2 - \Delta]^3$.

- B.4.112. We have

$$\bar{u}_2 \Sigma_2^\mu u_1 = [z^2m^2 - y(y+z)p^2] \bar{u}_2 \gamma^\mu u_1 - imz^2 \bar{u}_2 p_\nu \sigma^{\mu\nu} u_1 - mz(2y+z) \bar{u}_2 p^\mu u_1 \quad (\text{B.4.25})$$

$$\begin{aligned} \bar{u}_2 \Sigma_3^\mu u_1 &= \bar{u}_2 \not{p} \gamma^\mu (-y \not{p} + z \not{q}_1) u_1 = -y \bar{u}_2 \not{p} \gamma^\mu \not{p} u_1 + z \bar{u}_2 \not{p} \gamma^\mu \not{q}_1 u_1 \\ &= y p^2 \bar{u}_2 \gamma^\mu u_1 + imz \bar{u}_2 p_\nu \sigma^{\mu\nu} u_1 + mz \bar{u}_2 p^\mu u_1 \end{aligned} \quad (\text{B.4.26})$$

For $x + y + z = 1$, $1 - 2y - z = x - y$ and

$$\bar{u}_2 [\Sigma_2^\mu + \Sigma_3^\mu] u_1 = \bar{u}_2 [(z^2 m^2 + y(1-y-z)p^2) \gamma^\mu + imz(1-z) p_\nu \sigma^{\mu\nu} + mz(x-y) p^\mu] u_1 \quad (\text{B.4.27})$$

B.4.113. The numerator

$$\begin{aligned} N^\mu &= \bar{u}_2 [(\not{k} + \not{p} + m) \gamma^\mu (\not{k} + m)] u_1 \\ &\quad (\text{shift } k \text{ and drop all } k\text{-linear terms}) \\ &\rightarrow \bar{u}_2 [(\not{k} + \not{p} - y \not{p} + z \not{q}_1 + m) \gamma^\mu (\not{k} - y \not{p} + z \not{q}_1 + m)] u_1 \\ &= \bar{u}_2 [\not{k} \gamma^\mu \not{k} + (\not{p} - y \not{p} + z \not{q}_1 + m) \gamma^\mu (-y \not{p} + z \not{q}_1 + m)] u_1 \\ &= \bar{u}_2 [\not{k} \gamma^\mu \not{k} + \Sigma_3^\mu + \Sigma_2^\mu + m(\not{p} - y \not{p} + z \not{q}_1) \gamma^\mu + m \gamma^\mu (-y \not{p} + z \not{q}_1) + m^2 \gamma^\mu] u_1 \\ &= \bar{u}_2 [\not{k} \gamma^\mu \not{k} + \Sigma_3^\mu + \Sigma_2^\mu + (1-y) \not{p} \gamma^\mu \not{q}_1 + z \not{q}_1 \gamma^\mu \not{q}_1 - y \not{q}_2 \gamma^\mu \not{q}_2 + m^2 (1+y+z) \gamma^\mu] u_1 \\ &= -\frac{1}{2} k^2 \bar{u}_2 \gamma^\mu u_1 + \bar{u}_2 [(z^2 m^2 + y(1-y-z)p^2) \gamma^\mu + imz(1-z) p_\nu \sigma^{\mu\nu} + mz(x-y) p^\mu] u_1 \\ &\quad + m(1-y) \bar{u}_2 [ip_\nu \sigma^{\mu\nu} + p^\mu] u_1 + mz \bar{u}_2 [m \gamma^\mu - ip_\nu \sigma^{\mu\nu} - p^\mu] u_1 \\ &\quad - my \bar{u}_2 [m \gamma^\mu - ip_\nu \sigma^{\mu\nu} + p^\mu] u_1 + m^2 (1+y+z) \bar{u}_2 \gamma^\mu u_1 \\ &= -\frac{1}{2} k^2 \bar{u}_2 \gamma^\mu u_1 + \{p^2 y(1-y-z) + m^2 (1+2z+z^2)\} \bar{u}_2 \gamma^\mu u_1 \\ &\quad + im(1-z^2) \bar{u}_2 p_\nu \sigma^{\mu\nu} u_1 + m(1+z)(x-y) \bar{u}_2 p^\mu u_1 \end{aligned} \quad (\text{B.4.28})$$

B.4.114. From Ward identity $p_\mu N^\mu = 0$ because $\bar{u}_2 \not{p} u_1 = 0$, $p_\mu p_\nu \bar{u}_2 \sigma^{\mu\nu} u_1 = 0$ from symmetry issue of μ, ν , and, finally, the last term $(1+z)(x-y)p^\mu \bar{u}_2 u_1$ is antisymmetric in x, y while Δ is symmetric in x, y and the contribution of this

term vanishes identically by integration. Thus we only consider the numerator

$$N^\mu = \left[-\frac{1}{2}k^2 + p^2y(1-y-z) + m^2(1+2z+z^2) \right] \bar{u}_2\gamma^\mu u_1 + im(1-z^2) \bar{u}_2 p_\nu \sigma^{\mu\nu} u_1 \quad (\text{B.4.29})$$

B.4.115. As before, and as $\frac{G_F}{\sqrt{2}} = \frac{g^2}{8M_W^2}$

$$\begin{aligned} F_2^h(0) &= \frac{2m}{e} \left(\frac{eg^2m^2}{4M_W^2} \right) (im)(2) \int_0^1 dz dy dx \delta(1-x-y-z) (1-z^2) \\ &\quad \times \mathcal{I}(0, 3; \Delta(x, y, z; p^2 = 0)) \\ &= \frac{G_F m^4}{4\pi^2 \sqrt{2}} \int_0^1 dz dy dx \delta(1-x-y-z) \frac{1-z^2}{\Delta(x, y, z; p^2 = 0)} \\ &= \frac{G_F m^4}{4\pi^2 \sqrt{2}} \int_0^1 dz \int_{y=0}^{1-z} dy \frac{1-z^2}{zm_h^2 + (1-z)^2 m^2} \\ &= \frac{G_F m^2}{4\pi^2 \sqrt{2}} \int_0^1 dz \int_{y=0}^{1-z} dy \frac{1-z^2}{(1-z)^2 + z \frac{m_h^2}{m^2}} \\ &= \frac{G_F m^2}{4\pi^2 \sqrt{2}} \int_0^1 dz \frac{(1+z)(1-z)^2}{(1-z)^2 + z \frac{m_h^2}{m^2}} \\ &\approx \frac{G_F m^2}{4\pi^2 \sqrt{2}} \int_0^1 dz \left[\frac{1}{1+z \frac{m_h^2}{m^2}} - \frac{1+z-z^2}{\frac{m_h^2}{m^2}} \right] \\ &\approx \frac{G_F m^2}{4\pi^2 \sqrt{2}} \frac{m^2}{m_h^2} \left[\ln \frac{m_h^2}{m^2} - \frac{7}{6} \right] \\ &= \frac{7}{3} \cdot \frac{G_F m^2}{8\pi^2 \sqrt{2}} \frac{m^2}{m_h^2} \left[\frac{6}{7} \ln \frac{m_h^2}{m^2} - 1 \right] \end{aligned} \quad (\text{B.4.30})$$

B.4.116. The Higgs boson contributes only at $\mathcal{O}(\frac{m^4}{M_W^2 m_h^2})$. The final Higgs-loop contribution to $\mathcal{O}(\frac{m^4}{M_W^2 m_h^2})$ and for $G_F = 1.1663787 \times 10^{-5} \text{ GeV}^{-2}$, $m = 0.1056583755 \text{ GeV}$ and $m_h = 125.25 \text{ GeV}$ is

$$a_\mu^h = \frac{7}{3} \cdot \frac{G_F m^2}{8\pi^2 \sqrt{2}} \frac{m^2}{m_h^2} \left[\frac{6}{7} \ln \frac{m_h^2}{m^2} - 1 \right] = 0.002 \times 10^{-11} \quad (\text{B.4.31})$$

B.4.117. The EW contribution to a_μ is the sum of the W, Z and Higgs contributions

$$a_\mu^{\text{EW}} = a_\mu^{W-\nu} + a_\mu^Z + a_\mu^h$$

$$= \frac{1}{3} \cdot \frac{G_F m^2}{8\pi^2 \sqrt{2}} \left[10 + \{(4s_w^2 - 1)^2 - 5\} + 7 \frac{m^2}{m_h^2} \left[\frac{6}{7} \ln \frac{m_h^2}{m^2} - 1 \right] \right] = 194.604 \times 10^{-11}$$

(B.4.32)

B.4.118. Finally, the SM (nonhadronic) contribution is the sum of both the QED and the EW ones

$$\begin{aligned} a_\mu^{\text{SM-nonhad}} &= a_\mu^{\text{QED}} + a_\mu^{\text{EW}} \\ &= \frac{\alpha}{2\pi} + \frac{1}{3} \cdot \frac{G_F m^2}{8\pi^2 \sqrt{2}} \left[10 + \{(4s_w^2 - 1)^2 - 5\} + 7 \frac{m^2}{m_h^2} \left[\frac{6}{7} \ln \frac{m_h^2}{m^2} - 1 \right] \right] \\ &= 116171685.904 \times 10^{-11} \\ a_\mu^{\text{Exp}} &= 116592061(41) \times 10^{-11} \\ \Delta a_\mu &= a_\mu^{\text{Exp}} - a_\mu^{\text{SM}} = (251 \pm 59) \times 10^{-11}. \end{aligned}$$

(B.4.33)

C

VLSM Appendix

C.1 Details of the model

C.1.1 Diagonalization of vector boson mass matrix

We show the explicit form of the diagonalization matrix to obtain the canonically normalized mass basis of the vector bosons. We decompose the diagonalization matrix as

$$\begin{pmatrix} W_\mu^3 \\ B_\mu \\ V_\mu \end{pmatrix} =: \mathcal{E} R_1 R_2 \begin{pmatrix} A_\mu \\ A'_\mu \\ Z_\mu \end{pmatrix}, \quad (\text{C.1.1})$$

C.1 Details of the model

where \mathcal{E} canonically normalizes the kinetic terms, R_1 block diagonalize the massless photon and the others, and R_2 diagonalize the 2×2 block of the massive bosons. Their explicit forms are given by

$$\mathcal{E} = \frac{1}{\sqrt{2}} \begin{pmatrix} \sqrt{2} & 0 & 0 \\ 0 & \eta_+ & -\eta_- \\ 0 & \eta_+ & \eta_- \end{pmatrix}, \quad R_1 = \frac{1}{\sqrt{2}} \begin{pmatrix} \sqrt{2}s_W & \sqrt{2}c_W & 0 \\ c_W/\eta_+ & -s_W/\eta_+ & 1/\eta_- \\ -c_W/\eta_- & s_W/\eta_- & 1/\eta_+ \end{pmatrix}, \quad R_2 = \begin{pmatrix} 1 & 0 & 0 \\ 0 & c_V & s_V \\ 0 & -s_V & c_V \end{pmatrix}, \quad (\text{C.1.2})$$

where $\eta_{\pm} := 1/\sqrt{1 \pm \epsilon}$ and

$$c_V := \sqrt{\frac{1}{2} \left(1 - \frac{1 - (1 + s_W^2)\epsilon^2 - c_W^2 t_V^2}{\sqrt{d_V}} \right)}, \quad s_V := \text{sign}(\epsilon) \sqrt{\frac{1}{2} \left(1 + \frac{1 - (1 + s_W^2)\epsilon^2 - c_W^2 t_V^2}{\sqrt{d_V}} \right)}, \quad (\text{C.1.3})$$

with

$$d_V := (1 - \epsilon^2 c_W^2)^2 - 2 \{ 1 - (1 + s_W^2)\epsilon^2 \} c_W^2 t_V^2 + c_W^4 t_V^4. \quad (\text{C.1.4})$$

Altogether, the diagonalization matrix has the form

$$\mathcal{E} R_1 R_2 = \begin{pmatrix} s_W & c_W c_V & c_W s_V \\ c_W & -s_W c_V + \epsilon s_V \eta_+ \eta_- & -s_V s_W - \epsilon c_V \eta_+ \eta_- \\ 0 & -s_V \eta_+ \eta_- & c_V \eta_+ \eta_- \end{pmatrix} =: \begin{pmatrix} s_W & c_W C_{WA'} & c_W C_{WZ} \\ c_W & -s_W C_{BA'} & -s_W C_{BZ} \\ 0 & C_{VA'} & C_{VZ} \end{pmatrix}. \quad (\text{C.1.5})$$

The masses after diagonalization are given by

$$m_{A'}^2 = \frac{m_W^2}{2c_W^2(1 - \epsilon^2)} \left(1 + c_W^2(t_V^2 - \epsilon^2) - \sqrt{d_V} \right), \quad (\text{C.1.6})$$

$$m_Z^2 = \frac{m_W^2}{2c_W^2(1 - \epsilon^2)} \left(1 + c_W^2(t_V^2 - \epsilon^2) + \sqrt{d_V} \right). \quad (\text{C.1.7})$$

Up to the second order in ϵ and t_V ,

$$C_{WA'} \sim s_W \epsilon, \quad C_{BA'} \sim -\frac{c_W^2}{s_W} \epsilon, \quad C_{VA'} \sim -\left(1 + \frac{c_W^2}{2} \epsilon^2 \right) \quad (\text{C.1.8})$$

$$C_{WZ} \sim 1 - \frac{s_W^2}{2}\epsilon^2, \quad C_{BZ} \sim 1 + \left(1 - \frac{s_W^2}{2}\right)\epsilon^2, \quad C_{VZ} \sim s_W\epsilon,$$

and

$$m_{A'}^2 \sim m_V^2(1 + c_W^2\epsilon^2), \quad m_Z^2 \sim \frac{m_W^2}{c_W^2} (1 + s_W^2\epsilon^2). \quad (\text{C.1.9})$$

C.1.2 Diagonalization of the fermion mass matrices

We show the diagonalization matrices of the leptons,

$$\mathcal{M}_e = \begin{pmatrix} y_1 v_H & 0 & \lambda_L v_\Phi \\ 0 & \lambda_e v_H & m_L \\ \lambda_E v_\Phi & m_E & \lambda'_e v_H \end{pmatrix}, \quad \mathcal{M}_n = \begin{pmatrix} 0 & \lambda_L v_\Phi \\ \lambda_n v_H & m_L \\ m_N & \lambda'_n v_H \end{pmatrix}, \quad (\text{C.1.10})$$

for $v_\Phi, m_N \ll v_H \lesssim m_L, m_E$. Here, we omit the second and third generations under the assumption of Eq. (6.1.10). We also assume that $m_L, m_E, m_N > 0$. The diagonalization matrices of the charged leptons are given by

$$U_{e_L} = \begin{pmatrix} 1 & 0 & 0 \\ 0 & c_{e_L} & s_{e_L} \\ 0 & -s_{e_L} & c_{e_L} \end{pmatrix} \begin{pmatrix} 1 - (\eta_{L_1}^2 + \eta_{L_2}^2)/2 & \eta_{L_1} & -\eta_{L_2} \\ -\eta_{L_1} & 1 & 0 \\ \eta_{L_2} & 0 & 1 \end{pmatrix}, \quad (\text{C.1.11})$$

$$U_{e_R} = \begin{pmatrix} 1 & 0 & 0 \\ 0 & s_{e_R} & c_{e_L} \\ 0 & c_{e_R} & -s_{e_L} \end{pmatrix} \begin{pmatrix} 1 - (\eta_{R_1}^2 + \eta_{R_2}^2)/2 & -\eta_{R_1} & \eta_{R_2} \\ \eta_{R_1} & 1 & 0 \\ -\eta_{R_2} & 0 & 1 \end{pmatrix},$$

up to the second order in $\eta := \mathcal{O}(\eta_{L_1,2}, \eta_{R_1,2})$. The first matrices diagonalize the right-lower 2×2 block of \mathcal{M}_e . The angles are given by

$$c_{e_L} = \sqrt{\frac{1}{2} \left(1 - \frac{T_{e_L}}{\sqrt{D_e}}\right)}, \quad s_{e_L} = \sigma_{e_L} \sqrt{\frac{1}{2} \left(1 + \frac{T_{e_L}}{\sqrt{D_e}}\right)}, \quad (\text{C.1.12})$$

$$c_{e_R} = \sqrt{\frac{1}{2} \left(1 + \frac{T_{e_R}}{\sqrt{D_e}}\right)}, \quad s_{e_R} = -\sigma_{e_R} \sqrt{\frac{1}{2} \left(1 - \frac{T_{e_R}}{\sqrt{D_e}}\right)},$$

where

$$S_e := m_E^2 + m_L^2 + (\lambda_e^2 + \lambda_e'^2) v_H^2, \quad D_e := S_e^2 - 4(m_L m_E - \lambda_e \lambda'_e v_H^2)^2, \quad (\text{C.1.13})$$

C.1 Details of the model

$$T_{e_L} := m_L^2 - m_E^2 + (\lambda_e^2 - \lambda'_e)^2 v_H^2, \quad T_{e_R} := m_E^2 - m_L^2 + (\lambda_e^2 - \lambda'_e)^2 v_H^2,$$

and

$$\sigma_{e_L} := \text{sign}(\lambda_e m_E + \lambda'_e m_L), \quad \sigma_{e_R} := \text{sign}(\lambda_e m_L + \lambda'_e m_E). \quad (\text{C.1.14})$$

The second matrices diagonalize the mixing between the first generation and the vector-like lepton. The singular values are given by ¹

$$m_{e_1} \simeq y_1 v_H + v_\Phi \eta_e, \quad m_{E_1} \simeq \sqrt{\frac{S_e - \sqrt{D_e}}{2}}, \quad m_{E_2} \simeq \sqrt{\frac{S_e + \sqrt{D_e}}{2}}, \quad (\text{C.1.17})$$

where

$$\eta_e := \lambda_L \lambda_E v_\Phi \left(\frac{s_{e_L} c_{e_R}}{m_{E_1}} + \frac{c_{e_L} s_{e_R}}{m_{E_2}} \right) \sim \lambda_e \lambda_L \lambda_E \frac{v_\Phi v_H}{m_L m_E} + \mathcal{O}\left(\frac{v_H^3}{m_E^3}\right). \quad (\text{C.1.18})$$

For the neutrinos, the diagonalization matrices are given by

$$U_{n_L} = \begin{pmatrix} 1 & 0 & 0 \\ 0 & c_{L_1} & s_{L_1} \\ 0 & -s_{L_1} & c_{L_1} \end{pmatrix} \begin{pmatrix} c_{L_2} & s_{L_2} & 0 \\ -s_{L_2} & c_{L_2} & 0 \\ 0 & 0 & 1 \end{pmatrix} \begin{pmatrix} 1 & 0 & 0 \\ 0 & c_{n_L} & s_{n_L} \\ 0 & -s_{n_L} & c_{n_L} \end{pmatrix}, \quad U_{n_R} = \begin{pmatrix} s_{n_R} & c_{n_R} \\ c_{n_R} & -s_{n_R} \end{pmatrix}, \quad (\text{C.1.19})$$

where

$$c_{L_1} := \frac{m_N}{\sqrt{m_N^2 + \lambda_n^2 v_H^2}}, \quad s_{L_1} := \frac{\lambda_n v_H}{\sqrt{m_N^2 + \lambda_n^2 v_H^2}}, \quad c_{L_2} := \frac{c_{L_1} m_L - s_{L_1} \lambda'_n v_H}{\tilde{m}_L}, \quad s_{L_2} := \frac{\lambda_L v_\Phi}{\tilde{m}_L}, \quad (\text{C.1.20})$$

¹The diagonal elements after the rotation by the first matrix are given by,

$$\begin{aligned} \mu_{E_1} &= \frac{\lambda_e v_H}{2 c_{e_L} s_{e_R}} \left[1 - \frac{1}{\sqrt{D_e}} \left\{ S_e + 2 \frac{\lambda'_e}{\lambda_e} (m_L m_E - \lambda_e \lambda'_e v_H^2) \right\} \right], \\ \mu_{E_2} &= \frac{\lambda_e v_H}{2 s_{e_L} c_{e_R}} \left[1 + \frac{1}{\sqrt{D_e}} \left\{ S_e + 2 \frac{\lambda'_e}{\lambda_e} (m_L m_E - \lambda_e \lambda'_e v_H^2) \right\} \right], \end{aligned} \quad (\text{C.1.15})$$

such that

$$\begin{pmatrix} c_{e_L} & s_{e_L} \\ -s_{e_L} & c_{e_L} \end{pmatrix} \begin{pmatrix} \lambda_e v_H & m_L \\ m_E & \lambda'_e v_H \end{pmatrix} \begin{pmatrix} s_{e_R} & c_{e_R} \\ c_{e_R} & -s_{e_R} \end{pmatrix} = \text{diag}(\mu_{E_1}, \mu_{E_2}), \quad (\text{C.1.16})$$

where $\mu_{E_{1,2}}$ are, in general, not positive. Under the assumption, $m_L, m_E > 0$ and $v_H \ll m_E$, $\mu_{E_a} > 0$, and thus $\mu_{E_a} = m_{E_a}$ given by Eq. (C.1.17).

with $\tilde{m}_L := \sqrt{\lambda_L^2 v_\Phi^2 + (c_{L_1} m_L - s_{L_1} \lambda'_n v_H)^2}$. The first matrix is to rotate away the $(2, 1)$ element, and then the $(1, 2)$ element is rotated away by the second matrix. The angles in the last matrix, $c_{n_{L,R}}$ and $s_{n_{L,R}}$, are given by formally replacing $\lambda_e \rightarrow 0$, $m_E \rightarrow \sqrt{m_N^2 + \lambda_n^2 v_H^2}$, $m_L \rightarrow \tilde{m}_L$ and $\lambda'_e v_H \rightarrow s_{L_1} m_L + c_{L_1} \lambda'_n v_H$ from $c_{e_{L,R}}$ and $s_{e_{L,R}}$ shown in Eq. (C.1.12). The singular values m_{N_1} and m_{N_2} are respectively obtained by the same replacement from m_{E_1} and m_{E_2} in Eq. (C.1.17). Note that the diagonalization for \mathcal{M}_n is exact, not relying on any approximation.

For $v_H \ll m_E$ and $m_L < m_E$, the mixing angles are approximately given by

$$s_{e_L} \sim v_H \frac{\lambda_e m_E + \lambda'_e m_L}{|m_E^2 - m_L^2|}, \quad s_{e_R} \sim -v_H \frac{\lambda_e m_L + \lambda'_e m_E}{|m_E^2 - m_L^2|}. \quad (\text{C.1.21})$$

The masses of the vector-like leptons are given by

$$m_{E_1} \sim m_L - v_H^2 \frac{(\lambda_e^2 + \lambda'_e^2)m_L + 2\lambda_e \lambda'_e m_E}{2(m_E^2 - m_L^2)}, \quad m_{E_2} \sim m_E + v_H^2 \frac{(\lambda_e^2 + \lambda'_e^2)m_E + \lambda_e \lambda'_e m_L}{2(m_E^2 - m_L^2)}, \quad (\text{C.1.22})$$

for $m_L < m_E$ and $m_E - m_L \gg v_H$. For the neutrinos, $\lambda_n v_H \lesssim m_N \lesssim \mathcal{O}(1)$ GeV is necessary to make the vector-like neutrino N_1 light so that the dark photon can decay. We shall assume $\lambda_n = 0$ for simplicity. The neutrino mixing angles are approximately given by

$$c_{n_L} \sim \frac{\lambda'_n v_H}{\sqrt{m_L^2 + \lambda_n'^2 v_H^2}}, \quad s_{n_L} \sim \frac{m_L}{\sqrt{m_L^2 + \lambda_n'^2 v_H^2}}, \quad c_{n_R} \sim 0, \quad s_{n_R} \sim -1, \quad (\text{C.1.23})$$

and the vector-like neutrino masses are given by

$$m_{N_1} \simeq \frac{m_N m_L}{m_L^2 + \lambda_n'^2 v_H^2}, \quad m_{N_2} \simeq \sqrt{m_L^2 + \lambda_n'^2 v_H^2}. \quad (\text{C.1.24})$$

C.1.3 Lepton couplings

The approximate forms of \mathcal{E}_A , \mathcal{N}_A and h_A are given by

$$\mathcal{E}_L \sim \begin{pmatrix} 1 - \eta_e^2/\lambda_E^2 & s_{e_L}\eta_e/\lambda_E & -c_{e_L}\eta_e/\lambda_E \\ s_{e_L}\eta_e/\lambda_E & c_{e_L}^2 & c_{e_L}s_{e_L} \\ -c_{e_L}\eta_e/\lambda_E & c_{e_L}s_{e_L} & s_{e_L}^2 \end{pmatrix}, \quad \mathcal{E}_R \sim \begin{pmatrix} \eta_e^2/\lambda_L^2 & c_{e_R}\eta_e/\lambda_L & -s_{e_R}\eta_e/\lambda_L \\ c_{e_R}\eta_e/\lambda_L & c_{e_R}^2 & -c_{e_R}s_{e_R} \\ -s_{e_R}\eta_e/\lambda_L & -s_{e_R}c_{e_R} & s_{e_R}^2 \end{pmatrix}, \quad (\text{C.1.25})$$

$$\mathcal{N}_L \sim \begin{pmatrix} 1 & 0 & 0 \\ 0 & c_{n_L}^2 & c_{n_L}s_{n_L} \\ 0 & c_{n_L}s_{n_L} & s_{n_L}^2 \end{pmatrix}, \quad \mathcal{N}_R = \begin{pmatrix} c_{n_R}^2 & -c_{n_R}s_{n_R} \\ -c_{n_R}s_{n_R} & s_{n_R}^2 \end{pmatrix},$$

$$h_L \sim \begin{pmatrix} 1 - \frac{1}{2}(\eta_{L_1}^2 + \eta_{L_2}^2 + s_{L_2}^2) + s_{L_2}(c_{e_L}\eta_{L_1} - s_{e_L}\eta_{L_2}) & \eta_{L_1} - c_{e_L}s_{L_2} & -\eta_{L_2} - s_{e_L}s_{L_2} \\ c_{n_L}(s_{L_2} - c_{e_L}\eta_{L_1} + s_{e_L}\eta_{L_2}) & c_{e_L}c_{n_L} & s_{e_L}c_{n_L} \\ s_{n_L}(s_{L_2} - c_{e_L}\eta_{L_1} + s_{e_L}\eta_{L_2}) & c_{e_L}s_{n_L} & s_{e_L}s_{n_L} \end{pmatrix}, \quad (\text{C.1.26})$$

$$h_R \sim \begin{pmatrix} c_{n_R}(c_{e_R}\eta_{R_1} + s_{e_R}\eta_{R_2}) & c_{e_R}c_{n_R} & -c_{n_R}s_{e_R} \\ -s_{n_R}(c_{e_R}\eta_{R_1} + s_{e_R}\eta_{R_2}) & -c_{e_R}s_{n_R} & s_{e_R}s_{n_R} \end{pmatrix},$$

up to $\mathcal{O}(\eta^2)$ and $\mathcal{O}(s_{L_2}^2)$. Here, we take $s_{L_1} = 0$ and the sub-dominant contributions in the lower-right 2×2 block are omitted. For the Z' -boson couplings,

$$Q'_{e_L} \sim \begin{pmatrix} \eta_{L_1}^2 + \eta_{L_2}^2 & -\eta_{L_1} & \eta_{L_2} \\ -\eta_{L_1} & 1 & 0 \\ \eta_{L_2} & 0 & 1 \end{pmatrix}, \quad Q'_{e_R} \sim \begin{pmatrix} \eta_{R_1}^2 + \eta_{R_2}^2 & \eta_{R_1} & -\eta_{R_2} \\ \eta_{R_1} & 1 & 0 \\ -\eta_{R_2} & 0 & 1 \end{pmatrix}, \quad (\text{C.1.27})$$

$$Q'_{n_L} \sim \begin{pmatrix} s_{L_2}^2 & -c_{n_L}s_{L_2} & -s_{n_L}s_{L_2} \\ -c_{n_L}s_{L_2} & 1 & 0 \\ -s_{n_L}s_{L_2} & 0 & 1 \end{pmatrix}, \quad Q'_{n_R} = \begin{pmatrix} 1 & 0 \\ 0 & 1 \end{pmatrix}.$$

The Yukawa couplings are given by

$$Y_e^\chi \sim \begin{pmatrix} 2\eta_e & c_{e_R}\lambda_L & -s_{e_R}\lambda_L \\ -s_{e_L}\lambda_E & \lambda_E s_{e_L}\eta_{R_1} + \lambda_L c_{e_R}\eta_{L_1} & -\lambda_E s_{e_L}\eta_{R_2} - \lambda_L s_{e_R}\eta_{L_1} \\ c_{e_L}\lambda_E & -\lambda_E c_{e_L}\eta_{R_1} - \lambda_L c_{e_R}\eta_{L_2} & \lambda_E c_{e_L}\eta_{R_2} + \lambda_L s_{e_R}\eta_{L_2} \end{pmatrix}, \quad (\text{C.1.28})$$

$$Y_n^\chi \sim \lambda_L \begin{pmatrix} c_{n_R} & -s_{n_R} \\ c_{n_L} c_{n_R} s_{L_2} & -c_{n_L} s_{n_R} s_{L_2} \\ s_{n_L} c_{n_R} s_{L_2} & -s_{n_L} s_{n_R} s_{L_2} \end{pmatrix}.$$

C.2 Loop functions

The loop functions for Δa_ℓ are given by

$$F_Z(x) = \frac{5x^4 - 14x^3 + 39x^2 - 38x + 8 - 18x^2 \ln(x)}{12(1-x)^4}, \quad G_Z(x) = \frac{x^3 + 3x - 4 - 6x \ln(x)}{2(1-x)^3}, \quad (\text{C.2.1})$$

and

$$F_S(y) = -\frac{y^3 - 6y^2 + 3y + 6y \ln(y) + 2}{6(1-y)^4}, \quad G_S(y) = \frac{y^2 - 4y + 2 \ln(y) + 3}{(1-y)^3}. \quad (\text{C.2.2})$$

The loop functions for the oblique parameters are given by

$$\theta_+(y_1, y_2) = y_1 + y_2 - \frac{2y_1 y_2}{y_1 - y_2} \log \frac{y_1}{y_2}, \quad \theta_-(y_1, y_2) = 2\sqrt{y_1 y_2} \left(\frac{y_1 + y_2}{y_1 - y_2} \log \frac{y_1}{y_2} - 2 \right), \quad (\text{C.2.3})$$

$$\chi_+(y_1, y_2) = \frac{y_1 + y_2}{2} - \frac{(y_1 - y_2)^2}{3} + \left(\frac{(y_1 - y_2)^3}{6} - \frac{1}{2} \frac{y_1^2 + y_2^2}{y_1 - y_2} \right) \log \frac{y_1}{y_2} \quad (\text{C.2.4})$$

$$\begin{aligned} \chi_-(y_1, y_2) = & -\sqrt{y_1 y_2} \left[2 + \left(y_1 - y_2 - \frac{y_1 + y_2}{y_1 - y_2} \right) \log \frac{y_1}{y_2} + \frac{f(y_1, y_1) + f(y_2, y_2)}{2} - f(y_1, y_2) \right], \\ & + \frac{y_1 - 1}{6} f(y_1, y_1) + \frac{y_2 - 1}{6} f(y_2, y_2) + \left(\frac{1}{3} - \frac{y_1 + y_2}{6} - \frac{(y_1 - y_2)^2}{6} \right) f(y_1, y_2), \end{aligned} \quad (\text{C.2.5})$$

and

$$\psi_+(y_1, y_2) = \frac{2y_1 + 10y_2}{3} + \frac{1}{3} \log \frac{y_1}{y_2} + \frac{y_1 - 1}{6} f(y_1, y_1) + \frac{5y_2 + 1}{6} f(y_2, y_2), \quad (\text{C.2.6})$$

$$\psi_-(y_1, y_2) = -\sqrt{y_1 y_2} \left(4 + \frac{f(y_1, y_1) + f(y_2, y_2)}{2} \right). \quad (\text{C.2.7})$$

Here, the function f is defined as

$$f(y_1, y_2) = \begin{cases} \sqrt{d} \log \left| \frac{y_1 + y_2 - 1 + \sqrt{d}}{y_1 + y_2 - 1 - \sqrt{d}} \right| & d > 0 \\ 0 & d = 0 \\ -2\sqrt{|d|} \left[\tan^{-1} \frac{y_1 - y_2 + 1}{\sqrt{|d|}} - \tan^{-1} \frac{y_1 - y_2 - 1}{\sqrt{|d|}} \right] & d < 0 \end{cases} \quad (\text{C.2.8})$$

with $d = (1 + y_1 - y_2)^2 - 4y_1$.

Bibliography

- [1] Aaboud, M., et al. *Search for heavy resonances decaying into a W or Z boson and a Higgs boson in final states with leptons and b-jets in 36 fb⁻¹ of $\sqrt{s} = 13$ TeV pp collisions with the ATLAS detector*. JHEP **03** (2018), 174. [Erratum: JHEP 11, 051 (2018)].
- [2] Aaboud, M., et al. *Search for pair production of Higgs bosons in the b \bar{b} b \bar{b} final state using proton-proton collisions at $\sqrt{s} = 13$ TeV with the ATLAS detector*. JHEP **01** (2019), 030.
- [3] Aad, G., et al. *Observation of a new particle in the search for the Standard Model Higgs boson with the ATLAS detector at the LHC*. Phys. Lett. B **716** (2012), 1–29.
- [4] Aad, G., et al. *Observation of a new particle in the search for the Standard Model Higgs boson with the ATLAS detector at the LHC*. Phys. Lett. B **716** (2012), 1–29.
- [5] Aad, G., et al. *A search for heavy Higgs bosons decaying into vector bosons in same-sign two-lepton final states in pp collisions at $\sqrt{s} = 13$ TeV with the ATLAS detector*. JHEP **07** (2023), 200.
- [6] Aad, G., et al. *Search for t \bar{t} H/A → t \bar{t} t \bar{t} production in the multilepton final state in proton–proton collisions at $\sqrt{s} = 13$ TeV with the ATLAS detector*. JHEP **07** (2023), 203.

BIBLIOGRAPHY

- [7] Aaij, R., et al. *Search for Dark Photons Produced in 13 TeV pp Collisions.* Phys. Rev. Lett. **120** (2018), 061801.
- [8] Aaij, R., et al. *Measurement of lepton universality parameters in $B^+ \rightarrow K^+ \ell^+ \ell^-$ and $B^0 \rightarrow K^{*0} \ell^+ \ell^-$ decays.* Phys. Rev. D **108** (2023), 032002.
- [9] Aaltonen, T., et al. *High-precision measurement of the W boson mass with the CDF II detector.* Science **376** (2022), 170–176.
- [10] Abdallah, W., Ashry, M., Kawamura, J., and Moursy, A. *Semivisible dark photon in a model with vectorlike leptons for the $(g-2)_e, \mu$ and W -boson mass anomalies.* Phys. Rev. D **109** (2024), 015031.
- [11] Abdallah, W., Awad, A., Khalil, S., and Okada, H. *Muon Anomalous Magnetic Moment and mu -> e gamma in B-L Model with Inverse Seesaw.* Eur. Phys. J. C **72** (2012), 2108.
- [12] Abdallah, W., Gandhi, R., and Roy, S. *Understanding the MiniBooNE and the muon and electron $g - 2$ anomalies with a light Z' and a second Higgs doublet.* JHEP **12** (2020), 188.
- [13] Abdallah, W., Hammad, A., Khalil, S., and Moretti, S. *Search for Mono-Higgs Signals at the LHC in the B-L Supersymmetric Standard Model.* Phys. Rev. D **95** (2017), 055019.
- [14] Abdallah, W., Hammad, A., Khalil, S., and Moretti, S. *Searching for Charged Higgs Bosons in the B – L Supersymmetric Standard Model at the High Luminosity Large Hadron Collider.* Phys. Lett. B **788** (2019), 65–69.
- [15] Abdallah, W., Khalil, S., and Moretti, S. *Double Higgs peak in the minimal SUSY B-L model.* Phys. Rev. D **91** (2015), 014001.

BIBLIOGRAPHY

- [16] Abdelalim, A. A., Das, B., Khalil, S., and Moretti, S. *Di-photon decay of a light Higgs state in the BLSSM*. Nucl. Phys. B **985** (2022), 116013.
- [17] Abdullahi, A. M., Hostert, M., Massaro, D., and Pascoli, S. *Semi-Visible Dark Photon Phenomenology at the GeV Scale*. Phys. Rev. D **108** (2023), 015032.
- [18] Abe, T., et al. *Belle II Technical Design Report* (2010).
- [19] Abi, B., et al. *Measurement of the Positive Muon Anomalous Magnetic Moment to 0.46 ppm*. Phys. Rev. Lett. **126** (2021), 141801.
- [20] Abi, B., et al. *Measurement of the Positive Muon Anomalous Magnetic Moment to 0.46 ppm*. Phys. Rev. Lett. **126** (2021), 141801.
- [21] Abi, B., et al. *Measurement of the Positive Muon Anomalous Magnetic Moment to 0.46 ppm*. Phys. Rev. Lett. **126** (2021), 141801.
- [22] Adam, J., et al. *A limit for the mu → e gamma decay from the MEG experiment*. Nucl. Phys. B **834** (2010), 1–12.
- [23] Adhikary, A., Bhattacherjee, B., Godbole, R. M., Khan, N., and Kulkarni, S. *Searching for heavy Higgs in supersymmetric final states at the LHC*. JHEP **04** (2021), 284.
- [24] Aebischer, J., Altmannshofer, W., Guadagnoli, D., Reboud, M., Stangl, P., and Straub, D. M. *B-decay discrepancies after Moriond 2019*. Eur. Phys. J. C **80** (2020), 252.
- [25] Aguillard, D. P., et al. *Measurement of the Positive Muon Anomalous Magnetic Moment to 0.20 ppm*. Phys. Rev. Lett. **131** (2023), 161802.
- [26] Ahmad, Q., et al. *Direct evidence for neutrino flavor transformation from neutral current interactions in the Sudbury Neutrino Observatory*. Phys. Rev. Lett. **89** (2002), 011301.

BIBLIOGRAPHY

- [27] Ahmad, Q. R. e. a. *Measurement of the Rate of $\nu_e + d \rightarrow pp + e^-$ Interactions Produced by 8B Solar Neutrinos at the Sudbury Neutrino Observatory.* Phys. Rev. Lett. **87** (2001), 071301.
- [28] Ahmad, Q. R. e. a. *Direct Evidence for Neutrino Flavor Transformation from Neutral-Current Interactions in the Sudbury Neutrino Observatory.* Phys. Rev. Lett. **89** (2002), 011301.
- [29] Ahn, M., et al. *Indications of neutrino oscillation in a 250 km long baseline experiment.* Phys. Rev. Lett. **90** (2003), 041801.
- [30] Aitchison, I. J. R. *Supersymmetry and the MSSM: An Elementary introduction* (2005).
- [31] Aitchison, I. J. R. *Supersymmetry in Particle Physics. An Elementary Introduction.* Cambridge University Press, Cambridge, 2007.
- [32] Algueró, M., Capdevila, B., Crivellin, A., Descotes-Genon, S., Masjuan, P., Matias, J., Novoa Brunet, M., and Virto, J. *Emerging patterns of New Physics with and without Lepton Flavour Universal contributions.* Eur. Phys. J. C **79** (2019), 714. [Addendum: Eur.Phys.J.C 80, 511 (2020)].
- [33] Ali, M. I., Chakraborti, M., Chattopadhyay, U., and Mukherjee, S. *Muon and electron ($g - 2$) anomalies with non-holomorphic interactions in MSSM.* Eur. Phys. J. C **83** (2023), 60.
- [34] Allanach, B., Queiroz, F. S., Strumia, A., and Sun, S. *Z' models for the LHCb and $g - 2$ muon anomalies.* Phys. Rev. **D93** (2016), 055045. [Erratum: Phys. Rev.D95,no.11,119902(2017)].
- [35] Alok, A. K., Dighe, A., Gangal, S., and Kumar, D. *Continuing search for new physics in $b \rightarrow s\mu\mu$ decays: two operators at a time.* JHEP **06** (2019), 089.

- [36] Alonso, R., Dhen, M., Gavela, M. B., and Hambye, T. *Muon conversion to electron in nuclei in type-I seesaw models.* JHEP **01** (2013), 118.
- [37] Altmannshofer, W., Carena, M., and Crivellin, A. *$L_\mu - L_\tau$ theory of Higgs flavor violation and $(g-2)_\mu$.* Phys. Rev. **D94** (2016), 095026.
- [38] Altmannshofer, W., et al. *The Belle II Physics Book.* PTEP **2019** (2019), 123C01. [Erratum: PTEP 2020, 029201 (2020)].
- [39] Alwall, J., Herquet, M., Maltoni, F., Mattelaer, O., and Stelzer, T. *MadGraph 5 : Going Beyond.* JHEP **06** (2011), 128.
- [40] An, F., et al. *Observation of electron-antineutrino disappearance at Daya Bay.* Phys. Rev. Lett. **108** (2012), 171803.
- [41] Anastasi, A., et al. *Limit on the production of a low-mass vector boson in $e^+e^- \rightarrow U\gamma$, $U \rightarrow e^+e^-$ with the KLOE experiment.* Phys. Lett. B **750** (2015), 633–637.
- [42] Andreev, Y. M., et al. *Constraints on New Physics in Electron $g-2$ from a Search for Invisible Decays of a Scalar, Pseudoscalar, Vector, and Axial Vector.* Phys. Rev. Lett. **126** (2021), 211802.
- [43] Antusch, S., Biggio, C., Fernandez-Martinez, E., Gavela, M. B., and Lopez-Pavon, J. *Unitarity of the Leptonic Mixing Matrix.* JHEP **10** (2006), 084.
- [44] Antusch, S., Fischer, O., Hammad, A., and Scherb, C. *Explaining excesses in four-leptons at the LHC with a double peak from a CP violating Two Higgs Doublet Model.* JHEP **08** (2022), 224.
- [45] Aoyama, T., et al. *The anomalous magnetic moment of the muon in the Standard Model.* Phys. Rept. **887** (2020), 1–166.

BIBLIOGRAPHY

- [46] Aoyama, T., Hayakawa, M., Kinoshita, T., and Nio, M. *Complete Tenth-Order QED Contribution to the Muon $g - 2$.* Phys. Rev. Lett. **109** (2012), 111808.
- [47] Aoyama, T., Kinoshita, T., and Nio, M. *Theory of the Anomalous Magnetic Moment of the Electron.* Atoms **7** (2019), 28.
- [48] Appelquist, T., Dobrescu, B. A., and Hopper, A. R. *Nonexotic Neutral Gauge Bosons.* Phys. Rev. D **68** (2003), 035012.
- [49] Arbey, A., Hurth, T., Mahmoudi, F., Martínez Santos, D., and Neshatpour, S. *Update on the $b \rightarrow s$ anomalies.* Phys. Rev. D **100** (2019), 015045.
- [50] Arkani-Hamed, N., Dimopoulos, S., Dvali, G. R., and March-Russell, J. *Neutrino masses from large extra dimensions.* Phys. Rev. D **65** (2001), 024032.
- [51] Artamonov, A. V., et al. *Study of the decay $K^+ \rightarrow \pi^+ \nu \bar{\nu}$ in the momentum region $140 < P_\pi < 199$ MeV/c.* Phys. Rev. D **79** (2009), 092004.
- [52] Ashry, M. *TeV Scale Left-Right Symmetric Model with Minimal Higgs Sector.* Master's thesis, Faculty of Science, Cairo University, 2015.
- [53] Ashry, M., Ezzat, K., and Khalil, S. *Search for Heavy Neutral Higgs Bosons at the LHC.* In *Beyond Standard Model: From Theory to Experiment* (2021).
- [54] Ashry, M., Ezzat, K., and Khalil, S. *Muon $g-2$ anomaly in a left-right model with an inverse seesaw mechanism.* Phys. Rev. D **107** (2023), 055044.
- [55] Ashry, M., and Khalil, S. *Phenomenological aspects of a TeV-scale alternative left-right model.* Phys. Rev. D **91** (2015), 015009. [Addendum: Phys. Rev. D **96**, 059901 (2017)].
- [56] Ashry, M., Khalil, S., and Moretti, S. *Searching for a heavy neutral CP-even Higgs boson in the BLSSM at the LHC Run 3 and HL-LHC.* Eur. Phys. J. C **84** (2024), 433.

- [57] Aulakh, C. S., Benakli, K., and Senjanovic, G. *Reconciling supersymmetry and left-right symmetry*. Phys. Rev. Lett. **79** (1997), 2188–2191.
- [58] Aulakh, C. S., Melfo, A., and Senjanovic, G. *Minimal supersymmetric left-right model*. Phys. Rev. **D57** (1998), 4174–4178.
- [59] Babu, K. S., Kolda, C. F., and March-Russell, J. *Implications of generalized Z - Z-prime mixing*. Phys. Rev. D **57** (1998), 6788–6792.
- [60] Babu, K. S., and Patra, A. *Higgs Boson Spectra in Supersymmetric Left-Right Models*. Phys. Rev. **D93** (2016), 055030.
- [61] Badziak, M., and Sakurai, K. *Explanation of electron and muon g – 2 anomalies in the MSSM*. JHEP **10** (2019), 024.
- [62] Baer, H., and Tata, X. *Weak scale supersymmetry: From superfields to scattering events*. Cambridge University Press, 5 2006.
- [63] Baglio, J., Campanario, F., Glaus, S., Mühlleitner, M., Spira, M., and Streicher, J. *Gluon fusion into Higgs pairs at NLO QCD and the top mass scheme*. Eur. Phys. J. C **79** (2019), 459.
- [64] Bahl, H., Bechtle, P., Heinemeyer, S., Liebler, S., Stefaniak, T., and Weiglein, G. *HL-LHC and ILC sensitivities in the hunt for heavy Higgs bosons*. Eur. Phys. J. C **80** (2020), 916.
- [65] Bailin, D., and Love, A. *Supersymmetric Gauge Field Theory and String Theory*. Taylor & Francis, 1994.
- [66] Baldini, A. M., et al. *Search for the lepton flavour violating decay $\mu^+ \rightarrow e^+ \gamma$ with the full dataset of the MEG experiment*. Eur. Phys. J. C **76** (2016), 434.
- [67] Banerjee, S., Mitra, M., and Spannowsky, M. *Searching for a Heavy Higgs boson in a Higgs-portal B – L Model*. Phys. Rev. D **92** (2015), 055013.

BIBLIOGRAPHY

- [68] Barbieri, R., Nanopoulos, D. V., Morchio, G., and Strocchi, F. *Neutrino Masses in Grand Unified Theories*. Phys. Lett. B **90** (1980), 91–97.
- [69] Basso, L. *Phenomenology of the minimal $B-L$ extension of the Standard Model at the LHC*. PhD thesis, Southampton U., 2011.
- [70] Basso, L. *The Higgs sector of the minimal SUSY $B-L$ model*. Adv. High Energy Phys. **2015** (2015), 980687.
- [71] Basso, L., Moretti, S., and Pruna, G. M. *A Renormalisation Group Equation Study of the Scalar Sector of the Minimal $B-L$ Extension of the Standard Model*. Phys. Rev. D **82** (2010), 055018.
- [72] Batell, B., Freitas, A., Ismail, A., and McKeen, D. *Flavor-specific scalar mediators*. Phys. Rev. D **98** (2018), 055026.
- [73] Batell, B., Lange, N., McKeen, D., Pospelov, M., and Ritz, A. *Muon anomalous magnetic moment through the leptonic Higgs portal*. Phys. Rev. D **95** (2017), 075003.
- [74] Batley, J. R., et al. *Search for the dark photon in π^0 decays*. Phys. Lett. B **746** (2015), 178–185.
- [75] Bauer, M., Neubert, M., Renner, S., Schnubel, M., and Thamm, A. *Axionlike Particles, Lepton-Flavor Violation, and a New Explanation of a_μ and a_e* . Phys. Rev. Lett. **124** (2020), 211803.
- [76] Bechtle, P., Brein, O., Heinemeyer, S., Stål, O., Stefaniak, T., Weiglein, G., and Williams, K. E. *HiggsBounds – 4: Improved Tests of Extended Higgs Sectors against Exclusion Bounds from LEP, the Tevatron and the LHC*. Eur. Phys. J. C **74** (2014), 2693.

- [77] Bechtle, P., Heinemeyer, S., Stål, O., Stefaniak, T., and Weiglein, G. *HiggsSignals: Confronting arbitrary Higgs sectors with measurements at the Tevatron and the LHC*. Eur. Phys. J. C **74** (2014), 2711.
- [78] Bennett, G. W., et al. *Measurement of the negative muon anomalous magnetic moment to 0.7 ppm*. Phys. Rev. Lett. **92** (2004), 161802.
- [79] Bhattacharyya, S. *Heavy Higgs boson searches at the LHC in light of a left-right symmetric model*. Phys. Rev. D **109** (2024), 015034.
- [80] Bigaran, I., and Volkas, R. R. *Getting chirality right: Single scalar leptoquark solutions to the $(g - 2)_{e,\mu}$ puzzle*. Phys. Rev. D **102** (2020), 075037.
- [81] Bijnens, J., Hermansson-Truedsson, N., and Rodríguez-Sánchez, A. *Short-distance constraints for the HLbL contribution to the muon anomalous magnetic moment*. Phys. Lett. **B798** (2019), 134994.
- [82] Bjorken, J. D., and Drell, S. D. *Relativistic quantum mechanics*. International series in pure and applied physics. McGraw-Hill, New York, NY, 1964.
- [83] Bjorken, J. D., Ecklund, S., Nelson, W. R., Abashian, A., Church, C., Lu, B., Mo, L. W., Nunamaker, T. A., and Rassmann, P. *Search for Neutral Metastable Penetrating Particles Produced in the SLAC Beam Dump*. Phys. Rev. D **38** (1988), 3375.
- [84] Blum, T., Christ, N., Hayakawa, M., Izubuchi, T., Jin, L., Jung, C., and Lehner, C. *The hadronic light-by-light scattering contribution to the muon anomalous magnetic moment from lattice QCD*. Phys. Rev. Lett. **124** (2020), 132002.
- [85] Bolton, P. D., Deppisch, F. F., and Bhupal Dev, P. S. *Neutrinoless double beta decay versus other probes of heavy sterile neutrinos*. JHEP **03** (2020), 170.

BIBLIOGRAPHY

- [86] Borah, D., Dutta, M., Mahapatra, S., and Sahu, N. *Lepton anomalous magnetic moment with singlet-doublet fermion dark matter in a scotogenic $U(1)L\mu-L\tau$ model.* Phys. Rev. D **105** (2022), 015029.
- [87] Borah, D., Patra, S., and Sarkar, U. *TeV scale Left Right Symmetry with spontaneous D-parity breaking.* Phys. Rev. D **83** (2011), 035007.
- [88] Borah, D., and Yajnik, U. A. *Supersymmetric Left-Right models with Gauge Coupling Unification and Fermion Mass Universality.* Phys. Rev. D **83** (2011), 095004.
- [89] Borsanyi, S., et al. *Leading hadronic contribution to the muon magnetic moment from lattice QCD.* Nature **593** (2021), 51–55.
- [90] Botella, F. J., Cornet-Gomez, F., and Nebot, M. *Electron and muon $g - 2$ anomalies in general flavour conserving two Higgs doublets models.* Phys. Rev. D **102** (2020), 035023.
- [91] Boubaa, D., Khalil, S., Moretti, S., and Un, C. S. *Explaining the $R(D)$ and $R(D^*)$ anomalies in the $B-L$ supersymmetric standard model with inverse seesaw mechanism.* Phys. Rev. D **107** (2023), 075024.
- [92] Braam, F., and Reuter, J. *A Simplified Scheme for GUT-inspired Theories with Multiple Abelian Factors.* Eur. Phys. J. C **72** (2012), 1885.
- [93] Brdar, V., and Smirnov, A. Y. *Low Scale Left-Right Symmetry and Naturally Small Neutrino Mass.* JHEP **02** (2019), 045.
- [94] Cao, J., Meng, L., and Yue, Y. *Electron and muon anomalous magnetic moments in the $Z3$ -NMSSM.* Phys. Rev. D **108** (2023), 035043.
- [95] Cárcamo Hernández, A. E., King, S. F., Lee, H., and Rowley, S. J. *Is it possible to explain the muon and electron $g - 2$ in a Z model?* Phys. Rev. D **101** (2020), 115016.

- [96] Carena, M., Daleo, A., Dobrescu, B. A., and Tait, T. M. P. *Z' gauge bosons at the Tevatron*. Phys. Rev. D **70** (2004), 093009.
- [97] Carrazza, S., Degrande, C., Iranipour, S., Rojo, J., and Ubiali, M. *Can New Physics hide inside the proton?* Phys. Rev. Lett. **123** (2019), 132001.
- [98] Casas, J., and Ibarra, A. *Oscillating neutrinos and $\mu \rightarrow e, \gamma$* . Nuclear Physics B **618** (2001), 171–204.
- [99] Cavoto, G., Papa, A., Renga, F., Ripicci, E., and Voena, C. *The quest for $\mu \rightarrow e\gamma$ and its experimental limiting factors at future high intensity muon beams*. Eur. Phys. J. C **78** (2018), 37.
- [100] Cazzaniga, C., et al. *Probing the explanation of the muon ($g-2$) anomaly and thermal light dark matter with the semi-visible dark photon channel*. Eur. Phys. J. C **81** (2021), 959.
- [101] Chang, J., Cheung, K., Lee, J. S., Lu, C.-T., and Park, J. *Higgs-boson-pair production $H(\rightarrow bb)H(\rightarrow \gamma\gamma)$ from gluon fusion at the HL-LHC and HL-100 TeV hadron collider*. Phys. Rev. D **100** (2019), 096001.
- [102] Chankowski, P. H., Pokorski, S., and Wagner, J. *Z-prime and the Appelquist-Carrazzone decoupling*. Eur. Phys. J. C**47** (2006), 187–205.
- [103] Chatrchyan, S., et al. *Observation of a New Boson at a Mass of 125 GeV with the CMS Experiment at the LHC*. Phys. Lett. B **716** (2012), 30–61.
- [104] Chatrchyan, S., et al. *Observation of a new boson at a mass of 125 GeV with the CMS experiment at the LHC*. Phys. Lett. B**716** (2012), 30–61.
- [105] Chatrchyan, S., et al. *Observation of a new boson at a mass of 125 GeV with the CMS experiment at the LHC*. Phys.Lett. **B716** (2012), 30–61.

BIBLIOGRAPHY

- [106] Chen, K.-F., Chiang, C.-W., and Yagyu, K. *An explanation for the muon and electron $g - 2$ anomalies and dark matter.* JHEP **09** (2020), 119.
- [107] Chen, X., Xu, Y., Wu, Y., Kuang, Y.-P., Wang, Q., Chen, H., Hsu, S.-C., Hu, Z., and Li, C. *Search for a generic heavy Higgs at the LHC.* Phys. Lett. B **804** (2020), 135358.
- [108] Cheng, T. P., and Li, L. F. *Gauge theory of elementary particle physics.* Oxford University Press, Oxford, UK, 1984.
- [109] Chernyavskaya, N. *Di-Higgs searches at the LHC.* In *55th Rencontres de Moriond on Electroweak Interactions and Unified Theories* (2 2023).
- [110] Ciccolini, M., Denner, A., and Dittmaier, S. *Electroweak and QCD corrections to Higgs production via vector-boson fusion at the LHC.* Phys. Rev. D **77** (2008), 013002.
- [111] Ciuchini, M., Coutinho, A. M., Fedele, M., Franco, E., Paul, A., Silvestrini, L., and Valli, M. *New Physics in $b \rightarrow s\ell^+\ell^-$ confronts new data on Lepton Universality.* Eur. Phys. J. C **79** (2019), 719.
- [112] Colangelo, G., Hagelstein, F., Hoferichter, M., Laub, L., and Stoffer, P. *Longitudinal short-distance constraints for the hadronic light-by-light contribution to $(g - 2)_\mu$ with large- N_c Regge models.* JHEP **03** (2020), 101.
- [113] Colangelo, G., Hoferichter, M., Procura, M., and Stoffer, P. *Dispersion relation for hadronic light-by-light scattering: two-pion contributions.* JHEP **04** (2017), 161.
- [114] Colangelo, G., Hoferichter, M., and Stoffer, P. *Two-pion contribution to hadronic vacuum polarization.* JHEP **02** (2019), 006.

- [115] Coleman, S. R., and Mandula, J. *All Possible Symmetries of the S Matrix*. Phys. Rev. **159** (1967), 1251–1256.
- [116] Conte, E., Dumont, B., Fuks, B., and Wymant, C. *Designing and recasting LHC analyses with MadAnalysis 5*. Eur. Phys. J. **C74** (2014), 3103.
- [117] Conte, E., Fuks, B., and Serret, G. *MadAnalysis 5, A User-Friendly Framework for Collider Phenomenology*. Comput. Phys. Commun. **184** (2013), 222–256.
- [118] Cornella, C., Paradisi, P., and Sumensari, O. *Hunting for ALPs with Lepton Flavor Violation*. JHEP **01** (2020), 158.
- [119] Cortina Gil, E., et al. *Search for production of an invisible dark photon in π^0 decays*. JHEP **05** (2019), 182.
- [120] Cortina Gil, E., et al. *Search for a feebly interacting particle X in the decay $K^+ \rightarrow \pi^+ X$* . JHEP **03** (2021), 058.
- [121] Cortina Gil, E., et al. *Search for π^0 decays to invisible particles*. JHEP **02** (2021), 201.
- [122] Cox, P., Kusenko, A., Sumensari, O., and Yanagida, T. T. *SU(5) Unification with TeV-scale Leptoquarks*. JHEP **03** (2017), 035.
- [123] Crivellin, A., Hoferichter, M., and Schmidt-Wellenburg, P. *Combined explanations of $(g - 2)_{\mu,e}$ and implications for a large muon EDM*. Phys. Rev. D **98** (2018), 113002.
- [124] Curtin, D., Essig, R., Gori, S., and Shelton, J. *Illuminating Dark Photons with High-Energy Colliders*. JHEP **02** (2015), 157.
- [125] Czarnecki, A., Marciano, W. J., and Vainshtein, A. *Refinements in electroweak contributions to the muon anomalous magnetic moment*. Phys. Rev. **D67** (2003), 073006. [Erratum: Phys. Rev. **D73**, 119901 (2006)].

BIBLIOGRAPHY

- [126] Darmé, L., Kowalska, K., Roszkowski, L., and Sessolo, E. M. *Flavor anomalies and dark matter in SUSY with an extra U(1)*. JHEP **10** (2018), 052.
- [127] Datta, A., Kumar, J., and London, D. *The B anomalies and new physics in $b \rightarrow se^+e^-$* . Phys. Lett. B **797** (2019), 134858.
- [128] Davidson, S., and Haber, H. E. *Basis-independent methods for the two-Higgs-doublet model*. Phys. Rev. D **72** (2005), 035004. [Erratum: Phys.Rev.D 72, 099902 (2005)].
- [129] Davidson, S., Kuno, Y., and Yamanaka, M. *Selecting $\mu \rightarrow e$ conversion targets to distinguish lepton flavour-changing operators*. Phys. Lett. B **790** (2019), 380–388.
- [130] Davier, M., Hoecker, A., Malaescu, B., and Zhang, Z. *Reevaluation of the hadronic vacuum polarisation contributions to the Standard Model predictions of the muon $g - 2$ and $\alpha(m_Z^2)$ using newest hadronic cross-section data*. Eur. Phys. J. C**77** (2017), 827.
- [131] Davier, M., Hoecker, A., Malaescu, B., and Zhang, Z. *A new evaluation of the hadronic vacuum polarisation contributions to the muon anomalous magnetic moment and to $\alpha(m_Z^2)$* . Eur. Phys. J. C**80** (2020), 241.
- [132] Davier, M., and Nguyen Ngoc, H. *An Unambiguous Search for a Light Higgs Boson*. Phys. Lett. B **229** (1989), 150–155.
- [133] Davoudiasl, H., and Marciano, W. J. *Tale of two anomalies*. Phys. Rev. D**98** (2018), 075011.
- [134] De, B., Das, D., Mitra, M., and Sahoo, N. *Magnetic moments of leptons, charged lepton flavor violations and dark matter phenomenology of a minimal radiative Dirac neutrino mass model*. JHEP **08** (2022), 202.

- [135] de Favereau, J., Delaere, C., Demin, P., Giannanco, A., Lemaître, V., Mertens, A., and Selvaggi, M. *DELPHES 3, A modular framework for fast simulation of a generic collider experiment.* JHEP **02** (2014), 057.
- [136] de Giorgi, A., Merlo, L., and Pokorski, S. *The Low-Scale Seesaw Solution to the M_W and $(g - 2)_\mu$ Anomalies.* Fortsch. Phys. **71** (2023), 2300020.
- [137] Delle Rose, L., Khalil, S., and Moretti, S. *Explaining electron and muon $g - 2$ anomalies in an Aligned 2-Higgs Doublet Model with right-handed neutrinos.* Phys. Lett. B **816** (2021), 136216.
- [138] Dermisek, R., Hermanek, K., and McGinnis, N. *Muon $g-2$ in two-Higgs-doublet models with vectorlike leptons.* Phys. Rev. D **104** (2021), 055033.
- [139] Dermisek, R., Kawamura, J., Lunghi, E., McGinnis, N., and Shin, S. *Leptonic cascade decays of a heavy Higgs boson through vectorlike leptons at the LHC.* JHEP **10** (2022), 138.
- [140] Dermisek, R., and Raval, A. *Explanation of the Muon $g-2$ Anomaly with Vectorlike Leptons and its Implications for Higgs Decays.* Phys. Rev. D **88** (2013), 013017.
- [141] Deshpande, N., Gunion, J., Kayser, B., and Olness, F. I. *Left-right symmetric electroweak models with triplet Higgs.* Phys. Rev. D **44** (1991), 837–858.
- [142] Dev, P. S. B., and Mohapatra, R. N. *TeV Scale Inverse Seesaw in $SO(10)$ and Leptonic Non-Unitarity Effects.* Phys. Rev. D **81** (2010), 013001.
- [143] Dev, P. S. B., Mohapatra, R. N., and Zhang, Y. *Explanation of the 95 GeV $\gamma\gamma$ and bb^- excesses in the minimal left-right symmetric model.* Phys. Lett. B **849** (2024), 138481.

BIBLIOGRAPHY

- [144] Dinh, S. Q., and Tran, H. M. *Muon g-2 and semileptonic B decays in the Bélanger-Delaunay-Westhoff model with gauge kinetic mixing.* Phys. Rev. D **104** (2021), 115009.
- [145] Djouadi, A. *The Anatomy of electro-weak symmetry breaking. II. The Higgs bosons in the minimal supersymmetric model.* Phys.Rept. **459** (2008), 1–241.
- [146] Djouadi, A., Kalinowski, J., Ohmann, P., and Zerwas, P. M. *Heavy SUSY Higgs bosons at e^+e^- linear colliders.* Z. Phys. C **74** (1997), 93–111.
- [147] Drees, M., Godbole, R., and Roy, P. *Theory and phenomenology of sparticles: An account of four-dimensional N=1 supersymmetry in high energy physics.* Hackensack, USA: World Scientific (2004) 555 p (2004).
- [148] Duerr, M., Ferber, T., Garcia-Cely, C., Hearty, C., and Schmidt-Hoberg, K. *Long-lived Dark Higgs and Inelastic Dark Matter at Belle II.* JHEP **04** (2021), 146.
- [149] Duerr, M., Ferber, T., Hearty, C., Kahlhoefer, F., Schmidt-Hoberg, K., and Tunney, P. *Invisible and displaced dark matter signatures at Belle II.* JHEP **02** (2020), 039.
- [150] Dutta, B., and Mimura, Y. *Electron g – 2 with flavor violation in MSSM.* Phys. Lett. **B790** (2019), 563–567.
- [151] Eguchi, K., et al. *First results from KamLAND: Evidence for reactor anti-neutrino disappearance.* Phys. Rev. Lett. **90** (2003), 021802.
- [152] El Kheishen, M. M., Aboshousha, A. A., and Shafik, A. A. *Analytic formulas for the neutralino masses and the neutralino mixing matrix.* Phys. Rev. D **45** (1992), 4345–4348.

- [153] El-Zant, A., Khalil, S., and Sil, A. *Warm dark matter in a $B-L$ inverse seesaw scenario*. Phys. Rev. D **91** (2015), 035030.
- [154] Ellis, J. R., Ridolfi, G., and Zwirner, F. *On radiative corrections to supersymmetric Higgs boson masses and their implications for LEP searches*. Phys. Lett. B **262** (1991), 477–484.
- [155] Ellis, J. R., Ridolfi, G., and Zwirner, F. *Radiative corrections to the masses of supersymmetric Higgs bosons*. Phys. Lett. B **257** (1991), 83–91.
- [156] Elsayed, A., Khalil, S., and Moretti, S. *Higgs Mass Corrections in the SUSY $B-L$ Model with Inverse Seesaw*. Phys. Lett. B **715** (2012), 208–213.
- [157] Endo, M., and Yin, W. *Explaining electron and muon $g - 2$ anomaly in SUSY without lepton-flavor mixings*. JHEP **08** (2019), 122.
- [158] Esteban, I., Gonzalez-Garcia, M. C., Maltoni, M., Schwetz, T., and Zhou, A. *The fate of hints: updated global analysis of three-flavor neutrino oscillations*. JHEP **09** (2020), 178.
- [159] et al, G. A. *Search for non-resonant Higgs boson pair production in the $b\bar{b}\ell\nu\ell\nu$ final state with the ATLAS detector in pp collisions at $s=13$ TeV*. Physics Letters B **801** (2020), 135145.
- [160] Ezzat, K., Ashry, M., and Khalil, S. *Search for a heavy neutral Higgs boson in a left-right model with an inverse seesaw mechanism at the LHC*. Phys. Rev. D **104** (2021), 015016.
- [161] Ezzat, K., Faisel, G., and Khalil, S. *Investigating R_D and R_{D^*} anomalies in a left-right model with an inverse seesaw*. Eur. Phys. J. C **83** (2023), 731.
- [162] Farley, F. J. M., Jungmann, K., Miller, J. P., Morse, W. M., Orlov, Y. F., Roberts, B. L., Semertzidis, Y. K., Silenko, A., and Stephenson, E. J. *A New*

BIBLIOGRAPHY

- method of measuring electric dipole moments in storage rings.* Phys. Rev. Lett. **93** (2004), 052001.
- [163] Fileviez Perez, P., and Spinner, S. *Spontaneous R-Parity Breaking and Left-Right Symmetry.* Phys. Lett. **B673** (2009), 251–254.
- [164] Fonseca, R. M., Malinsky, M., Porod, W., and Staub, F. *Running soft parameters in SUSY models with multiple U(1) gauge factors.* Nucl. Phys. B **854** (2012), 28–53.
- [165] Frank, M., Özdal, O., and Poulose, P. *Relaxing LHC constraints on the W_R mass.* Phys. Rev. D **99** (2019), 035001.
- [166] Fukuda, Y., et al. *Evidence for oscillation of atmospheric neutrinos.* Phys. Rev. Lett. **81** (1998), 1562–1567.
- [167] Fukuda, Y. e. a. *Evidence for Oscillation of Atmospheric Neutrinos.* Phys. Rev. Lett. **81** (1998), 1562–1567.
- [168] Gell-Mann, M., Ramond, P., and Slansky, R. *Complex Spinors and Unified Theories.* Conf. Proc. C **790927** (1979), 315–321.
- [169] Gérardin, A., Meyer, H. B., and Nyffeler, A. *Lattice calculation of the pion transition form factor with $N_f = 2 + 1$ Wilson quarks.* Phys. Rev. **D100** (2019), 034520.
- [170] Giudice, G. F., Paradisi, P., and Passera, M. *Testing new physics with the electron g-2.* JHEP **11** (2012), 113.
- [171] Glashow, S. L., Iliopoulos, J., and Maiani, L. *Weak Interactions with Lepton-Hadron Symmetry.* Phys. Rev. D **2** (1970), 1285–1292.

- [172] Gnendiger, C., Stöckinger, D., and Stöckinger-Kim, H. *The electroweak contributions to $(g - 2)_\mu$ after the Higgs boson mass measurement.* Phys. Rev. **D88** (2013), 053005.
- [173] Gonzalez-Garcia, M., and Valle, J. *Fast Decaying Neutrinos and Observable Flavor Violation in a New Class of Majoron Models.* Phys. Lett. B **216** (1989), 360–366.
- [174] Grimus, W., Lavoura, L., Ogreid, O. M., and Osland, P. *The Oblique parameters in multi-Higgs-doublet models.* Nucl. Phys. B **801** (2008), 81–96.
- [175] Grossman, Y., and Neubert, M. *Neutrino masses and mixings in nonfactorizable geometry.* Phys. Lett. B **474** (2000), 361–371.
- [176] Gu, J., Li, H., Liu, Z., Su, S., and Su, W. *Learning from Higgs Physics at Future Higgs Factories.* JHEP **12** (2017), 153.
- [177] Guchait, M. *Exact solution of the neutralino mass matrix.* Z. Phys. C **57** (1993), 157–164. [Erratum: Z.Phys.C 61, 178 (1994)].
- [178] Gunion, J. F., and Haber, H. E. *Higgs Bosons in Supersymmetric Models. 1.* Nucl. Phys. B **272** (1986), 1. [Erratum: Nucl.Phys.B 402, 567–569 (1993)].
- [179] Haag, R., Lopuszanski, J. T., and Sohnius, M. *All Possible Generators of Supersymmetries of the s Matrix.* Nucl. Phys. **B88** (1975), 257. [,257(1974)].
- [180] Haba, N., Shimizu, Y., and Yamada, T. *Muon and electron $g - 2$ and the origin of the fermion mass hierarchy.* PTEP **2020** (2020), 093B05.
- [181] Haber, H. E., and Hempfling, R. *Can the mass of the lightest Higgs boson of the minimal supersymmetric model be larger than $m(Z)$?* Phys. Rev. Lett. **66** (1991), 1815–1818.

BIBLIOGRAPHY

- [182] Haber, H. E., and Kane, G. L. *The Search for Supersymmetry: Probing Physics Beyond the Standard Model.* Phys. Rept. **117** (1985), 75–263.
- [183] Haber, H. E., and O’Neil, D. *Basis-independent methods for the two-Higgs-doublet model. II. The Significance of $\tan\beta$.* Phys. Rev. D **74** (2006), 015018. [Erratum: Phys.Rev.D 74, 059905 (2006)].
- [184] Haber, H. E., and O’Neil, D. *Basis-independent methods for the two-Higgs-doublet model III: The CP-conserving limit, custodial symmetry, and the oblique parameters S , T , U .* Phys. Rev. D **83** (2011), 055017.
- [185] Hahn, T. *Generating Feynman diagrams and amplitudes with FeynArts 3.* Comput. Phys. Commun. **140** (2001), 418–431.
- [186] Hahn, T., and Schappacher, C. *The Implementation of the minimal supersymmetric standard model in FeynArts and FormCalc.* Comput. Phys. Commun. **143** (2002), 54–68.
- [187] Hammad, A., Khalil, S., and Moretti, S. *Higgs boson decays into $\gamma\gamma$ and $Z\gamma$ in the MSSM and the B-L supersymmetric SM.* Phys. Rev. D **92** (2015), 095008.
- [188] Hammad, A., Khalil, S., and Moretti, S. *LHC signals of a B-L supersymmetric standard model CP -even Higgs boson.* Phys. Rev. D **93** (2016), 115035.
- [189] Han, X.-F., Li, T., Wang, L., and Zhang, Y. *Simple interpretations of lepton anomalies in the lepton-specific inert two-Higgs-doublet model.* Phys. Rev. D **99** (2019), 095034.
- [190] Hanneke, D., Fogwell, S., and Gabrielse, G. *New Measurement of the Electron Magnetic Moment and the Fine Structure Constant.* Phys. Rev. Lett. **100** (2008), 120801.

- [191] Hanneke, D., Hoogerheide, S. F., and Gabrielse, G. *Cavity Control of a Single-Electron Quantum Cyclotron: Measuring the Electron Magnetic Moment*. Phys. Rev. A **83** (2011), 052122.
- [192] Harigaya, K., Petrosky, E., and Pierce, A. *Precision electroweak tensions and a dark photon*. JHEP **07** (2024), 201.
- [193] Harlander, R. V., and Kilgore, W. B. *Inclusive Higgs production at next-to-next-to leading order*. eConf **C010630** (2001), P506.
- [194] Harlander, R. V., and Kilgore, W. B. *Next-to-Next-to-Leading Order Higgs Production at Hadron Colliders*. Phys. Rev. Lett. **88** (2002), 201801.
- [195] Hiller, G., Hormigos-Feliu, C., Litim, D. F., and Steudtner, T. *Anomalous magnetic moments from asymptotic safety*. Phys. Rev. D **102** (2020), 071901.
- [196] Hocker, A., et al. *TMVA - Toolkit for Multivariate Data Analysis* (2007).
- [197] Hoferichter, M., Hoid, B.-L., and Kubis, B. *Three-pion contribution to hadronic vacuum polarization*. JHEP **08** (2019), 137.
- [198] Hoferichter, M., Hoid, B.-L., Kubis, B., Leupold, S., and Schneider, S. P. *Dispersion relation for hadronic light-by-light scattering: pion pole*. JHEP **10** (2018), 141.
- [199] Ibarra, A., Molinaro, E., and Petcov, S. T. *Low Energy Signatures of the TeV Scale See-Saw Mechanism*. Phys. Rev. D **84** (2011), 013005.
- [200] Ignatov, F. V., et al. *Measurement of the $e^+e^- \rightarrow \pi^+\pi^-$ cross section from threshold to 1.2 GeV with the CMD-3 detector*. Phys. Rev. D **109** (2024), 112002.
- [201] Jana, S., K., V. P., and Saad, S. *Resolving electron and muon $g - 2$ within the 2HDM*. Phys. Rev. D **101** (2020), 115037.

BIBLIOGRAPHY

- [202] Jegerlehner, F., and Nyffeler, A. *The Muon g-2*. Phys. Rept. **477** (2009), 1–110.
- [203] Kane, G. L., Kolda, C. F., Roszkowski, L., and Wells, J. D. *Study of constrained minimal supersymmetry*. Phys. Rev. **D49** (1994), 6173–6210.
- [204] Kannike, K. *Vacuum Stability Conditions From Copositivity Criteria*. Eur.Phys.J. **C72** (2012), 2093.
- [205] Kawamura, J., Okawa, S., and Omura, Y. *W boson mass and muon g-2 in a lepton portal dark matter model*. Phys. Rev. D **106** (2022), 015005.
- [206] Kawamura, J., and Raby, S. *W mass in a model with vectorlike leptons and U(1)'*. Phys. Rev. D **106** (2022), 035009.
- [207] Kawamura, J., Raby, S., and Trautner, A. *Complete vectorlike fourth family and new U(1)' for muon anomalies*. Phys. Rev. **D100** (2019), 055030.
- [208] Kawamura, J., Raby, S., and Trautner, A. *Complete vectorlike fourth family with U(1)': A global analysis*. Phys. Rev. D **101** (2020), 035026.
- [209] Keshavarzi, A., Marciano, W. J., Passera, M., and Sirlin, A. *Muon g - 2 and Δα connection*. Phys. Rev. D **102** (2020), 033002.
- [210] Keshavarzi, A., Nomura, D., and Teubner, T. *Muon g - 2 and α(M_Z^2): a new data-based analysis*. Phys. Rev. **D97** (2018), 114025.
- [211] Keshavarzi, A., Nomura, D., and Teubner, T. *g - 2 of charged leptons, α(M_Z^2), and the hyperfine splitting of muonium*. Phys. Rev. D **101** (2020), 014029.
- [212] Khalil, S. *TeV-scale gauged B-L symmetry with inverse seesaw mechanism*. Phys. Rev. **D82** (2010), 077702.
- [213] Khalil, S. *Radiative symmetry breaking in supersymmetric B – L models with an inverse seesaw mechanism*. Phys. Rev. D **94** (2016), 075003.

- [214] Khalil, S., and Masiero, A. *Radiative B-L symmetry breaking in supersymmetric models*. Phys. Lett. **B665** (2008), 374–377.
- [215] Kim, O., et al. *Reduction of coherent betatron oscillations in a muon g – 2 storage ring experiment using RF fields*. New J. Phys. **22** (2020), 063002.
- [216] Kitano, R., Koike, M., and Okada, Y. *Detailed calculation of lepton flavor violating muon electron conversion rate for various nuclei*. Phys. Rev. D **66** (2002), 096002. [Erratum: Phys.Rev.D 76, 059902 (2007)].
- [217] Kowalska, K., Kumar, D., and Sessolo, E. M. *Implications for new physics in $b \rightarrow s\mu\mu$ transitions after recent measurements by Belle and LHCb*. Eur. Phys. J. C **79** (2019), 840.
- [218] Kribs, G. D., McKeen, D., and Raj, N. *Breaking up the Proton: An Affair with Dark Forces*. Phys. Rev. Lett. **126** (2021), 011801.
- [219] Kulkarni, H., and Raby, S. *An $SU(5) \times U(1)'$ SUSY GUT with a "vector-like chiral" fourth family to fit all low energy data, including the muon g - 2*. JHEP **05** (2023), 152.
- [220] Kumar, D., Kowalska, K., and Sessolo, E. M. *Global Bayesian Analysis of new physics in $b \rightarrow s\mu\mu$ transitions after Moriond-2019*. In *17th Conference on Flavor Physics and CP Violation* (6 2019).
- [221] Kundu, A., Le Yaouanc, A., Mondal, P., and Richard, F. *Searches for scalars at LHC and interpretation of the findings*. In *2022 ECFA Workshop on e+e-Higgs/EW/Top factories* (11 2022).
- [222] Kurz, A., Liu, T., Marquard, P., and Steinhauser, M. *Hadronic contribution to the muon anomalous magnetic moment to next-to-next-to-leading order*. Phys. Lett. **B734** (2014), 144–147.

BIBLIOGRAPHY

- [223] Lavoura, L., and Silva, J. P. *The Oblique corrections from vector - like singlet and doublet quarks.* Phys. Rev. D **47** (1993), 2046–2057.
- [224] Lee, H. M., Song, J., and Yamashita, K. *Seesaw lepton masses and muon $g - 2$ from heavy vector-like leptons.* J. Korean Phys. Soc. **79** (2021), 1121–1134.
- [225] Lee, H. M., and Yamashita, K. *A model of vector-like leptons for the muon $g - 2$ and the W boson mass.* Eur. Phys. J. C **82** (2022), 661.
- [226] Lees, J. P., et al. *Search for a Dark Photon in e^+e^- Collisions at BaBar.* Phys. Rev. Lett. **113** (2014), 201801.
- [227] Lees, J. P., et al. *Search for Invisible Decays of a Dark Photon Produced in e^+e^- Collisions at BaBar.* Phys. Rev. Lett. **119** (2017), 131804.
- [228] LÉVY, M., BASDEVANT, J.-L., SPEISER, D., WEYERS, J., GASTMANS, R., AND JACOB, M., Eds. *QUARKS AND LEPTONS. PROCEEDINGS, SUMMER INSTITUTE, CARGESE, FRANCE, JULY 9-29, 1979*, vol. 61 of *NATO Science Series B:* Springer, 1980.
- [229] Li, S.-P., Li, X.-Q., Li, Y.-Y., Yang, Y.-D., and Zhang, X. *Power-aligned 2HDM: a correlative perspective on $(g - 2)_{e,\mu}$.* JHEP **01** (2021), 034.
- [230] Lindner, M., Platscher, M., and Queiroz, F. S. *A Call for New Physics : The Muon Anomalous Magnetic Moment and Lepton Flavor Violation.* Phys. Rept. **731** (2018), 1–82.
- [231] Lipkin, H. J. *What is coherent in neutrino oscillations.* Phys. Lett. B **579** (2004), 355–360.
- [232] Liu, J., McGinnis, N., Wagner, C. E. M., and Wang, X.-P. *A light scalar explanation of $(g - 2)_\mu$ and the KOTO anomaly.* JHEP **04** (2020), 197.

- [233] Liu, J., Wagner, C. E. M., and Wang, X.-P. *A light complex scalar for the electron and muon anomalous magnetic moments.* JHEP **03** (2019), 008.
- [234] Liu, Y.-S., McKeen, D., and Miller, G. A. *Electrophobic Scalar Boson and Muonic Puzzles.* Phys. Rev. Lett. **117** (2016), 101801.
- [235] Ma, E. *Pathways to naturally small neutrino masses.* Phys. Rev. Lett. **81** (1998), 1171–1174.
- [236] Maiezza, A., Nemevsek, M., Nesti, F., and Senjanovic, G. *Left-Right Symmetry at LHC.* Phys. Rev. **D82** (2010), 055022.
- [237] Maki, Z., Nakagawa, M., and Sakata, S. *Remarks on the unified model of elementary particles.* Prog. Theor. Phys. **28** (1962), 870–880.
- [238] Maksymyk, I., Burgess, C. P., and London, D. *Beyond S, T and U.* Phys. Rev. D **50** (1994), 529–535.
- [239] Malinsky, M., Ohlsson, T., Xing, Z.-z., and Zhang, H. *Non-unitary neutrino mixing and CP violation in the minimal inverse seesaw model.* Phys. Lett. B **679** (2009), 242–248.
- [240] Martin, S. P. *A Supersymmetry primer.* Adv. Ser. Direct. High Energy Phys. **18** (1998), 1–98.
- [241] Masjuan, P., and Sánchez-Puertas, P. *Pseudoscalar-pole contribution to the $g_\mu - 2$: a rational approach.* Phys. Rev. **D95** (2017), 054026.
- [242] McCullough, M., Moore, J., and Ubiali, M. *The dark side of the proton.* JHEP **08** (2022), 019.
- [243] Megias, E., Quiros, M., and Salas, L. *$g_\mu - 2$ from Vector-Like Leptons in Warped Space.* JHEP **05** (2017), 016.

BIBLIOGRAPHY

- [244] Melnikov, K., and Vainshtein, A. *Hadronic light-by-light scattering contribution to the muon anomalous magnetic moment revisited.* Phys. Rev. **D70** (2004), 113006.
- [245] Messier, M. D. *Review of neutrino oscillations experiments.* eConf **C060409** (2006), 018.
- [246] Minkowski, P. $\mu \rightarrow e\gamma$ at a Rate of One Out of 10^9 Muon Decays? Phys. Lett. B **67** (1977), 421–428.
- [247] Mohapatra, R. *Mechanism for Understanding Small Neutrino Mass in Superstring Theories.* Phys. Rev. Lett. **56** (1986), 561–563.
- [248] Mohapatra, R., and Valle, J. *Neutrino Mass and Baryon Number Nonconservation in Superstring Models.* Phys. Rev. D **34** (1986), 1642.
- [249] Mohapatra, R. N., Paige, F. E., and Sidhu, D. *Symmetry Breaking and Naturalness of Parity Conservation in Weak Neutral Currents in Left-Right Symmetric Gauge Theories.* Phys. Rev. **D17** (1978), 2462.
- [250] Mohapatra, R. N., and Pati, J. C. *A Natural Left-Right Symmetry.* Phys. Rev. **D11** (1975), 2558.
- [251] Mohapatra, R. N., and Senjanovic, G. *Neutrino Mass and Spontaneous Parity Violation.* Phys. Rev. Lett. **44** (1980), 912.
- [252] Mohlabeng, G. *Revisiting the dark photon explanation of the muon anomalous magnetic moment.* Phys. Rev. D **99** (2019), 115001.
- [253] Morel, L., Yao, Z., Cladé, P., and Guellati-Khélifa, S. *Determination of the fine-structure constant with an accuracy of 81 parts per trillion.* Nature **588** (2020), 61–65.

- [254] Moretti, S., and Khalil, S. *Supersymmetry Beyond Minimality: From Theory to Experiment*. CRC Press, 2019.
- [255] Muller-Kirsten, H. J. W., and Wiedemann, A. *SUPERSYMMETRY: AN INTRODUCTION WITH CONCEPTUAL AND CALCULATIONAL DETAILS*. Hackensack, USA: World Scientific (2010) 439 p (1986).
- [256] Nemevsek, M., Senjanovic, G., and Tello, V. *Left-Right Symmetry: from Majorana to Dirac*. Phys.Rev.Lett. **110** (2013), 151802.
- [257] Okada, N., and Papapietro, N. *Radiative breaking of the minimal supersymmetric left-right model*. Phys. Lett. **B756** (2016), 47–51.
- [258] Okada, Y., Yamaguchi, M., and Yanagida, T. *Upper bound of the lightest Higgs boson mass in the minimal supersymmetric standard model*. Prog. Theor. Phys. **85** (1991), 1–6.
- [259] O’Leary, B., Porod, W., and Staub, F. *Mass spectrum of the minimal SUSY B - L model*. JHEP **05** (2012), 042.
- [260] Osland, P., Pankov, A. A., and Serenkova, I. A. *Bounds on the mass and mixing of Z' and W' bosons decaying into different pairings of W , Z , or Higgs bosons using CMS data at the LHC* (2022).
- [261] Pankov, A. A., Osland, P., Serenkova, I. A., and Bednyakov, V. A. *High-precision limits on WW' and ZZ' mixing from diboson production using the full LHC Run 2 ATLAS data set*. Eur. Phys. J. C **80** (2020), 503.
- [262] Parker, R. H., Yu, C., Zhong, W., Estey, B., and Müller, H. *Measurement of the fine-structure constant as a test of the Standard Model*. Science **360** (2018), 191.

BIBLIOGRAPHY

- [263] Patra, S., Sarkar, A., Sarkar, U., and Yajnik, U. *Spontaneous Parity Violation in a Supersymmetric Left-Right Symmetric Model.* Phys. Lett. **B679** (2009), 386–389.
- [264] Peskin, M. E., and Schroeder, D. V. *An Introduction to quantum field theory.* Addison-Wesley Publishing Company, 1995.
- [265] Peskin, M. E., and Takeuchi, T. *A New constraint on a strongly interacting Higgs sector.* Phys. Rev. Lett. **65** (1990), 964–967.
- [266] Peskin, M. E., and Takeuchi, T. *Estimation of oblique electroweak corrections.* Phys. Rev. D **46** (1992), 381–409.
- [267] Ping, L., and Yu, F. Y. *Criteria for copositive matrices of order four.* Linear Algebra and its Applications **194** (1993), 109 – 124.
- [268] Pontecorvo, B. *Inverse beta processes and nonconservation of lepton charge.* Zh. Eksp. Teor. Fiz. **34** (1957), 247.
- [269] Pontecorvo, B. *Mesonium and anti-mesonium.* Sov. Phys. JETP **6** (1957), 429.
- [270] Porod, W. *SPheno, a program for calculating supersymmetric spectra, SUSY particle decays and SUSY particle production at e+ e- colliders.* Comput. Phys. Commun. **153** (2003), 275–315.
- [271] Porod, W., and Staub, F. *SPheno 3.1: Extensions including flavour, CP-phases and models beyond the MSSM.* Comput. Phys. Commun. **183** (2012), 2458–2469.
- [272] Pospelov, M. *Secluded U(1) below the weak scale.* Phys. Rev. D **80** (2009), 095002.
- [273] Raby, S., and Trautner, A. *Vectorlike chiral fourth family to explain muon anomalies.* Phys. Rev. **D97** (2018), 095006.

- [274] Randall, L., and Sundrum, R. *A Large mass hierarchy from a small extra dimension.* Phys. Rev. Lett. **83** (1999), 3370–3373.
- [275] Riordan, E. M., et al. *A Search for Short Lived Axions in an Electron Beam Dump Experiment.* Phys. Rev. Lett. **59** (1987), 755.
- [276] Schmidt, T., and Spira, M. *Higgs Boson Production via Gluon Fusion: Soft-Gluon Resummation including Mass Effects.* Phys. Rev. D **93** (2016), 014022.
- [277] Schwartz, M. D. *Quantum Field Theory and the Standard Model.* Cambridge University Press, 3 2014.
- [278] Seif, M. A. I. *TEV SCALE LEFT-RIGHT SYMMETRIC MODEL WITH MINIMAL HIGGS SECTOR.* Msc thesis, Cairo University, Cairo, 2015.
- [279] Senjanovic, G., and Mohapatra, R. N. *Exact Left-Right Symmetry and Spontaneous Violation of Parity.* Phys. Rev. **D12** (1975), 1502.
- [280] Shifman, M. *Large Extra Dimensions: Becoming acquainted with an alternative paradigm.* Int. J. Mod. Phys. **A25** (2010), 199–225.
- [281] Shirman, Y. *Introduction to Supersymmetry and Supersymmetry Breaking* (2010). 359–422.
- [282] Shtabovenko, V., Mertig, R., and Orellana, F. *New Developments in FeynCalc 9.0.* Comput. Phys. Commun. **207** (2016), 432–444.
- [283] Sirunyan, A. M., et al. *Search for resonant and nonresonant Higgs boson pair production in the $b\bar{b}\ell\nu\ell\nu$ final state in proton-proton collisions at $\sqrt{s} = 13$ TeV.* JHEP **01** (2018), 054.
- [284] Sirunyan, A. M., et al. *Search for nonresonant Higgs boson pair production in the $bb\bar{b}\bar{b}$ final state at $\sqrt{s} = 13$ TeV.* JHEP **04** (2019), 112.

BIBLIOGRAPHY

- [285] Sirunyan, A. M., et al. *Search for physics beyond the standard model in multi-lepton final states in proton-proton collisions at $\sqrt{s} = 13$ TeV*. JHEP **03** (2020), 051.
- [286] Sirunyan, A. M., et al. *Search for a heavy vector resonance decaying to a Z boson and a Higgs boson in proton-proton collisions at $\sqrt{s} = 13$ TeV*. Eur. Phys. J. C **81** (2021), 688.
- [287] Sjostrand, T., Mrenna, S., and Skands, P. Z. *A Brief Introduction to PYTHIA 8.1*. Comput. Phys. Commun. **178** (2008), 852–867.
- [288] Sjöstrand, T., Ask, S., Christiansen, J. R., Corke, R., Desai, N., Ilten, P., Mrenna, S., Prestel, S., Rasmussen, C. O., and Skands, P. Z. *An Introduction to PYTHIA 8.2*. Comput. Phys. Commun. **191** (2015), 159–177.
- [289] Staub, F. *From Superpotential to Model Files for FeynArts and CalcHep/CompHep*. Comput. Phys. Commun. **181** (2010), 1077–1086.
- [290] Staub, F. *SARAH 4 : A tool for (not only SUSY) model builders*. Comput. Phys. Commun. **185** (2014), 1773–1790.
- [291] Staub, F. *A closer look at non-decoupling D-Terms*. Phys. Lett. B **758** (2016), 200–204.
- [292] Susskind, L. *Dynamics of Spontaneous Symmetry Breaking in the Weinberg-Salam Theory*. Phys. Rev. **D20** (1979), 2619–2625.
- [293] 't Hooft, G. *Naturalness, chiral symmetry, and spontaneous chiral symmetry breaking*. NATO Sci. Ser. B **59** (1980), 135–157.
- [294] 't Hooft, G., Itzykson, C., Jaffe, A., Lehmann, H., Mitter, P. K., Singer, I. M., and Stora, R. *Recent Developments in Gauge Theories. Proceedings, Nato*

Advanced Study Institute, Cargese, France, August 26 - September 8, 1979.
NATO Sci. Ser. B **59** (1980), pp.1–438.

- [295] Tanabashi, M., et al. *Review of Particle Physics.* Phys. Rev. **D98** (2018), 030001.
- [296] The-ATLAS-Collaboration. *Study of the double Higgs production channel $H(\rightarrow b\bar{b})H(\rightarrow \gamma\gamma)$ with the ATLAS experiment at the HL-LHC.* ATLAS NOTE **ATL-PHYS-PUB-2017-001** (2017).
- [297] Therhaag, J. *TMVA Toolkit for multivariate data analysis in ROOT.* PoS **ICHEP2010** (2010), 510.
- [298] Therhaag, J. *TMVA: Toolkit for multivariate data analysis.* AIP Conf. Proc. **1504** (2012), 1013–1016.
- [299] Thomas, A. W., Wang, X., and Williams, A. G. *Sensitivity of Parity-Violating Electron Scattering to a Dark Photon.* Phys. Rev. Lett. **129** (2022), 011807.
- [300] Thomas, A. W., Wang, X. G., and Williams, A. G. *Constraints on the dark photon from deep inelastic scattering.* Phys. Rev. D **105** (2022), L031901.
- [301] Tumasyan, A., et al. *Inclusive nonresonant multilepton probes of new phenomena at $\sqrt{s}=13$ TeV.* Phys. Rev. D **105** (2022), 112007.
- [302] Tumasyan, A., et al. *Search for new heavy resonances decaying to WW, WZ, ZZ, WH, or ZH boson pairs in the all-jets final state in proton-proton collisions at $s=13$ TeV.* Phys. Lett. B **844** (2023), 137813.
- [303] Tumasyan, A., et al. *Search for a new resonance decaying into two spin-0 bosons in a final state with two photons and two bottom quarks in proton-proton collisions at $\sqrt{s} = 13$ TeV.* JHEP **05** (2024), 316.

BIBLIOGRAPHY

- [304] Un, C. S., and Ozdal, O. *Mass Spectrum and Higgs Profile in BLSSM*. Phys. Rev. D **93** (2016), 055024.
- [305] Veltman, M. J. G. *The Infrared - Ultraviolet Connection*. Acta Phys. Polon. **B12** (1981), 437.
- [306] Weiland, C. *Enhanced lepton flavour violation in the supersymmetric inverse seesaw*. J. Phys. Conf. Ser. **447** (2013), 012037.
- [307] Weinberg, S. *Baryon and Lepton Nonconserving Processes*. Phys. Rev. Lett. **43** (1979), 1566–1570.
- [308] Weinberg, S. *Varieties of Baryon and Lepton Nonconservation*. Phys. Rev. D **22** (1980), 1694.
- [309] Wess, J., and Bagger, J. *Supersymmetry and supergravity*. Princeton University Press, Princeton, NJ, USA, 1992.
- [310] Wess, J., and Zumino, B. *Supergauge Transformations in Four-Dimensions*. Nucl. Phys. **B70** (1974), 39–50. [,24(1974)].
- [311] Wilczek, F., and Zee, A. *Operator Analysis of Nucleon Decay*. Phys. Rev. Lett. **43** (1979), 1571–1573.
- [312] Yao, W., et al. *Review of Particle Physics*. J.Phys. **G33** (2006), 1–1232.
- [313] Zhou, Q., Han, X.-F., and Wang, L. *The CDF W-mass, muon $g - 2$, and dark matter in a $U(1)_{L_\mu - L_\tau}$ model with vector-like leptons*. Eur. Phys. J. C **82** (2022), 1135.
- [314] Zyla, P. A., et al. *Review of Particle Physics*. PTEP **2020** (2020), 083C01.